UNIVERSIDADE DE BRASÍLIA - UnB

INSTITUTO DE GEOCIÊNCIAS - IG

GEOCRONOLOGIA U/PB EM ZIRCÕES DETRÍTICOS E A EVOLUÇÃO TECTÔNICA E ESTRATIGRÁFICA DA BACIA ESPINHAÇO NO SETOR MERIDIONAL

Tese de Doutorado

Nº 124

MARCELO NASCIMENTO DOS SANTOS

ORIENTADOR: PROF. DR. FARID CHEMALE JÚNIOR

COORIENTADOR: PROF. DR. IVO ANTÔNIO DUSSIN

BRASÍLIA – DF

2015

UNIVERSIDADE DE BRASÍLIA - UnB

INSTITUTO DE GEOCIÊNCIAS - IG

GEOCRONOLOGIA U/PB EM ZIRCÕES DETRÍTICOS E A EVOLUÇÃO TECTÔNICA E ESTRATIGRÁFICA DA BACIA ESPINHAÇO NO SETOR MERIDIONAL

Tese de Doutorado

Nº124

Marcelo Nascimento dos Santos

Tese de doutorado elaborada junto ao Programa de Pós-Graduação em Geologia (Área de Concentração Geologia Regional), do Instituto de Geociências (IG) da Universidade de Brasília (UnB) para obtenção do Título de Doutor em Geologia.

Orientador: Prof. Dr. Farid Chemale Júnior

Coorientador: Prof. Dr. Ivo Antônio Dussin

Banca examinadora: Prof. Dr. Alexandre Uhlein (UFMG)

Prof. Dr. Carlos José Souza de Alvarenga (UnB)

Prof. Dr. Fernando Flecha de Alkmim (UFOP)

Prof[a]. Dr[a]. Lucieth Cruz Vieira (UnB)

BRASÍLIA – DF

2015

AGRADECIMENTOS

Gostaria de agradecer a todas as pessoas e instituições que ajudaram no desenvolvimento da presente tese. Se esquecer de alguém, me perdoem, por favor!

Antes de tudo, agradeço à minha família! À minha esposa Fernanda pela paciência e compreensão pelos momentos de ausência decorrentes da elaboração da tese e aos meus filhos, Arthur e Lucas, pelos diversos momentos de descontração. À minha família do sul, meus pais e irmãos, por todo apoio e por acreditarem nessa realização.

Um agradecimento especial ao grande amigo e orientador, Farid, por todo apoio, críticas, discussões e ensinamentos, tanto do ponto de vista profissional, quanto pessoal. Ajudou-me em escolhas importantes e sempre acertadas. Um verdadeiro orientador, valeu Faridão!

Não poderia deixar de agradecer ao meu outro grande amigo e coorientador, Dussin, pelos ensinamentos e momentos compartilhados em campo, sempre acrescentando sabedoria, alegria e descontração em todas as conversas, principalmente às boêmias! Tentei seguir um pouco da sua história, saindo do Rio Grande do Sul direto para Diamantina, para desbravar os quartzitos da Serra do Espinhaço.

Aos amigos geólogos Max, Gláucia, Feijão, Raphael, Peixinho e Felipe Guadagnin que também ajudaram no desenvolvimento do projeto, principalmente durante as etapas de mapeamento, e ensinaram muito sobre a geologia regional da Bacia Espinhaço.

Agradeço à Universidade de Brasília, ao Instituto de Geociências e a todos os professores e funcionários do IG, bem como aos membros da banca examinadora e aos revisores dos artigos pelo tempo despendido na leitura e críticas para a melhoria da tese.

À Capes pela bolsa de estudos, essencial para que eu conseguisse me manter na pós-graduação.

Ao Instituto Casa da Glória (Eschwege) da UFMG pelo abrigo e estrutura durante parte do período de mapeamento, bem como a todos os seus funcionários, sempre tão prestativos e companheiros.

À Petrobras pelo financiamento do projeto.

RESUMO

Marcelo Nascimento dos Santos, 2015. Geocronologia U/PB em zircões detríticos e a evolução tectônica e estratigráfica da Bacia Espinhaço no setor meridional. Tese de Doutorado, Universidade de Brasília.

Orientador: Farid Chemale.

O Supergrupo Espinhaço em Minas Gerais representa um importante registro de bacias sedimentares intracontinentais desenvolvidas no Orógeno Araçuaí e no Cráton do São Francisco durante o Proterozoico. A presente tese tem o objetivo de esclarecer aspectos relacionados à proveniência sedimentar da Bacia Espinhaço e propor um modelo de evolução paleogeográfica para o Grupo Conselheiro Mata com base na integração de dados sedimentológicos e estratigráficos, geoquímica em rocha total, datação U-Pb e análise Lu-Hf em grãos de zircão.

Os dados geoquímicos indicam que as unidades estudadas foram formadas a partir de sedimentos provenientes de rochas félsicas e de rochas sedimentares. Picos de idade Paleoproterozoica ocorrem em todas as unidades da bacia, mas as proporções relativas entre as populações de cada período são nitidamente diferentes, o que pode refletir as frequentes mudanças no padrão de paleocorrentes ao longo do tempo. As análises Lu-Hf na maior parte das populações sugerem reciclagem de uma crosta antiga (T_{DM} com assinaturas Paleo- a Mesoarqueanas). Os valores de ε_{Hf}(t) negativos para as populações Neoarqueanas (c. 2,7 Ga) são similares aos valores encontrados nas amostras de xisto da Formação Barão de Guaicuí, indicando que essa unidade foi uma potencial fonte para os sedimentos. Os dados isotópicos de Hf da Sequência Espinhaço Inferior apresentam arranjos verticais de ε_{Hf}(t) pobremente definidos em c. 2,4 Ga (ε_{Hf}(t) -8,4 a +4,2) e 2,1 Ga (ε_{Hf}(t) −18,8 a +4,4), indicando que esses grãos de zircão refletem a mistura de uma crosta Arqueana em magmas juvenis do Sideriano e Riaciano. A Fm. São João da Chapada apresenta uma pequena população de grãos de zircão que cristalizou durante o Arqueano, possuindo uma composição isotópica de Hf muito próxima da amostra de gnaisse do Complexo Basal, datado em 2828 Ma e apresentando ε_{Hf}(t) de -1 a +1,3. Essas evidências sugerem que o embasamento cristalino foi uma importante fonte de sedimentos para a Formação São João da Chapada. A ausência de grãos ígneos de zircão com composição isotópica de Hf juvenil no filito hematítico sugere que não havia componentes derivados do manto presentes na fonte do filito hematítico.

O presente estudo mostra que a população Esteniana da Fm. Sopa-Brumadinho possui composição isotópica de Hf juvenil e não é restrita à borda leste do rifte (Região de Extração), mas também ocorre na borda oeste. As fontes formadas entre 1,4 e 1,6 Ga registram o retrabalhamento de uma crosta Arqueana, enquanto as fontes formadas entre 1,5 e 2,2 Ga envolveram a mistura de uma crosta arqueana com material juvenil. Na fase sag há uma mudança de ambiente de sedimentação de continental para marinho, que é caracterizada pela progressiva diminuição da quantidade relativa de sedimentos formados no Período Riaciano e concomitante aumento na proporção dos sedimentos do Período Orosiriano. A fonte Orosiriana, formada pela mistura de magma juvenil com uma crosta antiga, ainda não foi identificada nas regiões adjacentes. As fácies sedimentares identificadas nos ciclos transgressivo-regressivos do Grupo Conselheiro Mata foram agrupadas em seis associações de fácies: 1) offshore a lower shoreface, com períodos de quiescência e outros com deposição episódica (Fm. Santa Rita); 2) upper shoreface a foreshore, com retrabalhamento das unidades sotopostas (Fm. Córrego dos Borges); 3) ambiente costeiro desértico representado por depósitos eólicos de duna e interduna (Fm. Córrego dos Borges); 4) upper shoreface a foreshore influenciados pela maré, caracterizados pela migração de dunas subaquosas, colapso das ondas na região de espraiamento e ciclos de maré de sizígia e quadratura (Fm. Córrego Pereira); 5) lower shoreface, com decantação dos sedimentos finos e uma combinação de fluxos unidirecionais e oscilatórios gerados por tempestades (fms. Córrego da Bandeira e Rio Pardo Grande); e 6) plataforma carbonática (estromatolítica)-siliciclástica, com influxo siliciclástico reduzido e precipitação subaquosa (Fm. Rio Pardo Grande).

Keywords: Esteniano; Estateriano; Bacia Espinhaço; Geocronologia U-Pb em zircão; análises isotópicas Lu-Hf; Supercontinente Columbia.

ABSTRACT

Marcelo Nascimento dos Santos, 2015. U/PB detrital zircon geochronology and the tectonic and stratigraphic evolution of the Southern Espinhaço Basin. Ph. D. Thesis, Universidade de Brasília.

Thesis advisor: Farid Chemale.

The Espinhaço Supergroup in Minas Gerais is an important record of intracontinental sedimentary basins developed in the Araçuaí Fold Belt and the São Francisco Craton during the Proterozoic. This thesis has the objective of examining the sediment provenance of the Espinhaço Basin and propose a regional paleogeographic evolution model for the Conselheiro Mata Group by an integration of sedimentological and stratigraphic data, whole-rock geochemistry, U-Pb dating and Lu-Hf analysis of zircon grains.

The geochemical data indicate that the studied units contain input from felsic rocks and sedimentary rocks. Paleoproterozoic age peaks occur in all geological units of the Espinhaço Basin, but the relative proportions of the population are clearly distinct, which may reflect the changes in paleocurrent pattern over the time. The Lu-Hf analyzes in most of the populations suggest recycling of an older crust (T_{DM} with Paleo- to Mesoarchean signatures). The negative $\varepsilon_{Hf}(t)$ values for the Neoarchean population (c. 2.7 Ga) are similar to values found in the schist sample of the Barão do Guaicuí Formation, indicating that this unit was a potential source of sediments. The Hf isotope data of the Lower Espinhaço Sequence show a poorly defined vertical $\varepsilon_{Hf}(t)$ array at c. 2.4 ($\varepsilon_{Hf}(t)$ -8.4 to +4.2) and 2.1 Ga ($\varepsilon_{Hf}(t)$ −18.8 to +4.4) and indicate that those zircons reflect the mixing of Archean crust into juvenile Siderian and Rhyacian magmas. The São João da Chapada Fm. shows a small population of zircon that crystallized during the Archean with Hf isotope compositions that are very similar to the gneiss of the Basal Complex, dated at 2828 Ma and presenting $\varepsilon_{Hf}(t)$ values of -1 to +1.3. This finding suggests that the crystalline basement was an important source for the sediments of the São João da Chapada Formation. The absence of igneous zircons with juvenile Hf isotope compositions in the hematitic phyllite suggests that no major depleted mantle-derived components were present in the source of the hematitic phyllite.

This study shows that the Stenian population in the Sopa-Brumadinho Fm. has juvenile Hf isotope composition and it is not restricted to the eastern edge of the rift (Extração region), but also occurs in the western edge. The sources formed between 1.4 and 1.6 Ga record a reworking of Archean crust, whereas the sources formed between 1.5 and 2.2 Ga involve the mixing of zircons derived from the reworking of the Archean crust and from juvenile material. During the sag phase, a change from a continental to marine environment occurred, which is marked by a progressive decrease in sediments from the Rhyacian Period and a concomitant increase in sediments from the Orosirian Period. The Orosirian source rocks, formed by mixing of a juvenile magma with an older crust, have not yet been identified in the adjacent regions. The sedimentary facies identified in the transgressive-regressive cycles of the Conselheiro Mata Group were grouped into six facies associations: 1) offshore to lower shoreface with quiescent periods and episodic sediment supply (Santa Rita Fm.); 2) upper shoreface to foreshore with a reworking of the underlying units (Córrego dos Borges Fm.); 3) coastal desert environment represented by eolian dune and interdune deposits (Córrego dos Borges Fm.); 4) tidal-influenced upper shoreface to foreshore with the migration of subaqueous dunes, wave swash in a beach environment and cycles of neap-spring tides (Córrego Pereira Fm.); 5) lower shoreface with fallout of suspended fine sediments and a combination of unidirectional and oscillatory flows generated by storm waves (Córrego da Bandeira and Rio Pardo Grande fms.); and 6) stromatolitic carbonate-siliciclastic platform with reduced siliciclastic influx and subaqueous precipitation (Rio Pardo Grande Fm.).

Keywords: Stenian; Statherian; Espinhaço Basin; U-Pb zircon geochronology; Lu-Hf isotope analyses; Columbia Supercontinent.

SUMÁRIO

LISTA DE FIGURAS

TEXTO EXPLICATIVO – ESTRUTURA DA QUALIFICAÇÃO

A presente tese de doutorado está segmentada em quatro capítulos. O Capítulo I oferece uma revisão conceitual da Bacia Espinhaço e traz à tona a problemática envolvida em sua estratigrafia, compreendendo os seguintes tópicos: 1. Introdução; 2. Revisão do Estado da Arte; 3. Metodologia empregada na aquisição dos dados de campo; 4. Referências.

O Capítulo II apresenta o artigo científico publicado na revista Sedimentary Geology e incorporado à tese, intitulado “Provenance and paleogeographic reconstruction of a mesoproterozoic intracratonic sag basin (Upper Espinhaço Basin, Brazil)”. O Capítulo III, por sua vez, apresenta o artigo científico submetido à revista Gondwana Research, intitulado “Lu-Hf and U-Pb signature of the Espinhaço intracratonic basin for tracking evidence of the Columbia Supercontinent and the Grenville Orogeny in the São Francisco Craton”.

No Capítulo IV estão as conclusões da tese.

Os apêndices A, B, C, D e E correspondem, respectivamente, às tabelas com os dados de localização das amostras, geoquímica dos elementos maiores, geoquímica dos elementos terras raras, geocronologia U-Pb e análises isotópicas do sistema Lu-Hf.

CAPÍTULO I

1 Introdução

1.1 Caracterização do Problema

A Bacia Espinhaço é de longa data conhecida por apresentar questões controversas acerca de sua evolução tectono-estratigráfica, tendo em vista que grande parte dos modelos geológicos foram baseados essencialmente em dados de campo. Os últimos seis anos, no entanto, representam um período de significante avanço no conhecimento dessa bacia, principalmente a partir da publicação de dados geocronológicos (Chemale *et al*., 2010; Chemale *et al*., 2012; Santos *et al*., 2013), que permitem entender e posicionar temporalmente os eventos geológicos ocorridos de forma mais precisa.

O início da sedimentação na Bacia Espinhaço está relacionado a processos de rifteamento que, segundo parte da comunidade científica, teria ocorrido em contexto intracratônico ensiálico (Dussin & Dussin, 1995; Martins-Neto, 1998). No entanto, Almeida-Abreu (1993) propõe um modelo de bacia rifte que teria evoluído para uma margem passiva. As evidências de rifteamento podem ser observadas a partir de linhas sísmicas 2D e de dados de campo, que indicam a presença de vulcanismo em associação com sistemas deposicionais característicos desse contexto tectônico (Chemale *et al*., 2012; Dossin *et al*., 1987; Garcia & Uhlein, 1987; Chaves, 2013; Santos *et al*., 2013).

A caracterização das sequências deposicionais da fase rifte da Bacia Espinhaço Meridional encontra-se atualmente em estágio relativamente avançado do ponto de vista de mapeamento geológico e entendimento dos sistemas deposicionais. No entanto, os modelos apresentados até então para a fase sag carecem de informações detalhadas sobre evolução estratigráfica e sedimentar. Adicionalmente, a aplicação em conjunto dos métodos de datação U-Pb e Lu-Hf em zircão detrítico, na presente tese, permite uma abordagem diferenciada na análise de proveniência sedimentar para todas as unidades da bacia. É nesse contexto de mitigar parte das incertezas vigentes e compreender de forma acurada os aspectos sedimentológicos, estratigráficos e tectônicos da Bacia Espinhaço que se justifica a necessidade do presente estudo.

1.2 Objetivos

Os principais objetivos da tese são: analisar a proveniência sedimentar da Bacia Espinhaço Meridional com a aplicação dos métodos U-Pb e Lu-Hf em grãos de zircão detríticos, caracterizar de forma detalhada as fácies sedimentares e discriminar os subsistemas deposicionais da sequência marinha do Grupo Conselheiro Mata, para reconstruir de forma mais acurada possível a paleogeografia de cada unidade analisada.

1.3 Localização da Área de Estudo e Vias de Acesso

O acesso a Diamantina, partindo de Belo Horizonte (Fig. 1), pode ser realizado por via aérea (Aeroporto Presidente Juscelino Kubitschek, Diamantina) ou terrestre. Para o segundo caso, é necessário acessar as estradas BR-040 e BR-135, respectivamente em direção a Paroapeba e Curvelo. No entroncamento de Curvelo, segue-se em direção nordeste pelas estradas BR-259 e BR-367 rumo a Diamantina.

Por meio da estrada BR-367, que corta parte da área estudada, é possível obter o acesso a diversos afloramentos da sequência rifte. Existem algumas estradas secundárias, tanto em direção a leste como a oeste, porém cabe ressaltar a abundância de estradas vicinais e trilhas abertas para garimpos de ouro e diamante.

A estrada para Conselheiro Mata/Corinto e a estrada de ferro desativada, a partir da BR-367, permitem o acesso às unidades do Grupo Conselheiro Mata.

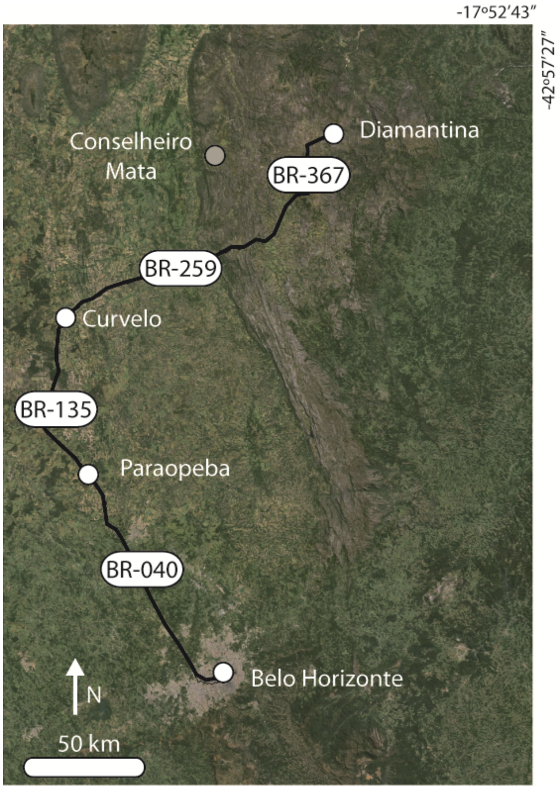

Figura 1 – Mapa com a localização das estradas (BRs) para o acesso a Diamantina a partir de Belo Horizonte com locais de referência citados no texto. Círculos brancos – cidades, círculo cinza – distrito de Diamantina. Imagem de satélite retirada do site maps.google.com (acesso em 29/04/2015).

2 Revisão do Estado da Arte

2.1 Litoestratigrafia

O termo Cordilheira Espinhaço foi atribuído por Eschwege (1822, *apud* Pflug, 1965) aos depósitos predominantemente quartzíticos que formam relevo acentuado que se estende na direção norte-sul, do centro do Estado de Minas Gerais até o norte da Bahia. A Serra do Espinhaço está subdividida em dois domínios fisiográficos: meridional e setentrional (Fig. 2; Saadi, 1995).

A Serra do Espinhaço compreende uma sucessão de rochas agrupadas da seguinte maneira, da base para o topo: Complexo Basal, Supergrupo Rio Paraúna, Supergrupo Espinhaço e Supergrupo São Francisco.

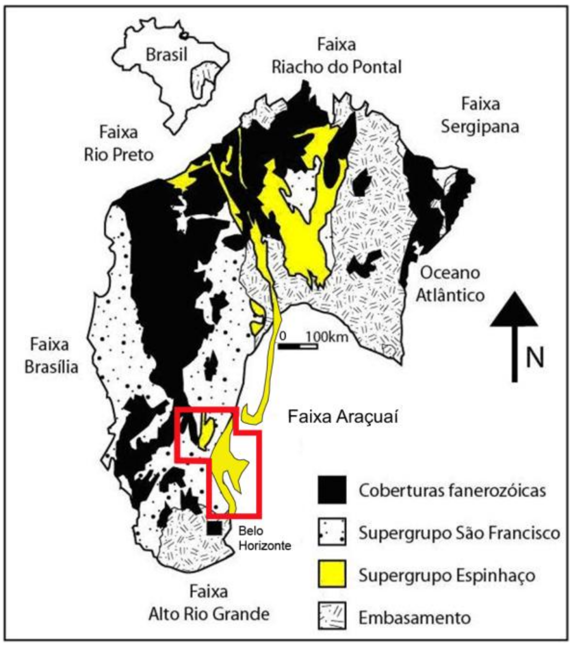

Figura 2 – Mapa de localização do Supergrupo Espinhaço com relação ao Cráton do São Francisco, com o quadrado vermelho destacando o Espinhaço Meridional (modificado de Alkmim *et al*., 1996).

Deve-se a Pflug (1968) a primeira divisão estratigráfica formal da Bacia Espinhaço Meridional. Ele a separou em oito formações: São João da Chapada, Sopa-Brumadinho, Galho do Miguel, Santa Rita, Córrego dos Borges, Córrego da Bandeira, Córrego Pereira e Rio Pardo Grande, da base para o topo, respectivamente. Schöll & Fogaça (1979) denominaram de Supergrupo Espinhaço as rochas quartzíticas abrangendo as oito formações supracitadas, em substituição a "Série Minas", termo utilizado por Pflug (1965), por correlacionar as rochas adjacentes a Diamantina com as rochas metassedimentares do Quadrilátero Ferrífero. Dossin *et al*. (1984) agruparam as oito formações em duas unidades hierarquicamente superiores, com base nos sistemas deposicionais e no contexto de evolução da bacia, Grupo Diamantina, incluindo as três primeiras formações e Grupo Conselheiro Mata, incluindo as cinco últimas formações. A Formação Bandeirinha foi posteriormente incluída à base da bacia, principalmente devido à presença de grãos de zircão formados no Período Estateriano (Fig. 3; Almeida-Abreu, 1993; Chemale *et al*., 2012; Santos *et al*., 2013).

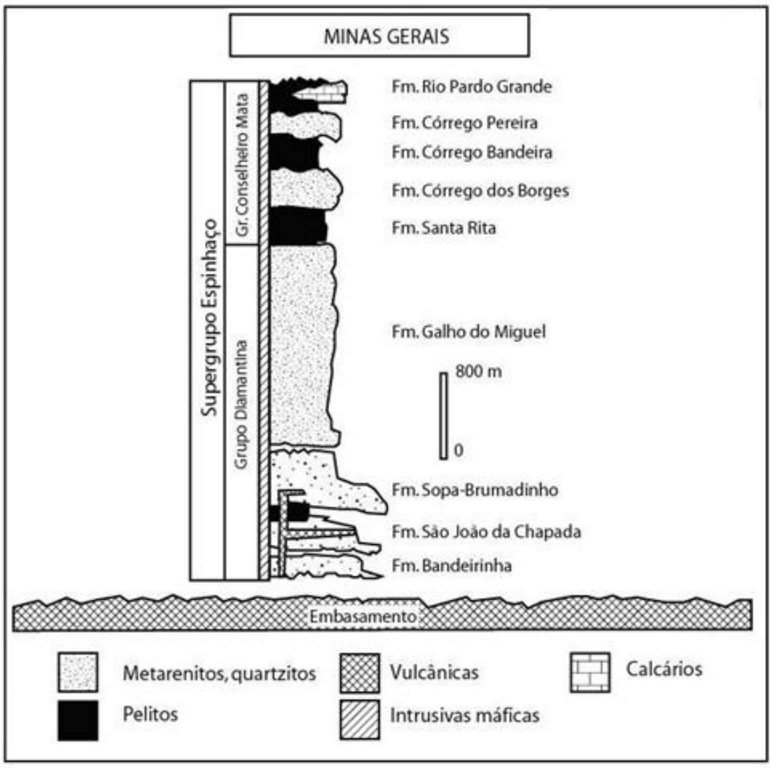

Figura 3 – Coluna estratigráfica esquemática simplificada do Supergrupo Espinhaço em Minas Gerais (modificado de Alkmim *et al.*,1996).

2.1.1 Complexo Basal

O Complexo Basal corresponde às porções inferiores do embasamento arqueano (Fig. 4), denominado por Pflug (1965) de Supergrupo Pré-Minas e posteriormente de Supergrupo Pré-Rio das Velhas por Schöll & Fogaça (1979). O embasamento compreende rochas graníticas, gnáissicas e migmatíticas e, secundariamente, anfibolitos isolados que podem ser observados na região de Barão do Guaicuí. Segundo Pflug (1965), o Complexo Basal ocorre em áreas restritas, ou como mega-anticlinais com eixo de orientação norte-sul (*e.g.* Anticlinório de Gouveia), ou como escamas geradas por falhamentos reversos.

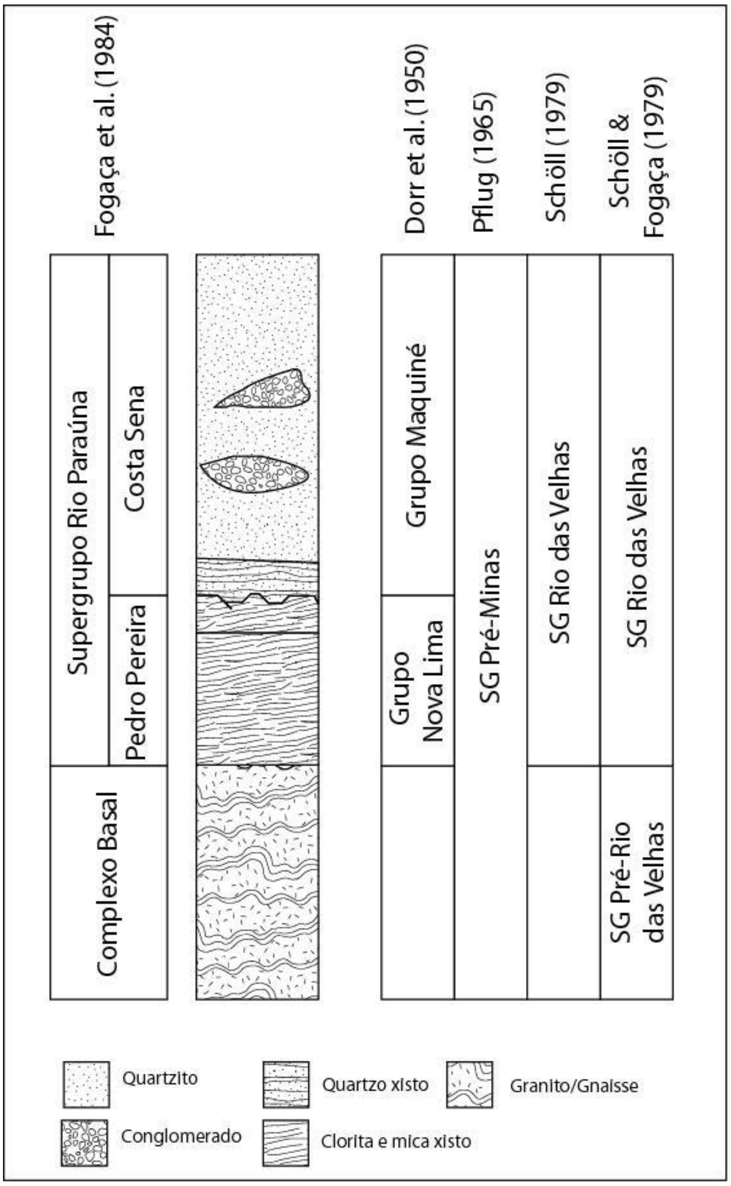

Figura 4 – Síntese da evolução da nomenclatura do embasamento da Bacia Espinhaço.

2.1.2 Supergrupo Rio Paraúna

Dorr *et al.* (1950 *apud* Schöll & Fogaça, 1979) identificaram duas unidades litoestratigraficamente correlacionáveis ao Quadrilátero Ferrífero, denominando-as de Grupo Nova Lima e Grupo Maquiné. Trabalhando na região de Gouveia, Hoffman (1978 *apud* Schöll & Fogaça, 1979), concluiu que as rochas graníticas do Complexo Basal formaram-se a temperaturas mais altas do que os xistos sobrepostos, permitindo clara individualização entre o Complexo Basal e a Série Pré-Minas. Posteriormente, Schöll (1979) atribuiu o nome Supergrupo Rio das Velhas em substituição ao termo Série Pré-Minas, mantendo em uso os grupos Nova Lima e Maquiné.

A atual nomenclatura, inserida por Fogaça *et al.* (1984), utiliza o termo Supergrupo Rio Paraúna e sua subdivisão nos grupos Pedro Pereira e Costa Sena, da base para o topo. Adicionalmente, no contato entre o Complexo Basal e o Supergrupo Rio Paraúna, é possível identificar seu caráter tectônico, cujas rochas geralmente encontram-se cisalhadas (Schöll & Fogaça, 1979), corroborando a separação proposta por Hoffman (1978 *apud* Schöll & Fogaça, 1979).

2.1.2.1 Grupo Pedro Pereira

O Grupo Pedro Pereira corresponde à unidade inferior do Supergrupo Rio Paraúna. Constituída por uma associação de clorita xistos e mica xistos com xistosidade para NNW, ocorrendo principalmente nas bordas N e NE do "Granito de Gouveia" (Schöll & Fogaça, 1979). Datações pelo método U/Pb em grãos de zircão realizadas por Chaves (2013) em uma rocha vulcânica que era mapeada como pertencente ao Grupo Pedro Pereira nessa região, no entanto, forneceram a idade de 1.16 Ga, indicando que o mapeamento ou o posicionamento estratigráfico dessa unidade precisa ser revista. Segundo Chaves (2013), a rocha datada representa o registro do vulcanismo que ocorrera durante o momento da deposição da Formação Sopa-Brumadinho.

2.1.2.2 Grupo Costa Sena

O Grupo Costa Sena, por sua vez, corresponde à unidade superior e menos espessa do Supergrupo Rio Paraúna. Esse grupo foi subdividido por Schöll & Fogaça (1979) em duas unidades distintas: a Formação Barão do Guaicuí, composta essencialmente por quartzo-mica xistos com cianita e a Formação Bandeirinha. Esta, no entanto, foi recentemente considerada como pertencente à Bacia Espinhaço (Chemale *et al.*, 2012; Santos *et al.*, 2013), tendo em vista que apresenta grãos de zircão datados em 1785 Ma, valor que representa a idade máxima dessa unidade. Por conseguinte, a

Formação Bandeirinha foi considerada como o registro do primeiro pulso de rifteamento da Bacia Espinhaço (Almeida-Abreu, 1993; Santos *et al.*, 2013).

2.1.3 A Sequência Espinhaço Inferior

Chemale *et al.* (2010) obtiveram a idade de 1.180 Ma para a matriz tufácea de um conglomerado pertencente à Formação Sopa-Brumadinho, na região de Extração, possibilitando a separação da bacia em duas sequências, uma estateriana e outra esteniana (*i.e.*, Sequência Espinhaço Inferior e Superior). A revisão da subdivisão litoestratigráfica do Supergrupo Espinhaço, aqui apresentada, leva em consideração as propostas de Pflug (1968), Dossin *et al*., (1984) e de Almeida-Abreu (1993), adaptadas conforme os dados recentes obtidos por Chemale *et al.* (2012) e Santos *et al*. (2013).

A sedimentação da Sequência Espinhaço inferior evoluiu em dois estágios de rifteamento distintos. A primeira fase condicionou a deposição da Formação Bandeirinha, enquanto que a Formação São João da Chapada representa o registro da segunda fase (Almeida-Abreu, 1993, 1995; Santos *et al*., 2013).

Durante a primeira fase de extensão mecânica, responsável pela abertura da bacia, as falhas normais de pequeno porte geradas resultaram na implantação de sistemas deposicionais característicos dessa fase (*i.e.*, predominando depósitos de canais de sistemas fluviais entrelaçados com padrão axial), ocupando áreas pequenas e desconexas (Silva, 1998; Santos *et al*., 2013). Com a evolução do rifte na segunda fase extensional, ou seja, com o aumento na taxa de extensão e subsidência, teria ocorrido a geração de atividade magmática por descompressão astenosférica (Dussin & Dussin, 1995) e a propagação das falhas anteriormente geradas, de grande importância para a ampliação da área de sedimentação e para o pleno desenvolvimento dos sistemas deposicionais.

A seguir são descritas as unidades litoestratigráficas já consagradas na Sequência Espinhaço inferior.

2.1.3.1 Formação Bandeirinha

A Formação Bandeirinha aflora a sudoeste de Diamantina de maneira restrita em relação à área, sendo composta por quartzitos finos de coloração rosada e lentes de metaconglomerados, perfazendo cerca de 200 m de espessura (Santos *et al.*, 2013). As estruturas sedimentares encontradas nos quartzitos incluem a estratificação plano-paralela, que é predominante, estratificações cruzadas acanaladas e cruzadas planares de pequeno porte. Os quartzitos localizados na base da formação geralmente apresentam cianita. Os coglomerados ocorrem de forma subordinada, possuem geometria lenticular, são maciços e suportados tanto pela matriz arenosa, quanto pelos clastos. Três sistemas deposicionais principais são reconhecidos para a Formação Bandeirinha: fluvial entrelaçado, leques aluviais e eólico.

A unidade tem sido alvo de muitas polêmicas quanto ao seu posicionamento estratigráfico (Espinhaço ou pré-Espinhaço?), sendo considerada por Almeida-Abreu (1993) e parte dos trabalhos subsequêntes (Silva, 1995; Alkmim *et al.*, 1996; Martins-Neto, 1998), como unidade integrante da Bacia Espinhaço. Os dados geocronológicos obtidos em zircão detrítico por Chemale *et al.*, (2012) e Santos *et al.* (2013) corroboram a inclusão da Formação Bandeirinha no Supergrupo Espinhaço.

2.1.3.2 Formação São João da Chapada

A Formação São João da Chapada é litologicamente caracterizada por quartzitos, ora puros, ora micáceos, com granulometria variável, que conferem a essa porção da Serra do Espinhaço aspectos geomorfológicos distintos, resultado de erosão diferencial, o que permitiu uma separação dessa formação em unidades hierarquicamente inferiores.

Schöll & Fogaça (1979) e Schöll (1979) separaram a Formação São João da Chapada em três níveis litoestratigráficos informais, designados pelas letras A, B e C, da base para o topo, respectivamente, conforme as rochas envolvidas. Recentemente o nível D foi incorporado à Formação São João da Chapada (Santos *et al.*, 2013).

Nível A – Composto essencialmente por quartzitos mal selecionados. Ocorrem de forma subordinada metabrechas com clastos de quartzitos angulosos, que passam a quartzitos tanto lateral, quanto verticalmente.

Nível B – Composto por filito hematítico, clorita xisto e rochas essencialmente a base de cloritóide. O filito hematítico apresenta predominância de sericita e hematita, além de agregados de turmalina em arranjo radial. A origem do filito hematítico também é alvo de controvérsias. Origem vulcânica de filiação alcalina potássica, com alteração metamórfica (Dussin, 1994) ou intempérica (Knauer & Schrank, 1994) são propostas. Segundo Cabral *et al*. (2012) a geoquímica das turmalinas presentes no filito hematítico reflete a alteração metassomática de rochas basálticas ou riolíticas a partir de soluções formadas pelo metamorfismo de evaporitos não marinhos. Datação Pb/Pb em zircão dos filitos hematíticos forneceu a idade de 1.710 Ma (Dossin *et al.*,1993), indicando uma idade aproximada do inicio da sedimentação do Supergrupo Espinhaço.

Nível C – Caracterizado pela preponderância de quartzitos de granulação média a grossa sobre filitos e quarzitos finos micáceos. Estrutura maciça e estratificações cruzadas tabulares são comuns (Schöll & Turinsky, 1979 *apud* Schöll & Fogaça, 1979). As espessuras desse nível geralmente perfazem 100 m, podendo chegar a 185 m (Pflug, 1968; Schöll & Fogaça, 1979).

Nível D – Denominado de Membro Datas por Almeida-Abreu (1993). A unidade é formada por filitos, filitos quartzosos e quartzitos micáceos, cuja espessura pode atingir até 35 m (Schöll & Fogaça, 1979). Do ponto de vista geomorfológico, seus afloramentos tendem a formar áreas mais deprimidas em virtude da relativamente baixa resistência à erosão, dada pela predominância de muscovita e de clorita.

2.1.4 Sequência Espinhaço Superior

Os depósitos sedimentares da Formação Sopa-Brumadinho representam o registro de um novo rifteamento e formação de uma nova bacia no mesmo lócus deposicional da Sequência Espinhaço inferior. Essa unidade é sucedida pela Formação Galho do Miguel e pelas unidades do Grupo Conselheiro Mata, que registram a implantação de sistemas deposicionais costeiros caracterizados por frequentes incursões marinhas e extrapolação da área de sedimentação para além dos limites do rifte (Martins-Neto, 1998). A seguir são apresentadas as descrições das unidades litoestratigráficas da Sequência Espinhaço superior.

2.1.4.1 Formação Sopa-Brumadinho

É a unidade sedimentar mais estudada na Serra do Espinhaço em virtude da presença de diamantes em metaconglomerados. A denominação de Formação Sopa advém de longa data (Moraes & Guimarães, 1930 *apud* Schöll & Fogaça, 1979), cujos metaconglomerados eram correlacionados com os metadiamictitos da Formação Macaúbas e considerados igualmente de origem glacial.

Denominada por Pflug (1968) como Formação Sopa-Brumadinho, aflora principalmente na região de Sopa, Guinda e Curralinho, distritos de Diamantina (Dossin et al., 1984; Alvarenga, 1982). Foi posteriormente subdividida por Schöll & Fogaça (1979) e Schöll (1979) em três níveis litoestratigráficos informais designados pelas letras D, E e F, em virtude de critérios observados em campo. Estudos de detalhe, no entanto, resultaram no reposicionamento dos filitos do nível D no topo da Formação São João da Chapada (Santos *et al.*, 2013).

Nível E – Constituído por quartzitos de granulometria grossa, com grande quantidade de óxidos de ferro em alguns setores, e por metaconglomerados polimíticos suportados pela matriz, intercalados com quartzitos. Os referidos metaconglomerados são localmente portadores de diamantes e apresentam clastos variados, como quartzo leitoso, quartzitos, filitos, ígneas ácidas e de metaconglomerados (Schöll & Fogaça, 1979). O Nível E foi posteriormente denominado de Membro Caldeirões (Almeida-Abreu, 1993).

Nível F – Formado por filitos, metassiltitos e intercalações de metabrecha diamantífera de matriz filítica, com clastos predominantemente de quartzitos. A metabrecha grada verticalmente para quartzitos micáceos e quartzitos finos (Schöll & Fogaça, 1979). Almeida-Abreu (1993) sugeriu o termo Membro Campo Sampaio para esse nível.

2.1.4.2 Formação Galho do Miguel

A Formação Galho do Miguel é composta predominantemente por quartzitos finos puros com estruturas sedimentares bem preservadas, tais como estratificações cruzadas acanaladas de grande porte. Secundariamente, é composta por quartzitos finos micáceos e finas camadas de metargilito. Os quartzitos atingem espessuras da ordem de 500 m nas proximidades de Gouveia até prováveis 2.000 m em direção ao norte (Schöll & Fogaça, 1979). O conjunto das características deposicionais indica um sistema eólico para a Formação Galho do Miguel (Dossin *et al*., 1987; Garcia & Uhlein, 1987).

2.1.4.3 Grupo Conselheiro Mata

O Grupo Conselheiro Mata compreende as formações Santa Rita, Córrego dos Borges, Córrego da Bandeira, Córrego Pereira e Rio Pardo Grande, da base para o topo, respectivamente (Dossin *et al*., 1984). Esse grupo inclui sedimentos pelíticos e arenosos alternados, representando três ciclos deposicionais caracterizados por bases transgressivas e topos regressivos (Dupont, 1995; Martins-Neto, 2007). Descrição detalhada das fácies do Grupo Conselheiro Mata é apresentada no Capítulo II.

2.1.4.4 Suíte Intrusiva Pedro Lessa

Compreende as rochas toleíticas subalcalinas máficas, metamorfizadas a baixo grau, que intrudem o Supergrupo Espinhaço e não intrudem o Supergrupo São Francisco (Uhlein *et al*., 1998). Machado *et al*. (1989) dataram grãos de badeleíta e zircão de um *sill* dessa unidade, que aflora na região de Pedro Lessa, obtendo a idade de 906 $\pm$ 2 Ma. Essa idade representa a idade mínima de deposição para o Supergrupo Espinhaço.

2.2 Geocronologia do Supergrupo Espinhaço e do Embasamento

Dados geocronológicos na Serra do Espinhaço Meridional são relativamente escassos. A seguir são apresentados os dados disponíveis:

- 2.971 ± 16 Ma para grãos de zircão de um metarriolito da região de Pedro Pereira, pertencente ao Supergrupo Rio Paraúna (Machado *et al.*,1989);
- 2,8 Ga pelo método U-Pb em zircão do Complexo Basal por Brito Neves *et al.* (1979) e Machado *et al.* (1989);
- 2.049 ± 3/-2 Ma para zircão de um metarriolito da região de Ouro Fino, pertencente ao Supergrupo Rio Paraúna (Machado *et al*.,1989);
- 1.730 Ma. Idade relacionada à abertura do rifte, conforme datações realizadas em um granito, pelo método U-Pb em zircão, que intrude o embasamento granito-gnáissico (Dossin *et al*., 1993);
- 1.770, 1.711 e 1.719 Ma pelo método U-Pb em metavulcânicas ácidas da região de Conceição do Mato Dentro e Serro, interpretadas como a base da sequência (Brito Neves *et al*., 1979; Machado *et al*., 1989);
- 1.710 Ma para o filito hematítico, datação obtida pelo método Pb/Pb em zircão (Dossin *et al*.,1993), nas proximidades do município de Diamantina, indicando uma idade aproximada do inicio da sedimentação no Supergrupo Espinhaço;
- 1.703 ± 16 Ma para o filito hematítico pelo método U-Pb (Chemale et al., 2012);
- 1.180 ± 16 Ma para a Formação Sopa-Brumadinho (Chemale *et al*., 2010);
- 906 ± 2 Ma pelo método U/Pb para as intrusivas máficas (*i.e.* Suíte Intrusiva Pedro Lessa) que cortam o Supergrupo Espinhaço, mas não cortam o Supergrupo São Francisco, datadas por Machado *et al.* (1989).

3 Metodologia empregada na aquisição dos dados de campo

3.1 Revisão Bibliográfica

O contato com diferentes interpretações, técnicas e pressupostos já empregados, forneceu o embasamento teórico necessário sobre a região, principalmente no que se refere à cobertura proterozóica: Bacia Espinhaço (alvo do estudo) e Bacia São Francisco; além do Cráton do São Francisco (embasamento) e dos cinturões orogênicos circundantes.

3.2 Análise Estrutural Prévia por Imagens de Satélite e Fotos Aéreas

A análise estrutural e estratigráfica preliminar da região foi realizada com o auxílio de imagens de satélite e fotografias aéreas (escala 1/25.000), com a posterior observação das feições no campo.

A observação de megaestruturas geológicas, no período que antecedeu e durante o trabalho de campo, foi de suma importância para a determinação de lineamentos e padrões estruturais e estratigráficos das unidades estudadas, permitindo a definição prévia dos locais a serem mapeados e a orientação preferencial para os levantamentos das seções estratigráficas.

O emprego de imagens de satélite a fim de analisar essas feições geológicas foi realizado por meio de uma série de composições coloridas geradas a partir de imagens multiespectrais do sensor *Landsat*, com resolução de 30 m, e do *Google Earth*, com resolução de 6 m.

3.3 Trabalho de Campo

A etapa de campo envolveu o mapeamento geológico na escala 1/25.000 realizado na região a leste de Conselheiro Mata, distrito de Diamantina. A etapa de campo foi realizada ao longo do ano de 2012, totalizando cerca de 120 dias.

O trabalho de campo envolveu a identificação e mapeamento das fácies sedimentares, medida de estruturas e coleta de amostras, utilizando equipamentos indispensáveis como GPS, bússola, marreta e trena (Fig. 5).

Figura 5 – Levantamento das seções utilizando uma trena.

3.4 Confecção dos Mapas Geológicos e das Seções Estratigráficas

A confecção dos mapas geológicos presentes no artigo envolveu os seguintes procedimentos:

(i) Delineação das feições estruturais a partir de imagens de satélite;

(ii) *Scannerização* do mapa em papel vegetal; e

(iv) Digitalização e georreferenciamento do mapa geológico por meio do *software* ArcGis 9.2.

Os mapas geológicos dos artigos estão no sistema geodésico *World Geodetic System* 1984 (WGS 84). As áreas mapeadas encontram-se no fuso 23 sul, cujo meridiano central é o -45°.

As seções estratigráficas foram digitalizadas no *software* Adobe Illustrator 10.

4 Referências

Alkmim F.F., Chemale Jr. F., Endo I. 1996. A deformação das coberturas proterozóicas do Cráton do São Francisco e o seu significado tectônico. Revista Escola de Minas 49, 22-38.

Almeida-Abreu, P.A., 1993. A Evolução Geodinâmica da Serra do Espinhaço Meridional, Minas Gerais, Brasil. Ph. D. Thesis, Univ. Freiburg, Freiburg, Germany, 150 pp.

Almeida-Abreu, P.A., 1995. O Supergrupo Espinhaço na Serra do Espinhaço Meridional, Minas Gerais: O rifte, a bacia e o orógeno. Geonomos 3, 1-18.

Brito Neves, B.B., Cordani, U.G., Kawashita, K., DelhalL, J., 1979. A evolução geocronológica da Cordilheira do Espinhaço; dados novos e integração. Rev Bras. Geociências 9, 71-85.

Cabral, A.R., Wiedenbeck, M., Koglin, N., Lehmann, B., Abreu, F.R., 2012. Boron-isotopic constraints on the petrogenesis of hematitic phyllite in the southern Serra do Espinhaço, Minas Gerais, Brazil. Lithos 140–141, 224–233.

Chaves, M.L.S., Silva, M.C.R., Scholz, R., Babinski, M., 2013. Grenvillian age magmatism in the Southern Espinhaço Range (Minas Gerais): evidence from U-Pb zircon ages. Braz. J. Geol. 43, 477–486.

Chemale Jr., F., Dussin, I.A., Martins, M.S., Alkmim, F.F., Queiroga, G., 2010. The Espinhaço Supergroup in Minas Gerais: a Stenian Basin? 7th South American Symposium on Isotope Geology, Brasília, pp. 552–555.

Chemale Jr., F., Dussin, I.A., Alkmim, F.F., Martins, M.S., Queiroga, G., Armstrong, R., Santos, M.N., 2012. Unravelling a Proterozoic basin history through detrital zircon geochronology: The case of the Espinhaço Supergroup, Minas Gerais, Brazil. Gondwana Research 22, 200-206.

Dossin, I.A., Uhlein, A., Dossin, T.M., 1984. Geologia da Faixa Móvel Espinhaço em sua porção meridional, MG. Congresso Brasileiro de Geologia, 33, Rio de Janeiro: Anais, Sociedade Brasileira de Geologia, 2, pp. 3118–3132.

Dossin, I.A., Garcia, A.J.V., Uhlein, A., Dardenne, M.A., Dossin, T.M., 1987. Fácies eólico na Formação Galho do Miguel. Supergrupo Espinhaço (MG). Simpósio sobre Sistemas Deposicionais no Pre-Cambriano, Ouro Preto: Atas, Sociedade Brasileira de Geologia, pp. 85–96.

Dossin, I.A., Dossin, T.N., Charvet, J., Cocherie, A., Rossi, P., 1993. Single-zircon dating by step-wise Pb-evaporation of Middle Proterozoic magmatismo in the Espinhaço range, southeastern São Francisco Craton. Minas Gerais, Brazil. Simpósio sobre o Cráton do São Francisco, 2, Salvador, 1993: Anais, Sociedade Brasileira de Geologia/Superintendência de Geologia e Recursos Minerais da Bahia, 1, pp. 39–42.

Dupont, H., 1995. O Grupo Conselheiro Mata no seu quadro paleogeográfico e estratigráfico. Simpósio de Geologia de Minas Gerais, Diamantina: Anais, Sociedade Brasileira de Geologia, 13, pp. 9–10.

Dussin, T.M., 1994. Associations plutono-volcaniques de l'"EspinhaçoMeridional (SE-Brésil): um exemple d'évolution de la croûte protérozoïque. Ph.D.Thesis, Orleans,Universited' Orleans, 177pp.

Dussin, I.A., Dussin, T.M., 1995. Supergrupo Espinhaço:modelo de evolução geodinâmica. Geonomos 3, 19–26.

Fogaça, A.C.C., Almeida-Abreu, P.A., Schorscher, H.D., 1984. Estratigrafia da sequência supracrustal arqueana na porção mediana central da Serra do Espinhaço – M.G. In: Congresso Brasileiro de Geologia, 33., Rio de Janeiro,SBG. Anais… p. 2652-2667.

Garcia, A.J.V., Uhlein, A., 1987. Sistemas deposicionais do Supergrupo Espinhaço na Região de Diamantina (MG). Simpósio sobre Sistemas Deposicionais no Pre-Cambriano, Ouro Preto: Atas, Sociedade Brasileira de Geologia, pp. 113–136.

Knauer, L.G., Schrank, A., 1994. A origem dos filitos hematíticos da Serra do Espinhaço Meridional, Minas Gerais. Geonomos 1, 33-38.

Machado, N., Schrank, A., Abreu, F.R., Knauer, L.G., Almeida-Abreu, P.A., 1989. Resultados preliminares da geocronologia U/Pb na Serra do Espinhaço Meridional. Boletim da Sociedade Brasileira de Geologia, Núcleo Minas Gerais, 10, pp. 171–174.

Martins-Neto, M.A., 1998. O Supergrupo Espinhaço em Minas Gerais: Registro de uma Bacia Rifte-Sag do Paleo/Mesoproterozóico. Revista Brasileira de Geociências 48, 151-168.

Martins-Neto, M.A., 2007. Sequence stratigraphic framework of Proterozoic successions in eastern Brazil. Marine and Petroleum Geology 26, 163-176.

Pflug, R. 1965. A Geologia da Parte Meridional da Serra do Espinhaço e Zonas Adjacentes, Minas Gerais. Boletim da Divisão de Geologia e Mineralogia do DNPM 226, 1-51.

Pflug, R., 1968. Observações sobre a estratigrafia da Série Minas na região de Diamantina, Minas Gerais. Boletim da Divisão de Geologia e Mineralogia do Departamento Nacional de Produção Mineral: Notas Preliminares 142 (20 pp.).

Saadi, A., 1995. A geomorfologia da Serra do Espinhaço em MinasGerais e de suas margens. Geonomos 3, 41–63.

Santos, M. N., Chemale Jr., F., Dussin, I.A., Martins, M.S., Assis, T.A.R., Jelinek, A. R., Guadagnin, F., Arsmtrong, R., 2013. Sedimentological and paleoenvironmental constraints of the Statherian and Stenian Espinhaço rift system, Brazil. Sedimentary Geology 290, 47-59.

Schöll W.U., 1979. Estratigrafia, sedimentologia e paleogeografia na região de Diamantina (Serra do Espinhaço, Minas Gerais, Brasil). Münster. Forsch. Geol. Palaont. 51, 223-240.

Schöll, W.U., Fogaça, A.C.C., 1979. Estratigrafia da Serra do Espinhaço na região de Diamantina. Simpósio de Geologia de Minas Gerais, Diamantina: Anais, Sociedade Brasileira de Geologia, pp. 55–73.

Silva, R.R., 1995. Contribution to the stratigraphy and paleogeography of the lower Espinhaço Supergroup (Mesoproterozoic) between Diamantina and Gouveia, Minas Gerais, Brazil. Ph. D. Thesis, Univ. Freiburg, Freiburg, Germany, Freiburger Geowiss. Beitr., 8, 115 pp.

Silva, R.R., 1998. As bacias proterozóicas do Espinhaço e São Francisco em Minas Gerais: uma abordagem do ponto de vista da estratigrafia de sequências. Geonomos 6, 1–12.

Uhlein, A., Trompette, R., Egydio-Silva,M., 1998. Proterozoic rifting and closure, SE border of the São Francisco Craton, Brazil. Journal of African Earth Sciences 11, 191–203.

CAPÍTULO II

Provenance and paleogeographic reconstruction of a Mesoproterozoic intracratonic sag basin (Upper Espinhaço Basin, Brazil)

M.N. Santos[1,2]*, F. Chemale Jr.[1], I.A. Dussin[3], M.S. Martins[4], G. Queiroga[4], R.T.R. Pinto[5], A.N. Santos[6], R. Armstrong[7]

1 – Programa de Pós-Graduação em Geologia, Instituto de Geociências, Universidade de Brasília, 70904-970, Brasília, DF, Brazil

2 – PETROBRAS/E&P-EXP, Avenida República do Chile, 330 – Centro, 20031-170, Rio de Janeiro, RJ, Brazil

3 – Faculdade de Geologia, Universidade do Estado do Rio de Janeiro, 20550-013, Rio de Janeiro, RJ, Brazil

4 – DEGEO/EM/UFOP, Morro do Cruzeiro, 35400-000, Ouro Preto, MG, Brazil

5 – Departamento de Geologia, Universidade Federal do Espírito Santo, 29500-000, Alegre, ES, Brazil

6 – Instituto de Geociências, Universidade Federal do Rio Grande do Sul, 91501-970, Porto Alegre, RS, Brazil

7 – RSES, ANU, Canberra, Australia

* Corresponding author at: PETROBRAS/E&P-EXP, Avenida República do Chile, 330 – Centro, 20031-170, Rio de Janeiro, RJ, Brazil.

Tel.: +55 38 9178 8699.

E-mail address: marcelodega@hotmail.com (M. Santos).

Received 22 September 2014, Revised 23 December 2014, Accepted 23 December 2014, Available online 30 December 2014 (doi:10.1016/j.sedgeo.2014.12.006).

Abstract

The Mesoproterozoic Conselheiro Mata Group is the uppermost sequence of the Proterozoic intracontinental Espinhaço basin that developed on the Congo-São Francisco Paleoplate. This sequence is represented by a marine shallow-water platform that experienced a sag phase followed by a rift phase in the Upper Espinhaço. We used combined sedimentological-stratigraphic descriptions of sections, whole-rock (WR) geochemistry and U-Pb detrital zircon dating to develop a regional paleogeographic evolution model of the sag phase. The succession corresponds to transgressive-regressive cycles in the following ascending order: 1) offshore to lower shoreface facies represented by quiescent periods and episodic sediment supply (Santa Rita Formation); 2) upper shoreface to foreshore and coastal desert facies with a reworking of the underlying units (Córrego dos Borges Formation); 3) lower shoreface with fallout of suspended fine sediments and a combination of unidirectional and oscillatory flows generated by storm waves (Córrego da Bandeira Formation); 4) tidal-influenced upper shoreface to foreshore facies with the migration of subaqueous dunes, wave swash in a beach environment and cycles of neap-spring tides (Córrego Pereira Formation); and 5) the resumption of lower-shoreface sedimentation and the subsequent development of a stromatolitic carbonate-siliciclastic platform (Rio Pardo Grande Formation). The geochemical data indicate that the studied units contain input from felsic rocks and sedimentary rocks. The basal marine to eolian sediments of the Galho do Miguel Formation are dominated by Rhyacian sources (2.1 Ga). The basal and intermediate units of the Conselheiro Group contain Archean, Rhyacian, Statherian and Calymmian-Ectasian (1.6-1.33 Ga) zircon grains, whereas Orosirian (1.9-2.0 Ga) sources dominate in the upper strata of the group. The study of this Stenian (Mesoproterozoic) intracratonic sequence provides clues to understanding the history of sedimentation and the potential source areas on the São Francisco Craton and adjacent areas, which are very useful for comparison to Phanerozoic intracratonic basins and the reconstruction of Paleoproterozoic and Mesoproterozoic supercontinents.

Keywords: Stenian; Espinhaço Basin; U-Pb zircon geochronology; São Francisco Craton.

1 Introduction

Intracratonic basins are located on stable continental lithosphere comprising several basin phases or megasequences with preserved continental to shallow-water marine deposits separated by regional unconformities (e.g., Sloss, 1963; Lindsay, 2002; Allen and Armitage, 2012). The study of Precambrian cratonic basins, which are similar to Phanerozoic basins, can provide important information on the paleogeography and distribution of continents and the evolution of supercontinents (e.g., Lindsay, 2002) and can elucidate the composition and paleodrainage dispersion of basement rocks. The spatial and temporal evolution of depositional systems in intracratonic rift and rift-sag basins depends on a complex relationship between sediment supply, eustatic variations, climate and tectonic processes at the time of deposition (Bosence, 1998; Bergner et al., 2009; Allen and Armitage, 2012). Hence, different models of tectonic evolution imply different models of the distribution and evolution of depositional systems (Prosser, 1993; Gawthorpe and Leeder, 2000), although the latter are a direct result of the particularities of each basin and data available for analysis (e.g., seismic data versus well logs or outcrop observations; Catuneanu et al., 2009). Nevertheless, there are many similarities among depositional systems in most rift basins, such as fluvial and alluvial fans that developed during a syn-rift stage (Prosser, 1993; Gawthorpe and Leeder, 2000) or marine depositional environments during a basinal sag phase (e.g., Porcupine Basin; Tate, 1993), similar to the conditions observed in the intracratonic Espinhaço Basin, eastern Brazil.

The southern Espinhaço Basin has been widely interpreted as an intracontinental rift-sag basin that developed on the Paleoproterozoic Congo-São Francisco Paleoplate (e.g., Martins-Neto, 1998; Alkmim and Martins-Neto, 2012; Chemale et al., 2012) and on the Neoproterozoic to Eopaleozoic deformed Araçuai Belt along the margin of the São Francisco Craton (Marshak and Alkmim, 1989; Chemale et al., 1993). According to Chemale et al. (2012), the Espinhaço Supergroup in Minas Gerais comprises metasedimentary units that record two distinct rift phases separated by a gap of 500 Ma (i.e., a rift phase started at 1.7 Ga and a rift-sag phase started at approximately 1.2 Ga), named the Lower and Upper Espinhaço Sequences. The sag phase of the

Upper Sequence corresponds to the Conselheiro Group, which is characterized by a marine incursion over eolian sediments (Dupont, 1995; Martins-Neto, 2000).

This paper focuses on the evolution of the depositional systems and sediment provenance during the sag phase of the Conselheiro Mata Group by applying concepts of sequence stratigraphy and detrital zircon U-Pb geochronology to propose a regional paleogeographic evolution model. The study of the marine sequence associated with the sag phase in the Espinhaço Basin enables a better understanding of the sedimentation history along the São Francisco Craton and how the successive transgression-regression events controlled the extent of the basin and basement exposed to subaerial processes, sediment supply and paleocurrent patterns.

2 Geological setting

The Espinhaço Basin forms part of a complex rift system that extends approximately north-south from Minas Gerais to Bahia in Brazil. The basin in the study area comprises the Serra do Cabral region, located in the São Francisco Craton, and the western portion of the southern Serra do Espinhaço in the Araçuaí Fold Belt (Pflug, 1968; Dussin and Dussin, 1995; Uhlein et al., 1998; Martins-Neto, 2000) (Fig. 1).

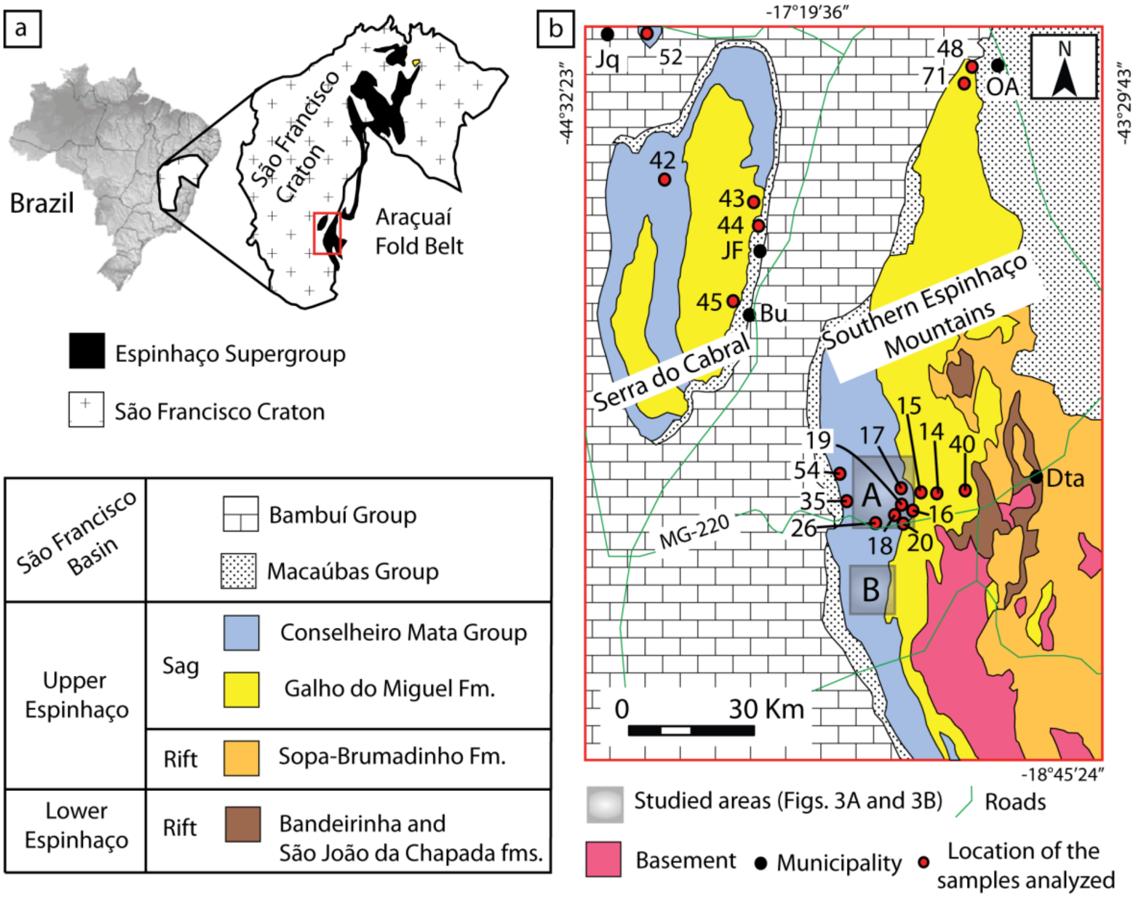

Fig. 1. Location (a) and simplified map (b) of the Espinhaço Basin in the southern Serra do Espinhaço and Serra do Cabral region, indicating the sampling sites of the dated samples and the two studied areas (Fig. 3a, 3b). Modified after Souza Filho (1995), Fogaça (1995) and Alkmim et al. (2006). Bu- Buenópolis; Dta- Diamantina; JF- Joaquim Felício; Jq- Jequitaí; OA- Olhos D'Água.

The São Francisco Craton is defined as one of the most stable parts of the South American Platform and was not involved in the Brasiliano Orogeny during the late Neoproterozoic (Alkmim, 2004). The transition from the eastern São Francisco Craton to the Araçuaí Fold Belt is marked by the deformation of the basin and the appearance of portions of basement reworked during the Brasiliano Orogeny with a clear vergence toward the craton (Marshak and Alkmim, 1989; Chemale et al., 1993; Dussin and Dussin, 1995; Uhlein et al., 1998). From a lithostratigraphic point of view, the Archean basement comprises the Basal Complex and the Rio Paraúna Supergroup. The Basal Complex includes granites (dated by U-Pb in zircon to 2938 ± 14 Ma; Machado et al., 1989), gneisses, amphibolites and migmatites (Schöll and Fogaça, 1979), whereas the Rio Paraúna Supergroup is composed mainly of schists and metavolcanic rocks (with zircon grains from a rhyolite dated to 2971 ± 16 Ma; Machado et al., 1989).

Recent geochronological data and detailed sedimentological–stratigraphic studies applying sequence stratigraphy have revealed three second-order depositional sequences (*sensu* Krapez, 1996) for the Espinhaço Supergroup deposits—the Lower, Middle and Upper Espinhaço (Chemale et al., 2012). The record of the Middle Espinhaço is preserved in the physiographic regions of the northern Serra do Espinhaço and Chapada Diamantina (Guadagnin et al., 2015). The absence of this sequence in the southern Serra do Espinhaço indicates either erosion or non-deposition; the latter hypothesis assumes that the region remained a topographic high during this period (Chemale et al., 2012).

The Lower Espinhaço Basin (Fig. 1) developed during the Statherian taphrogenesis (Plumb, 1991; Brito Neves et al., 1995). Sedimentation evolved through two distinct rifting stages, which were responsible for the deposition of the Bandeirinha and São João da Chapada formations (Almeida-Abreu, 1993; Santos et al., 2013). The magmatic events of the Lower Espinhaço Basin are represented by 1.77 to 1.73 Ga acidic alkaline volcanism and plutonism (Brito Neves et al., 1979; Dossin et al., 1993) and K-rich alkaline volcanics (hematite phyllite) dated to 1.71-1.70 Ga (Dossin et al., 1993; Chemale et al., 2012).

The opening of the Upper Espinhaço Basin occurred after 1.2 Ga. This age refers to volcanic zircon grains from the green clay matrix (tuffaceous contribution) of a diamond-bearing conglomerate in the Sopa-Brumadinho Formation (Fig. 2) and marks the time of deposition of this unit during the rift stage of the basin’s development (Chemale et al., 2010, 2012). The deposition of the eolian and marine sediments of the Galho do Miguel Formation (Figs. 1, 2) marks an expansion in the area of this basin based on an extrapolation of the limits of the rift and the subsequent transition from mechanical to thermal subsidence (Martins-Neto, 1998). The subsequent sediments represent three marine transgression-regression cycles of the Conselheiro Mata Group (Dossin et al., 1984; Dupont, 1995) (Fig. 2), which are marked by the intercalation of pelitic units (i.e., the Santa Rita, Córrego da Bandeira and Rio Pardo Grande formations) with sand units (i.e., the Córrego dos Borges and Córrego Pereira formations). Despite the large number of published papers that mention the Conselheiro Mata Group, questions regarding its sedimentary provenance and depositional environments remain due to a lack of quantitative analysis integrated with sedimentology.

The Espinhaço Supergroup is cut by basic dykes that have been dated to 0.9 Ga via the U-Pb method performed on crystals of baddeleyite and zircon (Machado et al., 1989) (Fig. 2). The Espinhaço rocks that are exposed along the southern Serra do Espinhaço were affected by the Neoproterozoic to Cambrian west-vergent fold-and-thrust Araçuaí Belt and experienced lower greenschist facies conditions (Chemale et al., 2012, and references therein).

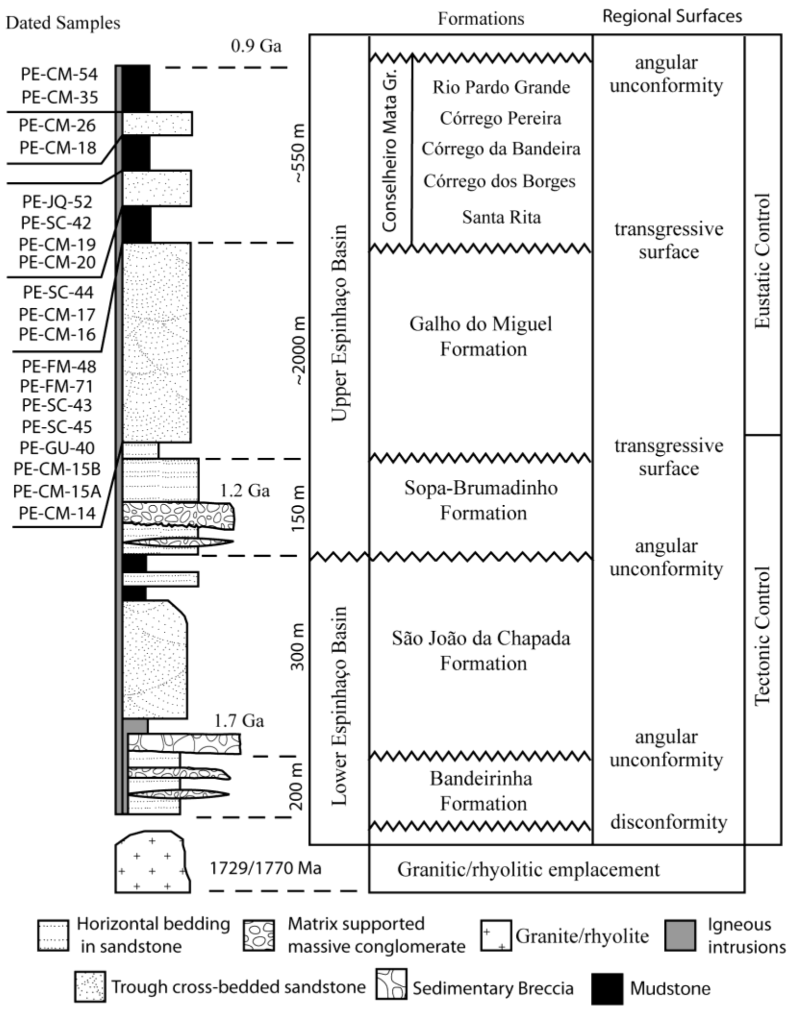

Fig. 2. Stratigraphic nomenclature for the Espinhaço Basin showing the location of the dated samples (after Santos et al., 2013). Not to scale.

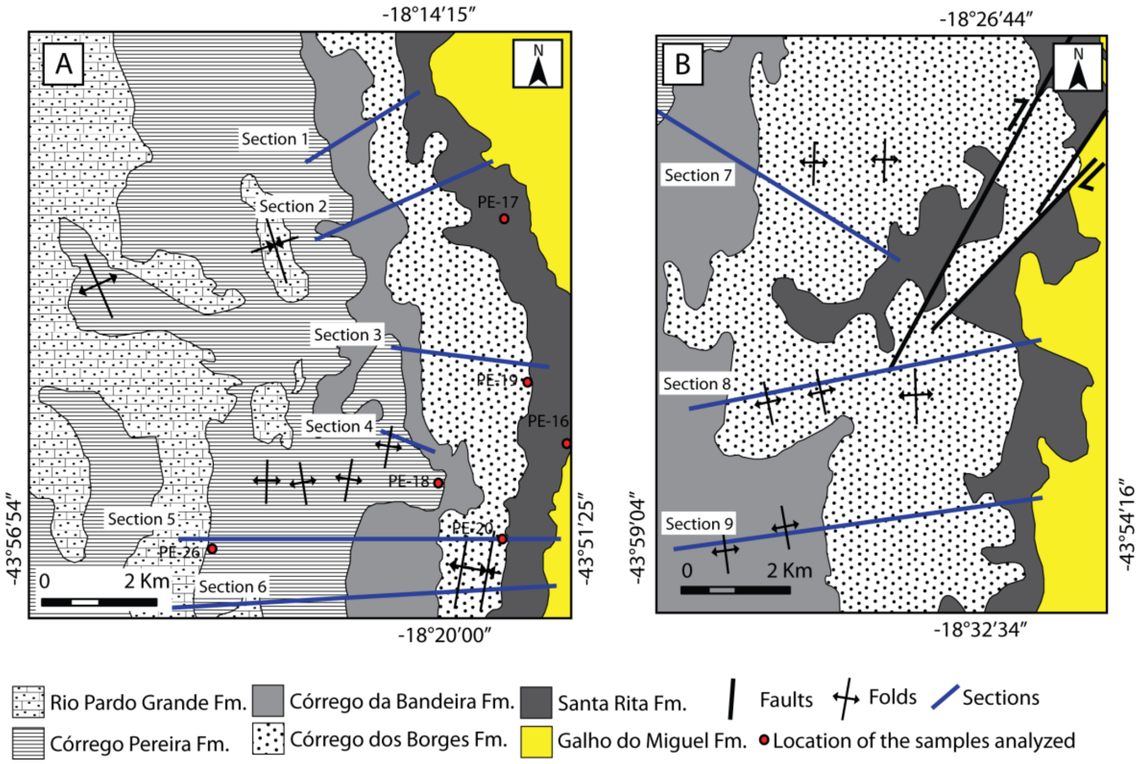

Fig. 3. Simplified geological maps of the Conselheiro Mata Group showing the locations of the dated samples (a) and stratigraphic sections in the southern Serra do Espinhaço (a and b). Location shown in Fig. 1.

3 Methods

For the development of this work, sedimentological and stratigraphic descriptions of sections in the Conselheiro Mata region were completed and complemented with geological mapping at a scale of 1:25,000 (Figs. 3a, 3b, 4) to investigate lateral facies variations. Stratigraphic sections were measured mainly with a Jacob's Staff. The sedimentary facies were recognized based on their texture, sedimentary structures, paleocurrent patterns, set geometry and lateral transitions. Several thin sections were made from the rocks collected along the measured sections to provide a more detailed account of the facies.

From the Galho do Miguel Formation and Conselheiro Mata Group, we analyzed twenty samples for geochemistry and nineteen samples for detrital zircon U-Pb geochronology and conducted a reinterpretation of seismic reflection data (from the Agência Nacional do Petróleo, Gás Natural e Biocombustíveis, previously published by Reis, 2011). The samples were collected in the southern Espinhaço Mountains (west of the Olhos D'Água municipality and along roadcuts of the MG-220 highway) on the eastern edge of the Serra do Cabral and east of the Jequitaí municipality (Fig. 1). We collected four samples of mature sandstones with large-scale tabular and trough cross-bedding (samples PE-CM-15A, PE-CM-15B, PE-SC-45 and PE-FM-48) and four with low-angle cross-bedding (samples PE-CM-14, PE-GO-40, PE-SC-43 and PE-FM-71) from the Galho do Miguel Formation. Two samples of pelite (PE-CM-16 and PE-SE-44) and a fine-grained sandstone sample (PE-CM-17) were collected from the Santa Rita Formation. Sandstone samples were also collected from the Córrego Borges (PE-CM-19, PE-CM-20, PE-SC-42 and PE-JQ-52), Córrego Pereira (PE-CM-18 and PE-CM-26) and Rio Pardo Grande (PE-CM-35 and PE-CM-54) formations.

The rock samples were crushed and milled using a jaw crusher. Zircon populations were separated by conventional procedures using hand-panning, a Frantz Isodynamic Magnetic Separator, heavy liquids and sorting by hand under a binocular lens. The zircon grains were photographed in transmitted and reflected light, imaged using BSE (backscattered electrons) and CL (cathodoluminescence), and dated using a laser ablation microprobe (New Wave UP213) coupled to a MC-ICP-MS (Neptune) at the isotope laboratories of the universities of Brasília and Rio Grande do Sul (Brazil). Isotope data were acquired in static mode with spot sizes of 25 and 40 μm. Laser-induced elemental fractionation and instrumental mass discrimination were corrected using a reference zircon (GJ-1; Jackson et al., 2004). Two GJ-1 analyses were measured after every ten sample zircon spots. To evaluate the accuracy and precision of the laser-ablation results, we analyzed an internal standard, PAD1, and Temora 2. The external error was calculated based on the propagation error of the GJ-1 mean and the individual sample zircons (or spots). The reproducibility obtained from GJ-1 was 0.6% for the $^{207}Pb/^{206}Pb$ ratio and 0.9% for the $^{206}Pb/^{238}U$ ratio. Details of the analytical procedures can be found in Chemale et al. (2011).

U-Pb SHRIMP (Sensitive High-Resolution Ion Microprobe) zircon geochronology was performed at the Research School of Earth Sciences, Australian National University, using SHRIMP II equipment. The zircon grains were analyzed with a 2-3 nA, 10 kV primary O2 beam focused to a ~25 to ~20 μm diameter spot. At a mass resolution of ~5500, the Pb, Th and U isotopes were resolved from all major interferences. The U and Th concentrations were determined relative to those measured in the RSES standard SL13. Histograms were prepared with Isoplot/Ex (Ludwig, 2003). For the detrital zircon histogram, we used zircon data with discordance equal to or less than 10%.

4 Results

4.1 Facies Association

Because the Conselheiro Mata Group is a Mesoproterozoic sequence affected by low-grade metamorphism and deformation during the Brasiliano Orogeny (Dussin, 1994), the metasedimentary facies are described with sedimentary nomenclature for practical purposes (Table 1).

The facies associations in the Conselheiro Mata Group were observed in the vicinity of the Conselheiro Mata district belonging to the Diamantina municipality (i.e., where the type sections were defined) and in the Serra do Cabral between Joaquim Felício and Buenópolis. These sites feature excellent and continuous outcrops and allow for the study of lateral and vertical variations in the sedimentary facies. The facies were grouped into six facies associations.

4.1.1 Facies Association 1 (FA 1): offshore to lower shoreface

Description

FA 1 is mainly composed of laminated and massive siltstones and mudstones with a light-gray color that becomes reddish and even yellow when weathered (Table 1). The pelites are primarily composed of sericite and quartz. Magnetite crystals altered to martite occur sparsely, as observed by Fogaça (1995). Toward the top of FA 1, siltstones are interbedded with tabular sand beds of centimeter-scale thicknesses (<10 cm thick in Conselheiro Mata and <50 cm in the Serra do Cabral). The sandstones are beige, fine- to very fine-grained, well-sorted, subrounded, composed of quartz with some mica and feldspar, and exhibit wave ripples and gradational contacts at the top and bottom. The presence of hummocky cross-stratification in the sandstones of the

Santa Rita Formation has been described in the southern Serra do Espinhaço (Dossin et al., 1990). Toward the top of FA 1, small sand dykes were observed in the siltstones at the top of the Santa Rita Formation (Schöll and Fogaça, 1979).

Interpretation

FA 1 records an upward increase in the energy and frequency of sediment deposition based on the upward-coarsening grain size coupled with increasing sandstone interbeds. The basal portions of FA 1, which consist essentially of horizontal, planar-laminated pelites, indicate low-energy deposition, interpreted as the fallout of suspended fine material deposited during fair-weather periods, most likely below the storm wave base, which is typical of offshore conditions (Clifton, 2006). At the top of FA 1, the appearance of sand beds (Fig. 4) marks the transition from offshore to lower shoreface conditions. The increased quantity of sandstones toward the top of FA 1 may indicate that storm waves removed sand from the proximal portions of the basin due to a relative sea-level fall (i.e., deposition above the storm wave base). The injection of sand dykes into the pelites in FA 1 most likely resulted from liquefaction during seismic events (Schöll and Walde, 1980; Fernandes et al., 2007). This interpretation is corroborated by the deposition of intraformational breccias and synsedimentary deformation structures (FA 2) above the pelitic facies.

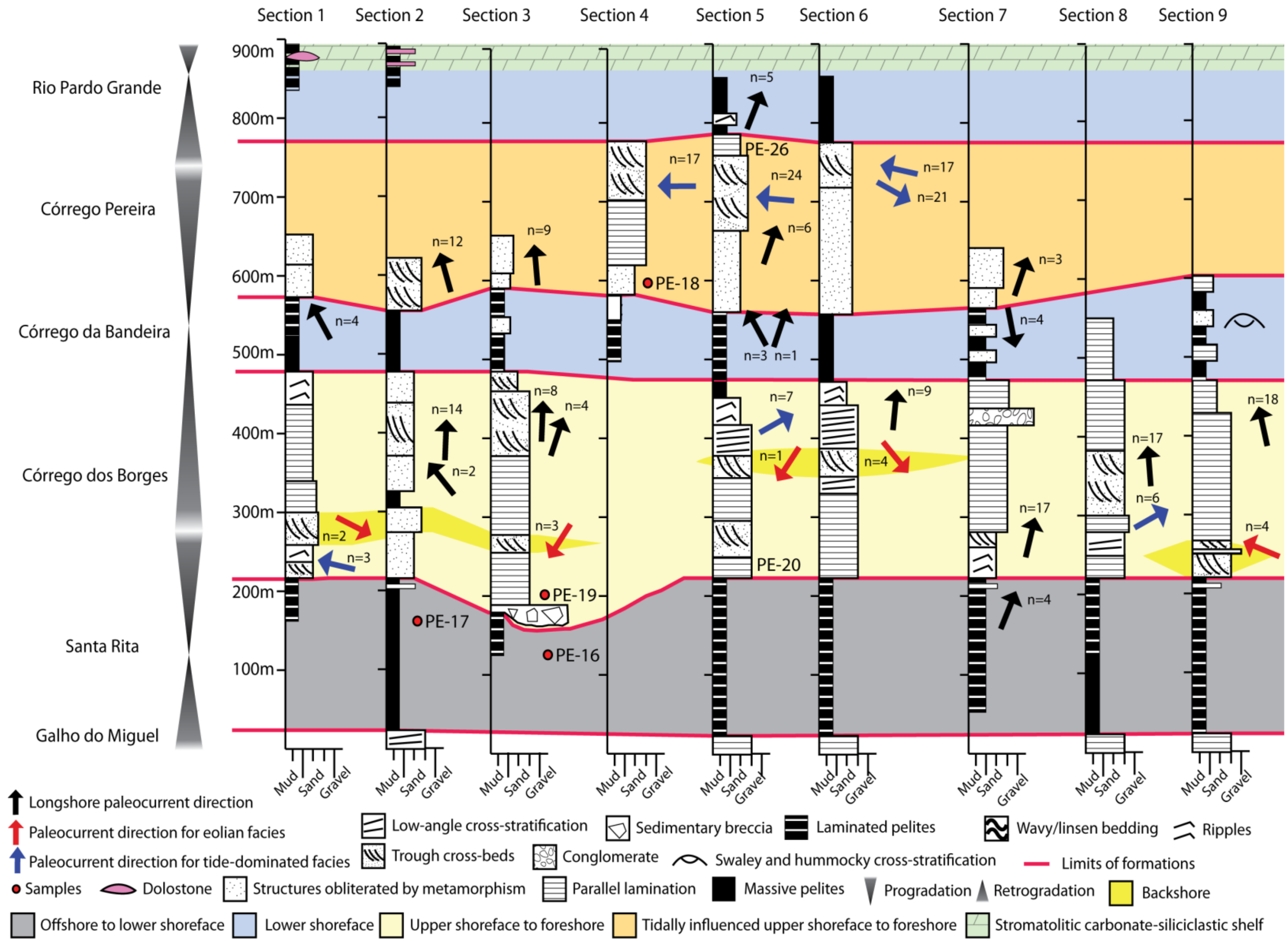

Section 1
Section 2
Section 3
Section 4
Section 5
Section 6
Section 7
Section 8
Section 9
900m
800m
700m
600m
500m
400m
300m
200m
100m
Rio Pardo Grande
Córrego Pereira
Córrego da Bandeira
Córrego dos Borges
Santa Rita
Galho do Miguel
PE-26
PE-18
PE-20
PE-19
PE-17
PE-16
Mud
Sand
Gravel
Longshore paleocurrent direction
Paleocurrent direction for eolian facies
Paleocurrent direction for tide-dominated facies
Samples
Dolostone
Structures obliterated by metamorphism
Low-angle cross-stratification
Trough cross-beds
Parallel lamination
Sedimentary breccia
Conglomerate
Laminated pelites
Massive pelites
Swaley and hummocky cross-stratification
Wavy/linsen bedding
Ripples
Limits of formations
Progradation
Retrogradation
Backshore
Offshore to lower shoreface
Lower shoreface
Upper shoreface to foreshore
Tidally influenced upper shoreface to foreshore
Stromatolitic carbonate-siliciclastic shelf

Fig. 4. Correlation of the measured sections in the Conselheiro Mata region. Location shown in Fig. 3. Arrows indicate the mean paleocurrent direction (up: north; down: south).

4.1.2 Facies Association 2 (FA 2): upper shoreface to foreshore

Description

The pelites of FA 1 transition gradually into an interval composed mainly of plane-parallel-stratified sandstone, which is designated Facies Association 2 (Table 1). FA 2 is composed of sandstones, conglomerates and massive sedimentary breccias. The sandstones are white and beige; their composition ranges from pure quartz to arkosic and micaceous, and they contain rare dispersed magnetite crystals that have altered to martite. The mineral grains are fine- to medium-grained, moderately to well sorted and subrounded sand. Horizontal planar stratification predominates, but symmetrical and asymmetrical ripples (Fig. 5a), low-angle cross-bedding and small- to medium-scale tabular and trough cross-bedding occur secondarily, indicating a predominantly north-south paleoflow (Fig. 7). Evidence for synsedimentary deformation is seen in folded and faulted foresets (Fig. 5b, 5c), where the deformed horizons can reach 1 m in thickness. The sedimentary breccias of FA 2 have abrupt lateral and vertical contacts with the surrounding sandstone, reach up to 10 m thick, and are massive and clast-supported, with variably sized angular clasts of laminated white sandstones ranging from cobbles to boulders. The monomictic nature of the sedimentary breccias has been observed by Fogaça (1995), who also identified features of erosive channels. The rare conglomerate bodies have lenticular geometries, can reach thicknesses of up to 3 m, and are massive or normally graded and clast supported, with rounded cobbles of sandstone (Fig. 5d).

Table 1 - Description and interpretation of sedimentary facies of the Conselheiro Mata Group.

		Description	Interpretation	Formation
Facies Association 1	offshore to lower shoreface	Laminated and massive siltstone/mudstone composed primarily of quartz and sericite.	These pelite beds represent fallout of suspended fine sediments in an offshore environment.	Santa Rita
		Fine- to very fine-grained sandstone with wave ripples and gradational contacts at the top and bottom. Small sand dykes in pelites toward the top of FA 1.	Deposited above storm wave base. Quiescent periods followed by episodic sediment supply. The sand dykes most likely resulted from liquefaction during seismic events.	
Facies Association 2	upper shoreface to foreshore	Massive sedimentary breccias and conglomerate (massive or normally graded, clast-supported).	Deposited by submarine fans. Reworking of previously lithified sandstones of the Galho do Miguel Formation, FA 1 and/or FA 2.	Córrego dos Borges
		Plane-parallel-stratified and low-angle cross-bedding sandstone. Symmetrical and asymmetrical ripples and small- to medium-scale tabular and trough cross-bedding occur secondarily.	Wave swash in a beach environment along low-angle dipping to sub-horizontal depositional surfaces in the foreshore area. Migration of subaqueous 2D and 3D dunes in the upper shoreface.	
Facies Association 3	coastal desert environment	Sandstones with large-scale tabular and trough cross-bedding. Locally exhibits alternating thin laminae of white and gray sand.	Eolian dunes with straight and sinuous crests. Cross-bedding produced by grain fall and grain flow processes.	Córrego dos Borges
		Massive and horizontally laminated, fine- to medium-grained sandstones. Layers of facetted pebbles occur secondarily.	Dry deflationary interdune deposits.	
Facies Association 4	tidally influenced upper shoreface to foreshore	Sandstones with small-scale tabular and trough cross-bedding. Bimodal paleocurrent distributions forming herringbone cross-bedding.	Migration of subaqueous 2D and 3D dunes during ebb- and flood-tides in the upper shoreface.	Córrego Pereira
		Sandstones with planar horizontal stratification, flaser lamination, symmetric and asymmetric ripples.	Wave swash in a beach environment along sub-horizontal depositional surfaces in the foreshore area.	

		Sandstones with tidal bundles and tidal bundles with sigmoid-shaped cross-strata.	Cycles of neap-spring tides. The mud drapes in tidal-bundles represent a decrease in energy during neap tides in some cycles.	
Facies Association 5	lower shoreface	Sandstone with convolute lamination and sand dykes.	High sedimentation rates and liquefaction of sand beds under shock loading.	Rio Pardo Grande
		Massive and hummocky/swaley stratified sandstone. Sandstones with small-scale truncated wave-ripple and medium-scale trough cross-bedding are less frequent.	Combination of unidirectional and oscillatory flows generated by storm waves in lower shoreface.	Córrego da Bandeira Rio Pardo Grande
		Laminated and massive siltstone/mudstone	Fallout of suspended fine sediments in a lower shoreface environment.	Córrego da Bandeira Rio Pardo Grande
Facies Association 6	stromatolitic carbonate-siliciclastic shelf	Pelites that may or may not contain layers of carbonate.	Fallout of suspended fine sediments in a upper shoreface environment, probably a result of reduced siliciclastic influx.	Córrego da Bandeira Rio Pardo Grande
		Massive and laminated dolostone. Layers with stratiform stromatolites with flat and crenulated lamination.	Subaqueous precipitation.	Rio Pardo Grande

Interpretation

The base level affected by the action of fair-weather waves is proposed by Leckie and Krystinik (1989) to be the lower limit of the upper shoreface. This zone is affected by longshore currents, rip currents and breaking waves in the surf zone. Such processes operating in the upper shoreface result in the formation of tabular and trough cross-bedded sandstones in response to the migration of subaqueous 2D and 3D dunes, respectively (Clifton, 2006). Sandstones with abundant horizontal planar stratification and low-angle cross-bedding commonly represent wave swash in a beach environment along low-angle to sub-horizontal depositional surfaces in the foreshore area (Clifton, 2006). Therefore, the formation of the sandstone described above most likely represents deposition in shallow water in the transition zone between the upper shoreface and foreshore. An approximately north-south-oriented coastline is inferred by the symmetrical ripples with this orientation. The mainly north and south orientations of the paleocurrent directions based on the subaqueous dunes suggest that deposition occurred during the action of longshore drift due to the obliquity of the waves against the shoreline.

The deposition of intraformational sedimentary breccias suggests a reworking of previously lithified sediments of the Galho do Miguel Formation or FA 1 and may represent a period of tectonic instability leading to the formation of submarine fans in the basin, particularly at the interface between FA 1 and FA 2, where the clastic dykes were noted (above).

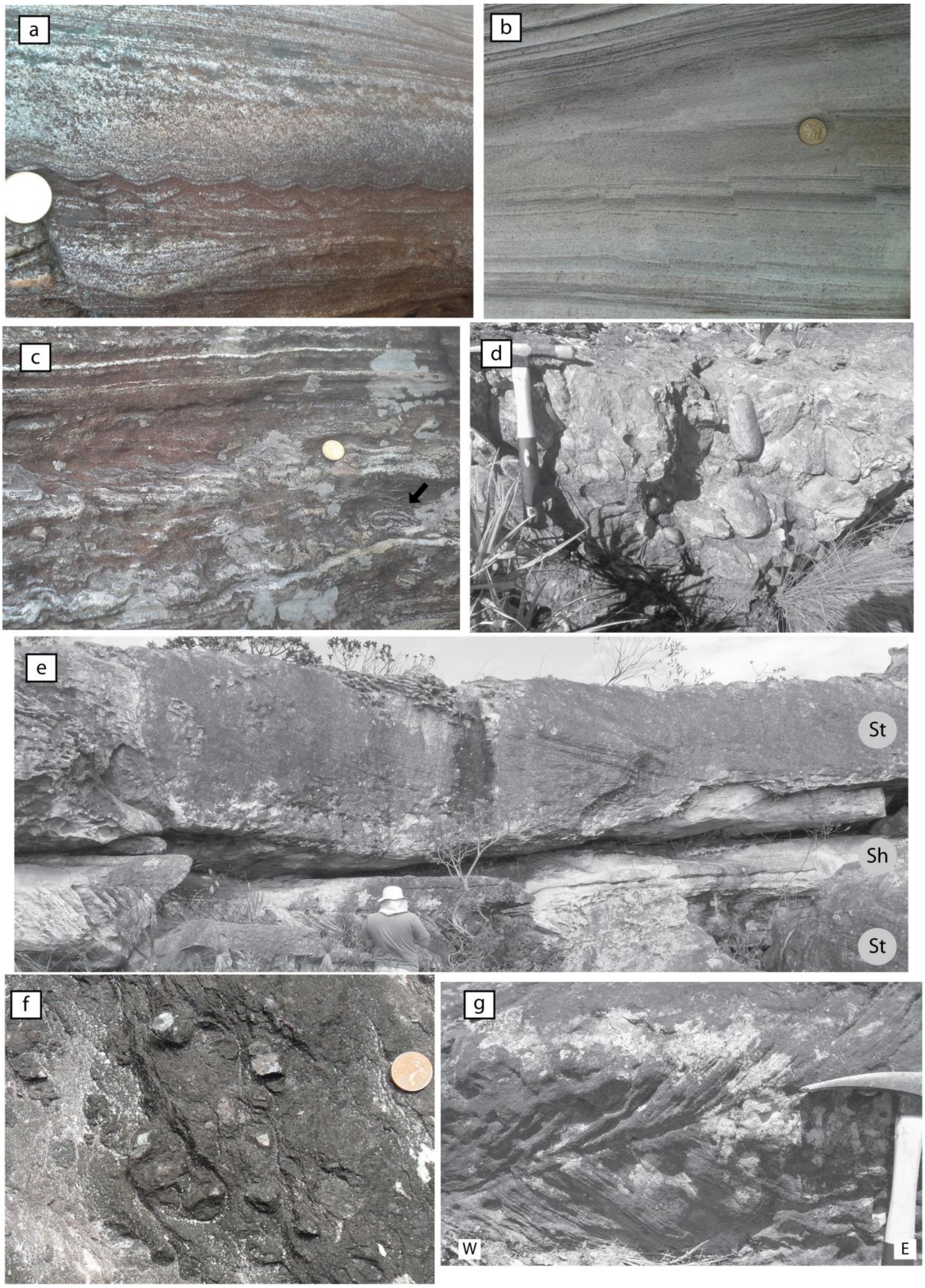

Fig. 5. Lithofacies examples of the Córrego dos Borges Fm. (a- f) and Córrego Pereira Fm. (g). (a) Fine-grained sandstone with wave ripples (FA 2); synsedimentary small scale faulting (b) and convolute lamination (c) in sandstones of FA 2 (black arrow); (d) clast-supported conglomerate with rounded cobbles of sandstone of FA 2; (e) large-scale trough cross-bedding

sandstone of FA 3 (note the person for scale); (f) massive sandstone with granules and small, faceted quartz pebbles of FA 3; and (g) herringbone cross-bedding in sandstone of FA 4.

4.1.3 Facies Association 3 (FA 3): coastal desert environment

Description

FA 3 comprises two intercalated sedimentary facies that reach a thickness of approximately 40 m (Table 1). The first facies comprises mineralogically and texturally mature sandstones. These sandstones are beige colored, and the predominantly medium-sized sand grains are generally well sorted and rounded. The sandstone beds exhibit tabular and lenticular geometry with sets ranging between 2 and 3 m thick. However, the main features of this facies are the presence of large-scale (2-3 m thick) tabular and trough cross-bedding with dips of approximately 30° (Fig. 5e) and paleocurrent directions to the southwest and southeast, which are quite distinct from the other facies associations (Figs. 4, 6, 7). The trough cross-bedding locally exhibits alternating thin laminae of white and gray sand. The second facies is composed of massive, poorly sorted, light-gray sandstone with predominantly medium to coarse grain sizes. This sandstone also contains granules and small, faceted quartz pebbles scattered throughout (Fig. 5f). Generally, FA 3 is positioned in the intermediate portions of the Córrego dos Borges Formation (i.e., in the middle of FA 2). However, in stratigraphic section 9, FA 3 directly overlies the Santa Rita Formation (i.e., on FA 1; Fig. 4).

Interpretation

The sandstones with large-scale cross-bedding most likely result from the migration of large eolian dunes with straight and sinuous crests (2D and 3D). The maturity of the sandstone with well-sorted and well-rounded grains is typical in many coastal deposits and, together with the large-scale and high-angle cross-bedding (produced by grain fall and grain flow processes), indicate the presence of eolian dunes with a well-developed slip face (Inman et al., 1966; Fryberger and Schenk, 1988; Mountney, 2006). The small, faceted pebbles in the massive sandstones most likely represent ventifacts formed in deflationary interdune areas. The conditions that favor the formation of ventifacts include a supply of loose sediment within an appropriate size range, relatively strong winds and appropriate direction, ground surface stability and exposed clast surfaces (pebble input) (Laity, 1994; Knight, 2008). Most ventifacts in modern environments are found in desert pavements (Cooke et al., 1993; Livingstone and Warren, 1996). FA 3 is interpreted to represent a coastal desert environment, similar to the Namib Desert. In stratigraphic section 9 (Fig. 4), the eolian deposits directly overlie offshore/lower shoreface deposits, indicating a local disconformity formed by subaerial exposure.

4.1.4 Facies Association 4 (FA 4): tidally influenced upper shoreface to foreshore

Description

FA 4 is present across almost the entire Córrego Pereira Formation and is modestly expressed in the Córrego dos Borges Formation. FA 4 consists of sandy bodies with lenticular and tabular geometry, predominantly small-scale tabular and trough cross-bedding (sets ranging from 10 to 50 cm defined by reactivation surfaces), generally forming herringbone cross-bedding, and bimodal paleocurrent patterns that are predominantly to the west and east (Figs. 5g, 7; Table 1). The grains of this facies range in size from fine to medium sand, are moderately to well sorted, and are sub-angular to sub-rounded. This facies rarely presents mud-draped foresets. Mineralogically, the sandstone consists of quartz and may contain varying amounts of plagioclase, mica and dispersed opaque minerals. The color varies from white to beige. Planar horizontal stratification, symmetric ripple marks oriented north-south, asymmetric ripple marks, and wavy and lenticular lamination occur rarely in FA 4 (Fig. 6b). The perpendicular direction of the asymmetric ripples with respect to the wave ripples often forms interference ripple marks.

Tabular and trough cross-bedding with sigmoidal cross-strata exhibit foreset thickening-thinning patterns. These facies are composed of medium- to coarse-grained sandstones, are moderately sorted and in some cases contain thin mud drapes (Fig. 6a). The sigmoidal cross-beds are medium in scale (sets of approximately 1 m) and feature progressive thinning toward the downdip direction, moderate dipping (approximately 20°) and reversals in paleocurrent directions.

Interpretation

Several authors (e.g., Davis and Hayes, 1984; Anthony and Orford, 2002) suggest that coastal systems can be classified into two main types: wave dominated and tide dominated. We interpret FA 4 as representative of tide-dominated shallow-marine systems. The presence of wave ripples, especially in the Serra do Cabral region, indicates the direct influence of waves and a north-south-oriented coastline, whereas the herringbone cross-bedding indicates ebb and flood tidal currents of approximately equal magnitude oriented perpendicular to the coastline (i.e., tidal currents to the east and west). The heterolithic bedding indicates repeated fluctuations in the energy regime, which are usually linked to tide-dominated depositional environments (Reineck and Singh, 1980).

The variation in the thickness of the foresets in certain outcrops with cross-beds represents cycles of neap-spring tides, in which relatively thin bundles are deposited during neap tides and relatively thick bundles are deposited during spring tides (Nio and Yang, 1991; Tape et al., 2003). The mud drapes in tidal bundles represent a decrease in energy (carrying capacity and competence) during neap tides in certain cycles. According to Kreisa and Moiola (1986), sigmoidal cross-stratification is formed as a result of the rapid transport and deposition of sediments during episodes of intense tidal flow. This type of flow in the Conselheiro Mata Group appears to be ephemeral and short lived because sigmoidal cross-stratification is rare and relatively thin bedded. The longshore currents have a secondary influence in FA 4, generating some cross-stratification and asymmetrical ripples with paleocurrent directions to the north and south.

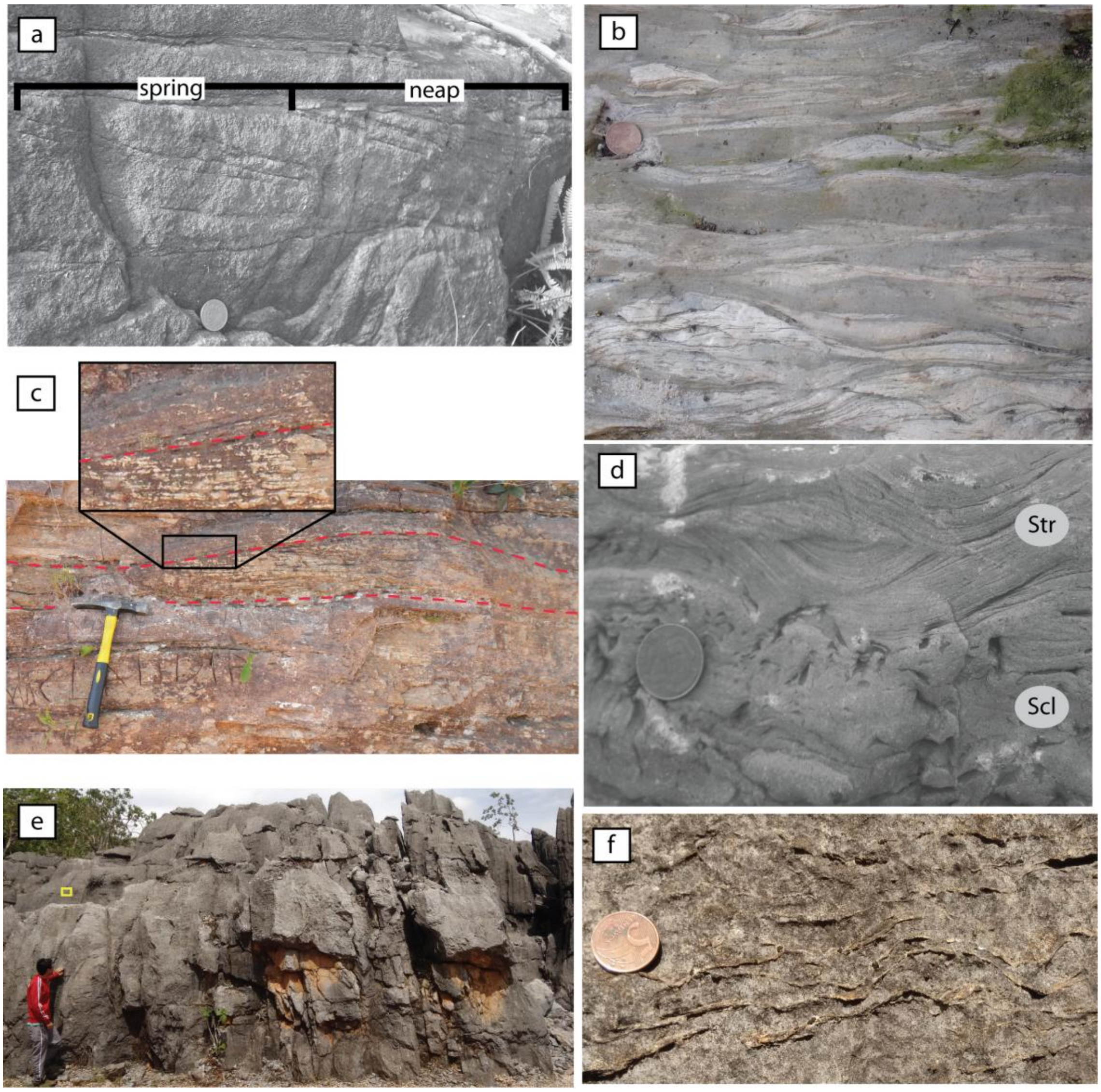

Fig. 6. (a) Sandstone with tidal bundles showing a spring-neap cycle (FA 4 - Córrego Pereira Formation); the bundle thickness is measured perpendicular to the dip of the foresets along a horizontal guided medial between the upper and lower bounding surfaces (Tape et al., 2003); (b) fine-grained heteroliths with wavy and lenticular bedding (FA 4 – Córrego Pereira Fm.); (c) hummocky cross-stratification in fine-grained sandstone of FA 5 (note the low-angle curved intersection of stratification; Córrego da Bandeira Formation); (d) sandstone with convolute lamination and small-scale truncated wave-ripples of FA 5 at the top of the Rio Pardo Grande Formation; and (e) massive dolostone with scattered layers of stromatolites (yellow box) with crenulated lamination (f) (FA 6 – Rio Pardo Grande Fm.). Str- sandstones with small-scale truncated wave-ripple; Scl- sandstone with convolute lamination.

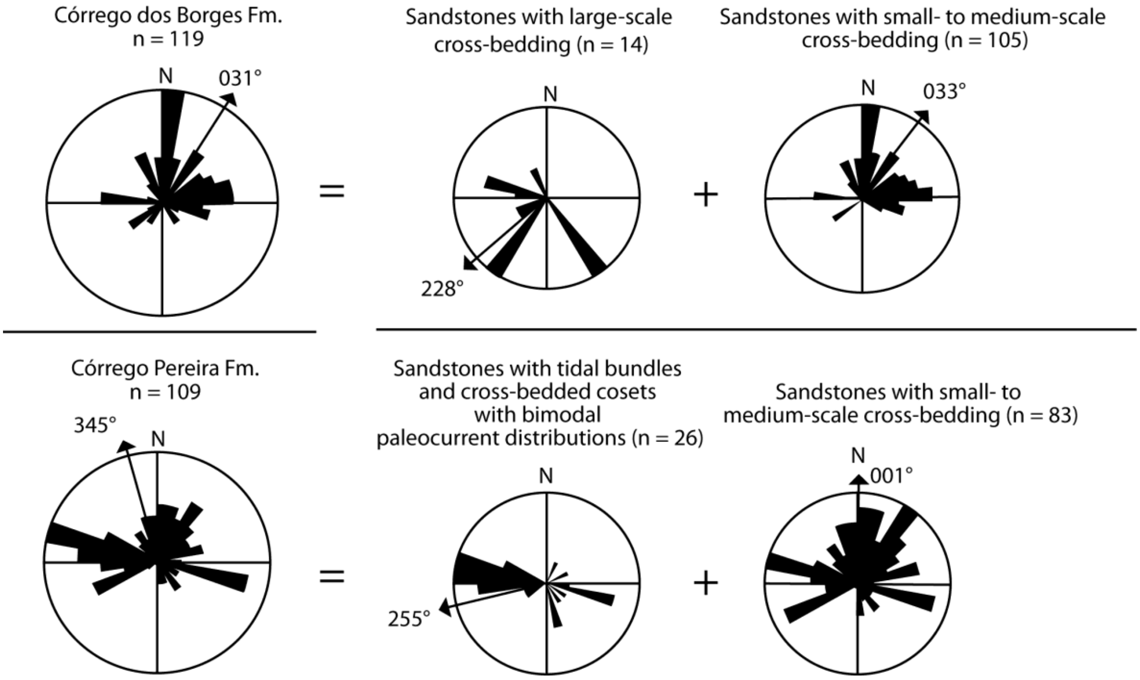

Fig. 7 Paleocurrent data of the Córrego dos Borges and Córrego Pereira formations plotted on rose diagrams.

4.1.5 Facies Association 5 (FA 5): lower shoreface

Description

The transition from upper shoreface (FA 2, FA 4) to lower shoreface conditions (FA 5) is gradual. FA 5 is mainly composed of pelites and quartz-sandy facies, which form rhythmites with a pelite/sandstone ratio that is commonly 1:1 in the Córrego da Bandeira Formation (Table 1). The pelitic beds can reach thicknesses of up to 15 m with sharp bed tops. These beds are predominantly massive, although lamination may occur rarely, and typically feature silt-sized grains. Magnetite crystals altered to martite occur sparsely and lend a gray and red color to the pelites. The sandstones that are interbedded with pelites predominantly feature fine-grained, well-sorted, and subrounded sand. These sandstones range from white to gray and can be massive or display medium-scale hummocky and swaley cross-stratification (HCS and SCS, respectively; Fig. 6c). Most beds consist of low-angle cross-stratification, have tabular or pinch and swell geometry, decrease by as much as 35% in thickness (commonly 25 cm average thickness), and define hummocks of antiform relief with wavelengths between 1.3 and 2 m. Asymmetrical ripples are rarely preserved on upper surfaces. Laminated micaceous sandstones, sandstones with sand dykes, convolute laminations, small-scale truncated wave ripples (Fig. 6d) and medium-scale trough cross-bedding also occur but are uncommon.

Interpretation

This facies association is interpreted to have been deposited between a fair-weather wave base and a storm wave base (Dott and Bourgeois, 1982; Walker, 1984; Leckie and Krystinik, 1989) in lower shoreface conditions. According to Galloway and Hobday (1996), sediments along the lower shoreface experience greater influence from storms and lesser influence from shorter-period fair-weather waves. The sandy facies described above (HCS, SCS and trough cross-bedding) are usually formed under a combination of unidirectional and oscillatory flow conditions caused by storm waves, indicating a high-energy context (Swift et al., 1983; Southard et al., 1990; Duke et al., 1991; DeCelles and Cavazza, 1992; Dumas and Arnott, 2006). Additionally, the presence of rhythmites, sandstones with convolute laminations, sand dykes and pelites/SCS intercalations is usually linked to a high-frequency episodic sediment supply (Reineck and Singh, 1980).

4.1.6 Facies Association 6 (FA 6): Stromatolitic carbonate-siliciclastic shelf

Description

FA 5 transitions gradually into an interval composed of mixed siliciclastic-chemical sedimentary rocks designated FA 6. This facies association occurs only in the southern Serra do Espinhaço and includes three main facies: a) pelite containing layers of carbonate, b) massive dolostone, and c) laminate dolostone. The pelite is thinly laminated, ranges from light gray to dark gray, and comprises quartz, sericite and thin layers of dolomitic limestone, although lenses (2 to 3 m) of limestone may occur rarely (Dossin et al., 1990). The presence of centimeter-scale layers of carbonate in the pelites has been reported only in the Rio Pardo Grande Formation in the Conselheiro Mata region (Pflug, 1968; Schöll and Fogaça, 1979; Fogaça 1995), but Lopes (2012) also identified carbonates in the Córrego da Bandeira Formation on the northwestern edge of the Serra do Cabral.

Massive gray dolostone occurs toward the top of the Rio Pardo Grande Formation and can reach thicknesses of up to 40 m (Batista et al., 1986; Fogaça, 1995) (Fig. 6e). Most of the primary structures have been obliterated by metamorphic recrystallization and deformation. Layers with stratiform stromatolites with flat and crenulated lamination (Fraga et al., 2014) occur scattered randomly throughout the massive dolostone (Fig. 6f).

Interpretation

The pelites are the product of the fallout of suspended fine sediments. The carbonate layers in the pelite rocks were most likely produced biologically or via biochemical mediation because this facies is overlain by dolostone with stromatolites. According to Dossin et al. (1990), these layers were deposited in a shallow marine environment, implying a substantial reduction in siliciclastic influx. Therefore, FA 6 is interpreted as resulting from a mixed carbonate-siliciclastic shelf (Garcia and Uhlein, 1987; Dupont, 1995). According to Droxler and Schlager (1985), the deposition rates of carbonate sediments are higher during sea-level highstands, a stage compatible with part of the Córrego da Bandeira and Rio Pardo Grande formations following an initial transgression phase.

4.2 Analytical results

The locations and complete results of the geochemistry and U-Pb detrital zircon geochronology are shown in Appendices A (electronic supplementary material) and in the charts in Figs. 8-12.

The Th/Sc and Zr/Sc ratios exhibit large variations in the analyzed samples. In the pelitic samples of the Santa Rita Formation (PE-CM-16, PE-SC-

44 and PE-SC-46) and sandstone samples of the Galho do Miguel Formation (PE-GO-40, PE-SC-43 and PE-FM-48) and Córrego dos Borges Formation (PE-CM-19 and PE-CM-21), the Th/Sc ratio is greater than 1, and almost all samples have a Zr/Sc ratio greater than 10 (Fig. 8). The chondrite-normalized REE patterns for the samples from the Galho do Miguel Formation and Conselheiro Mata Group are shown in Fig. 9. Because sandstones with high Zr contents (400 ± 200 ppm) may indicate the enrichment of heavy minerals (i.e., zircon), which characteristically have a abundant REEs (McLennan, 1989; Gromet et al., 1984), the samples with Zr contents of 400 ± 200 ppm (i.e., PE-16, PE-17, PE-44 and PE-21) were not included in the graph shown in Fig. 9 to avoid bias.

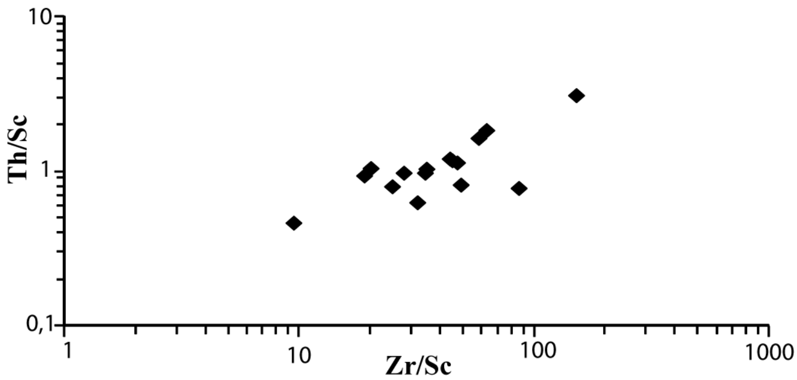

Fig. 8. Zr/Sc versus Th/Sc plot of the Galho do Miguel Formation and Conselheiro Mata Group.

The samples from the Galho do Miguel Formation and all the units from the Conselheiro Mata Group (with the exception of the Córrego da Bandeira Formation, which was not analyzed) show a steep LREE pattern, a relatively flat HREE pattern and significant enrichment in LREEs (~6-73 times greater than chondrite; Fig. 9). All the samples have moderately negative Eu anomalies, with Eu/Eu* values of 0.54-0.79. The REE pattern is similar to that of the NASC (Haskin et al., 1968). However, the REE abundances identified in the samples are depleted in comparison to the NASC's composition, most likely due to the quartz dilution effect (Taylor and McLennan, 1985).

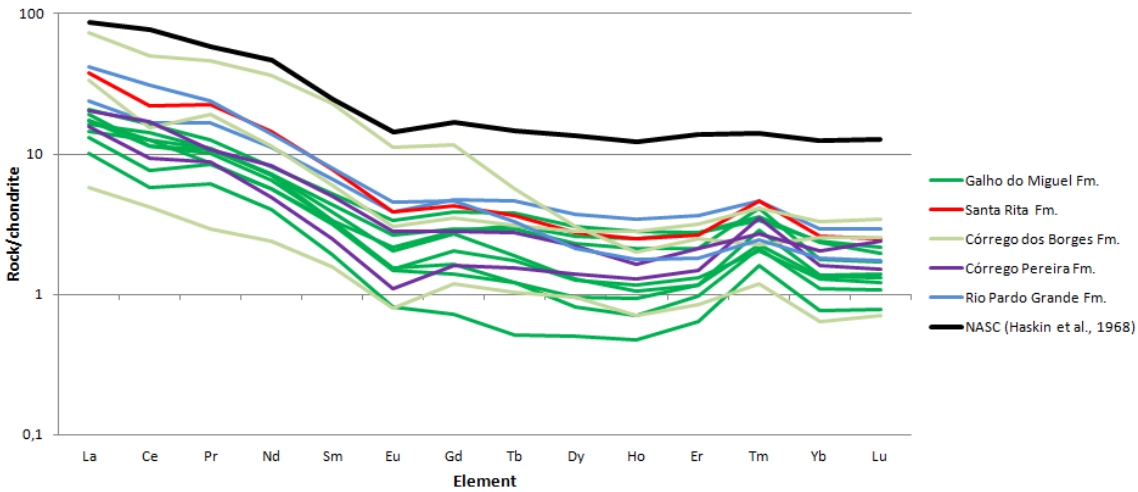

Fig. 9. Chondrite-normalized REE diagram for the Galho do Miguel Formation, Conselheiro Mata Group and North American Shale Composite (NASC; Haskin et al. 1968). The chondrite values are from Taylor and McLennan (1985).

The Galho do Miguel Formation is dominated by Rhyacian (Plumb, 1991) zircon grains (2.05-2.3 Ga) with a main peak at 2.1 Ga that is well marked in all the samples. Minor peaks occur at 1832 Ma, 2405 Ma, 2679 Ma and 3.4 Ga (Figs. 10a, 11a). The youngest ages obtained for the Galho do Miguel Formation are approximately 1581 Ma (Fig. 11f), which were found in three sandstone samples (PE-CM-14, PE-SC-43 and PE-FM-71). The outcrops of these samples do not exhibit the large-scale cross-stratification that is typical of the eolian environment attributed to the formation. In these places (Fig. 1), planar-laminated to low-angle cross-stratified sandstones predominate.

Two of the three Santa Rita Formation samples have a minimum age peak of approximately 1.5 Ga (Fig. 11b, 11f). This formation also features main peaks at 1947 Ma, 2048 Ma, 2118 Ma, and 2640 Ma and secondary peaks at 2908 Ma, 3156 Ma, 3298 Ma and 3520 Ma (Fig. 10b). There is a small discrepancy between samples PE-CM-16 (pelite from the lower portion of the Santa Rita Formation) and PE-CM-17 (sandstone from the middle portion of the Santa Rita Formation), with the former featuring a concentration of older zircons and the latter featuring younger zircons.

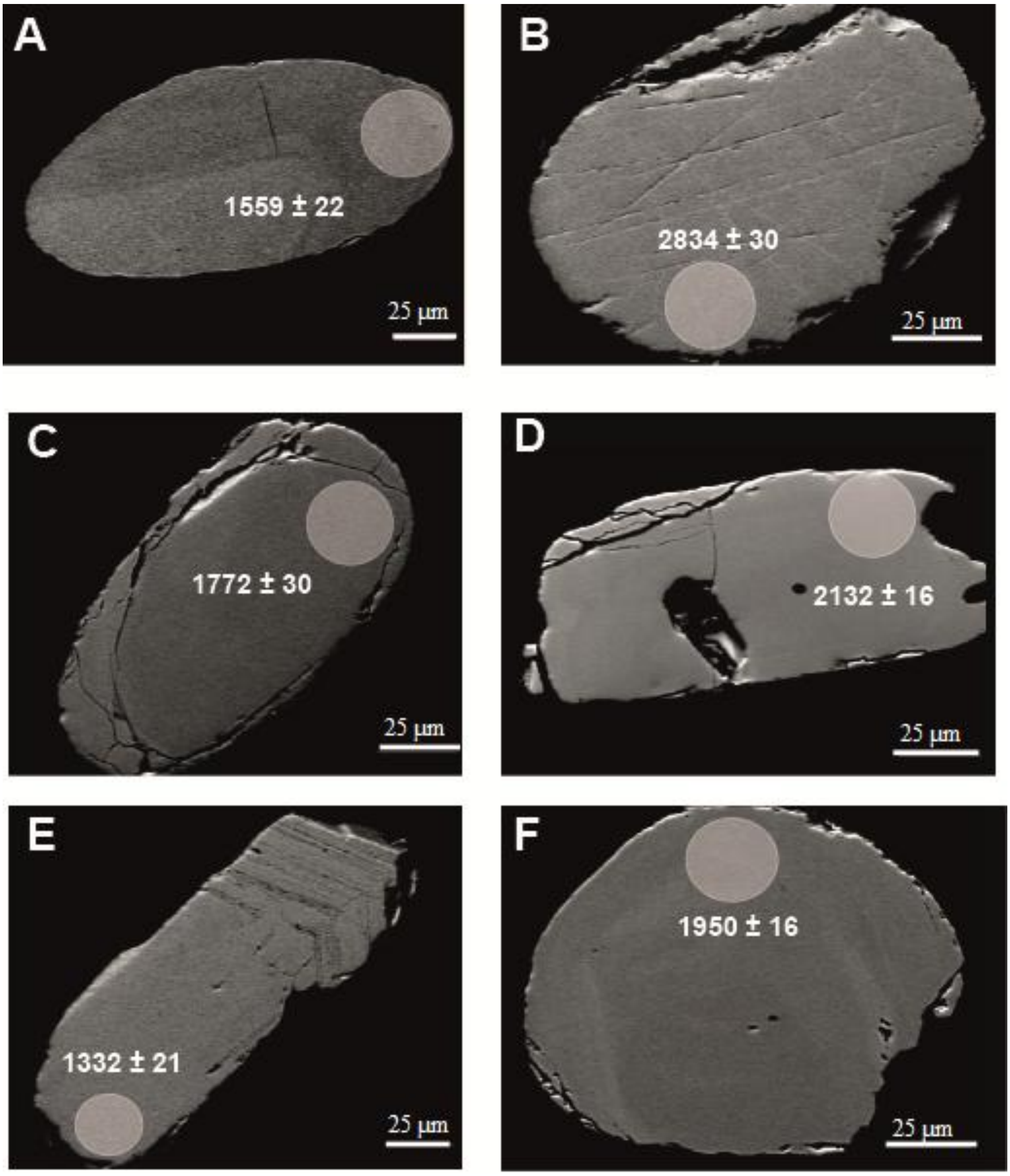

Fig. 10. SEM images of the dated zircon grains with circles representing in situ U-Pb dating and age plus error. The zircon grains are from samples as follow: A= PE-FM-71 E-37 (Galho do Miguel Fm.), B= PE-CM-CIII-19 (Santa Rita Fm.), C= PE-SC-42-D-IV-03 (Córrego dos Borges Fm.), D = PE-JQ-32 A-15 (Córrego dos Borges Fm.), E = PE-CM-26-DIV-16 (Córrego Pereira Fm.), and F = PE-CM-CIII-19 (Rio Pardo Grande Fm.).

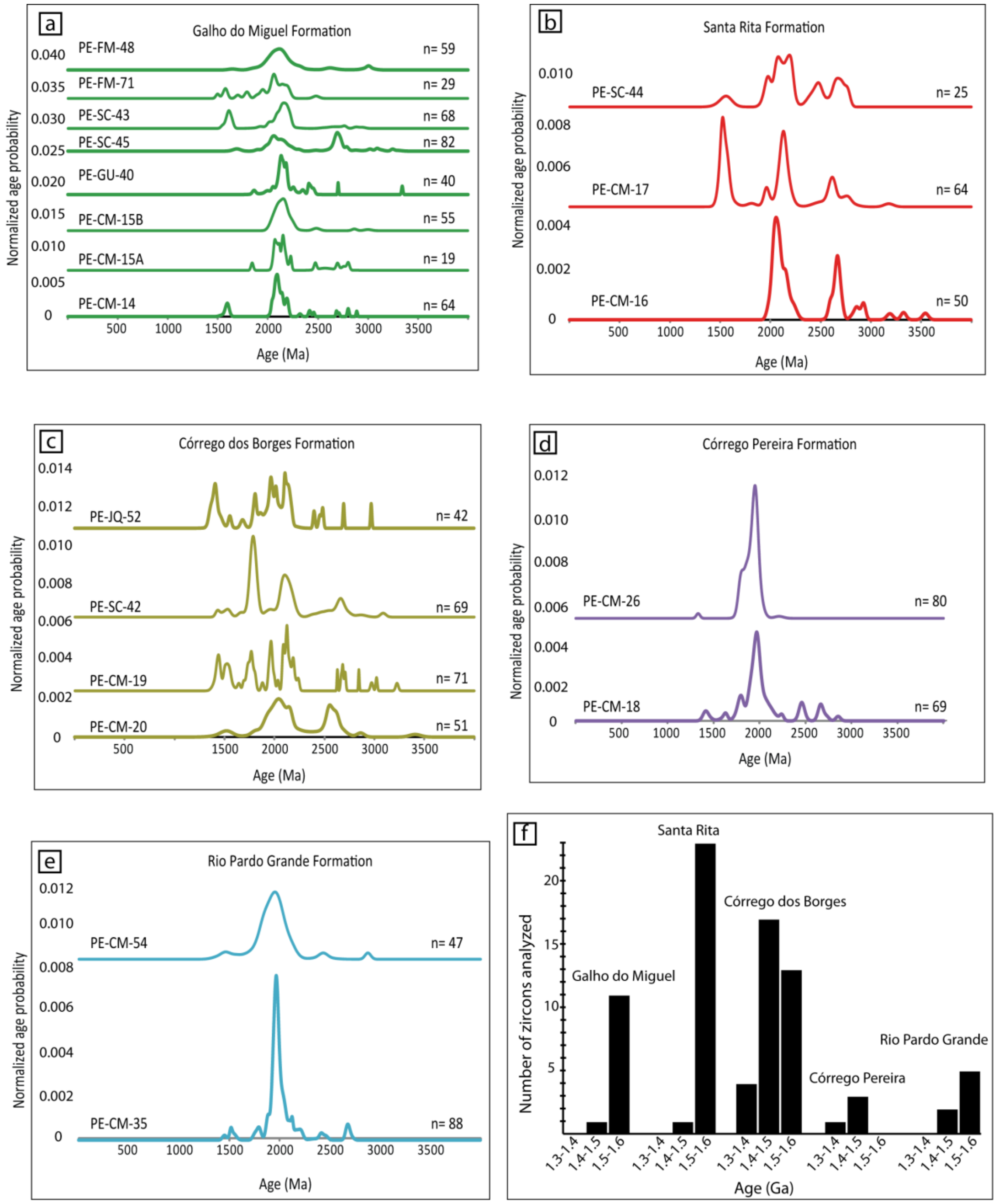

Fig. 11. Relative probability histograms for the studied samples from the southern Serra do Espinhaço and Serra do Cabral corresponding to (a) the Galho do Miguel Formation, (b) the Santa Rita Formation, (c) the Córrego dos Borges Formation, (d) the Córrego Pereira Formation, (e) the Rio Pardo Grande Formation, and (f) the younger zircon populations in the Galho do Miguel, Santa Rita, Córrego dos Borges, Córrego Pereira and Rio Pardo Grande formations. Detrital zircon data with discordance equal to or less than 10%.

Of all the units studied, the samples from the Córrego dos Borges Formation possess the age spectrum with the largest variation, characterized by several age peaks within relatively short intervals of time. The youngest zircon grains have ages of between 1.3 Ga and 1.4 Ga (Fig. 11f). There are also main age peaks at 1777 Ma, 1960 Ma, and 2183 Ma and secondary peaks at 2540 Ma, 2640 Ma, 2843 Ma, 2968 Ma, 3212 Ma and 3414 Ma (Figs. 10c, 10d, 11c).

The youngest zircon of the Conselheiro Mata Group (1332 ± 21 Ma) was found in sandstones from the Córrego Pereira Formation (Figs. 10e, 11f). However, most ages obtained for this formation are concentrated at approximately 1956 Ma. Zircon ages of 2434 Ma, 2636 Ma and 2812 Ma, listed in decreasing order of abundance, occur as subordinate peaks (Fig. 11d).

Five main peaks appear in the age spectra of the Rio Pardo Grande Formation: 1506 Ma, 1964 Ma, 2389 Ma, 2667 Ma and 2851 Ma (Figs. 10f, 11e). However, detrital zircon ages that are approximately 2.0 Ga (Orosirian Period; Plumb, 1991) are dominant, similar to the Córrego Pereira Formation. Three samples were analyzed geochemically, including one pelite and two sandstones.

5 Discussions

5.1 Provenance and geochronology

The use of REEs and ratios such as La/Sc, Th/Sc, Eu/Eu*, and LREE/HREE for sedimentary provenance analysis assumes that these elements have low mobility during sedimentary processes, diagenesis or metamorphism (Cullers et al., 1974; Taylor and McLennan, 1985; Slack and Stevens, 1994; Cullers, 1995; Shao et al., 2001). Therefore, the abundance of these elements most likely represent the bulk composition of their source rocks (McLennan et al., 1980; Raza et al., 2010). The chondrite-normalized REE patterns of the Galho do Miguel Formation and Conselheiro Mata Group are parallel, suggesting that there were no substantial changes in the source rocks or changes in the LREE/HREE ratio caused by secondary processes.

The sedimentary rocks in the Galho do Miguel Formation and Conselheiro Mata Group feature high concentrations of REEs, patterns similar to NASC, negative Eu anomalies, high LREE/HREE ratios (Fig. 9), and high La/Sc (>2.5) and Th/Sc (>0.8) ratios. These chemical characteristics generally indicate a granitic source rock for the sediments (Schieber, 1986; Condie, 1993; Rahman and Suzuki, 2007; Raza et al., 2010).

The Zr/Sc versus Th/Sc diagram (Fig. 8) allows us to discriminate the composition of the source rocks to the sedimentary rocks (Taylor and McLennan, 1985; McLennan, 1989; Raza et al., 2010). According to Taylor and McLennan (1985), samples with Th/Sc ratios greater than 1 reflect input from fairly evolved crustal igneous rocks, whereas Th/Sc ratios less than 0.8 most likely reflect input from mafic sources. A Zr/Sc ratio greater than 10 indicates a mature or recycled source. Additionally, the Th/U ratio can be considered complementary to the Zr/Sc ratio because Th/U values greater than 4 may indicate sediment recycling (Rahman and Suzuki, 2007). The selective sorting of heavy minerals caused by recycling can also result in a change in the pattern of REEs (Tripathi and Rajamani, 2003), which is not the case for the rocks analyzed here. Based on these assumptions, we found that both the Galho do Miguel Formation and all the units in the Conselheiro Mata Group may contain input from felsic rocks and sedimentary rocks that have experienced only a low degree of recycling, similar to the quartzites in the Aravalli Craton, NW Indian shield (Raza et al., 2010). In most cases, the analyzed zircon grains are rounded due to sedimentary transport. Some of the zircons, and therefore the sedimentary rocks, are recycled material (Fig. 10).

Analyzing the U-Pb detrital zircon results from the Conselheiro Mata Group's units suggests a major contribution of zircon grains that formed during the Paleoproterozoic and, subordinately, the Mesoproterozoic and Archean (Fig. 12). However, note that a source of zircons generated in the Calymmian to Ectasian (Plumb, 1991) (Fig. 11f) occurs in the stratigraphic formations Galho do Miguel (1497 ± 17 to 1599 ± 24 Ma, n = 12), Santa Rita (1489 ± 29 to 1576 ± 24 Ma, n = 24), Córrego dos Borges (1361 ± 19 to 1583 ± 31 Ma, n = 34), Córrego Pereira (1332 ± 21 to 1445 ± 40 Ma, n = 4) and Rio Pardo Grande (1400 ± 65 to 1547 ± 28 Ma, n = 7), which were formed in the Middle Espinhaço Sequence, as defined by Chemale et al. (2012) and Guadagnin et al.

(2015). These zircon grains correspond to the younger ages found in the studied uppermost stratigraphic units of the Upper Espinhaço Sequence in the Espinhaço Basin, which were deposited between 1.18 and 0.9 Ga.

The zircon age distribution patterns of the Galho do Miguel and Santa Rita formations are very similar to those of Neoarchean, Rhyacian and Calymmian zircons (Fig. 12), suggesting that the main source areas remained constant during the sag phase in the Upper Espinhaço Sequence.

The depositional period of the Córrego dos Borges Formation indicates a slightly different pattern with the presence of Statherian zircon input and few Orosirian grains together with Rhyacian, Neo- and Paleoarchean and Calymmian zircon grains, suggesting a change in the sediment supply (Fig. 12).

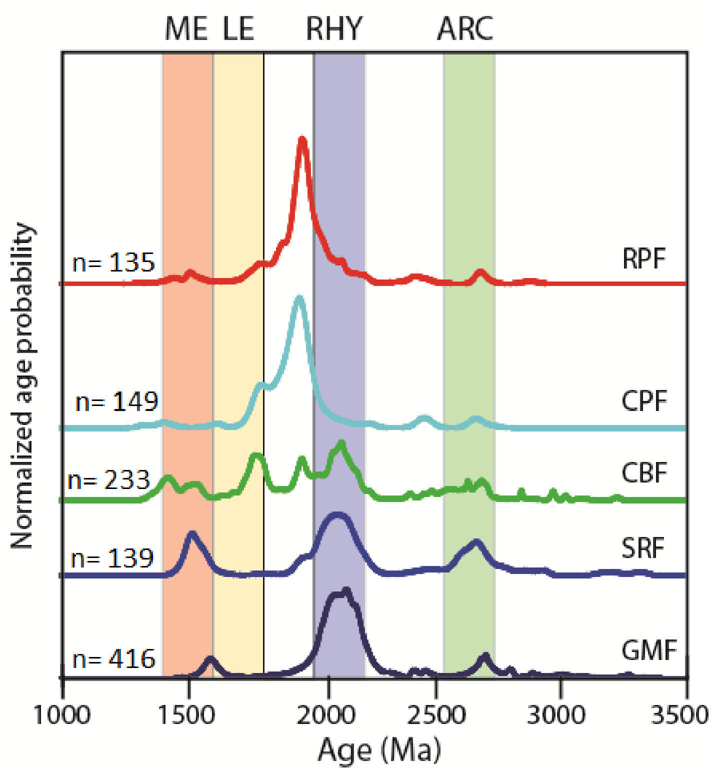

Fig. 12. Histogram with all detrital zircon ages for the main stratigraphic units of the Conselheiro Mata Group. The main domains correspond to Neoarchean (ARC), Rhiacyan (RHY), Statherian/Lower Espinhaço Sequence (LE), and Calymmian-Ectasian/ Middle Espinhaço Sequence (ME). The following abbreviations are: n= number of zircon grains analyzed, GMF= Galho do Miguel Fm., SRF= Santa Rita Fm., CBF= Córrego dos Borges Fm., CPF= Córrego Pereira Fm., and RPF= Rio Pardo Grande Fm.

During the deposition of the upper units of the Upper Espinhaço Sequence, specifically the Córrego Pereira and Rio Pardo Grande formations, there was a drastic change in the origin of the sediments, whose Orosirian sources (Fig. 12) have not yet been identified in the adjacent region. The main source areas in the surrounding areas of the Espinhaço Basin are Archean, Rhyacian, Statherian and Neoproterozoic to Early Paleozoic (e.g., Brito Neves et al., 1979; Chemale et al., 1993; Barbosa and Sabaté, 2004, Alkmin et al., 2006). There is very little contribution from the Calymnian (e.g., Silveira et al., 2013) and Stenian (Grenvillian) (e.g., Chemale et al., 2012; Chaves et al., 2013).

5.2 Depositional systems and palaeogeography

After the opening of the Lower Espinhaço Basin during the Statherian Period (~1.7 Ga), almost 500 Ma years elapsed before a new rifting of greater areal extent occurred at 1.2 Ga (Stenian Period; Chemale et al., 2012) via the reactivation of preexisting normal faults and the generation of new faults located west of the western limit of the possible Statherian rift (i.e., west of the sedimentary breccias of the São João da Chapada Formation). Reis (2011) has suggested the presence of rift deposits tens of km west of Guinda, which may represent the record of the Stenian Rift (1.2 Ga; Fig. 13a).

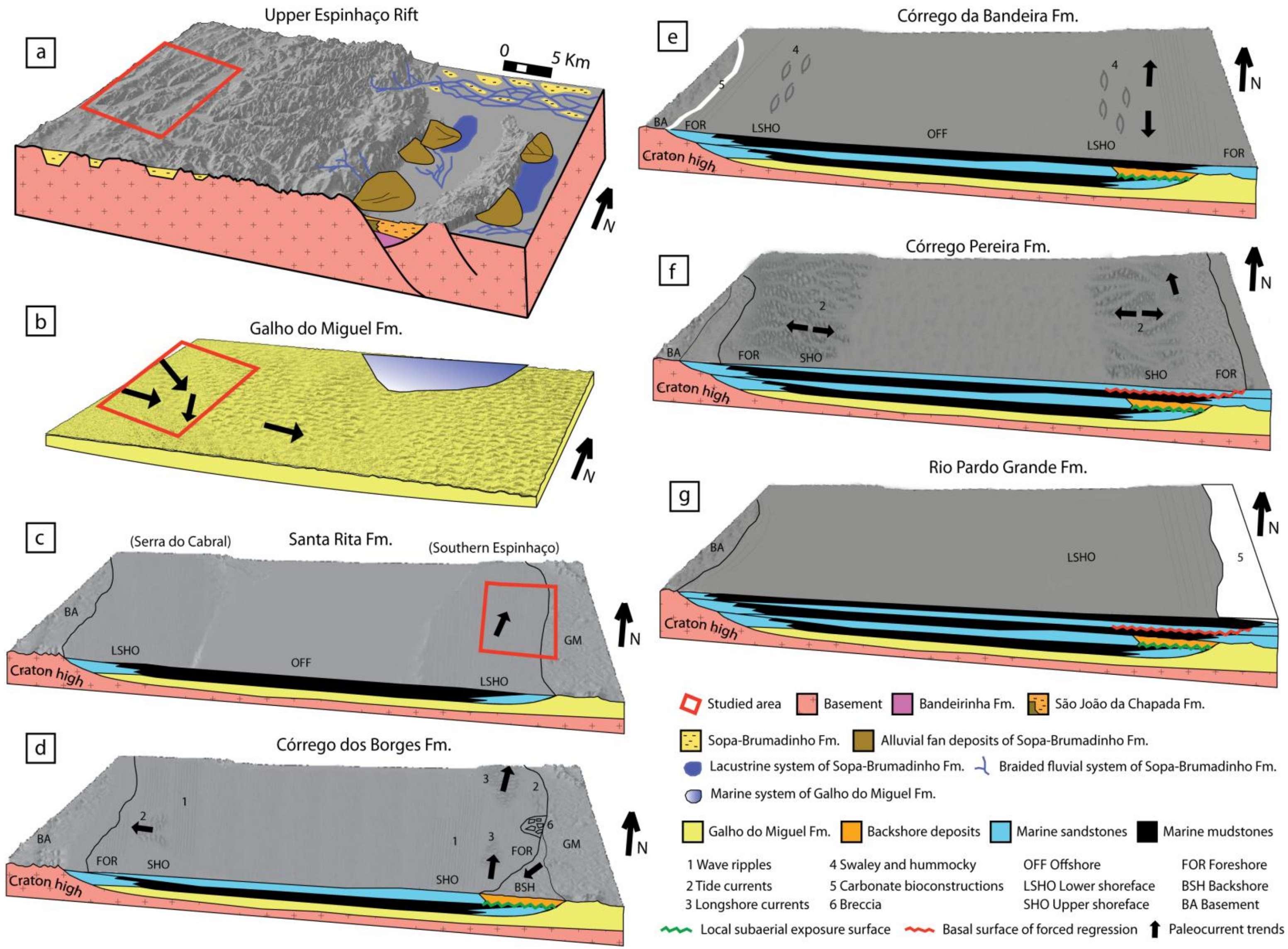

a
Upper Espinhaço Rift
0
5 Km
N
b
Galho do Miguel Fm.
N
c
(Serra do Cabral)
Santa Rita Fm.
(Southern Espinhaço)
BA
LSHO
OFF
LSHO
GM
Craton high
N
d
Córrego dos Borges Fm.
BA
FOR
SHO
SHO
FOR
BSH
GM
Craton high
N
e
Córrego da Bandeira Fm.
BA
FOR
LSHO
OFF
LSHO
FOR
Craton high
N
f
Córrego Pereira Fm.
BA
FOR
SHO
SHO
FOR
Craton high
N
g
Rio Pardo Grande Fm.
BA
LSHO
Craton high
N
Studied area
Basement
Bandeirinha Fm.
São João da Chapada Fm.
Sopa-Brumadinho Fm.
Alluvial fan deposits of Sopa-Brumadinho Fm.
Lacustrine system of Sopa-Brumadinho Fm.
Braided fluvial system of Sopa-Brumadinho Fm.
Marine system of Galho do Miguel Fm.
Galho do Miguel Fm.
Backshore deposits
Marine sandstones
Marine mudstones
1 Wave ripples
2 Tide currents
3 Longshore currents
4 Swaley and hummocky
5 Carbonate bioconstructions
6 Breccia
OFF Offshore
LSHO Lower shoreface
SHO Upper shoreface
FOR Foreshore
BSH Backshore
BA Basement
Local subaerial exposure surface
Basal surface of forced regression
Paleocurrent trends

Fig. 13. Depositional evolution of the Upper Espinhaço Basin. (a) Rifting at approximately 1.2 Ga with the development of major depocenters controlled by faults and reactivation of normal faults from the Statherian rift (1.7 Ga); (b) eolian sediment deposition of the Galho do Miguel Formation during the transition from a mechanical to a thermal subsidence phase (Martins-Neto et al., 2001); (c) relative sea-level rise during the deposition of the Santa Rita Formation mudstones; (d) regressive trend during the deposition of the Córrego dos Borges Formation; (e) storm activity during periods of marine transgression (Córrego da Bandeira Formation); (f) marine regression and deposition of tidally influenced upper shoreface to foreshore sediments of the Córrego Pereira Formation; and (g) mudstones of the Rio Pardo Grande Formation deposited during a new marine transgression.

The sedimentation in the Upper Espinhaço Basin in the southern Serra do Espinhaço began with the deposition of quartzites by braided fluvial systems and conglomerates that, in some cases, contain diamonds from deltaic and alluvial fans (Martins-Neto, 1996). Both systems belong to the Sopa-Brumadinho Formation (Martin-Neto, 2000, and references therein). During the transition from mechanical to thermal subsidence, a coastal system dominated by eolian deposits developed across a wide area of the region (Dossin et al., 1987; Martins-Neto et al., 2001; Fig. 13b). The thickness (2000-3000 m) and great areal extent of the eolian sandstones (Pflug, 1968; Schöll and Fogaça, 1979) suggest that the local paleotopography was buried. In addition, the lack of any substantial amount of coarse material in the Galho do Miguel Formation suggests low topographic relief during deposition, similar to the Jurassic eolian system in the western United States (Peterson, 1988). Marine facies at the base and top of the eolian sandstones have been described in the Guinda and Serra do Cabral regions, respectively (Martins-Neto, 1998; Espinoza, 1996). Gamma spectrometry data from an aerial survey conducted in the Guinda region (Megafísica Survey Aerolevantamentos S.A., 2001) show potassium anomalies occurring in some areas mapped as the Galho do Miguel Formation (Fogaça, 1995). These anomalies are associated with pelitic layers and fine-grained sandstones with wave ripples, low-angle cross-stratification and plane-parallel stratification. The absence of sandstones with large-scale cross-stratification; the geochemistry of the major elements, which indicates that the sandy facies have relatively high pelitic contents; and the geochronology, which indicates a distinct provenance signature that includes Calymmian detrital zircon age data (1.5 Ga), indicate a change in depositional conditions. Further studies are needed to fully clarify such depositional systems.

The Conselheiro Mata Group is characterized mostly by marine sedimentation. Three transgressive-regressive sequences were recognized based on facies analysis and stratal stacking patterns (Fig. 4). Mudstone facies record deposition in an offshore environment at the base of the group and most likely represent the continuity of the marine transgression at the top of the Galho do Miguel Formation (i.e., a gradational transition from shoreface to offshore conditions; Fig. 13c). As seen in Figs. 2 and 11b, zircon ages from the Calymmian Period (1.5 Ga) tend to occur in the lower shoreface deposits (middle and top of the Santa Rita Formation). The absence of zircon ages from this period in the pelitic sample PE-CM-16 most likely suggests a low terrigenous sediment supply to the offshore environment, and the subsequent regressive trend caused an increase in the sediment supply, thereby incorporating more Calymmian sediments.

The normal regression caused the development of a lower shoreface on offshore deposits and indicates that the rate of sediment supply to the coastal zone exceeded the rate of relative sea-level rise. The return of shallow marine conditions was most likely accompanied by seismic events that generated sedimentary breccias and synsedimentary deformation structures. Although the Espinhaço Supergroup was deposited in an intraplate setting, Grenvillian tectonism at the border of or within the São Francisco-Congo Craton may have influenced sedimentation (Chemale et al., 2012). Grenvillian zircon grains are scarce in the Upper Espinhaço Sequence, occurring only in the basal rift portion as thin volcaniclastic layers (Chemale et al., 2012) or volcaniclastic material on the basement structural high (Chaves et al., 2013). The sediments in the Córrego dos Borges Formation record periods of zircon generation (igneous or metamorphic) with relatively high frequencies between approximately 1.5 Ga and 2.1 Ga (Fig. 11c). Plane-parallel-stratified and low-angle cross-bedding sandstones were deposited on the upper shoreface to foreshore, where waves and currents continually reworked the sediments. We identified two main types of marine paleocurrent directions: longshore currents toward the north and south and predominantly eastward tidal currents on the eastern shore and westward tidal currents on the western shore (Fig. 13d). The oscillatory flow in the coastal region generally shows an orientation perpendicular to the shoreline when it is dominated by waves; thus, the orientation of the wave ripple crests can be used as an approximation of the tendency of the local paleoshoreline (Leckie and Krystinik, 1989). The shallow marine deposits in the southern Serra do Espinhaço exhibits wave ripples with crests oriented north-south, as observed by Espinoza (1996) in the Serra do Cabral region, indicating a paleoshoreline with the same orientation or that the shoreline influenced the wave orientation. In stratigraphic section 9, it is possible to observe a coastal desert environment (dune and interdune sandstones) directly overlying offshore deposits, indicating a possible local subaerial erosion surface.

The upper shoreface (FA 2) transitions gradually into the lower shoreface (FA 5) (Fig. 13e), recording the second marine transgression. A lower shoreface condition under the action of storm waves seems to have prevailed during the deposition of the Córrego da Bandeira Formation. In the Serra do Cabral region, the reduced siliciclastic input allowed for carbonate sedimentation, although to a limited extent.

The local transition from the lower shoreface (Córrego da Bandeira Formation) to the upper shoreface (Córrego Pereira Formation) is laterally abrupt. The surface between these deposits exhibits sharp relief, possibly marking a regressive surface of marine erosion, indicating a relative sea-level fall (*sensu* Catuneanu et al., 2009; Fig. 15). From this pattern, we infer that the substrate on which the Conselheiro Mata Group was deposited had a low-gradient slope because it would have been more susceptible to erosion by waves than a higher-gradient shoreface during base-level fall (Catuneanu, 2006). The sedimentary structures produced during the forced marine regression indicate tidal currents toward the east and west and, secondarily, longshore currents to the north and south (Fig. 13f). The ages of the detrital zircons show that the main source is Orosirian (~1.9-2.0 Ga) (Fig. 12). This change in sedimentary provenance may result from a change in the paleocurrent pattern and/or because of tectonic events in the source area. Of the two dated samples (Fig. 11d), sample PE-CM-18, which was collected at the base of the Córrego Pereira Formation (progradational trend; Fig. 4), contains Archean zircons, unlike sample PE-CM-26 from the top of the formation (retrogradational trend; Fig. 4). The textural characteristics of these zircons (e.g., roundness) suggest a high transport distance and/or recycling during the marine regression.

The last marine transgression of the sag phase recorded in the southern Serra do Espinhaço comprises the lower shoreface deposits of the Rio Pardo Grande Formation (Fig. 13g), which is dominated by Orosirian source rocks (~1.97 Ga), above the upper-shoreface deposits. During the subsequent period of sea-level highstand, the rate of base-level rise decreased, resulting in a normal regression and consequent change from a predominantly siliciclastic system to a carbonate system and led to the establishment of a mixed carbonate-siliciclastic shelf (Garcia and Uhlein, 1987; Dupont, 1995). The mudstones and carbonate sediments containing stratiform stromatolites were deposited during quiet phases of sedimentation characterized by low siliciclastic influx.

The change from the dominant Rhycian source in the Córrego dos Borges to an Orosirian source in the two last units of the Conselheiro Mata Group may reflect far-field stresses along the plate margins or tectonic process in the interior of the Congo-São Francisco Paleoplate.

Seismic reflection data (Reis, 2011; Fig. 14) show the presence of a basement topographic high west of the areas studied. Fig. 14 shows that two major depocenters were separated (south of Três Marias) during the Espinhaço rift-sag phase. The basement topographic high most likely had great influence on the coastline geometry during the marine development of the Conselheiro Mata Group. The upper part of the Espinhaço sequence progressively onlap the basement, recording periods of relative rises in sea level. This stratum is bounded at the top by an erosional surface and overlain by the Macaúbas Group.

Our studies suggest that this marine sequence extended to the north and east of the Meridional Espinhaço on the São Francisco Craton and can be used for the kinematic reconstruction of supercontinent masses such as Columbia and Rondinia.

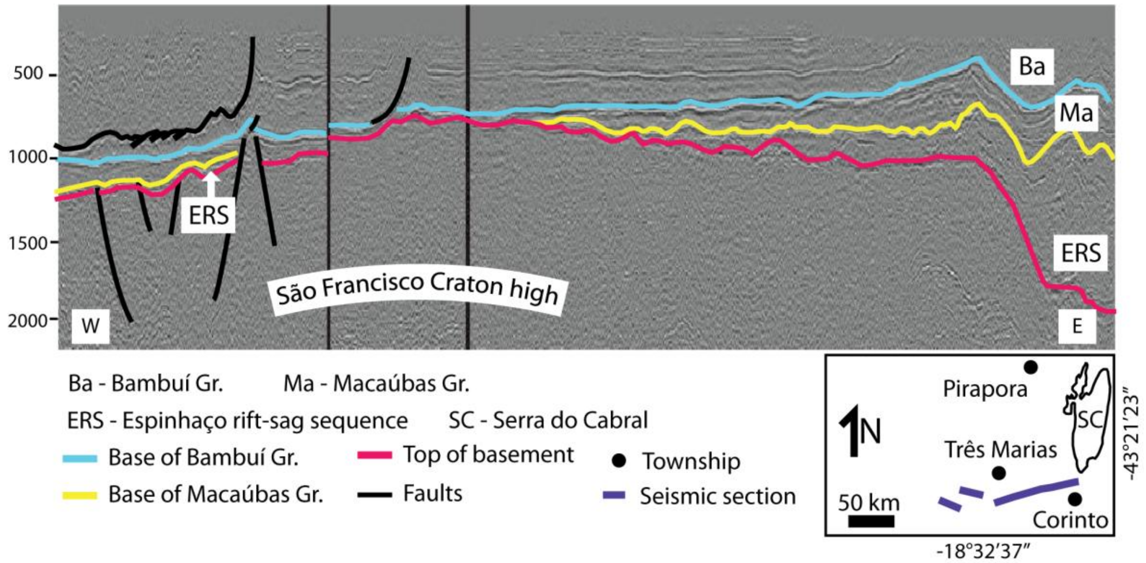

Fig. 14. Seismic reflection lines from the Espinhaço Basin (modified from Reis, 2011). Vertical scale: two-way travel time (TWT/ms).

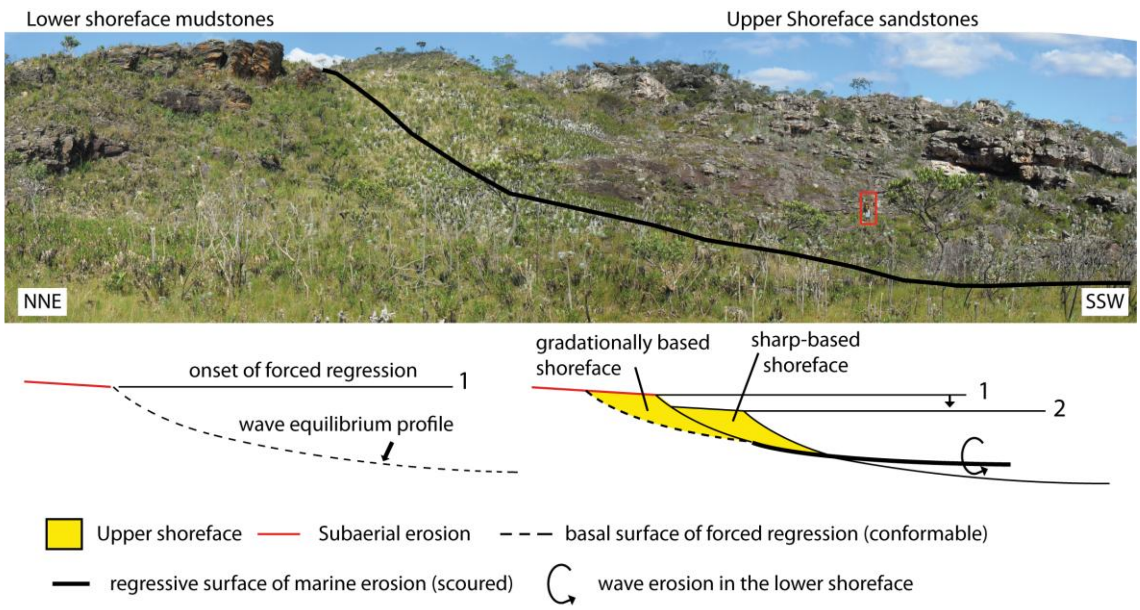

Fig. 15. Abrupt lateral changes of lithofacies separating the Córrego da Bandeira Formation (lower shoreface) from the Córrego Pereira Formation (upper shoreface). The surface between these formations shows sharp relief, possibly marking a regressive surface of marine erosion (drawing modified from Catuneanu, 2006).

6 Conclusions

The Conselheiro Mata Group represents an excellent example of transgressive-regressive cycles that developed in an intracratonic sag basin during the Stenian to early Tonian (Upper Mesoproterozoic to Lower Upper Proterozoic) as part of the Upper Espinhaço Sequence (or Megasequence) of the 1.8 to 0.92 Ga intracratonic Proterozoic Espinhaço Basin. The trace element geochemistry suggests that the provenance was mainly from granitic rocks, typical of a craton interior, and secondarily from sedimentary rocks that have experienced only a low degree of recycling, most likely from the underlying rift basin. The geochronological data indicate a provenance dominated by Paleoproterozoic and, subordinately, Paleo- to Neoarchean source terranes, coinciding with the main tectonic cycles of the basement rocks in the São Francisco Craton. Some contributions from Statherian and Calymmian sources that are part of scarce magmatism in the intracratonic Proterozoic Espinhaço Basin are also recognized.

Based on lithological and architectural element analysis, the Conselheiro Mata Group can be divided into six facies associations. FA 1, which mostly formed from mudstones, resulted from a marine transgression and deposition in offshore to lower shoreface conditions. The main sources of these sedimentary rocks are similar to those of the underlying Galho do Miguel Formation, with ages of approximately 1.5 Ga, 2.1 Ga and 2.6 Ga. The subsequent normal marine regression was characterized by a gradual change to an upper shoreface environment (FA 2) influenced by longshore currents to the north and south, resulting in provenances from several source rocks with ages of between 1.3 Ga and 3.4 Ga, including sediment inputs from the Lower Espinhaço Sequence. Locally, the eolian sandstones of FA 3 directly overlie offshore mudstones that record local subaerial erosion. The second transgressive-regressive cycle was marked by deposition in lower shoreface conditions under the action of storm waves followed by relative sea-level fall, represented locally by a regressive surface of marine erosion and the resumption of upper shoreface conditions. These sandstones (FA 4) were derived almost exclusively from Orosirian source rocks (peak at 1.97 Ga, whose sources have not yet been identified in the adjacent region), similar to those found in the overlying unit (FA 5 and FA 6), which marked a drastic change in the sediment supply that was likely due to changes in the paleocurrent pattern to the east and west caused by tidal influence and/or may reflect tectonic processes in the source area. A new transgression-regression cycle records a change from a predominantly siliciclastic system (pelites in FA 5) to a carbonate system (dolostones in FA 6) and led to the establishment of a mixed carbonate-siliciclastic shelf.

Acknowledgements

We would like to thank the CAPES, CNPq (grant no. 304045/2010-1) and PETROBRAS for their financial support for the field work and analysis. We also thank Giorgio Basilici, an anonymous reviewer and the Editor Jasper Knight, for improving the quality of the manuscript.

References

Alkmim, F.F., 2004. O que faz de um cráton um cráton? O cráton do São Francisco e as revelações almeidianas ao delimitá-lo. In: Mantesso-Neto, V., Bartorelli, A., Carneiro, C.D.R., Neves, B.B. (Eds.), Geologia do Continente Sul-Americano, Evolução da Obra de Fernando Flávio Marques de Almeida, Beca, São Paulo, pp. 17-35.

Alkmim, F.F., Marshak, S., Pedrosa-Soares, A.C., Peres, G.G., Cruz, S., Whittington, A., 2006. Kinematic evolution of the Araçuaí–West Congo orogen in Brazil and Africa: nutcracker tectonics during the Neoproterozoic assembly of Gondwana. Precambrian Research 149, 43-64.

Alkmim, F.F., Martins-Neto, M.A., 2012. Proterozoic first-order sedimentary sequences of the São Francisco craton, eastern Brazil. Marine and Petroleum Geology 33, 127-139.

Allen, P.A., Armitage, J.J., 2012. Cratonic basins. In: Busby, C., Perez, A.A. (Eds.), Tectonics of sedimentary basins: recent advances. Wiley-Blackwell, Oxford pp. 602-620.

Almeida-Abreu, P.A., 1993. A Evolução Geodinâmica da Serra do Espinhaço Meridional, Minas Gerais, Brasil. Ph. D. Thesis, Univ. Freiburg, Freiburg, Germany, 150 pp.

Anthony, E.J., Orford, J.D., 2002. Between wave- and tide-dominated coasts: the middle ground revisited. Journal of Coastal Research, Special Issue 36, 8-15.

Barbosa, J.S.F., Sabaté, P., 2004. Archean and Paleoproterozoic crust of the São Francisco Craton, Bahia, Brazil: geodynamic features. Precambrian Research 133, 1–27.

Batista, A.J., Castro, W.B.M., Greco, F.M., 1986. Geologia da Serra do Espinhaço entre Conselheiro Mata e Rodeador, Minas Gerais. XXXIV Congresso Brasileiro de Geologia, Goiânia, Anais 2, 949-959.

Bergner, A.G.N., Strecker, M.R., Trauth, M.H., Deino, A., Gasse, F., Blisniuk, P., Dühnforth, M., 2009. Tectonic and climatic control on evolution of rift lakes in the Central Kenya Rift, East Africa. Quaternary Science Reviews 28, 2804-2816.

Bosence, D.W.J., 1998. Stratigraphic and sedimentological models of ritf basins. In: Purser, B.H., Bosence, D.W.J. (Eds.), Sedimentation and Tectonics of Rift Basins: Red Sea - Gulf of Aden. Chapman and Hall, London, pp. 9-25.

Brito Neves, B.B., Cordani, U.G., Kawashita, K., Delhal, J., 1979. A evolução geocronológica da Cordilheira do Espinhaço; dados novos e integração. Revista Brasileira de Geociências 9, 71–85.

Brito Neves, B.B. de, SÁ, J.M., Nilson, A.A., Botelho, N.F., 1995. A Tafrogênese Estateriana nos blocos paleoproterozóicos da América do Sul e processos subsequentes. Geonomos 3, 1-21.

Catuneanu, O., 2006. Principles of Sequence Stratigraphy. Elsevier, Amsterdam, 375 pp.

Catuneanu, O., Abreu, V., Bhattacharya, J.P., Blum, M.D., Dalrymple, R.W., Eriksson, P.G., Fielding, C.R., Fisher, W.L., Galloway, W.E., Gibling, M.R., Giles, K.A., Holbrook, J.M., Jordan, R., Kendall, C.G.St.C., Macurda, B., Martinsen, O.J., Miall, A.D., Neal, J.E., Nummedal, D., Pomar, L., Posamentier, H.W., Pratt, B.R., Sarg, J.F., Shanley, K.W., Steel, R.J., Strasser, A., Tucker, M.E., Winker, C., 2009. Towards the standardization of sequence stratigraphy. Earth-Science Reviews 92, 1–33.

Chaves, M.L.S., Silva, M.C.R., Scholz, R., Babinski, M., 2013. Grenvillian age magmatism in the Southern Espinhaço Range (Minas Gerais): evidence from U-Pb zircon ages. Brazilian Journal of Geology 43, 477-486.

Chemale Jr., F., Alkmim, F.F., Endo, I., 1993. Late Proterozoic Tectonism in the interior of the São Francisco Craton. In: Findlay, R.H., Banks, H.R., Veevers, J.J., Unrug, R. (Eds.), Gondwana 8: assembly, evolution and dispersal. Balkema, Rotterdam, pp. 29–41.

Chemale Jr., F., Dussin, I.A., Martins, M.S., Alkmim, F.F., Queiroga, G., 2010. The Espinhaço Supergroup in Minas Gerais: a Stenian Basin? 7th South American Symposium on Isotope Geology, Brasília, pp. 552–555.

Chemale Jr., F., Philipp, R.P., Dussin, I.A., Formoso, M.L.L., Kawashita, K., Bertotti, A.L., 2011. Lu-Hf and U-Pb age determinations of Capivarita Anorthosite in the Dom Feliciano Belt, Brazil. Precambrian Research 186, 117-126.

Chemale Jr., F., Dussin, I.A., Alkmim, F.F., Martins, M.S., Queiroga, G., Armstrong, R., Santos, M.N., 2012. Unravelling a Proterozoic basin history through detrital zircon geochronology: The case of the Espinhaço Supergroup, Minas Gerais, Brazil. Gondwana Research 22, 200-206.

Clifton, H.E., 2006. A re-examination of facies models for clastic shorelines. In: Posamentier, H.W., Walker, R.G. (Eds.), Facies Models Revisited. SEPM, Special Publication 84, pp. 293–337.

Condie, K.C., 1993. Chemical composition and evolution of the upper continental crust: Contrasting results from surface samples and shales. Chemical Geology, 104, 1–37.

Cook, R., Warren, A., Goudie, A., 1993. Desert Geomorphology. UCL Press, London, 526 pp.

Cullers, R.L., Yeh, L.-T., Chaudhuri, S., Guidotti, C.V., 1974. Rare earth elements in Silurian pelitic schists from N.W. Maine. Geochimica et Cosmochimica Acta 38, 389-400.

Cullers, R.L., 1995. The controls of the major- and trace-element evolution of shales, siltstones and sandstones of Ordovician to Tertiary age in the Wet Mountains region, Colorado, USA. Chemical Geology 123, 107–131.

Davis Jr., R.A., Hayes, M.O., 1984. What is a wave dominated coast? Marine Geology 60, 313-329.

DeCelles, P.G., Cavazza, W., 1992. Constraints on the formation of Pliocene hummocky cross-stratification in Calabria (southern Italy) from consideration of hydraulic and dispersive equivalence, grain-flow theory, and suspended-load fallout rate. Journal of Sedimentary Petrology 62, 555-568.

Dossin, I.A., Dossin, T.M., Chaves, M.L.S.C., 1990. Compartimentação Estratigráfica do Supergrupo Espinhaço em Minas Gerais - os Grupos Diamantina e Conselheiro Mata. Revista Brasileira de Geociências 20, 178–186.

Dossin, I.A., Dossin, T.M., Charvet, J., Cocherie, A., Rossi, P., 1993. Single-zircon dating by step-wise Pb-evaporation of Middle Proterozoic magmatismo in the Espinhaço range, southeastern São Francisco Craton. Minas Gerais, Brazil. Simpósio sobre o Cráton do São Francisco, 2, Salvador, 1993: Anais, Sociedade Brasileira de Geologia/Superintendência de Geologia e Recursos Minerais da Bahia, 1, pp. 39–42.

Dossin, I.A., Garcia, A.J.V., Uhlein, A., Dardenne, M.A., Dossin, T.M., 1987. Fácies eólico na Formação Galho do Miguel. Supergrupo Espinhaço (MG). Simpósio sobre Sistemas Deposicionais no Pre-Cambriano, Ouro Preto: Atas, Sociedade Brasileira de Geologia, pp. 85–96.

Dossin, I.A., Uhlein, A., Dossin, T.M., 1984. Geologia da Faixa Móvel Espinhaço em sua porção meridional, MG. Congresso Brasileiro de Geologia, 33, Rio de Janeiro: Anais, Sociedade Brasileira de Geologia, 2, pp. 3118–3132.

Dott, R.H., Bourgeois, J., 1982. Hummocky crossstratification: significance of its variable bedding sequence. Geological Society of America Bulletin 93, 663-680.

Driese, S.G., Dott, R.H., 1984. Model for sandstone-carbonate “cyclothems” based on upper member of Morgan Formation (Middle Pennsylvanian) of Northern Utah and Colorado. AAPG Bulletin 68, 574-597.

Droxler, A.W., Schlager, W., 1985. Glacial versus interglacial sedimentation rates and turbidite frequency in the Bahamas. Geology 13, 799–802.

Duke, W.L., Arnott, R.W.C., Cheel, R.J., 1991. Shelf sandstones and hummocky cross-stratification: new insights on a stormy debate. Geology 19, 625-628.

Dumas, S., Arnott, R.W.C., 2006. Origin of hummocky and swaley cross-stratification— The controlling influence of unidirectional current strength and aggradation rate. Geology 34, 1073–1076.

Dupont, H., 1995. O Grupo Conselheiro Mata no seu quadro paleogeográfico e estratigráfico. Simpósio de Geologia de Minas Gerais, Diamantina: Anais, Sociedade Brasileira de Geologia 13, pp. 9–10.

Dussin, I.A.,1994. Evolution Structurale de la pertie méridional de L'Espinhaço sur la bordure orientale du Craton São Francisco. Minas Gerais – Brésil: Um exemple de tectonique protérozoique superposé. Ph. D. Thesis, Orleans, Universite d’Orleans, 200 pp.

Dussin, I.A., Dussin, T.M., 1995. Supergrupo Espinhaço: modelo de evolução geodinâmica. Geonomos 3, 19–26.

Espinoza, J.A.A., 1996. Sistemas deposicionais e relações estratigráficas da Tectonosseqüência Conselheiro Mata, na borda leste da Serra do Cabral, Minas Gerais, Brasil. MSc Thesis, Departamento de Geologia, Escola de Minas, Universidade Federal de Ouro Preto, Ouro Preto, 66 pp.

Fernandes, L.A., Castro, A.B., Basilici, G., 2007. Seismites in continental sand sea deposits of the Late Cretaceous Caiuá Desert, Bauru Basin, Brazil. Sedimentary Geology 199, 51-64.

Fogaça, A.C.C., 1995. Geologia da Folha Diamantina. Projeto Espinhaço. Belo Horizonte, COMIG-UFMG, 98 pp.

Fraga, L.M.S., Neves, S.C., Uhlein, A., Sial, A.N., Pimentel, M.M., Horn, A.H., 2014. C-, Sr-isotope stratigraphy of carbonate rocks from the Southern Espinhaço Ridge, Minas Gerais, southeastern Brazil. Anais da Academia Brasileira de Ciências 86, 633-648.

Fryberger, S.G., Schenk, C.J., 1988. Pin stripe lamination: A distinctive feature of modern and ancient eolian sediments. Sedimentary Geology 55, 1-15.

Galloway, W.E., Hobday, D.K., 1996. Terrigenous Clastic Depositional Systems; Applications to Fossil Fuel and Groundwater Resources, Second Edition. New York, Springer, 489 pp.

Garcia, A.J.V., Uhlein, A., 1987. Sistemas deposicionais do Supergrupo Espinhaço na Região de Diamantina (MG). Simpósio sobre Sistemas Deposicionais no Pre-Cambriano, Ouro Preto, Atas, Sociedade Brasileira de Geologia, pp. 113–136.

Gawthorpe, R.L., Leeder, M.R., 2000. Tectono-sedimentary evolution of active extensional basins. Basin Research 12, 195–218.

Gromet, L.P., Dymek, R.F., Haskin, L.A., Korotev, R.L., 1984. The “North American shale composite”; Its compilation, major and trace element characteristics. Geochimica et Cosmochimica Acta 48, 2469- 2482.

Guadagnin, F., Chemale Jr., F., Magalhães, A.J., Santana, A., Dussin, I., Takehara, L., 2015. Age constraints on crystal-tuff from the Espinhaço Supergroup - Insight into the Paleoproterozoic to Mesoproterozoic intracratonic basin cycles of the São Francisco Craton. Gondwana Research 27, 363-376.

Haskin, L.A., Wildeman, T.R., Haskin, M.A., 1968. An accurate procedure for the determination of the rare earths by neutron activation. Journal of Radioanalytical Chemistry 1, 337-348.

Inman, D.L., Ewing, G.C., Corliss, J.B., 1966. Coastal sand dunes of Guerrero Negro, Baja California, Mexico. Geological Society of America Bulletin 77, 787-802.

Jackson, S.E., Pearson, N.J., Griffin, W.L., Belousova, E.A., 2004. The application of laser ablation-inductively coupled plasma-mass spectrometry to in situ U–Pb zircon geochronology. Chemical Geology 211, 47-69.

Knight, J., 2008. The environmental significance of ventifacts: A critical review. Earth-Science Reviews 86, 89–105.

Krapez, B., 1996. Sequence stratigraphic concepts applied to the identification of basin-filling rhythms in Precambrian successions. Australian Journal of Earth Sciences 43, 355-380.

Kreisa, R.D., Moiola, R.J., 1986. Sigmoidal tidal bundles and other tide-generated sedimentary structures of the Curtis Formation, Utah, Geological Society of America Bulletin 97, 381-387.

Laity, J.E., 1994. Landforms of aeolian erosion. In: A. Abrahams, A. Parsons (Eds.) Geomorphology of Desert Environments. Chapman and Hall, London, pp. 506-535

Leckie, D.A., Krystinik, L.F., 1989. Is there evidence for geostrophic currents preserved in the sedimentary record of inner to middle shelf deposits? Journal of Sedimentary Petrology 59, 862-870.

Lindsay, J.F., 2002. Supersequences, superbasins, supercontinents – evidence from the Neoproterozoic-Early Palaeozoic basins of central Australia. Basin Research 14, 207-223.

Livingstone, I., Warren, A., 1996. Aeolian Geomorphology: An Introduction. Singapore: Addison-Wesley, 211 pp.

Lopes, T.C., 2012. O Supergrupo Espinhaço na Serra do Cabral, Minas Gerais: contribuição ao estudo de proveniência sedimentar. MSc Thesis, Instituto de Geociências, Universidade Federal de Minas Gerais, Belo Horizonte, Brazil, 110 pp.

Loope, D.B., 1985. Episodic deposition and preservation of eolian sands: a late Paleozoic example from southeastern Utah. Geology 13, 73-76.

Ludwig, K.R., 2003. Using Isoplot/Ex, version 3.00, a geochronological toolkit for Microsoft Excel. Berkeley Geochronology Center, Special Publication 1, 43 pp.

Machado, N., Schrank, A., Abreu, F.R., Knauer, L.G., Almeida-Abreu, P.A., 1989. Resultados preliminares da geocronologia U/Pb na Serra do Espinhaço Meridional. Boletim da Sociedade Brasileira de Geologia, Núcleo Minas Gerais 10, pp. 171–174.

Marshak, S., Alkmim, F.F., 1989. Proterozoic contraction/extension tectonics of the Southern São Francisco Region, Minas Gerais, Brazil. Tectonics 8, 555-571.

Martins-Neto, M.A., 1996. Lacustrine fan-deltaic sedimentation in a Proterozoic rift basin: the Sopa-Brumadinho Tectonosequence, southeastern Brazil. Sedimentary Geology 106, 65-96.

Martins-Neto, M.A., 1998. O Supergrupo Espinhaço em Minas Gerais: Registro de uma Bacia Rifte-Sag do Paleo/Mesoproterozóico. Revista Brasileira de Geologia 48, 151–168.

Martins-Neto, M.A., 2000. Tectonics and sedimentation in a paleo/mesoproterozoic rift-sag basin (Espinhaço basin, southeastern Brazil). Precambrian Research 103, 147-173.

Martins-Neto, M.A., Pedrosa-Soares, A.C., Lima S.A.A., 2001. Tectono-sedimentary evolution of sedimentary basins from Late Paleoproterozoic to Late

Neoproterozoic in the São Francisco craton and Araçuaí fold belt, eastern Brazil. Sedimentary Geology 141–142, 343-370.

McLennan, S.M., 1989. Rare earth elements in sedimentary rocks: influence of provenance and sedimentary processes. In: Lipin, B.R., McKay, G.A. (Eds.), Geochemistry and Mineralogy of Rare Earth Elements Reviews in Mineralogy 21, pp. 169-200.

McLennan, S.M., Nance, W.B.,Taylor, S.R., 1980. Rare earth element - thorium correlations in sedimentary rocks, and the composition of the continental crust. Geochimica et Cosmochimica Acta 44, 1833-1839.

Megafísica Survey Aerolevantamentos S.A., 2001. Relatório final do levantamento e processamento dos dados magnetométricos e gamaespectrométricos. Levantamento Aerogeofísico de Minas Gerais, Área 4 faixa São João Chapada - Datas. Volume I, Texto técnico.

Mountney, N.P., 2006. Eolian Facies Models. In: Posamentier, H.W., Walker, R.G. (Eds.), Facies Models Revisited. Society for Sedimentary Geology, Special Publication 84, pp. 19-83.

Nio, S.D., Yang, C., 1991. Diagnostic attributes of clastic tidal deposits: a review. In: Smith, D.G., Reinson, G.E., Zaitlin, B.A., Rahmani, R.A. (Eds.), Clastic Tidal Sedimentology: Canadian Society of Petroleum Geologists, Memoir 16, pp. 3-28.

Peterson, F., 1988. Pennsylvanian to Jurassic eolian transportation systems in the western United States. Sedimentary Geology 56, 207-260.

Pflug, R., 1968. Observações sobre a estratigrafia da Série Minas na região de Diamantina, Minas Gerais. Boletim da Divisão de Geologia e Mineralogia do Departamento Nacional de Produção Mineral: Notas Preliminares, 142, 20 pp.

Plumb, K.A., 1991. New Precambrian time scale. Episodes 14, 139-140.

Prosser, S., 1993. Rift-related linked depositional systems and their seismic expression. In: Williams, G.D., Dobb, A. (Eds.), Tectonics and Seismic Sequence Stratigraphy. Geological Society, London, Special Publications 71, pp. 35–66.

Rahman M.J.J., Suzuki S., 2007. Geochemistry of sandstones from the Miocene Surma Group, Bengal Basin, Bangladesh: Implications for Provenance, tectonic setting and weathering. Geochemical Journal 41, 415-428.

Raza, M., Bhardwaj, V.R., Ahmad, A.H.M., Mondal, M.E.A., Khan A., Khan, M.S., 2010. Provenance and weathering history of Archaean Naharmagra quartzite of Aravalli craton, NW Indian Shield: Petrographic and geochemical evidence. Geochemical Journal 44, 331-345.

Reineck, H.E., Singh, I.B., 1980. Depositional sedimentary environments. Springer-Verlag, Berlin, Heidelberg, New York, 551 pp.

Reis, H.L.S., 2011. Estratigrafia e tectônica da Bacia do São Francisco na zona de emanações de gás natural do baixo Rio Indaiá (MG). MSc Thesis, Universidade Federal de Ouro Preto, Ouro Preto, Brazil, 127 pp.

Santos, M.N., Chemale Jr., F., Dussin, I.A., Martins, M.S., Assis, T.A.R., Jelinek, A.R., Guadagnin, F., Armstrong, R., 2013. Sedimentological and Paleoenvironmental Constraints of the Statherian and Stenian Espinhaço Rift System, Brazil. Sedimentary Geology 290, 47-59.

Schieber, J., 1986. Stratigraphic control of rare-earth pattern types in Mid-Proterozoic sediments of the Belt Supergroup, Montana, U.S.A.: Implications for basin analysis. Chemical Geology 54, 135-148.

Schöll, W.U., 1980. Estratigrafia, sedimentologia e paleogeografia na região de Diamantina (Serra do Espinhaço, Minas Gerais, Brasil). Münstersche Forschungen zur Geologie und Paläontologie 51, 223–240.

Schöll, W.U., Fogaça, A.C.C., 1979. Estratigrafia da Serra do Espinhaço na região de Diamantina. Simpósio de Geologia de Minas Gerais, Diamantina: Anais, Sociedade Brasileira de Geologia, pp. 55–73.

Shao, L., Stettegger, K., Garbe-Schoenberg, C.D., 2001. Sandstone petrology and geochemistry of the Turpan basin (NW China): implications for the tectonic evolution of a continental basin. Journal of Sedimentary Research 71, 37-49.

Silveira, E.M., Söderlund, U., Oliveira, E.P., Ernst, R.E., Menezes Leal, A.B., 2013. First precise U-Pb baddeleyite ages of 1500 Ma mafic dykes from the São Francisco Craton, Brazil, and tectonic implications. Lithos 174, 144–156.

Slack, J.F., Stevens, B.P.J., 1994. Clastic Metasediments of the Early Proterozoic Broken-Hill Group, New-South-Wales, Australia - Geochemistry, Provenance, and Metallogenic Significance. Geochimica et Cosmochimica Acta 58, 3633-3652.

Sloss, L.L., 1963. Sequences in the Cratonic Interior of North America. Geological Society of America Bulletin 74, 93-114.

Southard, J.B., Lambie, J.M., Federico, D.C., Pile, H.T., Wideman, C. R., 1990. Experiments on bed configurations in fine sand under bidirectional purely oscillatory flow, and origin of hummocky cross stratification. Journal of Sedimentary Petrology 60, 1-17.

Souza Filho, R.C., 1995. Arcabouço estrutural da porção externa da Faixa Araçuaí na Serra do Cabral (MG) e o contraste de estilos deformacionais entre os Supergrupos Espinhaço e São Francisco. MSc Thesis, Universidade Federal de Ouro Preto, Ouro Preto, Brazil, 148 pp.

Swift, D.J.P., Figueiredo, A.G., Freeland, F.L., Oertel, G.F., 1983. Hummocky cross-stratification and megaripples: a geological double standard? Journal of Sedimentary Petrology 53, 1295-1318.

Tape, C.H., Cowan, C.A., Runkel, A.C., 2003. Tidal-bundle sequences in the Jordan Sandstone (Upper Cambrian), southeastern Minnesota, USA: Evidence for tides along inboard shorelines of the sauk epicontinental sea. Journal of Sedimentary Research 73, 354-366.

Tate, M.P., 1993. Structural framework and tectono-stratigraphic evolution of the Porcupine Seabight Basin, offshore western Ireland. Marine and Petroleum Geology 10, 95–123.

Taylor, S.R., McLennan, S.M., 1985. The continental crust: its composition and evolution. Oxford, Blackwell, 312pp.

Tripathi, K.J., Rajamani, V., 2003. Geochemistry of Proterozoic Delhi quartzite: Implications for the provenance and source area weathering. Journal of the Geological Society of India 62, 215–226.

Uhlein, A., Trompette, R., Egydio-Silva, M., 1998. Proterozoic rifting and closure, SE border of the São Francisco Craton, Brazil. Journal of African Earth Sciences 11, 191–203.

Walker, R.G., 1984. Shelf and shallow marine sands. In: Walker, R.G. (Ed.), Facies Models, Second Edition. Geological Association of Canada, Geoscience Canada Reprint Series 1, pp. 141-170.

CAPÍTULO III

Lu-Hf and U-Pb signature of the Espinhaço intracratonic basin for tracking evidence of the Columbia Supercontinent and the Grenville Orogeny in the São Francisco Craton

From: santosh@cugb.edu.cn
To: marcelodega@hotmail.com
Date: Mon, 8 Jun 2015 23:41:08 +0100
Subject: Submission Confirmation

Article Type: Research Paper

Dear Dr. Marcelo Santos,

Your submission entitled "Lu-Hf and U-Pb signature of the Espinhaço intracratonic basin for tracking evidence of the Columbia Supercontinent and the Grenville Orogeny in the São Francisco Craton" has been received by Gondwana Research

You may check on the progress of your paper by logging on to the Elsevier Editorial System as an author. The URL is http://ees.elsevier.com/gr/.

Your username is: marcelodega@hotmail.com
Your password is: *******

Your manuscript will be given a reference number once an Editor has been assigned.

Thank you for submitting your work to this journal.

Kind regards,

Elsevier Editorial System
Gondwana Research

Lu-Hf and U-Pb signature of the Espinhaço intracratonic basin for tracking evidence of the Columbia Supercontinent and the Grenville Orogeny in the São Francisco Craton

M.N. Santos[1,2]*, F. Chemale Jr.[1], I.A. Dussin[3], C. C. Lana

1 – Programa de Pós-Graduação em Geologia, Instituto de Geociências, Universidade de Brasília, 70904-970, Brasília, DF, Brazil

2 – PETROBRAS/E&P-EXP, Avenida República do Chile, 330 – Centro, 20031-170, Rio de Janeiro, RJ, Brazil

3 – Faculdade de Geologia, Universidade do Estado do Rio de Janeiro, 20550-013, Rio de Janeiro, RJ, Brazil

4 – Departmento de Geologia, Escola de Minas, Universidade Federal de Ouro Preto, 35400-000, Ouro Preto-MG, Brazil

* Corresponding author at: PETROBRAS/E&P-EXP, Avenida República do Chile, 330 – Centro, 20031-170, Rio de Janeiro, RJ, Brazil.

Tel.: +55 38 9178 8699.

E-mail address: marcelodega@hotmail.com (M. Santos).

Abstract

The Espinhaço Basin comprises two metasedimentary sequences developed in the São Francisco Craton and its margins during the Paleo- and Mesoproterozoic Eras in eastern Brazil. Whole-rock geochemistry and combined U-Pb and Lu-Hf in situ analyses of zircon indicate that an Archean continental crust periodically melted to generate magmatism at c. 2900–2600, 2200–1950, 1800–1680 and 1250–1150 Ma in the source areas of the basin. The main source, dated at 2-2.1 Ga, shows a predominance of juvenile materials (positive $\varepsilon_{Hf}(t)$ values) with some reworking of the Archean crust, suggesting the presence of a continental magmatic arc west of the craton that is related to the collisional event associated with the assembly of the Columbia Supercontinent. During the lifespan of this landmass, certain processes were imprinted in the Espinhaço Basin as sediment recycling and changes in the sedimentary provenance related to changes in the paleocurrent directions and the depositional systems. The upper sequence also records far-field stress transmissions from the Grenville Orogeny, leading to the reactivation of Paleoproterozoic extensional faults at c. 1.2 Ga. The investigation of such Proterozoic basins provides important information about the sedimentary and tectonic history of the São Francisco Craton and will therefore help researchers improve kinematic reconstruction models of the Columbia paleoplates.

Keywords: Stenian; Statherian; Espinhaço Basin; U-Pb zircon geochronology; Lu-Hf isotope analyses; Columbia Supercontinent; Grenville Orogeny.

1 Introduction

The lack of fossil content in Proterozoic basins is a major problem for the appropriate positioning of stratigraphic sequences contained therein and results in problems when correlating sedimentary units in different depocenters and preventing accurate tectonic and paleogeographic reconstructions. However, the study of sedimentary provenance applied to such basins is an important tool for elucidating the characteristics of stratigraphic and tectonic evolution and contributes to the identification of depositional sequences and potential source areas (Haughton et al., 1991). Some of the most accurate methods used for analyzing sedimentary provenance include the evaluation of detrital zircon age spectra with combinations of U-Pb and Lu-Hf during in situ analyses of zircon and whole-rock geochemical data (Howard et al., 2011; Thomas, 2011; Nebel-Jacobsen et al., 2011; Zhang et al., 2014).

A few recent papers have described the tectonic and sedimentological aspects of the Proterozoic sedimentary sequences that cover the São Francisco Craton based on their detrital zircon U-Pb ages (Chemale et al., 2012; Santos et al., 2013; Santos et al., 2015; Guadagnin and Chemale, 2015). However, the presence and abundance of a zircon population of a particular age in a given sedimentary rock sample is not sufficient to precisely identify the source rocks, given that different crustal blocks of the same age might have served as source areas (Bahlburg et al., 2010). Therefore, an additional procedure is necessary to recognize possible differences in the crustal evolution of these blocks. The combination of U-Pb with Lu-Hf isotope systems in detrital zircon grains with recently developed in situ analysis has become an important tool for dating magmatic events, distinguishing juvenile from evolved crustal sources, identifying the degree of crustal reworking in the source region and dating the crustal residence time of the zircon protoliths (Iizuka et al., 2005; Morag et al., 2011; Willner et al., 2011).

This paper examines two metasedimentary successions that occupy the same depositional locus in the Espinhaço Basin, which was developed at the border and within the São Francisco Craton during the Paleo- to Mesoproterozoic (Fig. 1; Alkmim et al., 1993; Dussin and Dussin, 1995; Brito Neves, 1995; Uhlein et al., 1998; Santos et al., 2013). Recent studies have shown that a gap of approximately 500 Ma exists between the two distinct rift phases of the basin, with sequences deposited during the Statherian (1.7 Ga) and Stenian (1.2 Ga; Chemale et al., 2010 and 2012; Santos et al., 2013). However, zircon grains dated to 1.2 Ga were found in a half-graben far from the defined type sections, which raised doubts regarding whether the value would be representative of the entire basin. Samples of the basement and all units of the basin were analyzed (with the exception of the Córrego da Bandeira

Formation), resulting in new detrital zircon U-Pb ages and Lu-Hf isotopes for the Espinhaço Basin. Based on these results, we constrained the age of the sequences and the zircon provenance and estimated the mode of crustal formation (juvenile vs. reworking) in the source region.

The data described in this paper contribute to a broad understanding of the development of Paleo- and Mesoproterozoic sequences in the São Francisco Craton and provide a basis for future correlations and supercontinent reconstructions. To determine the probable source rocks for the Espinhaço Basin, we compared our isotopic and geochemical data with data from gneiss and leucogranite from the Gouveia Complex (Chaves and Coelho, 2013), which is located near our study area (Fig. 1).

2 Geological setting

2.1 Espinhaço Basin

The Serra do Espinhaço mountain range has northern and southern geomorphological sectors located in the states of Bahia and Minas Gerais, Brazil, respectively (Saadi,1995). The Espinhaço Basin rocks outcrop in the Serra do Espinhaço and are generally partially deformed and metamorphosed at low grades due to the Brasiliano Event (Uhlein, 1991; I.A. Dussin, 1994; Dussin and Dussin, 1995). Recent geochronological data indicate that the basin in the northern sector contains a record of three second-order depositional sequences, which allows the lower, middle and upper Espinhaço Sequence layers that were deposited during the Statherian (~1.7 Ga), Calymmian to Ectasian (1.6 Ga to 1.38 Ga) and Stenian periods (~1.2 Ga; Plumb, 1991; Guadagnin et al., 2015), respectively, to be subdivided. However, in the southern sector, the record of the Middle Espinhaço Basin does not occur, potentially due to erosion or because the region would have remained as a topographic high during that period (Chemale et al., 2012; Santos et al., 2015). This paper describes and analyzes the geology in the southern Espinhaço sector.

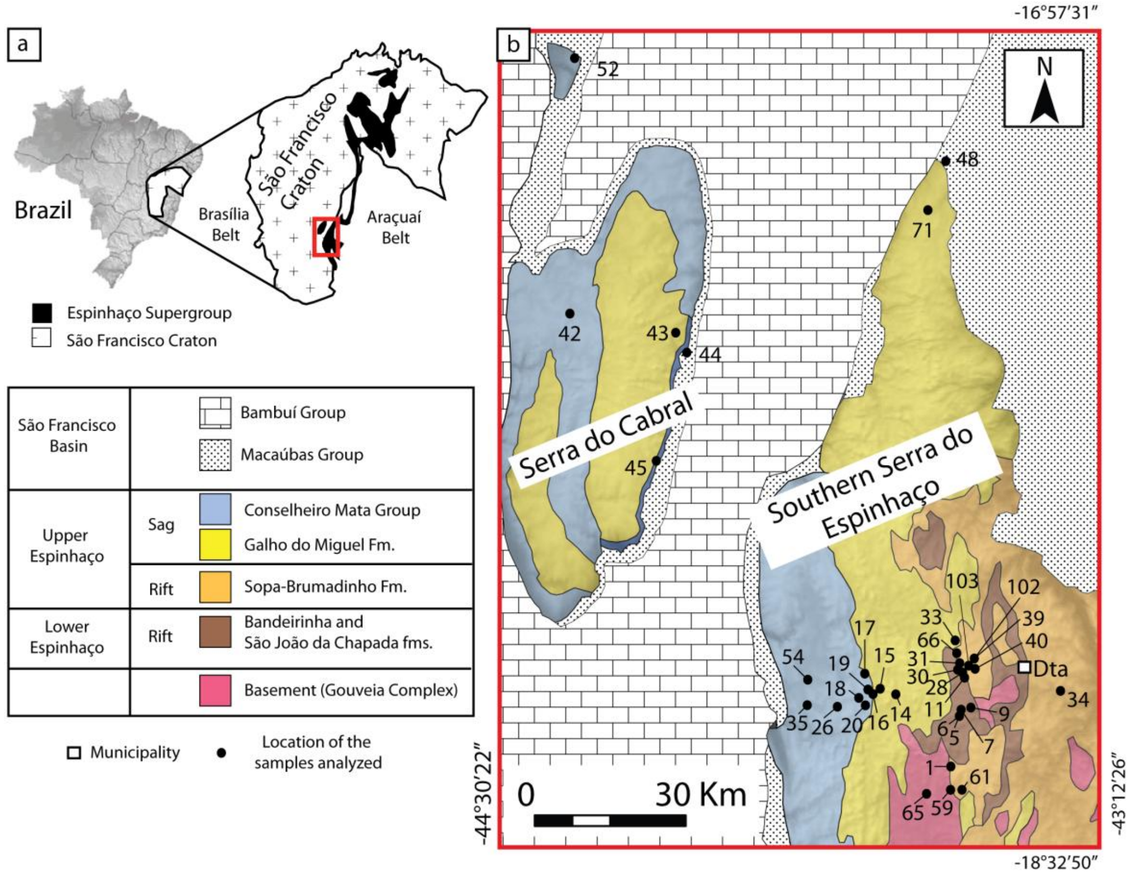

Fig. 1. Location (a) and simplified map (b) of the Espinhaço Basin in the southern Serra do Espinhaço and Serra do Cabral region indicating the sampling sites of the analyzed samples. Modified after Souza Filho (1995), Fogaça (1995) and Alkmim et al. (2006). Dta- Diamantina.

2.1.1 Lower Espinhaço Sequence

Integrated field and geochronological data indicate the opening of a rift and subsequent deposition of sedimentary and volcanic rocks during the Statherian Period (Dussin and Dussin, 1995; Almeida-Abreu, 1995; Uhlein et al., 1998; Martins-Neto, 2000; Uhlein and Chaves, 2001). In addition to the rocks of granitic composition at the base of the basin dated using U/Pb and Pb/Pb zircon methods (which provide ages of 1770 Ma and 1729 Ma, respectively; Brito Neves et al., 1979; Dossin et al., 1993), the zircon data from volcanic rocks intercalated with sedimentary rocks (1710 and 1703 Ma; Dossin et al., 1993; Chemale et al, 2012) indicate the approximate ages of the opening and deposition during that period.

Two distinct rifting stages conditioned the deposition of sediments in the Bandeirinha and São João da Chapada formations (Fig. 2). The Bandeirinha Formation contains fluvial sandstones, conglomerates of limited lateral continuity deposited by alluvial fans and subordinate eolian deposits (Silva, 1998). The São João da Chapada Formation contains sedimentary breccias at the base, predominance of quartzites deposited by a braided fluvial system and pelitic facies deposited by a lacustrine system at the top (Schöll and Fogaça, 1979; Garcia and Uhlein, 1987; Silva, 1998; Martins-Neto, 1998; Santos et al., 2013).

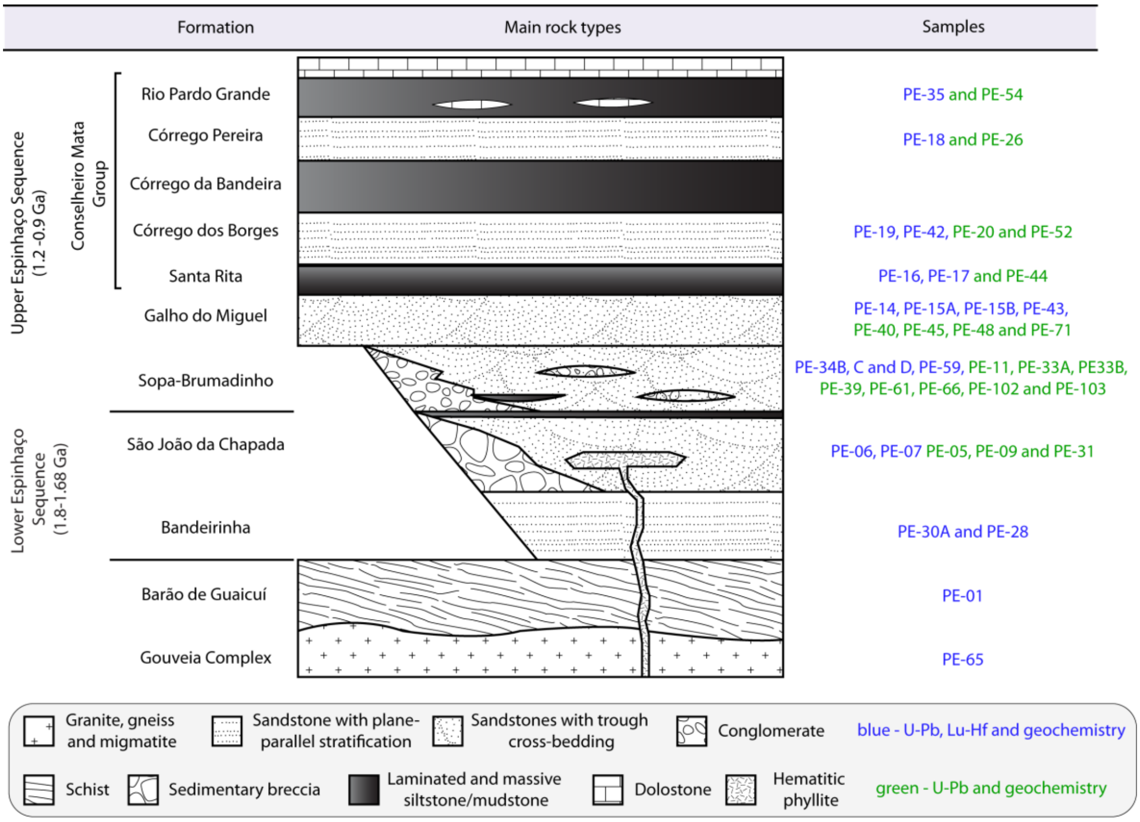

Fig. 2. Stratigraphic nomenclature for the Espinhaço Basin according to Pflug (1968) and Dossin et al. (1984) showing the locations of the analyzed samples. Not to scale.

2.1.2 Upper Espinhaço Sequence

The Upper Espinhaço Sequence is represented by the Sopa-Brumadinho Formation (rift phase), the Galho do Miguel Formation (transitional phase) and the Conselheiro Mata Group (sag phase), which were developed during the Stenian Period (Fig. 2; Uhlein, 1991; Martins-Neto, 1998; Chemale et al., 2012;

Santos et al., 2013). Before the data obtained by Chemale et al. (2010), the Sopa-Brumadinho Formation was considered to contain the record of another pulse in the Statherian rift (Almeida-Abreu, 1995). However, this geological unit records the formation of a new basin, a rift-sag that developed after a gap of approximately 500 Ma. In addition, this unit consists of diamond-bearing conglomerates deposited by alluvial fans and lacustrine fan-delta and quartzite deposited by a braided fluvial system with a deposition age of 1.2 Ga (Pflug, 1968; Schöll and Fogaça, 1979; Dossin et al., 1990; Chaves, 1997; Martins-Neto et al., 2001; Chemale et al., 2012).

The transition to the sag phase is marked by the presence of a coastal system with eolian and shallow marine deposits, which resulted in the extrapolation of the sedimentation area beyond the rift boundaries (Uhlein et al., 1998; Martins-Neto et al., 2001), as evidenced by the Galho do Miguel Formation that lies directly on the basement (Schöll and Fogaça, 1979). The Conselheiro Mata Group is formed by the intercalation of units composed essentially of phyllites and quartzites and is subdivided into the Santa Rita, Córrego dos Borges, Córrego da Bandeira, Córrego Pereira and Rio Pardo Grande formations (Pflug, 1968; Dossin et al., 1984), which represent successive marine transgressions and regressions developed during the sag phase (Dupont, 1995; Espinoza, 1996; Santos et al., 2015).

3 Methodology

In this study, detailed geological mapping of the sequences deposited in the rift stages was performed at a scale of 1:3,000, and sag phase sequences were mapped at a scale of 1:25,000. Full descriptions of lithofacies were observed from the geological sections and are presented in detail by Santos et al. (2013) and Santos et al. (2015). We analyzed 2625 zircon grains using the U-Pb method (40 samples), 336 zircon grains using the Lu-Hf method (20 samples) and 45 samples for whole-rock geochemistry.

For isotopic analysis, each rock sample was crushed and milled using a jaw crusher. Zircon populations were separated using the conventional hand-panning procedure, a Frantz Isodynamic Magnetic Separator, heavy liquids and picking by hand under a binocular lens. The zircon grains were photographed in transmitted and reflected light and imaged using BSE (backscattered electrons) and CL (cathodoluminescence).

U-Pb dating of the zircon grains was performed using two different types of equipment. The first type was a laser ablation microprobe (New Wave UP213) coupled to a MC-ICP-MS (Neptune) located in the isotope laboratories at the Universities of Brasília and Rio Grande do Sul (Brazil). Isotope data were acquired in static mode using spot sizes of 25 and 40 µm. Laser-induced elemental fractionation and instrumental mass discrimination were corrected using a reference zircon (GJ-1; Jackson et al., 2004), and two GJ-1 measurements were performed after every ten zircon sample spots. The external error was calculated based on the propagation error of the GJ-1 mean and the individual sample zircons (or spots). The U-Pb SHRIMP (Sensitive High Resolution Ion Microprobe) zircon geochronology was performed at the Research School of Earth Sciences at Australian National University using SHRIMP II equipment. The zircon grains were analyzed with a 2-3 nA, 10 kV primary O2- beam focused to a ~25 to ~20 µm diameter spot size. At a mass resolution of ~5500, the Pb, Th and U isotopes were resolved from all major interferences. The U and Th concentrations were determined relative to those measured in the RSES standard SL13. Histograms were prepared using Isoplot/Ex (Ludwig, 2003). For the detrital zircon histogram, we used zircon data with discordance equal to or less than 10%. Detailed analytical procedures can be found in Chemale et al. (2011).

A Photon-Machines (ArF excimer laser 193 nm) laser ablation system coupled to a Neptune MC-ICPMS at the Isotope Facility of the Universidade Federal de Ouro Preto (UFOP) was used in this study to measure Lu, Yb and Hf isotopic signatures in zircons from sedimentary samples of the Espinhaço Supergroup - Meridional Espinhaço range. The standards used during Hf analysis were GJ-1 (Morel et al, 2008), 91500 and Mud Tank (Woodhead and Hergt, 2005). The $^{176}Hf/^{177}Hf$ accepted values for the standards were reproduced within acceptable error during all analytical sessions, yielding within-run results of 0.282010 ± 0.000011 (n = 18, 2SD) for GJ-1, 0.282293 ±

0.000015 (n = 4, 2SD) for 91500 and 0.282502 ± 0.000002 (n = 9, 2SD) for Mud Tank.

Laser energy of approximately 5 J/cm^2 with a repetition rate of 5 Hz and a spot size of 50 µm was used for all analyses. To improve the sensibility, N (~0.080 l/min) was mixed with Ar and He (+sample) gas in a gas mixer (Squid) before entering the torch. The typical signal intensity was 10 V for ^{180}Hf. A user-selected interval of approximately 60 data points covering the sample transient peak was used to calculate the Hf ratio with a mass bias correction by using the exponential law. The ^{175}Lu, ^{171}Yb and ^{173}Yb isotopes were monitored during analysis, and their relative abundances were used to calculate ^{176}Lu and ^{176}Yb interferences, which were subtracted from ^{176}Hf. The data were corrected in an Excel spreadsheet offline using ^{179}Hf/^{177}Hf = 0.7325 (Patchett et al., 1981), ^{176}Lu/^{175}Lu = 0.2658 (JWG in-house value), and ^{176}Yb/^{173}Yb = 0.796218 (Chu et al. 2002) (see Gerdes and Zeh 2006).

4 Results

4.1 Geochemistry

The geochemical classification of terrigenous sedimentary rocks is based on certain major elements (Si_2O/Al_2O_3, Na_2O/K_2O and Fe_2O_3/K_2O) and has been widely used to discriminate between mature and immature sediments (Pettijohn and Potter, 1972; Herron, 1988) and provide important information about the nature of source rocks. One of the most frequently used diagrams for classifying sedimentary rocks uses Si_2O/Al_2O_3 and Fe_2O_3/K_2O, of which Si_2O/Al_2O_3 reflects the abundance of quartz and feldspar and the clay content and Fe_2O_3/K_2O enables the separation of lithic sands (litharenites and sublitharenites) from feldspathic sands (arkoses and subarkoses) and is a measure of mineral stability because ferromagnesian minerals are more susceptible to chemical alteration by weathering (Herron, 1988). Based on the diagram presented by Herron (1988) (Fig. 3), the samples were primarily classified as quartzarenite (n = 29) and subarkose (n = 5), which is consistent with their petrographic classification. Three other samples were classified as arkose, one as greywacke and one as sublitharenite, which can be attributed to variations in the sericite contents among these rock types.

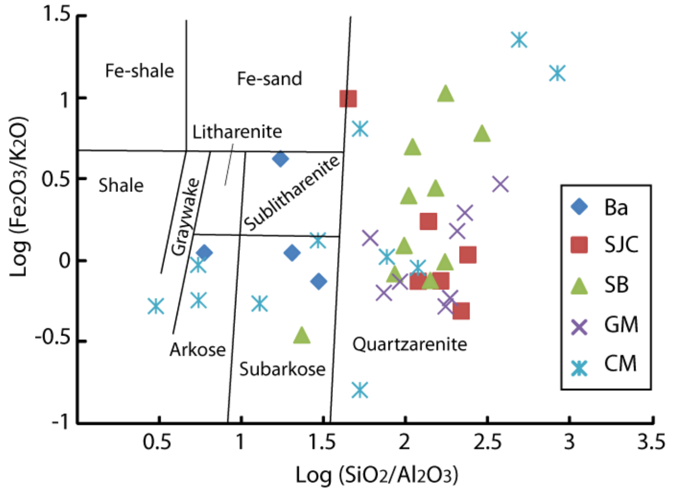

Fig. 3. Geochemical classification diagram of the Espinhaço Basin samples according to their logarithmic ratios of SiO_2/Al_2O_3 vs. Fe_2O_3/K_2O (after Herron, 1988). The samples mainly fall into the quartzarenite field. Ba- Bandeirinha Fm.; SJC- São João da Chapada Fm.; SB- Sopa-Brumadinho Fm.; GM- Galho do Miguel Fm.; and CM- Conselheiro Mata Group.

The major and trace element concentrations in the Espinhaço Basin are given in Appendix A (electronic supplementary material), and the ratios between elements are summarized in Table 1. Most of the analyzed samples have high chemical maturity because they are enriched in SiO_2 and depleted in other major and trace elements. A geochemical analysis shows that the SiO_2 content ranges from 66.75% to 99.95%, the Al_2O_3 content ranges from 0.12% to 22.9% and the Fe_2O_3 (total Fe as Fe_2O_3) + MgO content is approximately 0.34%. The depletion of Na_2O + CaO (usually below 0.2%) can be attributed to a relatively smaller amount of plagioclase in the rock samples, which is consistent with petrographic data and shows that, when present, K-feldspar (microcline) dominates over plagioclase feldspar.

All of the samples display negative linear trends for SiO_2 versus TiO_2, Al_2O_3, Fe_2O_3, MgO and K_2O. However, the same major oxides are positively correlated with Al_2O_3, most likely due to the presence of clay minerals that control the K_2O, Fe_2O_3 and MgO contents and may reflect the occurrence of Fe and Ti oxides associated with the clays. The strong negative correlation for SiO_2

vs. Al_2O_3 (r = -0.86), K_2O (r = -0.83), MgO (r = -0.82) and TiO_2 (r = -0.72) observed in the Sopa-Brumadinho Fm. indicates a decrease in the unstable components, such as feldspars and rock fragments, and an increase in mineralogical and chemical maturity. Samples more enriched in aluminum (22.9%), potassium (4.1%) and iron (3.9%) were found in the pelites of the Santa Rita Fm. because their modal compositions include high sericite, feldspar and hematite contents.

Positive correlations between Yb-Y (r = 0.98), Th-Ce (r = 0.66) and Ce-La (r = 0.96) for all sampling units (Fig. 4a, b and c) suggest coherent geochemical behavior that is most likely controlled by the stability of accessory monazite. Another significant correlation is observed between Zr-Hf (r = 0.98), which agrees with the expectation that the Hf abundance is controlled by chemical substitution in accessory minerals such as zircon. The abundances of light and heavy rare earth elements (LREE and HREE) are positively correlated with P_2O_5 (r = 0.64) and Zr (r = 0.61), respectively.

The $(La/Lu)_n$ values (subscript n refers to chondrite-normalized values) range from 4.6 to 57.6, the La/Sc values range from 1.0 to 14.75, the La/Yb values range from 6.7 to 82.2, the La/Th values range from 1.1 to 14.2 (Fig. 4d), the Th/Sc values range from 0.4 to 6.2, the Zr/Sc values range from 9.5 to 157.5, and the Th/U values range from 2.5 to 30.32 (Table 1). The ratios of the chemical elements are more effective for chemical comparisons than absolute abundances, mainly due to the dilution effect of quartz, which results in variations in the absolute abundances. All samples from the Espinhaço Basin (with the exception of the Córrego da Bandeira Formation, which was not analyzed) show significant enrichment in the LREE, with La values reaching approximately 5-128 times greater than that of chondrite. This enrichment results in a steep LREE pattern and a relatively flat HREE pattern (Fig. 5a, b and c). One sample of a conglomerate (PE-EX-34C) is distinctive because it has a very high light REE (LREE) content (La_n = 321). The Eu/Eu* values $(Eu/(Sm_n \times Gd_n)^{0.5})$ in chondrite are normalized over a range of 0.35 to 0.75, indicating significant depletion in Eu. Despite the depleted REE abundances in comparison with the NASC's composition, which most likely resulted from the quartz dilution effect (Taylor and McLennan, 1985), the REE pattern remains similar to that of the North American shale composite (NASC) (Haskin et al., 1968).

Table 1. Range of elemental ratios of the Espinhaço Basin samples compared with similar elemental ratios derived from felsic rocks, mafic rocks and the upper continental crust.

Elemental Ratio	Range of samples from Espinhaço Basin[1]	Range of sediment from felsic sources[2]	Range of sediment from mafic sources[2]	Upper continental crust[3]
(La/Lu)n	4.68-57.61	3.00-27.00	1.10-7.00	9.73
La/Sc	1.05-14.75	2.5-16.3	0.43-0.86	2.21
Th/Sc	0.46-6.25	0.84-20.5	0.05-0.22	0.79
Eu/Eu*	0.35-0.75	0.40-0.94	0.71-0.95	0.63

[1] This study; [2] Cullers (2000); [3] Taylor and McLennan (1985)

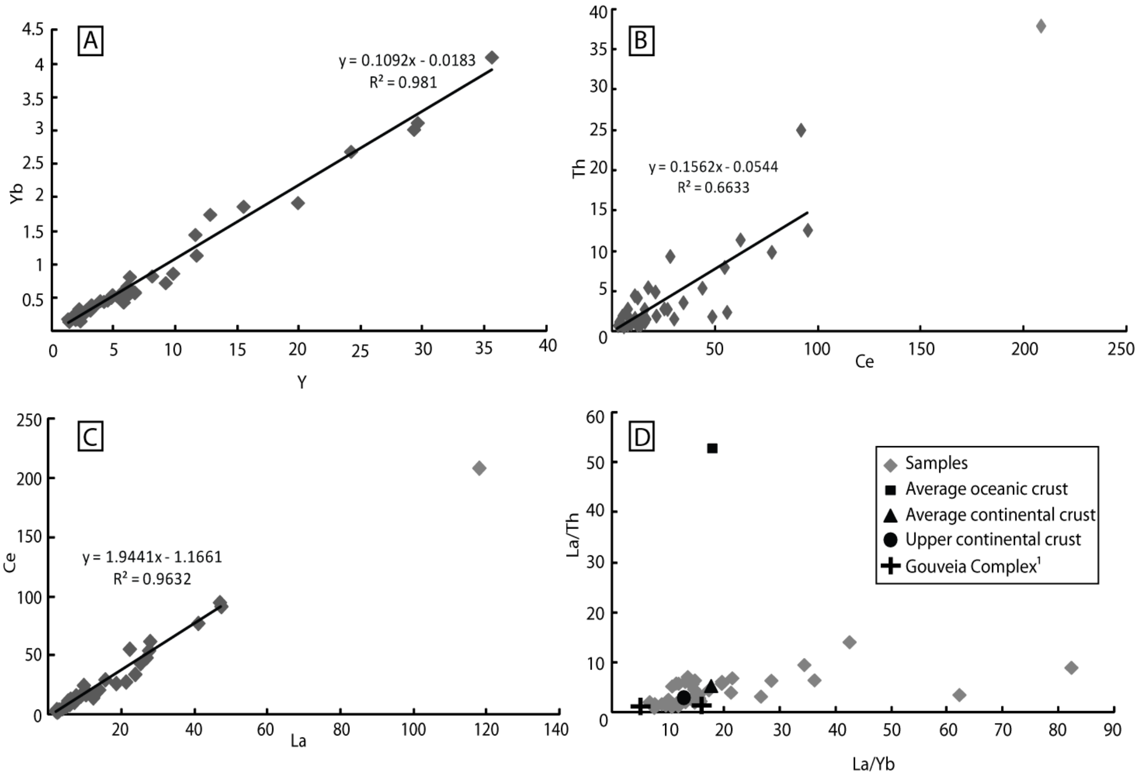

Fig. 4. Trace-element chemical variations (in ppm) for clastic metasediments of the Espinhaço Basin. (a) Y vs. Yb; (b) Ce vs. Th; (c) La vs. Ce; and (d) La/Yb vs. La/Th. Regression lines in (b) and (c) were calculated by excluding the data points with high Ce, Th and La values (sample PE-EX-34C). In (d), most samples are near the composition of the upper continental crust and the Gouveia Complex. The average values for the oceanic and continental crust were obtained

from Shao et al. (2001), and those for the Gouveia Complex were obtained from Chaves and Coelho (2013) (samples 1 and 18).

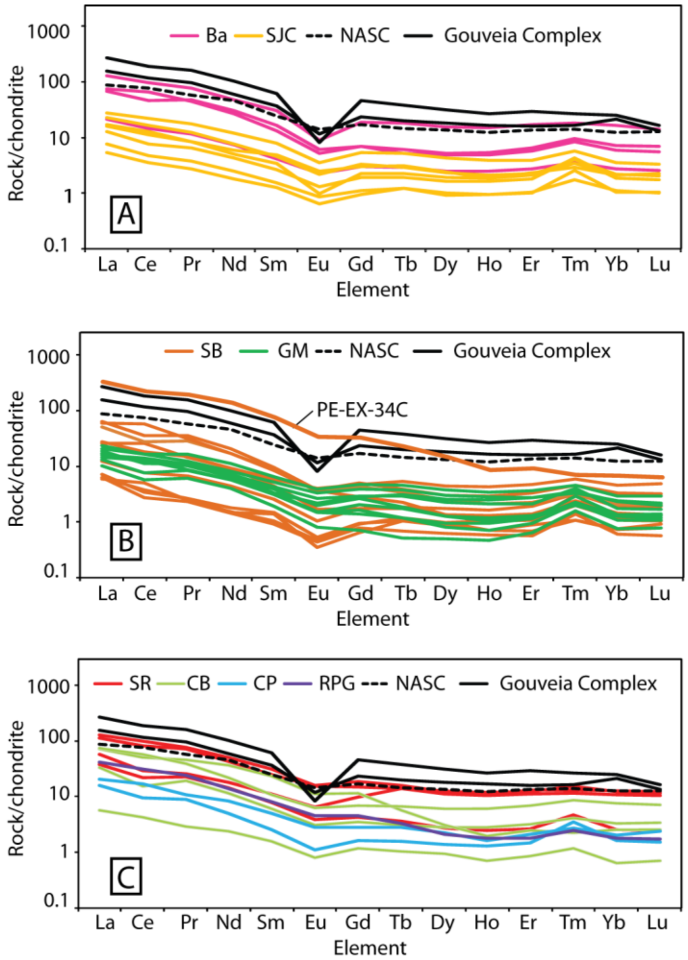

Fig. 5. Chondrite-normalized REE patterns for samples from the (a) Bandeirinha (Ba) and São João da Chapada formations (SJC); (b) Sopa-Brumadinho (SB) and Galho do Miguel formations (GM); (c) Santa Rita (SR), Córrego dos Borges (CB), Córrego Pereira (CP) and Rio Pardo Grande formations (RPG). For comparison, we use the North American shale composite (NASC) (Haskin et al., 1968) and the Gouveia Complex values (samples 1 and 18 from Chaves and Coelho, 2013). The chondrite values are from Taylor and McLennan (1985).

4.2 U-Pb zircon dating and Lu-Hf isotope analyses

The U-Pb and Lu–Hf data from the zircons are also given in Appendix A and are summarized in Figs. 6-9. The gneiss sample of the crystalline basement (PE-GO-65) has an upper-intersection U-Pb age of 2828 Ma and presents a homogenous initial $\varepsilon_{Hf}(t)$ ranging from -1 to +1.3 (Fig. 8), unlike the schist sample from the Barão de Guaicuí Formation (PE-GO-01), which is characterized by a wide variation in the initial $\varepsilon_{Hf}(t)$ in both the Archean (2692 to 3131 Ma) and Rhyacian zircon grains (2114 to 2124 Ma), with $\varepsilon_{Hf}(t)$ ranging from -11.8 to +6.2 and -18.7 to +1.4, respectively (Fig. 8).

The geochronological analyses of the two sandstone samples of the Bandeirinha Formation (PE-GO-28 and PE-GO-30A) show detrital zircon grains formed in the Archean and Paleoproterozoic. Only 98 out of the 180 analyzed grains were effectively used because they showed a degree of concordance of between 90 and 110%. The grain population formed in the Neoarchean (22%; 2.5 to 2.8 Ga) predominates over the Mesoarchean (7%; 2.8 to 3.2 Ga) and Paleoarchean grains (2%; 3.2 to 3.6 Ga), with peaks at 3272 Ma, 3076 Ma, 2838 Ma and 2664 Ma (Figs. 6 and 7). However, the Paleoproterozoic grains are dominant, with populations that formed during the Siderian (19%; 2.3 to 2.5 Ga), Rhyacian (25%; 2 to 2.3 Ga), Orosirian (8%; 1.8 to 2 Ga) and Statherian (17%; 1.6 to 1.8 Ga) periods (Plumb, 1991) and peaks at 2468 Ma, 2155 Ma and 1785 Ma (the last age is considered the maximum depositional age for the Banderinha Formation) (Santos et al., 2013). The two analyzed samples show similar Hf isotopic compositions (Fig. 8). Paleoarchean zircon grains with ^{207}Pb–^{206}Pb ages between 3.2 and 3.3 Ga are characterized by $\varepsilon_{Hf}(t)$ ranging from -3.9 to 0.4, whereas Neoarchean grains (2.5 to 2.8 Ga) have $\varepsilon_{Hf}(t)$ values from -8 to +8.2. Zircon grains with ages between 2 and 2.5 Ga show a wide variation in the initial $\varepsilon_{Hf}(t)$, with values ranging from -15.4 to +4.5. The grains formed during the Statherian Period (~1.7 Ga) show strongly negative $\varepsilon_{Hf}(t)$ values ranging from -16.9 to +0.8.

Four sandstone samples in the São João da Chapada Formation were analyzed (214 concordant zircon grains from 297). The detrital zircon grains provided similar ages to those of the Bandeirinha Formation but with a moderate change in the proportion of the population of grains formed during the Paleoproterozoic. The grains formed in the Paleoarchean (2%), Mesoarchean (7%) and Neoarchean (21%) maintained their relative proportions (Figs. 6 and 7). Compared with the Bandeirinha Formation, the percentage of Siderian grains decreased to 5%, the percentage of Rhyacian grains doubled to 48%, the percentage of Orosirian grains remained constant at 8% and the percentage of Statherian grains decreased to 9%. Main peaks occurred at 2138 Ma and 2702 Ma, and secondary peaks occurred at 1713 Ma, 2366 Ma, 2835 Ma and 3338 Ma. The sandstone sample PE-SM-07 analyzed for Lu-Hf shows Archean zircon grains (2.7 to 2.9 Ga) with Hf isotopic compositions similar to the basement sample and $\varepsilon_{Hf}(t)$ values from -0.3 to -1.1 (Fig. 8). Of the two Siderian grains analyzed, one has an $\varepsilon_{Hf}(t)$ value of -5.3, and another has a value of +4.2. The Rhyacian and Statherian grains have a relatively narrow initial $\varepsilon_{Hf}(t)$ range, with values ranging from +3.3 to +3.9 and -9.6 to -8.4, respectively. The hematitic phyllite sample (PE-SM-06), whose crystallization age is also Statherian (Dossin et al., 1993; Chemale et al, 2012), shows three grains with $\varepsilon_{Hf}(t)$ values of between -6.2 and -4.6 at 1.7 Ga. However, the hematitic phyllite also has inherited zircons with Neoarchean and Rhyacian ages and $\varepsilon_{Hf}(t)$ values ranging from -8.4 to -7.8 and +0.8 to +4.4, respectively, except for one grain that has an $\varepsilon_{Hf}(t)$ of -18.8.

Twelve samples of the Sopa-Brumadinho Formation were analyzed, including nine collected from hemigrabens located on the western edge of the Espinhaço rift system between the municipalities of Diamantina and Gouveia, and three from hemigrabens located on the eastern edge of the rift in the Extração region (accounting for 658 concordant zircon grains of the 806 analyzed). In the histogram shown in Fig. 7, it is possible to observe main peaks at 2148 Ma and 2719 Ma in the samples from both edges of the rift. The main difference in the geochronological signature between the two regions refers to a secondary peak at 1749 Ma present on the western edge and a secondary peak at 1182 Ma present on the eastern edge. Although the presence of zircon grains formed between 1.2 and 1.6 Ga is nearly imperceptible in Fig. 7C, these grains occur on the western edge, as evidenced by subordinated peaks (2% of the grains) with similar Hf isotopic compositions. The maximum depositional age for the Sopa-Brumadinho Formation is 1182 Ma (Chemale et al., 2010 and 2011), whose zircon grains are characterized by a wide range of $\varepsilon_{Hf}(t)$ values, from -20 to +4.7. The Archean grains with ages between 2.5 and 2.9 Ga have predominantly negative $\varepsilon_{Hf}(t)$ values, ranging from -12.5 to +0.9 (Fig. 9a). The only Paleoarchean grain analyzed has an initial $\varepsilon_{Hf}(t)$ value of -10.8. The populations of the Rhyacian and Orosirian Periods (ages between 1.8 and 2.2

Ga) show two distinct groups based on their initial Hf isotope values, one with strongly negative $\varepsilon_{Hf}(t)$ values from -17.5 to -9.5 and another with $\varepsilon_{Hf}(t)$ values from -4.2 to +4, which coincide with the values of a quartzite pebble sample contained in conglomerate with $\varepsilon_{Hf}(t)$ values from -4.1 to +6 (PE-EX-34B). The two analyzed Statherian grains have negative $\varepsilon_{Hf}(t)$ values of -9.9 to -9.6. Except for the Mesoproterozoic zircon grains, the relative proportions of the populations have remained approximately constant relative to the São João da Chapada Formation (Fig. 6).

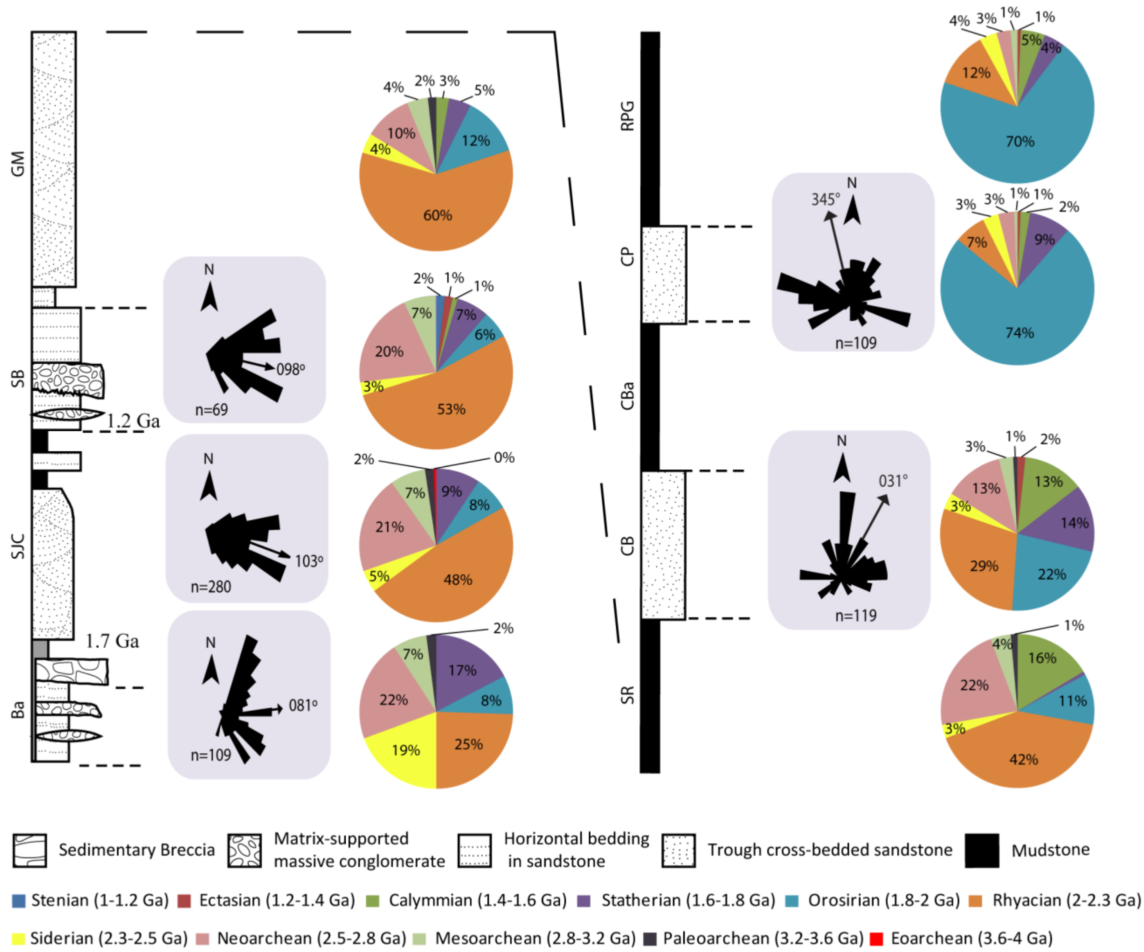

Fig. 6. Simplified stratigraphic arrangement of the Espinhaço Basin, paleocurrent data plotted on rose diagrams, and distribution of U-Pb ages of detrital zircons from the formations investigated in the present work. Ba- Bandeirinha Fm.; SJC- São João da Chapada Fm.; SB- Sopa-Brumadinho Fm.; GM- Galho do Miguel Fm.; SR- Santa Rita Fm.; CB- Córrego dos Borges Fm.; CBa- Córrego da Bandeira Fm.; CP- Córrego Pereira Fm.; and RPG- Rio Pardo Grande Fm. Not to scale.

Of the 512 detrital zircon grains dated from the Galho do Miguel Formation, 406 are concordant. The normalized age probability histogram of the eight samples analyzed in this formation (Fig. 7) show a main peak at 2159 Ma and secondary peaks at 1623 Ma, 2441 Ma and 2716 Ma. Among the units analyzed, the Galho do Miguel Formation has the highest proportion of zircon grains generated during the Rhyacian period (60%). In addition, a relative increase in the population of Orosirian grains (12%) and a decrease in Neoarchean grains is evident (10%; Fig. 6). Of the four sandstone samples analyzed for Lu-Hf, two were collected at intervals deposited by an eolian system (PE-CM-15A and B) and two were collected at intervals deposited by a shallow marine system (PE-CM-14 and PE-SC-43). The main difference between these two groups of samples is the absence of the zircon population formed during the Calymmian Period for the eolian deposits, which have negative $\varepsilon_{Hf}(t)$ values in the marine deposits, from -8 to -5.4 (Fig. 9a). Only one Paleoarchean zircon was analyzed (3272 Ma), showing an $\varepsilon_{Hf}(t)$ value of +0.6. Most of the grains formed in the Neo- and Mesoarchean have negative $\varepsilon_{Hf}(t)$ values, ranging from -6.1 to 5.8. Populations formed in the Rhyacian and Orosirian Periods (ages between 1.8 and 2.2 Ga) have initial $\varepsilon_{Hf}(t)$ values concentrated between -5.1 and 7.1, and two grains have $\varepsilon_{Hf}(t)$ values of -11.8 and -11.2.

The general trend of the Conselheiro Mata Group is a progressive increase in the proportion of zircon grains formed during the Orosirian and a progressive decrease in the proportion of grains formed during the Calymmian, Rhyacian and Archean periods (Fig. 6). All of their analyzed units have zircon grains with ^{207}Pb–^{206}Pb ages between 1.4 and 2.2 Ga and moderate variations in $\varepsilon_{Hf}(t)$ values from -7.9 to +3.2 (Fig. 9b). In the Santa Rita Fm. (140 concordant zircon grains from 154), age peaks can be seen at 1542 Ma, 2118 Ma and 2679 Ma, and a there is significant increase in the proportion of zircon grains formed during the Calymmian Period compared with the underlying units (and almost no Statherian grains). The zircon grains of the Santa Rita Formation of c. 2 Ga have strongly negative $\varepsilon_{Hf}(t)$ values of between -16 and -9.4 (Fig. 9b). The Córrego dos Borges Formation presents several peak ages, especially at 1446 Ma, 1547 Ma (one of grains with $\varepsilon_{Hf}(t)$ of -17.8), 1777 Ma, 1960 Ma and 2183 Ma, and presents secondary peaks at 2540 Ma, 2640 Ma, 2843 Ma, 2968 Ma, 3212 Ma and 3414 Ma, which mark a significant recovery in the zircon grains from Statherian (14%; Fig. 7). Both the Córrego Pereira Fm. and the Rio Pardo Grande Fm. are characterized as having most of their ages concentrated at approximately 1956 Ma, resulting in a significant increase in the proportion of grains formed during the Orosirian period (74%).

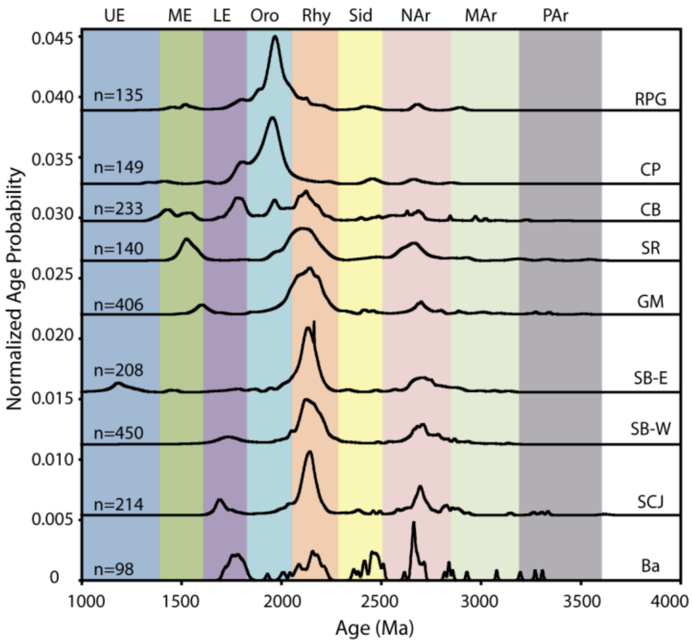

Fig. 7. Relative probability histograms for the studied samples from the southern Serra do Espinhaço and Serra do Cabral. The main domains correspond to Paleoarchean (PAr), Mesoarchean (MAr), Neoarchean (NAr), Siderian (Sid), Rhyacian (Rhy), Orosirian (Oro), Statherian/Lower Espinhaço Sequence (LE), Calymmian-Ectasian/Middle Espinhaço Sequence (ME) and Stenian/Upper Espinhaço Sequence (UE) (Plumb, 1991). The following abbreviations are used: Ba- Bandeirinha Fm.; SJC- São João da Chapada Fm.; SB-W and SB-E- Sopa-Brumadinho Fm. in the western and eastern edges of the rift, respectively; GM- Galho do Miguel Fm.; SR- Santa Rita Fm.; CB- Córrego dos Borges Fm.; CP- Córrego Pereira Fm.; and RPG- Rio Pardo Grande Fm.

The Lu-Hf analysis of sandstone samples from the Córrego dos Borges and Córrego Pereira formations (PE-SC-42 and PE-CM-18) indicated that their Siderian grains (c. 2.4 Ga) have $\varepsilon_{Hf}(t)$ values from -0.8 to +7.6 (Fig. 9b). Between 2.5 and 3.2 Ga, a predominance of negative $\varepsilon_{Hf}(t)$ values occurs in the Santa Rita Fm. (-7.4 to -3.7), Córrego dos Borges Fm. (-7.8 to +0.8) and Rio

Pardo Grande Fm. (-4.1 to -0.1). However, in the Córrego Pereira Fm., the $\varepsilon_{Hf}(t)$ values are slightly positive (+0.5 to +1.8). The Paleoarchean zircon grains of the Santa Rita and Córrego dos Borges formations have initial $\varepsilon_{Hf}(t)$ values scattered around zero (-2.2 to +2.5) and show a clear crustal evolution trend with hafnium model ages (T_{DM}) with Paleo- to Mesoarchean signatures when integrated with other grains from these two units with negative $\varepsilon_{Hf}(t)$ values (Fig. 9b).

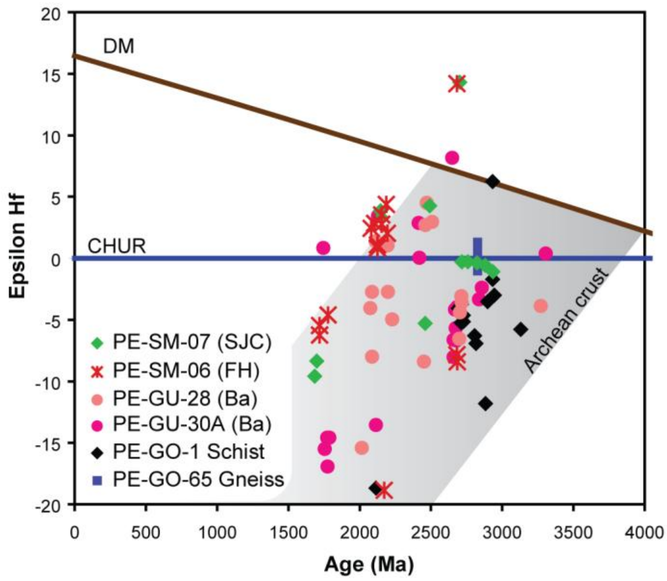

Fig. 8. U-Pb ages and $\varepsilon_{Hf}(t)$ values for single detrital zircon from a gneiss of the Gouveia Complex, a schist of the Barão de Guaicuí Fm., sandstones of the Bandeirinha Fm. (Ba) and hematitic phyllite (FH) and sandstone of the São João da Chapada Fm. (SJC). Crustal evolution path assuming a crustal $^{176}Lu/^{177}Lu$ ratio of 0.0113 (Taylor and McLennan, 1985).

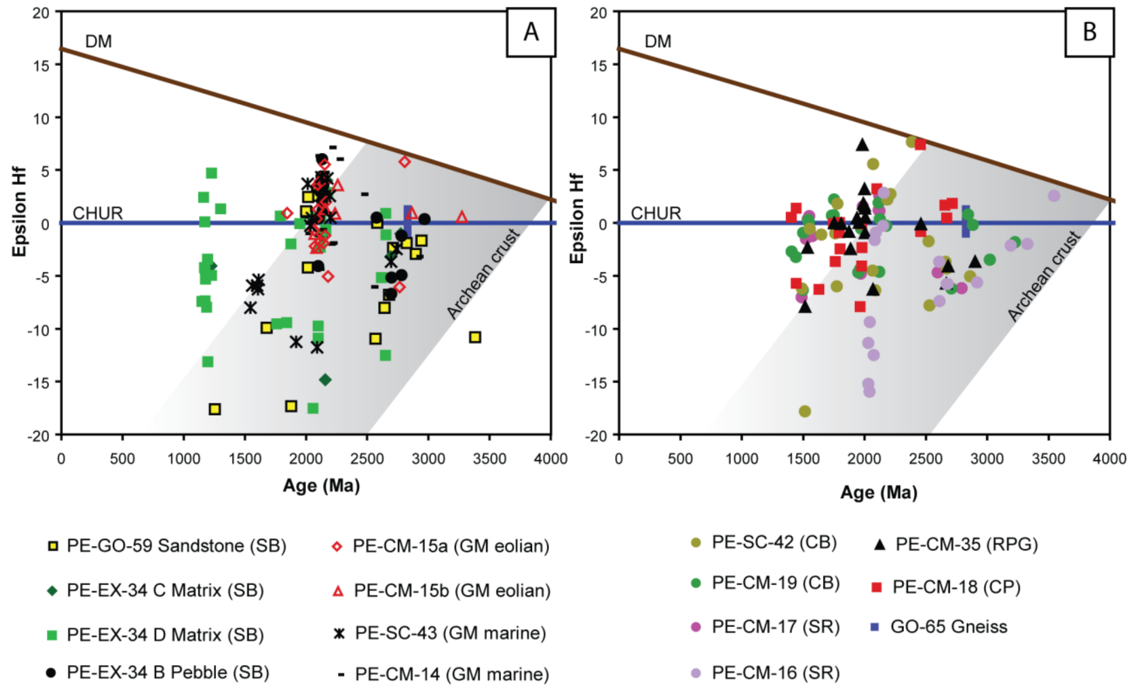

Fig. 9. U-Pb ages and $\varepsilon_{Hf}(t)$ values for a single detrital zircon from the Sopa Brumadinho and Galho do Miguel formations (A) and the Conselheiro Mata Group (B). SB- Sopa-Brumadinho Fm.; GM- Galho do Miguel Fm.; SR- Santa Rita Fm.; CB- Córrego dos Borges Fm.; CP- Córrego Pereira Fm.; and RPG- Rio Pardo Grande Fm. Crustal evolution path assuming a crustal $^{176}Lu/^{177}Lu$ ratio of 0.0113 (Taylor and McLennan, 1985).

5 Discussion

The predominance of SiO_2 and the depletion of other major elements in the chemical composition of the samples occur due to quartz enrichment, which suggests erosion from a low-relief source area under strong chemical weathering and would result in the removal of ferromagnesian minerals prior to deposition. Therefore, the composition of the units varies mainly from quartzarenite to subarkose. When present, the feldspars are mainly altered to sericite. An analysis of the Al_2O_3/TiO_2 ratio also adds important information for the provenance study of the major elements because of the likely chemical immobility of Ti and Al during weathering, sedimentation, diagenesis, and metamorphism (Slack and Stevens, 1994). The Al_2O_3/TiO_2 ratio values usually range from 3 to 8 for mafic magmatic rocks, from 8 to 21 for mixed-composition rocks and from 21 to 70 for felsic rocks, although the Al_2O_3/TiO_2 ratio also reflects Ti-bearing mafic phases derived from felsic and basic rocks

(Chakrabarti et al., 2009). Because the average value of the Al_2O_3/TiO_2 ratio of the Bandeirinha Fm. and part of the São João da Chapada Fm. (level below the hematitic phyllite) is 44.7, it is assumed that this interval receives contributions from felsic rocks (Fig. 10). The hematitic phyllite that represents the magmatism that occurs in the middle portions of the São João da Chapada Fm. (T.M. Dussin, 1994; Knauer and Schrank, 1994) and the basaltic trachyandesite of Stenian age analyzed by Chaves et al. (2013) have an average Al_2O_3/TiO_2 ratio of 5.0, which possibly contributes to the decrease of this ratio in the overlying units (average of 26.93, with oscillations below 21). Therefore, the Al_2O_3/TiO_2 ratio suggests contributions of Ti-bearing mafic phases (e.g., chlorite) that are derived from igneous rocks in the upper portions of the São João da Chapada Formation and in the Sopa-Brumadinho, Galho do Miguel and Córrego Pereira formations (Fig. 10).

The use of trace elements in sedimentary provenance analysis is based on the principle that they are substantially immobile in the sedimentary cycle. The Sc, Y, Zr, Hf, REE and Th elements exhibit low mobility during sedimentary processes (Taylor and McLennan, 1985; Getaneh, 2002) and can provide important information about the source of sediments. Although they represent a homogenized average source composition, the La_n/Lu_n, La/Sc and Th/Sc ratios enable the differentiation between the rocks predominantly generated by sediments from felsic sources and those generated by sediments from mafic sources because they have a range of significantly different values (Wronkiewicz and Condie 1989; Cullers, 1995, 2000; Cullers and Podkovyrov, 2000). In this study, the La_n/Lu_n, La/Sc and Th/Sc values of the analyzed samples are similar to the values for sediments that were derived from felsic source rocks as well as to UCC values than those derived from mafic source rocks (Table 1), which suggests that these samples were derived from felsic source rocks.

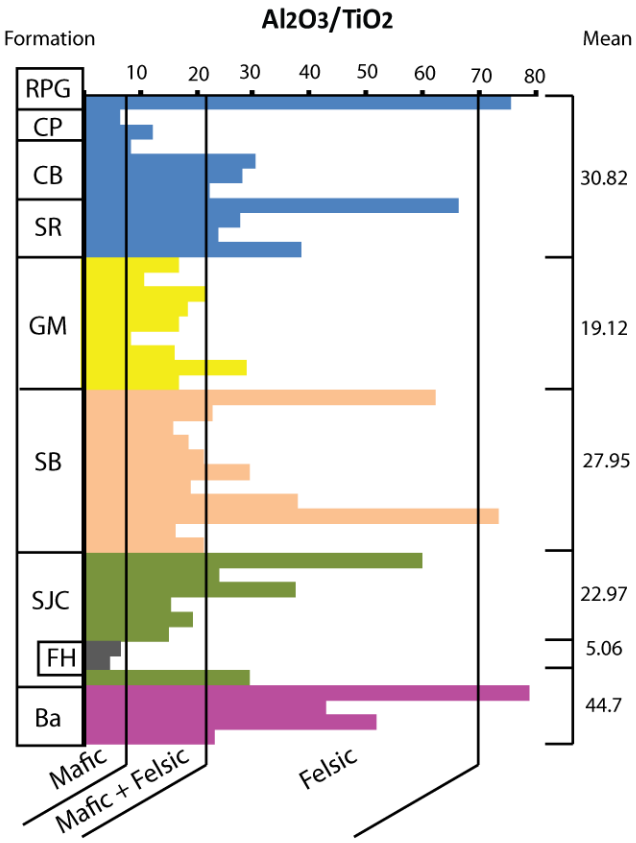

Fig. 10. Plot of the Al_2O_3/TiO_2 ratio for the Espinhaço Basin samples. Limits for mafic, mafic + felsic and felsic source rocks from Chakrabarti et al. (2009). Ba- Bandeirinha Fm.; FH- hematitic phyllite; SJC- São João da Chapada Fm.; SB- Sopa-Brumadinho Fm.; GM- Galho do Miguel Fm.; SR- Santa Rita Fm.; CB- Córrego dos Borges Fm.; CP- Córrego Pereira Fm.; and RPG- Rio Pardo Grande Fm.

The REE patterns and the sizes of the Eu anomalies are different among the felsic and mafic igneous rocks. Felsic rocks usually contain higher LREE/HREE ratios and negative Eu anomalies, whereas mafic rocks contain lower LREE/HREE ratios with few Eu anomalies (Cullers, 1994). All of the analyzed samples in the Espinhaço Basin have high LREE/HREE ratios (La_n/Yb_n ranging from 4.59 to 55.56) and a significantly negative Eu anomaly (0.35 to 0.75), which supports felsic igneous rocks as a possible source. Considering that the Gd_n/Yb_n ratio reflects depletion or enrichment in the HREE when these values are high or low, respectively (Muhs and Budahn, 2006), and that the Gd_n/Yb_n ratios of the analyzed samples are between 1.0 and 2.0 (Fig. 11a), it can be concluded through the Gd_n/Yb_n vs. Eu/Eu* graph that most of the samples show nearly flat chondrite-normalized HREE patterns and that these ratios are similar to the mean values for the UCC (Taylor and McLennan, 1985). PE-EX-34C, a conglomerate with a volcanogenic matrix from the Sopa-Brumadinho Formation, most likely contains significant detrital monazite as a host for the anomalous LREE in this sample.

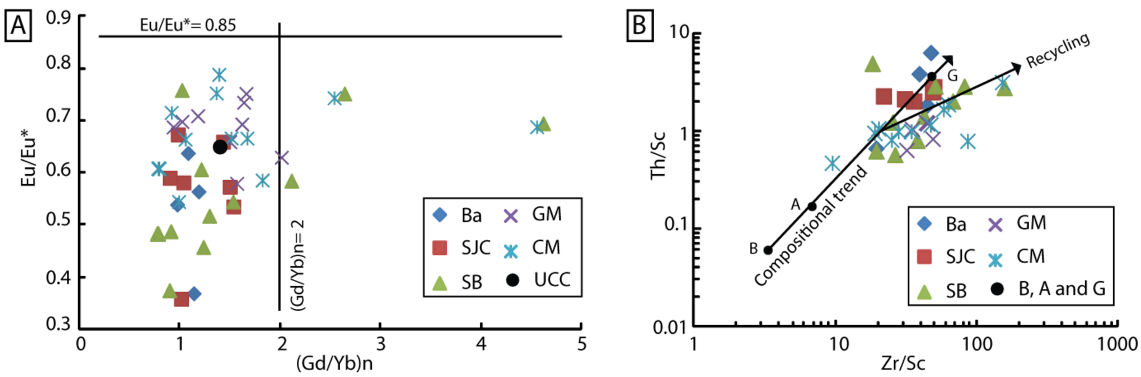

Fig. 11. (a) Plot of $(Gd/Yb)_n$ vs. Eu/Eu* for the Espinhaço Basin samples. Fields are after McLennan and Taylor (1991). The upper continental crust values (UCC) are from Taylor and McLennan (1985). (b) Zr/Sc vs. Th/Sc plot. Primary compositional trend defined by basalt (B), andesite (A) and granite (G) from average Proterozoic rock compositions (Condie, 1993). Samples depart from the compositional trend indicating zircon addition suggestive of a recycling effect. Ba- Bandeirinha Fm.; SJC- São João da Chapada Fm.; SB- Sopa-Brumadinho Fm.; GM- Galho do Miguel Fm.; and CM- Conselheiro Mata Group.

The leucogranite of the Gouveia Complex (the crystalline basement near the study area) has a fractionation pattern that is similar to that of REE and a depletion of Eu. According to Chaves and Coelho (2013), this pattern likely indicates that a portion of the HREE-bearing minerals were not melted during crustal anatexis, unlike the LREE-bearing minerals that would be hosted in the rare monazite crystals of leucogranite. The positive correlations between HREE and Zr (r = 0.61) and between LREE and P_2O_5 (r = 0.64) in the present study suggests that they are partially controlled by zircon and monazite, respectively. Similarly, the anomaly in the Eu, Sr, Rb, Ba and Nb elements found in both studies can be explained by the non-melting of Ca- and Nb-bearing minerals from the protolith during anatexis (Chaves and Coelho, 2013) and enhances the geochemical similarity between the leucogranite and sedimentary units. The

La/Yb ratios and La/Th ratios of the sediments are similar to those in the upper crust and in the two samples (1 and 18) analyzed by Chaves and Coelho (2013) (Fig. 4). Therefore, based on the geochemical data, we assumed that the Gouveia Complex was a potential source area for the rocks of the Espinhaço Basin.

Considering that the Th element is typically incompatible and Sc is typically compatible in igneous systems, the Th/Sc ratio is considered an indicator of igneous chemical differentiation processes (Taylor and McLennan, 1985).In contrast, the Zr/Sc ratio is often used to infer sedimentary processes, such as sorting and mineral recycling (McLennan et al., 1993; Hassan et al., 1999; Mongelli et al., 2006; Bakkiaraj et al., 2010) because Zr is usually concentrated in zircon grains. According to Taylor and McLennan (1985), in sedimentary rocks, a Th/Sc ratio greater than 1 is usually associated with provenance from fairly evolved crustal igneous rocks, a Th/Sc ratio less than 0.8 indicates a probable mafic source and a Zr/Sc ratio greater than 10 indicates a mature or recycled source. A felsic and recycled source for the analyzed samples is indicated by the Zr/Sc and Th/Sc ratios (Fig. 11b). In the Zr/Sc vs. Th/Sc plot (Fig. 11b), one of the lines shows the primary compositional trend defined by Proterozoic igneous rocks (i.e., basalt, andesite and granite; Condie, 1993), whereas the other shows the influence of heavy mineral addition during sediment recycling. According to McLennan et al. (1993), Zr/Sc ratios generally increase following the addition of zircon during recycling processes. A complementary geochemical criterion for the Zr/Sc ratio that also suggests sediment recycling is the Th/U ratio because most samples have values greater than 4 (Rahman and Suzuki, 2007). However, because there is no distortion in the REE pattern, it is likely that the analyzed units have only experienced a low degree of recycling (Tripathi and Rajamani, 2003).

5.1 The provenance of the Paleoproterozoic rift

According to Santos et al. (2013), the Lower Espinhaço Sequence presents two distinct system tracts, the rift initiation system tract and the early rift climax system tract, which are recorded in the Bandeirinha and São João da Chapada formations, respectively. During the deposition of the Bandeirinha

Formation, the paleorelief was likely controlled by small fault scarps that formed local areas with axial topographic highs and small and separated areas of deposition, predominantly under longitudinal drainage systems (paleocurrent pattern to N-NE) (Santos et al., 2013). The braided fluvial systems that developed during the deposition of the Bandeirinha Formation allowed a predominant sand supply from the south. The geochemical and geochronological data indicate different felsic sedimentary sources. The Lu-Hf analysis of the Paleoarchean grains (c. 3.3 Ga) suggests the recycling of an older crust. The negative $\varepsilon_{Hf}(t)$ values for the Neoarchean population (c. 2.7 Ga) suggest recycling of the same Paleoarchean crust and match the values found in the schist sample of the Barão do Guaicuí Formation, indicating that this unit was a potential sedimentary source during the early stages of the rift. In addition, the Hf isotope data show a poorly defined vertical $\varepsilon_{Hf}(t)$ array at c. 2.4 ($\varepsilon_{Hf}(t)$ -8.4 to +4.2) and 2.1 Ga ($\varepsilon_{Hf}(t)$ −18.8 to +4.4) and indicate that those zircons reflect the mixing of Archean crust into juvenile Siderian and Rhyacian magmas. Because the Bandeirinha Formation unit has the highest relative proportion of Siderian zircon grains and a predominant paleocurrent to the N-NE, it is likely that the source rock is located in the south (Fig. 6). The greatest relative proportion of Statherian sediments in this unit relative to the other formations in this basin likely occurs due to the provenance from magmatic rocks, which is related to the thermal events that are responsible for the opening of the basin at approximately 1.7 Ga. The negative $\varepsilon_{Hf}(t)$ values for the Statherian zircon grains suggest derivation from crustal domains from recycling of the Paleoarchean crust, whereas grains with $\varepsilon_{Hf}(t)$ values of +0.8 likely indicate the presence of another source of the same age.

The second tectonic pulse of the rift, which is responsible for the deposition of the São João da Chapada Formation, generated an angular discordance between this unit and the Bandeirinha Formation and resulted in the propagation of previously generated faults, deposition of sedimentary breccias next to fault scarps, expansion of the depocenters and formation of an extensive braided fluvial system with a drainage pattern transverse to the axis of the rift (Santos, 2011; Santos et al., 2013). The change of the N–NE longitudinal drainage pattern to an E–SE transverse drainage pattern was definitive because it remained during the later stages of rift sedimentation and reflects a change in sedimentary provenance. The contribution of sediments from the Siderian and Statherian sources decreased significantly in the São João da Chapada Formation, resulting in sedimentation predominantly from a juvenile Rhyacian source, likely from the west (Figs. 6 and 8). However, the proportion of Neoarchean zircon grains remained constant at approximately 21%, which indicated that the contributions of those sediments were not influenced by the local paleodrainage direction. A small population of zircon that crystallized during the Archean (sample PE-SM-07) shows age and Hf isotope compositions that are very similar to the gneiss of the Basal Complex, dated at 2828 Ma and presenting $\varepsilon_{Hf}(t)$ values of -1 to +1.3 (Fig. 8). This finding suggests that the crystalline basement was an important source for the sediments of the São João da Chapada Formation.

The absence of igneous zircons with juvenile Hf isotope compositions in the hematitic phyllite of the São João da Chapada Fm. suggests that no major depleted mantle-derived components were present in the source of the hematitic phyllite. This result indicates that part of the magmatism that occurred in the rift stage of the Lower Espinhaço Sequence represents crustal melting rather than differentiation of the mantle-derived parent material. Therefore, the analyses show that hematitic phyllite was not the rock that carried diamonds from the mantle to the Earth's surface in the Espinhaço Basin, as previously reported (Correns, 1932; Moraes, 1934; Barbosa, 1951). Instead, phyllite served as an important source of Statherian sediments for the São João da Chapada Formation, as seen by the similarities in the $\varepsilon_{Hf}(t)$ values of these populations. The inherited zircon grains of the hematitic phyllite also record the formation of juvenile magmas during the Rhyacian Period, which were contaminated by Archean crustal materials. The isotopic signature of the juvenile magmatic arc in the Rhyacian populations was identified by Rodrigues et al. (2012) and Matteini et al. (2012) in detrital zircon grains of the Meso- to Neoproterozoic sequences developed in the Brasília Belt (Vazante and Paranoá Groups) west of the São Francisco Craton. Potential source areas for these sediments include the rocks of the Mantiqueira and Juíz de Fora Complexes and the Mineiro Belt, south of the São Francisco Craton (Noce et al., 2007;

Ávila et al., 2010), and possible sources located west of the Espinhaço Basin that are currently covered by Neoproterozoic and Phanerozoic sedimentary sequences.

5.2 The provenance of the Mesoproterozoic rift

After a gap of approximately 500 Ma, a new tectonic-thermal event reactivated the Paleoproterozoic faults of the rift and generated other faults of the same orientation (north-south) in the east, expanding the area of deposition and forming a complex rift system. During the development of this new basin, the implementation of several alluvial fans and lacustrine fan deltas near the faults of the grabens and braided fluvial systems developed throughout the basin (Martins-Neto, 1996, 1998), forming the early rift climax systems tract described by Prosser (1993).

There is a close similarity between the São João da Chapada and Sopa-Brumadinho formations, especially regarding the depositional systems, paleocurrent patterns to E (transverse to the rift axis; Alvarenga, 1982; Santos et al., 2013) and proportion of different sedimentary sources in the analyzed samples. However, the presence of the zircon grains from the Stenian, Ectasian and Calymmian periods in the Sopa-Brumadinho Formation (n = 30) make such units completely timeless. Previously, only the samples located on the eastern edge of the rift indicated the provenance of such source rocks. Nevertheless, one of the samples studied in this paper (PE-GO-59), collected on the western edge of the rift, presented concordant grains (n = 3) with the same ages and similar Hf isotopic compositions. These grains have a fine grain size because of their tuffaceous provenance, and it is likely that some of the grains were lost during mineral separation procedures, mainly due to concentration by hand panning. Further analyses of the fine-sediment fractions may satisfactorily explain the actual proportions of the grains from the sources generated in the Mesoproterozoic Era. Recently, Chaves et al. (2013) identified the occurrence of volcanic rocks with a maximum deposition age of 1.16 Ga, which is the first record of such magmatism in the Southern Espinhaço. The rock dated by Chaves et al. (2013) was obtained only 8 km from the site where sample PE-

GO-59 was collected and is a likely source for zircon grains of the Stenian Period. The magmatic event that occurred at approximately 1.2 Ga may be associated with the transport of diamonds from a mantle source to the surface in the region because the radiogenic Hf isotopic compositions of the zircon grains (i.e., positive εHf(t) values) indicate that they were derived from juvenile (mantle-derived) sources (Gerdes and Zeh, 2006; Babu et al., 2008; Willner et al., 2008; Lamminen and Köykkä, 2010). A similar signature for that period was also reported by Rodrigues et al. (2012) for zircon grains from a quartzite sample of the Vazante Group in the Brasilia Belt. The negative $\varepsilon_{Hf}(t)$ values of the Stenian age detrital zircons from the Sopa-Brumadinho Formation also record the reworking of an older crust.

The provenance of the banded iron formation (BIF) pebbles present in the conglomerates of the Sopa-Brumadinho Formation on the eastern edge of the rift is interpreted to be coeval to the BIF of the Cauê Fm., Minas Supergroup. In addition, the quartzite pebble sample contained in one of the conglomerates had a population of zircon grains with a maximum Rhyacian age (c. 2.1 Ga; Fig. 9a) and might be part of the coeval upper section of the Minas Supergroup. Both clasts have provenance from the Serra da Serpentina Group in the east, where tectonic slices of Espinhaço Supergroup units, 1.7 Ga metarhyolites, Paleoproterozoic BIFs and quartzites and an Archean basement occur. The grains of the Sopa-Brumadinho Formation dated at c. 2.1 Ga show a vertical array of $\varepsilon_{Hf}(t)$ values ($\varepsilon_{Hf}(t)$−17.5 to +4), which suggests that the components of the Archean crust were mixed with juvenile magmas that were coeval to the global-scale collisional events associated with the assembly of the Columbia Supercontinent (Meert, 2012). The Archean population comprises ages between 2.5 and 2.9 Ga and only presents negative $\varepsilon_{Hf}(t)$ values, which suggests the recycling of an older Archean crust.

5.3 The provenance of the Mesoproterozoic sag

In contrast with the Paleoproterozoic rift, the Mesoproterozoic rift was succeeded by a sag phase that was characterized by regional subsidence and implementation of a regional eolian system, followed by an epicontinental sea.

The Galho do Miguel Formation and Conselheiro Mata Group present major zircon grain contributions that formed during the Paleoproterozoic (over 50% of the grains analyzed) and, subordinately, the Archean and Mesoproterozoic. Because these units overlap the Sopa-Brumadinho Formation, it is assumed that they were been deposited between 1.18 and 0.9 Ga (Chemale et al., 2012; Santos et al., 2015). In addition, zircon grains from the Stenian period were not found; only zircon grains from the Ectasian and Calymmian periods (Figs. 6 and 7)) that were formed in the Middle Espinhaço Sequence were found (Chemale et al., 2012; Guadagnin et al., 2015).

The beginning of the thermal subsidence was marked by the predominantly eolian sedimentation of the Galho do Miguel Formation (Dossin et al., 1987; Garcia and Uhlein, 1987), whose deposition likely occurred in a coastal context according to the evidence of marine sedimentation at some locations (Martins-Neto, 1998; Santos et al., 2013). The sedimentary provenance analysis of this unit indicates the predominance of a juvenile Rhyacian source (2 to 2.2 Ga), which accounts for 60% of the zircon grains (Fig. 6), and implies a progressive increase in the contributions of this source, with the highest percentage achieved in the Galho do Miguel Formation, even when considering the units of the Paleoproterozoic rift. The lack of detailed sedimentological studies in this unit, mainly due to access difficulties imposed by their relief, has resulted in a scarcity of paleocurrent measurements. The measurements of sandstones with large-scale cross-stratification indicate provenance from west and north (Santos et al., 2015). Only sandstones deposited in a marine environment in the Galho do Miguel Formation have a Calymmian population (c. 1.5 Ga), which was crystallized from recycled crust. Tuff samples analyzed by Guadagnin et al. (2015) in the Chapada Diamantina and located north of the São Francisco Craton indicated similar Hf isotopic compositions with some subordinate juvenile contribution, which suggests that the region may have been a potential source area for the marine deposits of the Upper Espinhaço Sequence. The Neoarchean grains indicate recycling of a Paleoarchean crust.

The change from a continental environment to the marine environment of the Conselheiro Mata Group is marked by a progressive decrease in sediments from the Rhyacian Period and a concomitant increase in the sediments from the Orosirian Period. However, the sedimentary provenance of the first unit deposited in an open-marine environment (i.e., the Santa Rita Formation) is similar to the underlying continental deposits, which indicates that a drastic change in the depositional system would have only partially affected the proportion of sediments from the different source rocks. The deposition in an offshore environment modified mainly the Statherian population, virtually absent in the samples, and Calymmian population, which reached its greatest relative proportion in the Santa Rita Formation (Fig. 6). According to Santos et al. (2015), the sediments of the Calymmian Period do not occur at the base of this unit due to the low terrigenous sediment supply to the offshore environment, which significantly increases toward the top due to subsequent marine regression, which would cause an increase in the sediment supply and result in the incorporation of more Calymmian sediments.

The Córrego dos Borges Formation, which was deposited under upper shoreface conditions, is characterized by paleocurrents of different directions and a prevailing trend to the north (Fig. 6). These paleocurrents resulted from the migration of subaqueous 2D and 3D dunes during the action of longshore drift due to the obliquity of the waves against the shoreline (Santos et al., 2015). The variations in the paleocurrent directions of this formation likely contributed to the provenance characterized by various sources of ages between approximately 1.4 Ga and 2.2 Ga, which record periods of zircon generation (igneous or metamorphic) with relatively high frequencies. The sources formed between 1.4 and 1.6 Ga record a reworking of the Archean crust, whereas the sources formed between 1.5 and 2.2 Ga involve the mixing of zircons derived from the reworking of the Archean crust and from juvenile material. As shown in Fig. 9b, some of the grains of the Santa Rita and Córrego dos Borges formations (i.e., grains with the lowest values of $\varepsilon Hf(t)$) form a linear array in plots of Hf isotope ratios against crystallization age, indicating that magmas of different ages are generated from a crust of the same mantle extraction age and composition. The Paleo- to Mesoarchean model ages indicate that the Gavião Block, the oldest segment of the São Francisco Craton (Barbosa and Sabaté, 2004), was a source area that contributed throughout the sedimentary evolution history of the Espinhaço Basin because all of the other units show this same trend, although not as clearly.

The Córrego Pereira and Rio Pardo Grande formations, deposited in tidally influenced upper shoreface and lower shoreface conditions, respectively, recorded a significant change in sedimentary provenance during the final stages of sedimentation of the Espinhaço Basin. In both of these formations, a large predominance of Orosirian zircon grains (70% - 74% of the grains) formed by mixing of a juvenile magma with an older crust occurs, whose source rocks have not yet been identified in the adjacent regions (Figs. 7 and 9b). According to Guadagnin and Chemale (2015), the provenance of zircon grains from the Orosirian Period is also notable in other relatively close sedimentary basins (e.g., Carandaí and Serra da Mesa basins) located in the Southern and Northern Brasilia Belt. The source rocks formed in the Orosirian Period are likely not currently exposed because younger rocks overlap them. Except for zircon grains of Orosirian age, all other identified populations likely reflect the provenance from sources located in the surrounding areas of the Espinhaço Basin (e.g., Brito Neves et al., 1979; Dossin et al., 1993; Barbosa and Sabaté, 2004; Hartmann et al., 2006; Danderfer et al., 2009; Chemale et al., 2012; Silveira et al., 2013; Chaves et al., 2013; Guadagnin et al., 2015). The populations of zircon grains of Archean, Rhyacian and Calymnian age show a mixing of juvenile materials with reworked older crustal materials, whereas the Statherian population was formed entirely during the recycling of older crust.

5.4 Imprints of the Columbia Supercontinent and Grenville Orogen in the Espinhaço Basin

After the identification of the Pangaea Supercontinent by Wegener (1915), many studies have been developed to refine the initial paleogeographic model and others to explain the arrangement of the lithospheric plates during very remote times. The evidence mainly generated from paleomagnetic and geochronological data suggests that two older supercontinents, called Rodinia and Columbia, assembled in the Meso-Neoproterozoic and Paleoproterozoic

Eras, respectively (Rogers and Santosh, 2002; Zhao et al., 2002; Li et al., 2008).

Many possible configurations of the Columbia Supercontinent have been proposed (e.g., Rogers and Santosh, 2002; Yakubchuk, 2010; D'Agrella-Filho et al., 2012; Zhang et al. 2012; Piper, 2013; Bispo-Santos et al., 2014; Pisarevsky et al., 2014), but the acceptance of every one of these configurations can be discussed mainly due to a lack of well-constrained paleopoles from the same period across all continental fragments (Roberts, 2013). However, there is a consensus that the assembly of this supercontinent occurred between 2.1 and 1.8 Ga based on global-scale collisional events (Zhao et al., 2002) that are well marked by peaks in U-Pb crystallization ages and the ages of juvenile granitoids (Condie and Aster, 2010). The isotopic and geochemical data presented in this paper suggest that the Espinhaço Basin preserves the imprints of magmatism in a convergent margin setting that would have occurred at 2 to 2.1 Ga and is associated with the formation of the Columbia Supercontinent (Fig. 12). The Lu-Hf isotopic signature of detrital zircons with ages of between 2 and 2.1 Ga contained in the sedimentary deposits of this basin show a predominance of juvenile materials (positive $\varepsilon_{Hf}(t)$ values) with some reworking of an Archean crust and provenance from the west. These sediments were likely formed in a continental magmatic arc coeval with a similar event found by Abati (2012) in the West African Craton but without clear evidence of continent-continent collision, which would be characterized by a predominance of negative $\varepsilon_{Hf}(t)$ values. This evidence suggests that the western region of the São Francisco Craton was most likely along the edge of the Columbia Supercontinent at 2 to 2.1 Ga.

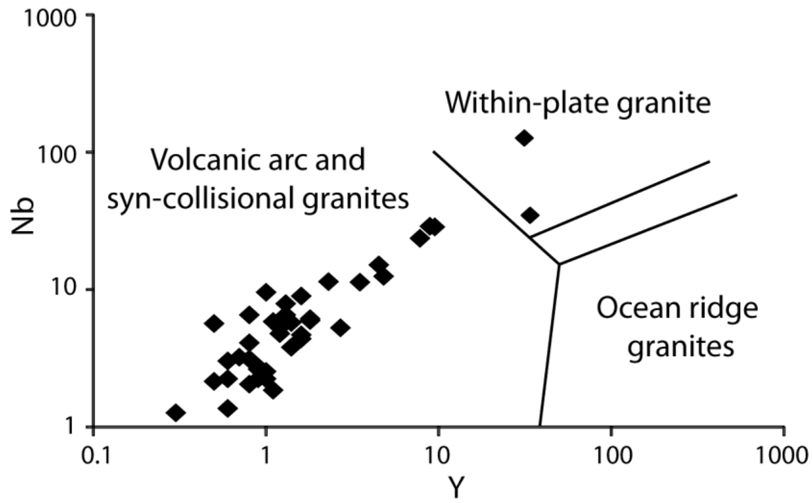

Fig. 12. Nb-Y composition in ppm of the metasediments from the Espinhaço Basin showing provenance from a magmatic arc. Discrimination fields from Pearce et al. (1984).

The Rodinia Supercontinent was assembled through worldwide orogenic events between 1.3 and 0.9 Ga (Li et al., 2008), where some exterior accretionary belts were transformed into interior collisional belts (Roberts et al., 2013). The development of the Upper Espinhaço Sequence at approximately 1.2 Ga likely records the influence within the São Francisco Craton from compressive events that occurred at the edge of the plate (i.e., the Grenville Orogeny; Chemale et al., 2012; Chaves et al., 2013; Santos et al., 2013; Guadagnin et al., 2015) because intracratonic basins, such as the Lower Espinhaço Sequence, are sites of thermal and/or rheological weakening that can be reactivated during compression, often in response to far-field stresses (Cawood et al., 2009).

6 Conclusions

In this study, we investigated the Paleoproterozoic and Mesoproterozoic units of the Espinhaço Basin by using whole-rock geochemistry and combined U-Pb and Lu-Hf in situ analyses of zircon to clarify their provenance and evolution with time. The geochemical data suggest that erosion from a low-relief source area occurred under strong chemical weathering. The Eu/Eu*, $(La/Lu)_n$, La/Sc, Th/Sc and Zr/Sc ratios support a felsic and recycled source for the sedimentary rocks. Chondrite-normalized REE patterns with LREE enrichment, flat HREE, and negative Eu anomalies are also attributed to felsic source rock. The decrease in the Al_2O_3/TiO_2 ratio in the upper portions of the São João da Chapada Formation and in the Sopa-Brumadinho, Galho do Miguel and Córrego Pereira formations suggest contributions from mafic phases, whose provenance can be attributed to volcanic rocks formed during the extensional events of the Statherian and Stenian periods (Dossin et al., 1993; Chemale et al, 2012; Chaves et al., 2013).

Detrital zircon grains of the Lower Espinhaço Basin show populations that were formed exclusively in the Archean and Paleoproterozoic. Although the Bandeirinha and São João da Chapada formations present similar age peaks (at 1.7, 2.1, 2.4, 2.7, 2.8 and 3.3 Ga), the relative proportions between the populations are clearly distinct, which may reflect the change from a N–NE longitudinal drainage pattern to an exclusively E–SE transverse drainage pattern (orthogonal to the rift axis). The Bandeirinha and São João da Chapada formations show a clear provenance from the schists of the Barão de Guaicuí Fm. and from the gneiss of the Complexo Basal, respectively. The Hf isotope compositions of the zircon grains dated at 1.7 Ga indicate provenance from the hematitic phyllite.

The Upper Espinhaço Basin contains detrital zircon populations formed during the Archean, Paleoproterozoic and Mesoproterozoic. Coeval to the Grenville Orogeny, the rift phase of this basin also shows paleocurrents to the east that resulted in a sedimentary provenance similar to the São João da Chapada Formation, except for the zircon grains from 1.2 to 1.5 Ga of the Sopa-Brumadinho Formation. This study indicates that this Mesoproterozoic population is not restricted to the eastern edge of the rift (Extração region) but also occurs along the western edge. The juvenile Hf isotope composition of the Stenian zircon grains suggests that their source was extracted from the mantle, whose magmatism was likely related to the transport of diamonds to the Earth's surface; therefore, the primary source of diamonds would not be related to the magmatic event of 1.7 Ga, characterized by the recycling of older crust. During the sag phase, a change from a continental to marine environment occurred, which is marked by a progressive decrease in sediments from the Rhyacian Period and a concomitant increase in sediments from the Orosirian Period formed by the mixing of a juvenile magma with an older crust. The positive $\varepsilon_{Hf}(t)$ values of the Paleoproterozoic zircon grains mainly suggest a distinct long-term (2 – 2.2 Ga) event of juvenile crust formation.

Coupled with Hf isotopes, the detrital spectra provide an important perspective on crustal growth and recycling in the São Francisco Craton. We conclude that the population of zircon grains with 2.1 Ga may be the result of contamination of Transamazonian juvenile arc magmas by Archean crust west of the craton during the assembly of the Columbia Supercontinent.

Acknowledgements

We would like to thank the CAPES, CNPq (grant for FCJ # 304045/2010-1) and PETROBRAS for their financial support for the field work and analysis.

References

Abati, J., Aghzer, A.M., Gerdes, A., Ennih, N., 2012. Insights on the crustal evolution of the West African Craton from Hf isotopes in detrital zircons from the Anti-Atlas belt. Precambrian Research 212–213, 263–274.

Alkmim, F.F., Brito Neves, B.B., Castro Alves, J.A., 1993. Arcabouço tectônico do Cráton do São Francisco: uma revisão. In: O Cráton do São Francisco. Dominguez, J.M.L. and Mis, A. (Eds), SBG - Núcleo BA/SE: 45-62.

Alkmim, F.F., Marshak, S., Pedrosa-Soares, A.C., Peres, G.G., Cruz, S.,Whittington, A., 2006. Kinematic evolution of the Araçuaí–West Congo orogen in Brazil and Africa: nutcracker tectonics during the Neoproterozoic assembly of Gondwana. Precambrian Res. 149, 43–64.

Almeida-Abreu, P.A., 1995. O Supergrupo Espinhaço na Serra do Espinhaço Meridional, Minas Gerais: O rifte, a bacia e o orógeno. Geonomos 3, 1–18.

Alvarenga, C.J.S., 1982. Comportamento estratigráfico da Formação Sopa-Brumadinho no distrito diamantífero de Extração (Diamantina,MG). Congresso Brasileiro de Geologia, 22, Salvador: Anais, 1, p. 168-176 .

Ávila,C.A., Teixeira, W., Cordani, U.G., Moura, C.A.V., Pereira, R.M., 2010. Rhyacian (2.23–2.20 Ga) juvenile accretion in the southern São Francisco craton, Brazil: Geochemical and isotopic evidence from the Serrinha magmatic suite, Mineiro belt. Journal of South American Earth Sciences 29, 464–482.

Babu, E.V.S.S.K., Griffin, W.L., Mukherjee, A., O'Reilly, S.Y., Belousova, E.A., 2008. Combined U-Pb and Lu-Hf analysis of megacrystic zircons from the Kalyandurg-4 kimberlite pipe, S. India: Implications for the emplacement age and Hf isotopic composition of the cratonic mantle. 9th International Kimberlite Conference. Extended Abstract No. 9IKC-A-00142.

Bahlburg, H., Vervoort, J.D., DuFrane, S.A., 2010. Plate tectonic significance of Middle Cambrian and Ordovician siliciclastic rocks of the Bavarian Facies, Armorican Terrane Assemblage, Germany — U–Pb and Hf isotope evidence from detrital zircons. Gondwana Research 17, 223–235.

Bakkiaraj, D., Nagendra, R., Nagarajan, R., Armstrong-Altrin, J.S., 2010. Geochemistry of sandstones from the Upper Cretaceous Sillakkudi Formation, Cauvery Basin, southern India: Implication for provenance. Journal of the Geological Society of India 76, 453-467.

Barbosa, O., 1951. Contribuição à origem do diamante em Diamantina, Estado de Minas Gerais. DNPM, DGM, 36 p.

Barbosa, J.S.F., Sabaté, P., 2004. Archean and Paleoproterozoic crust of the São Francisco Craton, Bahia, Brazil: geodynamic features. Precambrian Research 133, 1-27.

Bispo-Santos, F., D'Agrella-Filho, M.S., Trindade, R.I.F, Janikian, L.,Reis, N.J., 2014. Was there SAMBA in Columbia? Paleomagnetic evidence from 1790 Ma Avanavero mafic sills (northern Amazonian Craton). Precambrian Research 244, 139–155.

Brito Neves, B.B., 1995. A Tafrogênese Estateriana nos Blocos Paleoproterozóicos daAmérica do Sul e Processos Subseqüentes. Geonomos 3, 01–21.

Brito Neves, B.B., Cordani, U.G., Kawashita, K., Delhal, J., 1979. A evolução geocronológica da Cordilheira do Espinhaço; dados novos e integração. Revista Brasileira de Geociências 9, 71–85.

Cawood, P.A., Kröner, A., Collins, W.J., Kusky, T.M., Mooney, W.D., Windley, B.F., 2009. Accretionary orogens through Earth history. In: Cawood, P.A., Kröner, A. (Eds.), Earth Accretionary Systems in Space and Time, Geological Society of London, Special Publication 318, 1-36.

Chakrabarti, G., Shome, D., Bauluz, B., Sinha, S., 2009. Provenance and Weathering History of Mesoproterozoic Clastic Sedimentary Rocks from the Basal Gulcheru Formation, Cuddapah Basin. Journal of the Geological Society of India 74, 119-130.

Chaves, M.L. de S.C., 1997. Geologia e mineralogia do diamante da Serra do Espinhaço em Minas Gerais. Ph. D. Thesis, São Paulo, IG/Univ. São Paulo, 289 pp.

Chaves, A.O., Coelho, R.M., 2013. Petrografia, geoquímica e geocronologia do leucogranito peraluminoso do Complexo de Gouveia-MG. Geonomos 21, 1-12.

Chaves, M.L.S., Silva, M.C.R., Scholz, R., Babinski, M., 2013. Grenvillian age magmatism in the Southern Espinhaço Range (Minas Gerais): evidence from U-Pb zircon ages. Brazilian Journal of Geology 43, 477–486.

Chemale Jr., F., Dussin, I.A., Alkmim, F.F., Martins, M.S., Queiroga, G., Armstrong, R., Santos, M.N., 2012. Unravelling a Proterozoic basin history through detrital zircon geochronology: The case of the Espinhaço Supergroup, Minas Gerais, Brazil. Gondwana Research 22, 200-206.

Chemale Jr., F., Dussin, I.A., Martins, M.S., Alkmim, F.F., Queiroga, G., 2010. The Espinhaço Supergroup in Minas Gerais: a Stenian Basin? 7th South American Symposium on Isotope Geology, Brasília, pp. 552–555.

Chemale Jr., F., Philipp, R.P., Dussin, I.A., Formoso, M.L.L., Kawashita, K., Bertotti, A.L., 2011. Lu-Hf and U-Pb age determinations of Capivarita Anorthosite in the Dom Feliciano Belt, Brazil. Precambrian Research 186, 117-126.

Condie, K.C., Aster, R.C., 2010. Episodic zircon age spectra of orogenic granitoids: the supercontinent connection and continental growth. Precambrian Research 180, 227-236.

Chu, N.C., Taylor, R.N., Chavagnac, V., Nesbitt, R.W., Boella, M., Milton, J.A. 2002. Hf isotope ratio analysis using multi-collector inductively coupled plasma mass spectrometry: an evaluation of isobaric interference corrections. Journal of Analytical Atomic Spectrometry 17, 1567–1574.

Condie, K.C., 1993. Chemical composition and evolution of the upper continental crust: Contrasting results from surface samples and shales. Chemical Geology 104, 1-37.

Correns C.W., 1932. Die Diamanten des Hochlandes von Minas Geraes, Brasilien. Zeitschrift f Ur praktische Géologie. Jahrgang 40, 161 -176.

Cullers, R.L., 1994. The controls on the major and trace element variation of shales, siltstones and sandstones of Pennsylvanian – Permian age from uplifted continental blocks in Colorado to platform sediment in Kansas, USA. Geochimica et Cosmochimica Acta 58, 4955-4972.

Cullers, R.L., 1995. The controls on the major and trace element evolution of shales, siltstones and sandstones of Ordovician to Tertiary age in the Wet Mountain region, Colorado, U.S.A. Chemical Geology 123, 107-131.

Cullers, R.L., 2000. The geochemistry of shales, siltstones and sandstones of Pennsylvanian–Permian age, Colorado, USA: implications for provenance and metamorphic studies. Lithos 51, 181-203.

Cullers, R.L., Podkovyrov,V.N., 2000. Geochemistry of the Mesoproterozoic Lakhanda shales in southeastern Yakutia, Russia: Implications for mineralogical and provenance control, and recycling. Precambrian Research 104, 77-93.

D'Agrella-Filho, M.S., Trindade, R.I.F., Elming, S.-A., Teixeira, W., Yokoyama, E.,Tohver, E., Geraldes, M.C., Pacca, I.I.G., Barros, M.A.S., Ruiz, A.S., 2012. The 1420 Ma Indiavai Mafic Intrusion (SW Amazonian Craton): paleomagnetic results and implications for the Columbia supercontinent. Gondwana Reseach 22, 956–973.

Danderfer, A., De Waele, B., Pedreira, A.J, Nalini, H.A., 2009. New geochronological constraints on the geological evolution of Espinhaço basin within the São Francisco Craton-Brazil. Precambrian Research 170, 116-128.

Dossin, I.A., Dossin, T.N., Charvet, J., Cocherie, A., Rossi, P., 1993. Single-zircon dating by step-wise Pb-evaporation of Middle Proterozoic magmatismo in the Espinhaço range, southeastern São Francisco Craton. Minas Gerais, Brazil. Simpósio sobre o Cráton do São Francisco, 2, Salvador, 1993: Anais, Sociedade Brasileira de Geologia/Superintendência de Geologia e Recursos Minerais da Bahia, 1, pp. 39–42.

Dossin, I.A., Dossin, T.M., Chaves, M.L.S.C., 1990. Compartimentação Estratigráfica do Supergrupo Espinhaço em Minas Gerais - os Grupos Diamantina e Conselheiro Mata. Revista Brasileira de Geociências 20, 178–186.

Dossin, I.A., Garcia, A.J.V., Uhlein, A., Dardenne, M.A., Dossin, T.M., 1987. Fácies eólico na Formação Galho do Miguel. Supergrupo Espinhaço (MG). Simpósio sobre Sistemas Deposicionais no Pre-Cambriano, Ouro Preto: Atas, Sociedade Brasileira de Geologia, pp. 85–96.

Dossin, I.A., Uhlein, A., Dossin, T.M., 1984. Geologia da Faixa Móvel Espinhaço em sua porção meridional, MG. Congresso Brasileiro de Geologia, 33, Rio de Janeiro: Anais, Sociedade Brasileira de Geologia, 2, pp. 3118–3132.

Dupont, H., 1995. O Grupo Conselheiro Mata no seu quadro paleogeográfico e estratigráfico. Simpósio de Geologia de Minas Gerais, Diamantina: Anais, Sociedade Brasileira de Geologia, 13, pp. 9–10.

Dussin, I.A.,1994. Evolution Structurale de la pertie méridional de L'Espinhaço sur la bordure orientale du Craton São Francisco. Minas Gerais – Brésil: Um exemple de tectonique protérozoique superposé. Ph.D. Thesis, Orleans,Universited’ Orleans, 200pp.

Dussin, I.A., Dussin, T.M., 1995. Supergrupo Espinhaço: modelo de evolução geodinâmica. Geonomos 3, 19-26.

Dussin, T.M., 1994. Associations plutono-volcaniques de l"EspinhaçoMeridional (SE-Brésil): um exemple d'évolution de la croûte protérozoïque. Ph.D. Thesis, Orleans,Universited' Orleans, 177pp.

Espinoza, J.A.A., 1996. Sistemas deposicionais e relações estratigráficas da Tectonosseqüência Conselheiro Mata, na borda leste da Serra do Cabral, Minas Gerais, Brasil. MSc Thesis, Departamento de Geologia, Escola de Minas, Universidade Federal de Ouro Preto, Ouro Preto, 66 pp.

Fogaça, A.C.C., 1995. Geologia da Folha Diamantina. Projeto Espinhaço. COMIG-UFMG, Belo Horizonte (98 pp.).

Garcia, A.J.V., Uhlein, A., 1987. Sistemas deposicionais do Supergrupo Espinhaço na Região de Diamantina (MG). Simpósio sobre Sistemas Deposicionais no Pre-Cambriano, Ouro Preto: Atas, Sociedade Brasileira de Geologia, pp. 113–136.

Gerdes, A., Zeh, A., 2006. Combined U–Pb and Hf isotope LA-(MC-)ICP-MS analyses of detrital zircons: Comparison with SHRIMP and new constraints for the provenance and age of an Armorican metasediment in Central Germany. Earth and Planetary Science Letters 249, 47–62.

Getaneh, W., 2002. Geochemistry provenance and depositional tectonic setting of the Adigrat Sandstone northern Ethiopia. Journal of African Earth Sciences 35, 185–198.

Guadagnin, F., Chemale Jr., F., 2015. Detrital zircon record of the Paleoproterozoic to Mesoproterozoic cratonic basins in the São Francisco Craton. Journal of South American Earth Sciences 60, 104-116.

Guadagnin, F., Chemale Jr., F., Magalhães, A.J., Santana, A., Dussin, I., Takehara, L., 2015. Age constraints on crystal-tuff from the Espinhaço Supergroup - Insight into the Paleoproterozoic to Mesoproterozoic intracratonic basin cycles of the São Francisco Craton. Gondwana Research 27, 363-376.

Hartmann, L.A., Endo, I., Suita, M.T.F., Santos, J.O.S., Frantz, J.C., Carneiro, M.A., McNaughton, N.J., Barley, M.E., 2006. Provenance and age delimitation of Quadrilátero Ferrífero sandstones based on zircon U–Pb isotopes. Journal of South American Earth Sciences 20, 273–285.

Haskin, L.A., Wildeman, T.R., Haskin, M.A., 1968. An accurate procedure for the determination of the rare earths by neutron activation. Journal of Radioanalytical Chemistry 1, 337-348.

Hassan, S., Ishiga, H., Roser, B.P., Dozen, K., Naka, T., 1999. Geochemistry of Permian–Triassic shales in the Salt Range, Pakistan: implications for provenance and tectonism at the Gondwana margin. Chemical Geology 158, 293–314.

Haughton, P.D.W., Todd, S.P., Morton, A.C., 1991. Sedimentary provenance studies. In: Morton, A. C., Todd, S.P., Haughton, P.D.W. (Eds), Developments in Sedimentary Provenance Studies. Geological Society, Special Publication 57, pp. 1-11.

Herron, M.M., 1988. Geochemical classification of terrigenous sands and shales from core or log data. Journal of Sedimentary Petrology 58, 820–829.

Howard, K.E, Hand, M., Barovich, K.M., Payne, J.L., Belousova, E.A., 2011. U–Pb, Lu–Hf and Sm–Nd isotopic constraints on provenance and depositional timing of metasedimentary rocks in the western Gawler Craton: Implications for Proterozoic reconstruction models. Precambrian Research 184, 43–62.

Iizuka, T., Hirata, T., Komiya, T., Rino, S. Katayama, I., Motoki, A., 2005. U-Pb and Lu-Hf isotope systematics of zircons from the Mississippi River sand: Implications for reworking and growth of continental crust. Geology 33, 485–488.

Jackson, S.E., Pearson, N.J., Griffin, W.L., Belousova, E.A., 2004. The application of laser ablation-inductively coupled plasma-mass spectrometry to in situ U–Pb zircon geochronology. Chemical Geology 211, 47-69.

Knauer, L.G., Schrank, A., 1994. A origem dos filitos hematíticos da Serra do Espinhaço Meridional, Minas Gerais. Geonomos 1, 33–38.

Lamminen, J., Köykkä, J., 2010. The provenance and evolution of the Rjukan Rift Basin, Telemark, south Norway: The shift from a rift basin to an epicontinental sea along a Mesoproterozoic supercontinent. Precambrian Research 181, 129–149.

Li, Z.X., Bogdanova, S.V., Collins, A.S., Davidson, A., De Waele, B., Ernst, R.E., Fitzsimons, I.C.W., Fuck, R.A., Gladkochub, D.P., Jacobs, J., Karlstrom, K.E., Lu, S., Natapov, L.M., Pease, V., Pisarevsky, S.A., Thrane, K., Vernikovsky, V., 2008. Assembly, configuration, and break-up history of Rodinia: a synthesis. Precambrian Research 160, 179-210.

Ludwig, K.R., 2003. Using Isoplot/Ex, version 3.00, a geochronological toolkit for Microsoft Excel. Berkeley Geochronology Center, Special Publication 1 (43 pp.).

Martins-Neto, M.A., 1996. Lacustrine fan-deltaic sedimentation in a Proterozoic rift basin: the Sopa-Brumadinho Tectonosequence, southeastern Brazil. Sedimentary Geology 106, 65–96.

Martins-Neto, M.A., 1998. O Supergrupo Espinhaço em Minas Gerais: Registro de uma Bacia Rifte-Sag do Paleo/Mesoproterozóico. Revista Brasileira de Geologia 48, 151–168.

Martins-Neto, M.A., 2000. Tectonics and sedimentation in a paleo/mesoproterozoic rift-sag basin (Espinhaço basin, southeastern Brazil). Precambrian Research 103, 147-173.

Martins-Neto, M.A., Pedrosa-Soares, A.C., Lima, S.A.A., 2001. Tectono-sedimentary evolution of sedimentary basins from Late Paleoproterozoic to Late Neoproterozoic in the São Francisco craton and Araçuaí fold belt, eastern Brazil. Sedimentary Geology 141–142, 343–370.

Matteini, M., Dantas, E.L., Pimentel, M.M., Alvarenga, C.J.S., Dardenne, M.A., 2012. U–Pb and Hf isotope study on detrital zircons from the Paranoá Group, Brasília Belt Brazil: Constraints on depositional age at Mesoproterozoic –

Neoproterozoic transition and tectono-magmatic events in the São Francisco craton. Precambrian Research 206– 207, 168– 181.

McLennan, S.M., Hemming, S., McDaniel, D.K., Hanson, G.N., 1993. Geochemical approaches to sedimentation, provenance, and tectonics. In: M.J. Johnson and A. Basu (Eds.), Processes Controlling the Composition of Clastic Sediments. Geological Society of America Special Papers 284, 21-40.

McLennan, S.M., Taylor, S.R., 1991. Sedimentary rocks and crustal evolution: tectonic setting and secular trends. Journal of Geology 99, 1–21.

Meert, J.G., 2012. What's in a name? The Columbia (Paleopangaea/Nuna) supercontinent. Gondwana Research 21, 987–993.

Mongelli, G., Critelli, S., Perri, F., Sonnino, M., Perrone, V., 2006. Sedimentary recycling, provenance and paleoweathering from chemistry and mineralogy of Mesozoic continental redbed mudrocks, Peloritani mountains, southern Italy. Geochemical Journal 40, 197-209.

Moraes L.J., 1934. Depósitos diamantíferos no norte de Minas Geraes. Rio de Janeiro, DNPM/SFPM, 61 p.

Morag, N., Avigad, D., Gerdes, A., Belousova, E., Harlavan, Y., 2011. Detrital zircon Hf isotopic composition indicates long-distance transport of North Gondwana Cambrian–Ordovician sandstones. Geology 39, 955-958.

Morel, M.L.A., Nebel, O., Nebel-Jacobsen, Y.J., Miller, J.S., Vroon, P.Z. 2008. Hafnium isotope characterization of the GJ-1 zircon reference material by solution and laser-ablation MC-ICPMS. Chemical Geology 255, 231–235.

Muhs, D.R., Budahn, J.R., 2006. Geochemical evidence for the origin of late Quaternary loess in central Alaska: Canadian Journal of Earth Sciences 43, 323-337.

Nebel-Jacobsen, Y., Münker, C., Nebel, O., Mezger, K., 2011. Precambrian sources of Early Paleozoic SE Gondwana sediments as deduced from combined Lu–Hf and U–Pb systematics of detrital zircons, Takaka and Buller terrane, South Island, New Zealand. Gondwana Research 20, 427-442.

Noce, C.M., Pedrosa-Soares, A.C., Silva, L.C., Alkmim, F.F., 2007. O embasamento Arqueano E Paleoproterozóico do Orógeno Araçuaí. Geonomos 15, 17-23.

Patchett, P.J., Kouvo, O., Hedge, M., Tatsumoto, M., 1981. Evolution of the continental crust and mantle heterogeneity: evidence from Hf isotopes. Contributions to Mineralogy and Petrology 75, 263–267.

Pearce J.A., Harris N.B.W., Tindle, A.G., 1984. Trace element discrimination diagrams for the tectonic interpretation of granitic rocks. Journal of Petrology 25, 956-983.

Pettijohn, F.J., Potter, P.E., Siever, R., 1972. Sand and Sandstone. Springer-Verlag, New York, p. 618.

Pflug, R., 1968. Observações sobre a estratigrafia da Série Minas na região de Diamantina, Minas Gerais. Boletim da Divisão de Geologia e Mineralogia do Departamento Nacional de Produção Mineral: Notas Preliminares, 142 (20 pp.).

Piper, J.D.A., 2013. Continental velocity through Precambrian times: the link to magmatism, crustal accretion and episodes of global cooling. Geoscience Frontiers 4, 7-36.

Pisarevsky, S.A., Elming, S.Å., Pesonen, L.J., Li, Z.X., 2014. Mesoproterozoic paleogeography: Supercontinent and beyond. Precambrian Research 244, 207–225.

Plumb, K.A., 1991. New Precambrian time scale. Episodes 14, 139–140.

Prosser, S., 1993. Rift-related linked depositional systems and their seismic expression. In: Williams, G.D., Dobb, A. (Eds.), Tectonics and Seismic Sequence Stratigraphy: Geological Society, London, Special Publications, 71, pp. 35–66.

Rahman M.J.J., Suzuki S., 2007. Geochemistry of sandstones from the Miocene Surma Group, Bengal Basin, Bangladesh: Implications for Provenance, tectonic setting and weathering. Geochemical Journal 41, 415-428.

Roberts, N.M.W., 2013. The boring billion? e Lid tectonics, continental growth and environmental change associated with the Columbia supercontinent. Geoscience Frontiers 4, 681-691.

Rodrigues, J.B., Pimentel, M.M., Buhn, B., Matteini, M., Dardenne, M.A., Alvarenga, C.J.S., Armstrong, R.A., 2012. Provenance of the Vazante Group: New U–Pb, Sm–Nd, Lu–Hf isotopic data and implications for the tectonic evolution of the Neoproterozoic Brasília Belt. Gondwana Research 21, 439–450.

Rogers, J.J.W., Santosh, M., 2002. Configuration of Columbia, a Mesoproterozoic Supercontinent. Gondwana Research 5, 5–22.

Saadi, A., 1995. A geomorfologia da Serra do Espinhaço em Minas Gerais e de suas margens. Geonomos 3, 41–63.

Santos, M.N., 2011. Evolução sedimentológica e paleogeográfica do sistema de riftes do Espinhaço Meridional. MSc Thesis, Instituto de Geociências, Universidade Federal do Rio Grande do Sul, Porto Alegre, Brazil, 85 pp.

Santos, M.N., Chemale Jr., F., Dussin, I.A., Martins, M.S., Assis, T.A.R., Jelinek, A.R., Guadagnin, F., Arsmtrong, R., 2013. Sedimentological and Paleoenvironmental Constraints of the Statherian and Stenian Espinhaço Rift System, Brazil. Sedimentary Geology 290, 47-59.

Santos, M.N., Chemale Jr., F., Dussin, I.A., Martins, M.S., Queiroga, G., Pinto, R.T.R., Santos, A.N., Armstrong, R., 2015. Provenance and paleogeographic reconstruction of a mesoproterozoic intracratonic sag basin (Upper Espinhaço Basin, Brazil). Sedimentary Geology 318, 40–57.

Schöll, W.U., Fogaça, A.C.C., 1979. Estratigrafia da Serra do Espinhaço na região de Diamantina. Simpósio de Geologia de Minas Gerais, Diamantina: Anais, Sociedade Brasileira de Geologia, pp. 55–73.

Shao, L., Stettegger, K., Garbe-Schoenberg, C.D., 2001. Sandstone petrology and geochemistry of the Turpan basin (NW China): implications for the tectonic evolution of a continental basin. Journal of Sedimentary Research 71, 37-49.

Silva, R.R., 1998. As bacias proterozóicas do Espinhaço e São Francisco em Minas Gerais: uma abordagem do ponto de vista da estratigrafia de sequências. Geonomos 6, 1–12.

Silveira, E.M., Söderlund, U., Oliveira, E.P., Ernst, R.E.,Menezes Leal, A.B., 2013. First precise U-Pb baddeleyite ages of 1500 Ma mafic dykes from the São Francisco Craton, Brazil, and tectonic implications. Lithos 174, 144–156.

Slack, J.F., Stevens, B.P.J., 1994. Clastic Metasediments of the Early Proterozoic Broken-Hill Group, New-South-Wales, Australia: Geochemistry, provenance, and metallogenic significance. Geochimica et Cosmochimica Acta 58, 3633-3652.

Souza Filho, R.C., 1995. Arcabouço estrutural da porção externa da Faixa Araçuaí na Serra do Cabral (MG) e o contraste de estilos deformacionais entre os Supergrupos Espinhaço e São Francisco. (MSc Thesis), Universidade Federal de Ouro Preto, Ouro Preto, Brazil (148 pp.).

Taylor, S.R., McLennan, S.M., 1985. The continental crust: its composition and evolution. Oxford, Blackwell, 312pp.

Thomas, W.A., 2011. Detrital-zircon geochronology and sedimentary provenance. Lithosphere 3, 304-308.

Tripathi, K.J., Rajamani, V., 2003. Geochemistry of Proterozoic Delhi quartzite: Implications for the provenance and source area weathering. Journal of the Geological Society of India 62, 215–226.

Uhlein, A., 1991. Transição cráton-faixa dobrada: exemplo do Cráton do São Francisco e da Faixa Araçuaí (Ciclo Brasiliano) no Estado de Minas Gerais. Aspectos estratigráficos e estruturais. Ph.D. Thesis, São Paulo, Universidade de São Paulo, 295pp.

Uhlein, A., Chaves, M.L.S.C., 2001. O Supergrupo Espinhaço em Minas Gerais e Bahia: correlações estratigráficas, conglomerados diamantíferos e evolução geodinâmica. Revista Brasileira de Geociências 31, 433–444.

Uhlein, A., Trompette, R., Egydio-Silva, M., 1998. Proterozoic rifting and closure, SE borderof the São Francisco Craton, Brazil. Journal of African Earth Sciences 11, 191–203.

Wegener, A., 1915. Die Entstehung der Kontinente und Ozeane. On the Origin of Continents and Oceans, English translation of 3rd edition by J. G. A. Skerl (1924). Methuen, London. 212 pp.

Willner, A.P., Gerdes, A., Massonne, H.-J., 2008. History of crustal growth and recycling at the Pacific convergent margin of South America at latitudes 29°–36° S revealed by a U–Pb and Lu–Hf isotope study of detrital zircon from late Paleozoic accretionary systems. Chemical Geology 253, 114–129.

Woodhead, J.D., Hergt, J. M. 2005. A preliminary appraisal of seven natural zircon reference materials for in situ hf isotope determination. Geostandards and Geoanalytical Research 29, 183-195.

Wronkiewicz, D.J., Condie, K.C., 1989. Geochemistry and provenance of sediments from the Pongola Supergroup, South Africa: Evidence for a 3.0-Ga-old continental craton: Geochimica et Cosmochimica Acta 53, 1537–1549.

Yakubchuk, A., 2010. Restoring the supercontinent Columbia and tracing its fragments after its breakup: a new configuration and a Super-Horde hypothesis. Journal of Geodynamics 50, 166-175.

Zhang, S., Li, Z.-X., Evans, D.A.D., Wu, H., Li, H., Dong, J., 2012. Pre-Rodinia supercontinent Nuna shaping up: a global synthesis with new paleomagnetic results from North China. Earth and Planetary Science Letters 353-354, 145-155.

Zhang, Y., Pe-Piper, G., Piper, D.J.W., 2014. Sediment geochemistry as a provenance indicator: Unravelling the cryptic signatures of polycyclic sources, climate change, tectonism and volcanism. Sedimentology 61, 383–410.

Zhao, G., Cawood, P.A., Wilde, S.A., Sun, M., 2002. Review of global 2.1–1.8 Ga orogens: implications for a pre-Rodinia supercontinent. Earth-Science Reviews 59, 125–162.

CAPÍTULO IV

Conclusões da tese

Para a concepção da presente tese foram integrados dados de mapeamento geológico, análise geoquímica em rocha total e análise *in situ* dos isótopos U-Pb e Lu-Hf em grãos de zircão de amostras do embasamento, das unidades metassedimentares e metavulcânicas da Bacia Espinhaço. A partir desses dados foi possível chegar às conclusões descritas abaixo.

- Os dados geoquímicos dos elementos maiores sugerem proveniência a partir da erosão de uma área fonte com baixo relevo, provavelmente arrasada por forte intemperismo. O padrão dos elementos terras raras, caracterizado pelo enriquecimento em ETRs leves e tendência plana dos ETRs pesados, bem como as razões Eu/Eu*, $(La/Lu)_n$, La/Sc, Th/Sc e Zr/Sc indicam que a maior parte das fontes possuía composição félsica, embora a razão Al_2O_3/TiO_2 também aponte para a presença de fases máficas. Retrabalhamento das unidades sedimentares da própria bacia (autofagia) também contribuiu para a disponibilização dos sedimentos.
- Os grãos de zircão detríticos da Sequência Espinhaço Inferior (fms. Bandeirinha e São João da Chapada) apresentam picos de idade semelhantes em 1,7, 2,1, 2,4, 2,7, 2,8 e 3,3 Ga, porém a proporção relativa entre cada população é nitidamente distinta, provavelmente refletindo a mudança no padrão de paleocorrentes de longitudinal para transversal ao eixo do rifte. Os xistos da Fm. Barão de Guaicuí foram importantes rochas fontes para os sedimentos da Fm. Bandeirinha, pois em ambas as unidades há similaridade na composição isotópica de Hf dos grãos. Após a denudação de parte da Fm. Barão de Guaicuí da borda oeste do rifte (lapa), o embasamento cristalino (Complexo Gouveia), datado em 2828 Ma, teria ficado exposto e, por conseguinte, contribuído como fonte para a Fm. São João da Chapada. Os grãos de zircão detríticos de 1,7 Ga apresentam composição isotópica de Hf semelhante ao filito hamatítico, indicando que as rochas magmáticas relacionadas à abertura do rifte também contribuíram como áreas fontes.
- Os valores de $\varepsilon_{Hf}(t)$ exclusivamente negativos encontrados nos grãos de zircão do filito hamatítico evidenciam que o evento magmático que o formou não estaria relacionado ao transporte de diamantes do manto para a superfície da Terra.
- A manutenção das paleocorrentes transversais ao eixo do rifte durante a deposição da Fm. Sopa-Brumadinho resultou em proveniência sedimentar semelhante à Fm. São João da Chapada, mesmo após um hiato de 500 Ma, exceto pela presença de grãos de 1,2 a 1,5 Ga na primeira. A população de grãos de zircão do Mesoproterozoico da Fm. Sopa-Brumadinho não é restrita aos depósitos da borda leste do rifte (Região de Extração), mas também ocorre na

sua borda oeste. A composição juvenil dos grãos com 1,2 Ga indica que sua fonte foi extraída do manto, cujo magmatismo pode estar relacionado ao transporte de diamantes para a superfície da Terra.

- A Sequência Espinhaço Superior provavelmente registra a reativação das estruturas da Sequência Espinhaço Inferior devido à influência dentro do Cráton do São Francisco de eventos compressivos que ocorreram nas bordas da placa (Evento Grenvilleano). Eventos sísmicos decorrentes dessa compressão ficaram impressos, por exemplo, no Grupo Conselheiro Mata. Baseado na análise das litologias e elementos arquiteturais dessa unidade, foi possível discriminar os ambientes deposicionais presentes em seus ciclos de transgressão e regressão marinha, os quais incluem: sistema eólico desenvolvido em condições desérticas, foreshore, upper shoreface (dominado por correntes de deriva litorânea ou por maré), lower shoreface, offshore e plataforma carbonática-silisiclástica. A fase sag também é caracterizada por uma significativa mudança de proveniência, predominantemente Orosiriana nas formações Córrego Pereira e Rio Pardo Grande.
- A população de grãos com 2,1 Ga pode ter resultado da contaminação de magmas juvenis por uma crosta Arqueana, formados em arco continental a oeste do cráton durante a aglutinação do Supercontinente Columbia.

Apêndice A

Informações sobre a localização, litotipos e unidades estratigráficas das rochas datadas por U-Pb.

	Coordinates					
Sample	EM	NM	ALT (m)	Lithotype	Stratigraphic unit	Observation
PE-GO-65	631111	7957824	1049	Gneiss	Gouveia Complex	From this work
PE-GO-01	635338	7962289	1210	Schist	Barão de Guaicuí Fm.	From this work
PE-GO-28	637368	7981140	1390	Redish quartzite	Bandeirinha Fm.	Chemale et al. (2012)
PE-GO-30A	637083	7981560	1394	Redish quartzite	Bandeirinha Fm.	Santos et al. (2013)
PE-SM-05	637874	7972985	1435	Quartzite	São João da Chapada Fm.	Chemale et al. (2012)
PE-SM-06	637874	7972985	1435	Hematitic Phyllite	São João da Chapada Fm.	From this work
PE-SM-07	638742	7973393	1476	Quartzite	São João da Chapada Fm.	Santos et al. (2013)
PE-SM-09	638845	7973360	1482	Quartzite	São João da Chapada Fm.	Santos et al. (2013)
PE-GO-31	637230	7981774	1385	Quartzite	São João da Chapada Fm.	From this work
PE-CM-11A	638063	7980218	1430	Conglomerate	Sopa-Brumadinho Fm.	From this work
PE-GO-33A	636508	7986083	1314	Matrix of metaconglomerate	Sopa-Brumadinho Fm.	Santos et al. (2013)
PE-GO-33B	636508	7986083	1314	Quartzite	Sopa-Brumadinho Fm.	Santos et al. (2013)
PE-EX-34B	656286	7976528	1094	Pebble	Sopa-Brumadinho Fm.	Chemale et al. (2012)
PE-EX-34C	656286	7976528	1094	Matrix of metaconglomerate	Sopa-Brumadinho Fm.	Chemale et al. (2012)
PE-EX-34D	656286	7976528	1094	Matrix of metaconglomerate	Sopa-Brumadinho Fm.	Chemale et al. (2012)
PE-GO-39	639780	7982738	1346	Quartzite	Sopa-Brumadinho Fm.	From this work
PE-GO-59	635921	7958110	997	Quartzite	Sopa-Brumadinho Fm.	From this work
PE-GO-61	637571	7957980	1057	Quartzite	Sopa-Brumadinho Fm.	From this work
PE-GO-66	636924	7983947	1128	Phyllite	Sopa-Brumadinho Fm.	Santos et al. (2013)
PE-GO-102	639798	7982767	1364	Breccia	Sopa-Brumadinho Fm.	Santos et al. (2013)
PE-GO-103	639340	7981696	1380	Quartzite	Sopa-Brumadinho Fm.	Santos et al. (2013)
PE-CM-14	625338	7976007	1325	Quartzite	Galho do Miguel Fm.	From this work
PE-CM-15A	622219	7976999	1251	Quartzite	Galho do Miguel Fm.	From this work
PE-CM-15B	622219	7976999	1251	Quartzite	Galho do Miguel Fm.	From this work
PE-GO-40	640043	7980925	1364	Quartzite	Galho do Miguel Fm.	Chemale et al. (2012)
PE-SC-43	584364	8043721	1085	Quartzite	Galho do Miguel Fm.	From this work
PE-SC-45	580702	8019622	1103	Quartzite	Galho do Miguel Fm.	From this work
PE-FM-48	634692	8075344	865	Quartzite	Galho do Miguel Fm.	From this work
PE-FM-71	631404	8066797	1078	Quartzite	Galho do Miguel Fm.	From this work
PE-CM-16	620826	7975961	1228	Phyllite	Santa Rita Fm.	From this work
PE-CM-17	619629	7979809	1177	Quartzite	Santa Rita Fm.	From this work
PE-SC-44	586522	8039756	939	Phyllite	Santa Rita Fm.	Chemale et al. (2012)
PE-CM-19	620118	7976864	1255	Quartzite	Córrego dos Borges Fm.	Chemale et al. (2012)
PE-CM-20	619617	7974056	1191	Quartzite	Córrego dos Borges Fm.	From this work
PE-SC-42	564790	8047329	1058	Quartzite	Córrego dos Borges Fm.	From this work
PE-SC-52	565414	8094851	776	Quartzite	Córrego dos Borges Fm.	From this work
PE-CM-18	618496	7975080	1238	Quartzite	Córrego Pereira Fm.	From this work
PE-CM-26	614367	7973827	1120	Quartzite	Córrego Pereira Fm.	Chemale et al. (2012)
PE-CM-35	609206	7974105	987	Quartzite	Rio Pardo Grande Fm.	Chemale et al. (2012)
PE-CM-54	608983	7978824	1010	Quartzite	Rio Pardo Grande Fm.	From this work

Apêndice B

Dados de geoquímica dos elementos maiores.

Analyte Symbol		SiO2	Al2O3	Fe2O3(T)	MnO	MgO	CaO	Na2O	K2O	TiO2	P2O5	LOI	Total
Unit Symbol		%	%	%	%	%	%	%	%	%	%	%	%
PE- GO-01	Costa Sena Gr.	68.49	16.47	8.15	0.013	0.34	0.11	0.09	1.99	0.783	0.11	1.84	98.38
PE-SM-04	Bandeirinha Fm.	81.08	14.08	1.68	0.003	0.04	0.04	0.07	1.48	0.18	0.16	1.17	99.98
PE-GO-28	Bandeirinha Fm.	93.15	5.56	0.9	0.015	0.03	0.01	0.02	0.21	0.131	0.03	0.64	100.7
PE-GO-30A	Bandeirinha Fm.	91.83	4.66	1.25	0.005	0.04	0.01	0.05	1.1	0.207	0.04	1.06	100.2
PE-GO-30B	Bandeirinha Fm.	94.17	3.29	0.22	0.004	0.02	< 0.01	0.02	0.29	0.064	0.03	0.74	98.87
PE- GO-02	São João da Chapada Fm.	99.17	0.68	0.36	0.002	0.05	0.02	0.04	< 0.01	0.046	0.02	0.45	100.9
PE-GO-03	São João da Chapada Fm.	98.83	0.74	0.23	0.007	0.03	0.04	0.01	0.13	0.02	0.03	0.69	100.8
PE-SM-05	São João da Chapada Fm.	97.14	0.84	0.19	0.002	0.06	0.02	0.03	0.25	0.029	0.02	0.4	98.97
PE-SM-07	São João da Chapada Fm.	99.4	0.47	0.08	0.002	0.04	0.02	0.04	0.16	0.025	0.02	0.31	100.6
PE-GO-31	São João da Chapada Fm.	98.39	0.62	0.13	0.002	0.03	0.01	0.01	0.17	0.042	0.02	0.54	99.98
PE-CM-36	São João da Chapada Fm.	97.5	0.42	0.21	0.002	0.02	0.02	0.04	0.19	0.018	0.02	0.52	98.97
PE-GO-37	São João da Chapada Fm.	94.69	2.19	0.3	0.004	0.02	0.03	< 0.01	0.03	0.037	0.03	1.34	98.57
PE-GO-29	Hematitic Filite	32.48	22.22	29.33	0.097	1.01	< 0.01	0.29	7.48	3.64	0.03	3.66	100.2
PE-SM-06	Hematitic Filite	31.19	22.81	27.14	0.024	0.6	0.02	0.19	7.99	5.668	0.16	3.44	99.23
PE-SM-09	Sopa-Brumadinho Fm.	91.71	4.06	0.51	0.004	0.5	0.02	0.04	1.43	0.195	0.02	1.29	99.78
PE-SM-10	Sopa-Brumadinho Fm.	98.96	0.67	0.51	0.007	0.04	< 0.01	0.01	0.18	0.043	0.02	0.41	100.9
PE-CM-11A	Sopa-Brumadinho Fm.	96.82	1.02	0.34	0.004	0.07	0.02	< 0.01	0.27	0.014	0.02	0.52	98.97
PE-CM-11B	Sopa-Brumadinho Fm.	97.18	0.71	0.1	0.004	0.04	0.02	< 0.01	0.13	0.019	0.01	0.51	98.6
PE-GO-32	Sopa-Brumadinho Fm.	99.04	0.35	0.43	0.002	0.03	0.02	< 0.01	0.07	0.019	0.02	0.4	100.4
PE-GO-33B	Sopa-Brumadinho Fm.	96.17	0.9	0.66	0.002	0.04	0.02	< 0.01	0.13	0.031	0.03	0.74	100.8
PE-EX-34C	Sopa-Brumadinho Fm.	67.01	15.07	3.72	0.078	1.43	0.03	< 0.01	6	0.24	0.12	5.47	99.12
PE-EX-34B	Sopa-Brumadinho Fm.	96.12	0.95	0.89	0.032	0.11	0.02	0.03	0.35	0.046	0.03	0.6	99.16
PE-EX-34D	Sopa-Brumadinho Fm.	96.46	1.16	0.38	0.061	0.15	0.02	0.01	0.45	0.064	0.02	0.52	99.3
PE-GO-38	Sopa-Brumadinho Fm.	98.57	0.58	0.54	0.002	0.03	0.01	< 0.01	0.05	0.038	0.02	0.62	100.5

Analyte Symbol		SiO2	Al2O3	Fe2O3(T)	MnO	MgO	CaO	Na2O	K2O	TiO2	P2O5	LOI	Total
PE-GO-39	Sopa-Brumadinho Fm.	97.62	0.58	0.16	0.002	0.07	0.02	< 0.01	0.16	0.026	0.03	0.3	98.97
PE-GO-40	Galho do Miguel Fm.	98.53	1.1	0.31	0.002	0.1	< 0.01	< 0.01	0.41	0.065	0.02	0.35	100.9
PE-SC-43	Galho do Miguel Fm.	97.17	1.36	0.31	0.004	0.08	0.03	0.02	0.48	0.047	0.05	0.7	100.2
PE-SC-45	Galho do Miguel Fm.	99.5	0.55	0.09	0.002	0.02	0.02	0.03	0.15	0.034	0.04	0.45	100.9
PE-FM-48	Galho do Miguel Fm.	99.01	0.27	0.09	0.004	0.02	0.02	< 0.01	0.03	0.032	0.02	0.25	99.75
PE-CM-12	Galho do Miguel Fm.	98.46	0.58	0.08	0.002	0.02	0.03	0.01	0.15	0.034	0.03	0.42	99.82
PE-CM-13	Galho do Miguel Fm.	98.01	0.44	0.22	0.004	< 0.01	0.05	0.01	0.11	0.024	0.02	0.31	99.21
PE-CM-14	Galho do Miguel Fm.	97.35	1.65	0.63	0.003	0.02	0.01	0.03	0.45	0.075	0.03	0.61	100.9
PE-CM-15A	Galho do Miguel Fm.	99.27	0.17	0.08	0.007	< 0.01	< 0.01	< 0.01	< 0.01	0.016	0.02	0.42	100
PE-CM-15B	Galho do Miguel Fm.	97.85	0.49	0.17	0.004	0.02	0.03	0.11	0.11	0.029	0.02	0.46	99.3
PE-CM-16	Santa Rita Fm.	66.75	22.9	0.53	0.002	0.04	0.01	0.05	0.99	0.346	0.04	8.65	100.3
PE-CM-17	Santa Rita Fm.	96.63	1.89	0.72	0.002	0.05	0.03	0.05	0.11	0.068	0.04	1.18	100.8
PE-SC-44	Santa Rita Fm.	71.97	13.64	3.93	0.014	1.2	0.04	0.09	4.1	0.568	0.14	3.95	99.61
PE-SC-46	Santa Rita Fm.	73.6	13.86	2.27	0.005	1.22	0.08	0.07	3.9	0.359	0.06	4.1	99.53
PE-SC-42	Córrego dos Borges Fm.	97.81	0.12	0.43	0.004	0.02	0.03	< 0.01	0.03	0.014	0.02	0.42	98.79
PE-CM-19	Córrego dos Borges Fm.	95.88	1.88	0.1	0.002	< 0.01	0.03	0.01	0.61	0.062	0.03	0.75	99.38
PE-CM-20	Córrego dos Borges Fm.	96.09	1.29	0.29	0.012	0.05	0.02	< 0.01	0.27	0.046	0.09	0.49	98.56
PE-CM-21	Córrego dos Borges Fm.	86.95	6.96	0.9	0.002	0.44	0.02	0.02	1.62	0.312	0.03	2.45	99.7
PE-CM-26	Córrego Pereira Fm.	96.63	0.84	0.34	0.016	0.03	0.03	< 0.01	0.37	0.069	0.04	0.4	98.65
PE-CM-18	Córrego Pereira Fm.	99.95	0.21	0.23	0.004	0.01	0.02	0.01	0.01	0.033	0.04	0.47	101
PE-CM-35	Rio Pardo Grande Fm.	94.27	3.33	0.46	0.002	0.06	0.01	< 0.01	0.34	0.044	0.03	1.73	100.3

Apêndice C

Dados de geoquímica dos elementos-traço.

Analyte Symbol		La	Ce	Pr	Nd	Sm	Eu	Gd	Tb	Dy	Ho	Er	Tm	Yb	Lu
Unit Symbol		ppm	ppm	ppm	ppm	ppm	ppm	ppm	ppm	ppm	ppm	ppm	ppm	ppm	ppm
PE- GO-01	Costa Sena Gr.	25.8	52.5	5.33	20.7	4.56	1.3	5.26	1.08	6.16	1.07	3.77	0.495	3.25	0.512
PE-SM-04	Bandeirinha Fm.	47.3	91.5	10.5	33.6	7.03	0.769	5.78	1.04	5.84	1.27	4.19	0.655	4.1	0.54
PE-GO-28	Bandeirinha Fm.	27.8	62.1	6.11	18.9	3.06	0.448	2.11	0.35	1.98	0.45	1.61	0.337	1.75	0.266
PE-GO-30A	Bandeirinha Fm.	25.2	43.6	6.56	21.3	3.77	0.523	2.13	0.3	1.84	0.42	1.44	0.295	1.45	0.211
PE-GO-30B	Bandeirinha Fm.	7.85	13.7	1.61	5.24	0.97	0.196	0.91	0.17	0.94	0.21	0.69	0.126	0.68	0.098
PE- GO-02	São João da Chapada Fm.	10.1	20.8	2.44	8.45	1.85	0.306	1.65	0.3	1.61	0.33	0.97	0.201	0.87	0.126
PE-GO-03	São João da Chapada Fm.	5.91	10.8	1.14	3.6	0.78	0.086	0.69	0.13	0.73	0.16	0.53	0.145	0.55	0.079
PE-SM-05	São João da Chapada Fm.	4.62	7.36	0.89	3.04	0.62	0.115	0.59	0.11	0.62	0.14	0.45	0.153	0.46	0.066
PE-SM-07	São João da Chapada Fm.	2	3.34	0.37	1.27	0.29	0.056	0.29	0.07	0.35	0.08	0.25	0.09	0.26	0.04
PE-GO-31	São João da Chapada Fm.	8.44	15.6	1.69	5.46	1.06	0.193	1	0.17	0.88	0.18	0.57	0.123	0.54	0.077
PE-CM-36	São João da Chapada Fm.	2.84	4.49	0.52	1.77	0.35	0.076	0.34	0.07	0.39	0.08	0.26	0.063	0.28	0.039
PE-GO-37	São João da Chapada Fm.	6.19	12.2	1.15	4.27	1.11	0.218	0.92	0.18	0.92	0.16	0.58	0.103	0.52	0.085
PE-GO-29	Hematitic Filite	41.6	90.7	11.1	47.3	10	2.67	9.23	1.75	10.9	1.96	7.23	0.955	6.33	0.996
PE-SM-06	Hematitic Filite	69	171	17.5	75.9	18.1	5.15	17.6	2.84	13.8	2.2	7.04	0.913	5.96	0.878
PE-SM-09	Sopa-Brumadinho Fm.	10.2	17.3	2.08	6.6	1.35	0.346	1.44	0.31	1.72	0.37	1.18	0.214	1.14	0.185
PE-SM-10	Sopa-Brumadinho Fm.	4.55	7.41	0.93	3.2	0.6	0.09	0.53	0.11	0.67	0.14	0.48	0.113	0.47	0.074
PE-CM-11A	Sopa-Brumadinho Fm.	2.34	3.63	0.36	1.27	0.34	0.047	0.29	0.06	0.37	0.06	0.22	0.039	0.19	0.035
PE-CM-11B	Sopa-Brumadinho Fm.	2.67	3.27	0.37	1.05	0.32	0.031	0.2	0.06	0.33	0.06	0.17	0.039	0.18	0.03
PE-GO-32	Sopa-Brumadinho Fm.	2.33	2.66	0.32	1.02	0.21	0.038	0.24	0.04	0.24	0.05	0.14	0.05	0.15	0.022
PE-GO-33B	Sopa-Brumadinho Fm.	9.61	25.1	2	6.59	1.03	0.148	0.54	0.1	0.52	0.11	0.35	0.085	0.36	0.052
PE-EX-34C	Sopa-Brumadinho Fm.	118	208	26.8	99.4	18	3.14	10.7	1.42	6.03	0.81	2.48	0.277	1.88	0.27

Analyte Symbol		La	Ce	Pr	Nd	Sm	Eu	Gd	Tb	Dy	Ho	Er	Tm	Yb	Lu
PE-EX-34B	Sopa-Brumadinho Fm.	18.5	26.7	3.89	12.1	2	0.312	1.33	0.2	0.95	0.18	0.57	0.116	0.51	0.078
PE-EX-34D	Sopa-Brumadinho Fm.	23.7	34.4	4.85	14.7	2.21	0.332	1.57	0.23	1.16	0.25	0.82	0.166	0.83	0.123
PE-GO-38	Sopa-Brumadinho Fm.	2.21	4.8	0.34	1.09	0.24	0.041	0.28	0.07	0.37	0.09	0.27	0.07	0.29	0.045
PE-GO-39	Sopa-Brumadinho Fm.	22.2	55.6	4.29	12.3	1.96	0.323	0.88	0.13	0.52	0.09	0.28	0.108	0.27	0.04
PE-GO-40	Galho do Miguel Fm.	6.38	11	1.39	4.66	0.78	0.19	0.86	0.18	0.98	0.21	0.68	0.12	0.59	0.083
PE-SC-43	Galho do Miguel Fm.	7.62	15.7	1.71	5.76	1.2	0.294	1.19	0.22	1.17	0.24	0.68	0.126	0.58	0.075
PE-SC-45	Galho do Miguel Fm.	7.04	10.9	1.48	5.08	0.89	0.176	0.82	0.11	0.49	0.09	0.29	0.08	0.33	0.05
PE-FM-48	Galho do Miguel Fm.	6.35	12.1	1.5	4.99	0.77	0.131	0.62	0.1	0.48	0.1	0.33	0.072	0.32	0.046
PE-CM-12	Galho do Miguel Fm.	5.98	13.5	1.49	5.14	1.01	0.228	0.89	0.17	0.87	0.18	0.53	0.146	0.44	0.065
PE-CM-13	Galho do Miguel Fm.	5.32	12.1	1.18	4.03	0.76	0.133	0.5	0.07	0.31	0.06	0.24	0.076	0.27	0.041
PE-CM-14	Galho do Miguel Fm.	8.74	16	2.28	7.92	1.53	0.339	1.46	0.27	1.42	0.29	0.9	0.164	0.73	0.112
PE-CM-15A	Galho do Miguel Fm.	3.74	5.51	0.84	2.89	0.44	0.07	0.22	0.03	0.19	0.04	0.16	0.057	0.19	0.03
PE-CM-15B	Galho do Miguel Fm.	4.81	7.37	1.16	4.06	0.73	0.128	0.43	0.07	0.36	0.08	0.29	0.103	0.34	0.053
PE-CM-16	Santa Rita Fm.	21.2	28	3.54	12.8	2.55	0.555	3.05	0.8	4.9	0.91	3.25	0.465	3.12	0.47
PE-CM-17	Santa Rita Fm.	13.8	21.3	3.09	10.3	1.8	0.336	1.32	0.21	1.05	0.21	0.66	0.166	0.64	0.095
PE-SC-44	Santa Rita Fm.	46.9	94.8	10.6	35.6	7.1	1.38	5.64	0.91	4.69	1	3.09	0.545	3.02	0.438
PE-SC-46	Santa Rita Fm.	41	77.3	9.73	30.9	5.84	1.34	4.62	0.8	4.23	0.88	2.76	0.417	2.69	0.399
PE-SC-42	Córrego dos Borges Fm.	2.11	4.01	0.4	1.69	0.36	0.069	0.36	0.06	0.36	0.06	0.21	0.042	0.16	0.027
PE-CM-19	Córrego dos Borges Fm.	12.2	14.6	2.65	8.14	1.4	0.266	1.07	0.18	1.06	0.24	0.79	0.145	0.82	0.13
PE-CM-20	Córrego dos Borges Fm.	26.8	48.4	6.39	26.1	5.33	0.978	3.54	0.33	1.17	0.17	0.62	0.08	0.63	0.096
PE-CM-21	Córrego dos Borges Fm.	27.5	54.4	5.35	15.4	2.51	0.54	2.12	0.39	2.32	0.51	1.74	0.308	1.87	0.274
PE-CM-26	Córrego Pereira Fm.	7.51	16.4	1.48	5.85	1.16	0.246	0.86	0.16	0.85	0.14	0.53	0.097	0.51	0.092
PE-CM-18	Córrego Pereira Fm.	5.78	9.01	1.21	3.52	0.58	0.095	0.49	0.09	0.53	0.11	0.37	0.125	0.4	0.058
PE-CM-35	Rio Pardo Grande Fm.	15.5	29.9	3.27	9.85	1.85	0.393	1.41	0.19	0.81	0.15	0.45	0.087	0.45	0.066

Apêndice D

Resumo dos dados de U-Pb da amostra PE-GO-65 (Complexo Gouveia).

Grain.Spot	% $^{206}Pb_c$	ppm U	ppm Th	^{232}Th / ^{238}U	ppm $^{206}Pb^*$	(1) ^{206}Pb / ^{238}U Age		(1) ^{207}Pb / ^{206}Pb Age		% Dis-cor-dant	(1) $^{207}Pb^*$ / $^{206}Pb^*$	±%	(1) $^{207}Pb^*$ / ^{235}U	±%	(1) $^{206}Pb^*$ / ^{238}U	±%	err corr
A-2.1	0.14	481	379	0.81	165	2158	±33	2801.9	± 5.1	23	0.19705	0.31	10.8	1.8	0.3975	1.8	.985
A-4.1	0.31	207	166	0.83	73.1	2216	±34	2791.3	± 8	21	0.19578	0.49	11.08	1.9	0.4103	1.8	.966
A-6.1	0.08	206	90	0.45	90.1	2652	±39	2787.6	± 6.9	5	0.19533	0.42	13.71	1.8	0.5089	1.8	.973
A-8.1	0.12	306	128	0.43	144	2814	±40	2805.3	± 5.6	0	0.19746	0.34	14.9	1.8	0.5472	1.8	.982
A-9.1	0.28	431	730	1.75	101	1547	±25	2567.1	± 9.1	40	0.17096	0.55	6.39	1.9	0.2711	1.8	.956
A-10.1	0.86	562	176	0.32	104	1245	±20	2191	± 21	43	0.1371	1.2	4.03	2.1	0.2131	1.8	.829
A-11.1	0.92	488	322	0.68	133	1757	±27	2454	± 11	28	0.1599	0.66	6.91	1.9	0.3133	1.8	.938
A-22.1	0.20	427	116	0.28	151	2217	±33	2661.5	± 6.2	17	0.18094	0.37	10.24	1.8	0.4104	1.8	.978
A-23.1	1.07	532	157	0.31	140	1711	±26	2586	± 12	34	0.1729	0.72	7.25	1.9	0.304	1.7	.924
A-25.1	0.85	1238	365	0.30	172	961	±16	1806	± 14	47	0.11038	0.77	2.447	1.9	0.1608	1.8	.916
A-27.1	0.53	509	264	0.54	116	1513	±24	2387	± 11	37	0.15364	0.62	5.6	1.9	0.2646	1.8	.942
A-28.1	0.26	383	193	0.52	119	1978	±30	2685.3	± 9.2	26	0.1836	0.55	9.09	1.9	0.3592	1.8	.955
A-29.1	1.24	979	423	0.45	146	1023	±16	1845	± 17	45	0.1128	0.96	2.673	2	0.1719	1.7	.876
A-32.1	0.64	604	333	0.57	123	1362	±21	2263	± 14	40	0.1429	0.81	4.635	1.9	0.2352	1.7	.907
A-33.1	0.13	298	82	0.28	116	2405	±35	2734.9	± 6.1	12	0.18917	0.37	11.79	1.8	0.4522	1.8	.979
A-35.1	1.23	968	258	0.28	145	1025	±16	1870	± 17	45	0.1144	0.96	2.718	2	0.1724	1.7	.876
A-38.1	0.13	524	332	0.65	180	2167	±32	2664.7	± 7.2	19	0.18129	0.44	9.99	1.8	0.3995	1.7	.970
A-14.1	4.25	784	327	0.43	185	1503	±25	2660	± 83	43	0.1808	5	6.55	5.4	0.2626	1.9	.349

A-20.1	7.90	802	249	0.32	150	1179	±21	1909	±140	38	0.1169	7.5	3.23	7.8	0.2007	1.9	.245
A-18.1	0.66	954	746	0.81	160	1142	±18	2540.1	± 8.8	55	0.16823	0.52	4.494	1.8	0.1937	1.8	.959

Resumo dos dados de U-Pb da amostra PE-GO-01 (Formação Barão de Guaicuí).

Grain.Spot	% $^{206}Pb_c$	ppm U	ppm Th	^{232}Th / ^{238}U	ppm $^{206}Pb^*$	(1) ^{206}Pb / ^{238}U Age		(1) ^{207}Pb / ^{206}Pb Age		% Dis-cor-dant	(1) $^{207}Pb^*$ / $^{206}Pb^*$	±%	(1) $^{207}Pb^*$ / ^{235}U	±%	(1) $^{206}Pb^*$ / ^{238}U	±%	err corr
1.1	0.99	1390	934	0.69	217	1065	±11	2181	±18	51	0.1364	1	3.379	1.5	0.1797	1.1	.740
3.1	0.31	749	167	0.23	133	1209	±13	2850	±10	58	0.2029	0.62	5.773	1.3	0.2063	1.2	.882
4.1	0.03	497	77	0.16	218	2664	±27	2976.6	± 7	11	0.21944	0.43	15.48	1.3	0.5118	1.2	.945
5.1	0.23	479	121	0.26	150	1995	±21	3040.8	± 9	34	0.2284	0.56	11.42	1.4	0.3626	1.3	.912
6.1	0.02	276	92	0.34	141	3003	±33	2933	± 8.5	-2	0.2136	0.53	17.47	1.5	0.5934	1.4	.933
7.1	0.24	1207	471	0.40	184	1050	±11	2949.5	± 8.9	64	0.2158	0.55	5.265	1.2	0.177	1.1	.897
9.1	1.86	2772	720	0.27	244	618.6	± 6.4	1169	±49	47	0.0789	2.5	1.096	2.7	0.1007	1.1	.402
10.1	0.02	310	203	0.68	135	2640	±29	2806.4	± 9.2	6	0.1976	0.56	13.79	1.5	0.5062	1.3	.922
11.1	0.06	472	113	0.25	168	2237	±25	2958.7	± 7.8	24	0.217	0.48	12.41	1.4	0.4149	1.3	.941
13.1	0.25	781	222	0.29	210	1749	±18	2967.4	± 8	41	0.2182	0.5	9.37	1.3	0.3116	1.2	.921
14.1	2.74	2789	1074	0.40	210	527.1	± 5.5	2146	±41	75	0.1336	2.3	1.57	2.6	0.08521	1.1	.426
15.1	0.09	451	581	1.33	177	2426	±26	2692.1	± 8.8	10	0.18432	0.53	11.61	1.4	0.4569	1.3	.923
16.1	0.66	1660	465	0.29	169	716.3	± 7.5	2168	±16	67	0.1353	0.93	2.193	1.4	0.1175	1.1	.765
17.1	0.15	639	216	0.35	202	2013	±21	2798.7	± 8.3	28	0.19667	0.51	9.94	1.3	0.3665	1.2	.921
18.1	0.02	291	221	0.79	128	2668	±30	2714.6	± 9.7	2	0.1868	0.59	13.21	1.5	0.5127	1.4	.919
20.1	0.84	1650	610	0.38	287	1178	±12	2263	±14	48	0.1429	0.8	3.951	1.4	0.2005	1.1	.808
21.1	0.37	609	339	0.57	112	1251	±14	1985	±18	37	0.122	1	3.601	1.6	0.2142	1.2	.772

22.1	0.12	148	102	0.71	60.7	2518	±35	2726	±18	8	0.1881	1.1	12.39	2	0.4778	1.7	.839
23.1	0.01	665	424	0.66	296	2690	±26	2815.1	± 7.5	4	0.19865	0.46	14.18	1.3	0.5177	1.2	.932
26.1	2.67	2139	716	0.35	211	682.1	± 7.2	1393	±64	51	0.0885	3.3	1.362	3.5	0.1116	1.1	.318
29.1	2.21	2671	659	0.25	238	623.8	± 6.5	1791	±34	65	0.1095	1.9	1.534	2.2	0.1016	1.1	.503
30.1	0.06	327	89	0.28	80.8	1626	±19	2038	±19	20	0.1257	1.1	4.972	1.7	0.2869	1.3	.779
31.1	0.23	685	157	0.24	228	2105	±23	2681.8	± 8.6	22	0.18317	0.52	9.75	1.4	0.3861	1.3	.925
32.1	0.32	685	220	0.33	169	1622	±17	2876	±16	44	0.2062	0.99	8.14	1.5	0.2862	1.2	.765
33.1	0.00	392	41	0.11	185	2824	±30	2884	±14	2	0.2072	0.89	15.71	1.6	0.5497	1.3	.828
34.1	0.13	446	526	1.22	140	2004	±22	2114	±13	5	0.1312	0.73	6.597	1.5	0.3647	1.3	.863
1.1	0.19	69	26	0.39	30.1	2644	±49	2711	±21	2	0.1865	1.3	13.04	2.6	0.507	2.3	.868
2.1	0.14	682	202	0.31	204	1925	±20	2710.2	± 8.6	29	0.18635	0.52	8.94	1.3	0.3479	1.2	.916
3.1	0.09	501	142	0.29	222	2675	±27	3131.8	± 6.7	15	0.2418	0.42	17.15	1.3	0.5144	1.2	.947
4.1	1.26	1317	718	0.56	147	778.5	± 8.3	1706	±30	54	0.1045	1.6	1.85	2	0.1284	1.1	.575
5.1	1.27	2529	790	0.32	206	577.8	± 6	1646	±28	65	0.1012	1.5	1.309	1.8	0.0938	1.1	.589
6.1	0.01	334	253	0.78	159	2832	±31	2971.5	± 8.7	5	0.2187	0.54	16.64	1.5	0.5517	1.4	.930
7.1	0.85	1601	548	0.35	205	890.1	± 9.6	2196	±18	59	0.1375	1	2.807	1.6	0.1481	1.2	.741
8.1	0.19	123	175	1.47	55.8	2732	±41	2726	±16	0	0.1881	1	13.69	2.1	0.5277	1.8	.876
9.1	2.05	2573	824	0.33	228	620	± 6.6	2032	±31	69	0.1252	1.8	1.743	2.1	0.101	1.1	.537
10.1	1.69	2608	1186	0.47	235	633.5	± 6.6	1163	±42	46	0.0786	2.1	1.12	2.4	0.1033	1.1	.455
11.1	0.13	372	118	0.33	150	2481	±28	3334	± 7.8	26	0.2749	0.5	17.79	1.4	0.4695	1.3	.938
12.1	0.83	857	155	0.19	152	1204	±14	2615	±15	54	0.1759	0.9	4.982	1.5	0.2054	1.2	.811
13.1	0.16	477	486	1.05	122	1684	±19	2080	±15	19	0.1287	0.84	5.297	1.5	0.2986	1.3	.837
15.1	0.84	1277	225	0.18	188	1011	±11	2479	±15	59	0.1622	0.88	3.798	1.4	0.1698	1.1	.789
16.1	0.33	863	421	0.50	148	1172	±13	1934	±17	39	0.1185	0.94	3.258	1.5	0.1994	1.2	.780
17.1	0.24	542	139	0.26	117	1447	±16	2702	±12	46	0.1854	0.74	6.436	1.4	0.2517	1.2	.859
18.1	0.02	613	247	0.42	265	2629	±26	2899	± 7.7	9	0.20915	0.48	14.52	1.3	0.5036	1.2	.930
19.1	0.39	1048	249	0.25	254	1596	±16	2625.3	± 9.6	39	0.177	0.58	6.859	1.3	0.281	1.1	.891
20.1	0.02	288	213	0.76	139	2873	±33	3176.2	± 8.3	10	0.2487	0.52	19.25	1.5	0.5615	1.4	.937
21.1	0.71	1129	209	0.19	206	1235	±13	2544	±14	51	0.1686	0.85	4.911	1.4	0.2112	1.1	.798
22.1	1.46	1738	458	0.27	181	725.9	± 7.6	1927	±29	62	0.118	1.6	1.94	2	0.1192	1.1	.565

23.1	1.28	1650	618	0.39	200	840.3	± 8.7	2296	±27	63	0.1457	1.5	2.798	1.9	0.1392	1.1	.580
24.1	0.15	612	297	0.50	168	1786	±19	2061	±17	13	0.1273	0.97	5.606	1.6	0.3193	1.2	.783
25.1	0.08	234	76	0.34	68	1880	±24	2844	±13	34	0.2022	0.81	9.44	1.7	0.3385	1.4	.872
27.1	0.20	785	171	0.23	249	2023	±20	3004.7	± 6.8	33	0.22331	0.42	11.35	1.2	0.3687	1.2	.939
28.1	0.13	356	191	0.55	138	2394	±27	3063.1	± 8.9	22	0.2316	0.56	14.36	1.5	0.4497	1.3	.923
30.1	0.66	655	243	0.38	125	1285	±14	1973	±21	35	0.1211	1.2	3.684	1.7	0.2205	1.2	.727
31.1	0.49	944	552	0.60	226	1576	±17	2586	±10	39	0.1729	0.61	6.6	1.4	0.2769	1.2	.893
32.1	0.01	637	82	0.13	299	2813	±27	2878.8	± 6.2	2	0.20656	0.38	15.58	1.3	0.547	1.2	.953
34.1	0.18	650	352	0.56	234	2254	±23	3259.6	± 6.7	31	0.2621	0.43	15.13	1.3	0.4187	1.2	.943
35.1	0.21	466	193	0.43	125	1748	±20	2100	±14	17	0.1301	0.82	5.59	1.5	0.3116	1.3	.844
36.1	1.54	2683	948	0.37	264	689.9	± 7.1	1445	±33	52	0.0909	1.7	1.416	2	0.113	1.1	.532
37.1	1.65	2683	1127	0.43	263	686	± 7.3	1371	±36	50	0.0875	1.9	1.354	2.2	0.1123	1.1	.517
1.1	0.02	234	323	1.43	116	2939	±36	2946	± 10	0	0.2153	0.62	17.15	1.6	0.5776	1.5	.924
2.1	0.13	570	267	0.48	172	1935	±20	2124	± 12	9	0.13193	0.68	6.367	1.4	0.35	1.2	.875
3.1	0.45	847	156	0.19	194	1519	±17	1913	± 15	21	0.11711	0.85	4.289	1.5	0.2656	1.2	.823
5.1	1.89	2156	1894	0.91	182	594	± 6.2	1344	±200	56	0.0863	10	1.15	10	0.0965	1.1	.106
6.1	0.55	1281	328	0.26	205	1097	±11	2134	± 18	49	0.1327	1	3.395	1.5	0.1856	1.1	.740
7.1	0.00	149	107	0.74	73.8	2934	±41	2933	± 13	0	0.2136	0.79	16.97	1.9	0.5765	1.7	.909
8.1	0.02	475	115	0.25	209	2661	±27	2955.5	± 7.3	10	0.21659	0.45	15.26	1.3	0.5109	1.3	.941
9.1	0.49	1089	358	0.34	218	1344	±14	2998.9	± 8.7	55	0.2225	0.54	7.112	1.3	0.2318	1.1	.903
10.1	0.00	159	86	0.56	77.7	2906	±39	2947	± 12	1	0.2155	0.74	16.92	1.8	0.5695	1.7	.914
11.1	0.30	717	463	0.67	196	1776	±18	2777	± 11	36	0.1941	0.69	8.49	1.4	0.3172	1.2	.866
12.1	0.16	853	178	0.22	290	2147	±21	2772.7	± 7.3	23	0.19356	0.44	10.55	1.2	0.3951	1.2	.934
13.1	2.44	666	269	0.42	168	1628	±21	2636	± 73	38	0.1781	4.4	7.05	4.7	0.2872	1.5	.312
14.1	0.21	952	446	0.48	249	1709	±17	2928	± 10	42	0.2129	0.64	8.91	1.3	0.3036	1.2	.874
15.1	0.06	379	71	0.19	159	2558	±28	2808.2	± 8.9	9	0.1978	0.55	13.28	1.4	0.487	1.3	.923
16.1	0.02	581	307	0.55	278	2858	±30	2910.9	± 6.5	2	0.2107	0.4	16.21	1.4	0.5579	1.3	.956
19.1	0.08	550	123	0.23	153	1808	±20	2866.8	± 9.2	37	0.205	0.57	9.16	1.4	0.3238	1.2	.910
21.1	0.03	320	208	0.67	108	2126	±25	2143	± 13	1	0.1334	0.77	7.18	1.6	0.3907	1.4	.875
22.1	0.00	271	130	0.50	136	2971	±38	2976.8	± 9	0	0.2195	0.56	17.71	1.7	0.5854	1.6	.944
24.1	0.35	708	224	0.33	153	1440	±15	2777	± 11	48	0.194	0.64	6.697	1.4	0.2503	1.2	.882

25.1	0.38	808	245	0.31	151	1267 ±14	2764 ± 11	54	0.1925 0.64	5.763 1.4	0.2171 1.2	.890

Resumo dos dados de U-Pb da amostra PE-SM-06 (Formação São João da Chapada).

Spot number	Ratios							Age (Ma)						%		Best estimated	
	$^{207}Pb^{*}/^{235}U$	±	$^{206}Pb^{*}/^{238}U$	±	Rho 1	$^{207}Pb^{*}/^{206}Pb^{*}$	±	$^{206}Pb/^{238}U$	±	$^{207}Pb/^{235}U$	±	$^{207}Pb/^{206}Pb$	±	Disc.	f 206	Age (Ma)	±
Zr-219-A-I-01	7.09429	1.37	0.38982	0.55	0.41	0.13199	1.25	2122	12	2123	29	2125	27	0	0.0003	2125	27
Zr-219-A-I-02	13.06250	2.20	0.51716	1.30	0.59	0.18319	1.78	2687	35	2684	59	2682	48	0	0.0024	2682	48
Zr-219-A-I-03	6.69326	2.17	0.36173	0.69	0.32	0.13420	2.06	1990	14	2072	45	2154	44	8	0.0013	2154	44
Zr-219-A-I-04	6.82014	3.14	0.37900	2.74	0.87	0.13051	1.52	2072	57	2088	66	2105	32	2	0.0008	2105	32
Zr-219-A-I-05	13.12947	2.50	0.51878	1.26	0.51	0.18355	2.16	2694	34	2689	67	2685	58	0	0.0010	2685	58
Zr-219-A-I-06	7.64056	2.10	0.40528	0.99	0.47	0.13673	1.85	2193	22	2190	46	2186	40	0	0.0007	2186	40
Zr-219-A-I-07	7.13363	1.82	0.39173	1.23	0.68	0.13208	1.33	2131	26	2128	39	2126	28	0	0.0013	2126	28
Zr-219-A-I-08	6.65457	1.90	0.37486	1.29	0.68	0.12875	1.39	2052	26	2067	39	2081	29	1	0.0053	2081	29
Zr-219-A-I-09	6.78773	2.31	0.34631	1.26	0.55	0.14215	1.93	1917	24	2084	48	2254	43	15	0.0014	2254	43
Zr-219-A-I-10	4.80243	4.47	0.32132	4.18	0.94	0.10840	1.57	1796	75	1785	80	1773	28	-1	0.0247	1773	28
Zr-219-A-I-11	4.22417	2.42	0.22595	1.40	0.58	0.13559	1.98	1313	18	1679	41	2172	43	40	0.0428		
Zr-219-A-I-12	0.43651	6.16	0.04138	5.08	0.83	0.07650	3.48	261	13	368	23	1108	39	76	0.0444		
Zr-219-A-I-13	12.23157	1.52	0.48217	0.54	0.35	0.18398	1.42	2537	14	2622	40	2689	38	6	0.0018	2689	38
Zr-219-A-I-15	7.32423	2.66	0.39932	1.59	0.60	0.13303	2.14	2166	34	2152	57	2138	46	-1	0.0017	2138	46
Zr-219-A-I-17	6.89097	3.23	0.37859	2.41	0.75	0.13201	2.15	2070	50	2097	68	2125	46	3	0.0013	2125	46
Zr-219-A-I-18	4.00966	3.65	0.27648	2.42	0.66	0.10518	2.73	1574	38	1636	60	1718	47	8	0.0010	1718	47
Zr-219-A-I-19	4.53560	2.80	0.30262	1.88	0.67	0.10870	2.08	1704	32	1738	49	1778	37	4	0.0001	1778	37
Zr-219-A-I-20	7.45472	5.59	0.39345	1.92	0.34	0.13742	5.25	2139	41	2168	121	2195	115	3	0.0025	2195	115

Resumo dos dados de U-Pb da amostra PE-GO-31 (Formação São João da Chapada).

Grain.Spot	% $^{206}Pb_c$	ppm U	ppm Th	$^{232}Th/^{238}U$	ppm $^{206}Pb^*$	(1) $^{206}Pb/^{238}U$ Age		(1) $^{207}Pb/^{206}Pb$ Age		% Dis-cor-dant	(1) $^{207}Pb^*/^{206}Pb^*$	±%	(1) $^{207}Pb^*/^{235}U$	±%	(1) $^{206}Pb^*/^{238}U$	±%	err corr	Best estmated age (Ma)	
Sao Joao da Chapada Fm.																			
A1	3.10	1279	228	0.18	93.8	512.2	± 6.4	979	± 58	48	0.0718	2.9	0.818	3.1	0.0827	1.3	.416		
A3	0.27	118	92	0.81	46.2	2417	±28	2754.5	± 9.2	12	0.1914	0.56	12.01	1.5	0.455	1.4	.930		
A4	1.72	282	156	0.57	49	1167	±14	2629	± 14	56	0.1775	0.86	4.855	1.6	0.1984	1.4	.844		
A7	1.48	119	81	0.70	22	1238	±16	2585	± 19	52	0.1728	1.1	5.043	1.8	0.2117	1.4	.780		
A9	0.16	105	68	0.67	45.7	2634	±31	2678	± 12	2	0.1827	0.72	12.72	1.6	0.5048	1.4	.892	2678	12
A10	0.12	179	99	0.57	79.5	2684	±30	2856.3	± 6	6	0.20373	0.37	14.51	1.4	0.5165	1.4	.965	2856.3	6
A11	--	41	10	0.25	13.4	2095	±32	2147	± 16	2	0.1337	0.94	7.08	2	0.3841	1.8	.883	2147	16
A13	0.03	106	62	0.61	47.7	2716	±31	2720.1	± 7.5	0	0.18747	0.46	13.55	1.5	0.524	1.4	.951	2720.1	7.5
A15	0.16	102	46	0.46	42.7	2555	±30	2737	± 9.1	7	0.1894	0.55	12.7	1.5	0.4863	1.4	.932	2737	9.1
A16	0.09	87	122	1.45	37.8	2629	±31	2694.6	± 9.1	2	0.1846	0.55	12.82	1.6	0.5035	1.4	.934	2694.6	9.1
A17	0.03	123	114	0.96	54.5	2687	±31	2689.6	± 7.3	0	0.18404	0.44	13.12	1.5	0.5172	1.4	.953	2689.6	7.3
A20	0.15	221	112	0.52	65	1899	±22	2036	± 9.7	7	0.12551	0.55	5.929	1.4	0.3426	1.3	.926	2036	9.7
A21	0.38	133	127	0.98	45.7	2155	±25	2770.2	± 9.1	22	0.1933	0.55	10.58	1.5	0.397	1.4	.929		
A22	20.70	483	666	1.43	109	1223	±29	2434	±180	50	0.158	11	4.55	11	0.2089	2.6	.236		
A23	0.25	138	84	0.62	54.2	2413	±29	2750	± 9.3	12	0.1909	0.57	11.95	1.5	0.4541	1.4	.930		
A24	0.11	80	114	1.46	39.7	2925	±36	2899.5	± 9.8	-1	0.2092	0.61	16.56	1.6	0.5741	1.5	.930	2899.5	9.8
A26	0.00	30	37	1.25	12.9	2592	±42	2621	± 18	1	0.1766	1.1	12.05	2.2	0.495	1.9	.871	2621	18
A28	1.55	312	207	0.68	71	1493	±18	2727	± 14	45	0.1883	0.83	6.76	1.6	0.2606	1.4	.854		
A29	0.30	152	140	0.95	66.9	2659	±31	2670.3	± 9.7	0	0.1819	0.59	12.8	1.5	0.5105	1.4	.925	2670.3	9.7
A30	0.60	54	63	1.21	23	2588	±39	2613	± 21	1	0.1757	1.3	11.97	2.2	0.494	1.8	.824	2613	21
A33	0.45	213	169	0.82	78.9	2301	±27	2993.5	± 8.2	23	0.2218	0.51	13.11	1.5	0.4289	1.4	.938		
B1	0.94	123	44	0.37	41	2093	±27	2097	± 28	0	0.13	1.6	6.88	2.2	0.3837	1.5	.690	2097	28
B2	0.14	134	49	0.38	45.9	2161	±27	2146	± 14	-1	0.1336	0.82	7.34	1.7	0.3983	1.5	.872	2146	14

B5	0.20	164	79	0.50	68.5	2555	±30	2694.9	± 9.2	5	0.1846	0.56	12.38	1.5	0.4863	1.4	.931	2694.9	9.2
B9	1.22	97	63	0.67	22.8	1540	±21	2005	± 36	23	0.1233	2.1	4.59	2.6	0.2698	1.6	.605		
B11	0.53	142	112	0.81	44.2	1983	±25	2621	± 13	24	0.1766	0.79	8.77	1.7	0.3602	1.4	.877		
B12	2.46	365	391	1.11	55.3	1025	±13	2986	± 15	66	0.2208	0.91	5.246	1.7	0.1723	1.4	.836		
B14	1.83	284	129	0.47	50.6	1193	±16	1942	± 44	39	0.119	2.4	3.338	2.8	0.2034	1.4	.510		
B15	0.00	54	55	1.05	14.6	1777	±27	1882	± 23	6	0.1152	1.3	5.04	2.2	0.3175	1.7	.809	1882	23
B16	2.83	113	219	2.01	50.3	2633	±33	2646	± 28	1	0.1793	1.7	12.47	2.2	0.5045	1.5	.674	2646	28
B17	0.31	108	64	0.61	28.3	1710	±24	1704	± 23	0	0.1044	1.3	4.373	2	0.3037	1.6	.781	1704	23
B18	3.85	769	448	0.60	77.4	688.4	± 8.8	2443	± 27	72	0.1588	1.6	2.467	2.1	0.1127	1.3	.644		
B19	0.15	170	207	1.26	79.3	2790	±32	2813.9	± 9.3	1	0.1985	0.57	14.83	1.5	0.5417	1.4	.928	2813.9	9.3
B21	0.63	74	47	0.66	16	1440	±21	1721	± 42	16	0.1054	2.3	3.64	2.8	0.2502	1.6	.583		
B23	0.28	90	43	0.49	29.9	2095	±29	2156	± 26	3	0.1344	1.5	7.11	2.2	0.384	1.6	.742	2156	26
B24	2.29	1081	452	0.43	122	776.7	± 9.5	1863	± 26	58	0.1139	1.4	2.012	1.9	0.1281	1.3	.677		
B25	2.22	339	153	0.46	84.4	1608	±20	2536	± 24	37	0.1678	1.4	6.55	2	0.2833	1.4	.707		
B26	0.30	68	84	1.27	25.7	2334	±32	2380	± 18	2	0.1531	1	9.2	1.9	0.4362	1.6	.843	2380	18
B27	0.44	107	89	0.86	40.5	2345	±30	2745	± 13	15	0.1903	0.79	11.52	1.7	0.4388	1.5	.885	2745	13
B28	0.07	137	142	1.08	59.8	2650	±31	2707	± 13	2	0.186	0.77	13.04	1.6	0.5085	1.4	.884	2707	13
B32	0.22	232	112	0.50	85.5	2296	±27	2693.1	± 8.4	15	0.18443	0.51	10.88	1.5	0.4279	1.4	.938		
B33	0.02	169	44	0.27	78	2768	±32	2731.4	± 7.7	-1	0.18876	0.47	13.96	1.5	0.5364	1.4	.950	2731.4	7.7
B35	0.43	205	305	1.54	60	1886	±23	1988	± 17	5	0.1222	0.94	5.722	1.7	0.3398	1.4	.831	1988	17
B37	0.37	122	31	0.26	40.5	2106	±27	2123	± 17	1	0.1318	0.97	7.02	1.8	0.3864	1.5	.837	2123	17
B39	5.19	832	1343	1.67	40.2	335.1	± 4.5	2346	± 43	86	0.15	2.5	1.104	2.9	0.05336	1.4	.480		
C1	0.13	129	46	0.37	70.1	3164	±38	3263.4	± 9.7	3	0.2628	0.61	22.96	1.7	0.6337	1.5	.929	3263.4	9.7
C2	0.23	71	28	0.41	24.6	2182	±30	2199	± 21	1	0.1378	1.2	7.65	2	0.4028	1.6	.806	2199	21
C3	0.82	285	238	0.86	78.8	1786	±21	2656	± 12	33	0.1803	0.72	7.93	1.5	0.3192	1.4	.884		
C5	0.26	230	131	0.59	87.5	2358	±27	3048.4	± 6.9	23	0.22948	0.43	13.97	1.4	0.4416	1.4	.954		
C8	0.61	111	41	0.38	34.8	1993	±25	2005	± 22	1	0.1233	1.2	6.16	1.9	0.3622	1.5	.770	2005	22
C9	0.28	141	68	0.49	44.8	2019	±26	2050	± 16	2	0.1265	0.93	6.42	1.8	0.3679	1.5	.853	2050	16
C10	0.34	127	64	0.52	47.2	2311	±29	2786	± 14	17	0.1951	0.87	11.6	1.7	0.4311	1.5	.860	2786	14
C11	0.67	35	12	0.36	15.8	2721	±46	2768	± 22	2	0.193	1.3	13.97	2.5	0.525	2.1	.845	2768	22
C13	2.30	211	204	1.00	30.2	973	±13	3056	± 21	68	0.2305	1.3	5.18	2	0.163	1.5	.740		
C15	0.37	62	52	0.85	27.1	2634	±36	2654	± 16	1	0.1801	0.95	12.54	1.9	0.5048	1.7	.870	2654	16
C16	0.43	115	150	1.35	34.9	1947	±25	2829	± 14	31	0.2003	0.84	9.74	1.7	0.3526	1.5	.876		

C17	0.71	148	102	0.71	37.2	1639 ±21	2126 ± 23	23	0.1321	1.3	5.27	2	0.2896	1.5	.750		
C18	1.77	248	311	1.30	48.7	1307 ±17	1950 ± 34	33	0.1196	1.9	3.706	2.4	0.2248	1.4	.601		
C21	0.50	141	151	1.11	49	2185 ±27	2675 ± 12	18	0.1824	0.75	10.15	1.6	0.4034	1.5	.889		
C22	0.14	138	49	0.36	70	2987 ±40	3303.5 ± 8.6	10	0.2696	0.55	21.9	1.8	0.5893	1.7	.951	3303.5	8.6

Resumo dos dados de U-Pb da amostra PE-CM-11 (Formação Sopa-Brumadinho).

Grain.Spot	**% $^{206}Pb_c$**	**ppm U**	**ppm Th**	**$^{232}Th/^{238}U$**	**ppm $^{206}Pb^*$**	**(1) $^{206}Pb/^{238}U$ Age**	**(1) $^{207}Pb/^{206}Pb$ Age**	**% Dis-cor-dant**	**(1) $^{207}Pb^*/^{206}Pb^*$**	**±%**	**(1) $^{207}Pb^*/^{235}U$**	**±%**	**(1) $^{206}Pb^*/^{238}U$**	**±%**	**err corr**
A1	0.45	282	208	0.76	110	2399 ±22	2825.2 ± 6.3	15	0.19988	0.39	12.42	1.1	0.4508	1.1	.942
A2	0.04	263	168	0.66	86.9	2100 ±20	2113.3 ± 6.5	1	0.13114	0.37	6.962	1.2	0.385	1.1	.948
A3	0.12	138	54	0.40	60.9	2663 ±25	2681.8 ± 6.8	1	0.18317	0.41	12.92	1.2	0.5114	1.2	.944
A4	--	146	72	0.51	52.1	2242 ±22	2225.4 ± 8.9	-1	0.13986	0.51	8.02	1.3	0.4159	1.2	.915
A5	0.09	333	194	0.60	102	1969 ±18	2047.7 ± 6.4	4	0.12635	0.36	6.222	1.1	0.3572	1.1	.948
A6	0.12	77	44	0.59	31.3	2498 ±26	2669 ±12	6	0.1818	0.74	11.86	1.5	0.4733	1.3	.866
A7	0.05	134	43	0.33	45.4	2146 ±21	2136.1 ± 8.8	0	0.13286	0.5	7.235	1.3	0.395	1.2	.919
A8	0.01	56	28	0.52	26.3	2799 ±31	2769.2 ± 9.1	-1	0.1932	0.55	14.48	1.5	0.5437	1.4	.927
A9	0.00	58	47	0.85	15.3	1738 ±23	1776 ±16	2	0.10859	0.9	4.633	1.8	0.3094	1.5	.865
A10	0.05	106	37	0.36	37.1	2210 ±23	2170.7 ± 9.8	-2	0.13552	0.56	7.64	1.3	0.4089	1.2	.907
A11	0.08	84	30	0.37	27.8	2107 ±23	2161 ±12	2	0.13474	0.69	7.18	1.5	0.3866	1.3	.882
A12	0.18	182	144	0.82	58.5	2043 ±20	2131.8 ± 8.9	4	0.13253	0.51	6.814	1.2	0.3729	1.1	.912
A13	0.03	134	62	0.48	65.3	2888 ±27	2867.6 ± 5.8	-1	0.20515	0.36	15.99	1.2	0.5651	1.2	.957
A14	0.02	171	99	0.60	56.7	2098 ±21	2124.4 ± 7.9	1	0.13198	0.45	7.001	1.2	0.3847	1.1	.930
A15	0.02	63	27	0.44	29.9	2827 ±31	2867 ± 8.4	1	0.2051	0.52	15.56	1.4	0.5503	1.3	.933
A16	0.01	207	94	0.47	67.6	2079 ±20	2108.8 ± 7.3	1	0.1308	0.42	6.863	1.2	0.3806	1.1	.938

A17	0.09	45	25	0.58	15.2	2145	±27	2156	±16	1	0.1344	0.89	7.32	1.7	0.3948	1.5	.857
A18	0.05	47	18	0.40	16.1	2141	±27	2131	±15	0	0.1325	0.88	7.2	1.7	0.3939	1.5	.860
A20	0.01	108	103	0.98	36	2109	±22	2092	±10	-1	0.12956	0.58	6.915	1.4	0.3871	1.2	.906
A21	0.37	126	128	1.04	48.9	2389	±24	2684	± 9.1	11	0.1834	0.55	11.34	1.3	0.4485	1.2	.910
A22	0.15	335	140	0.43	105	1996	±19	2099.8	± 7.8	5	0.13014	0.44	6.511	1.2	0.3629	1.1	.925
A23	0.06	130	113	0.90	43.6	2121	±22	2130.4	± 9.8	0	0.13243	0.56	7.116	1.3	0.3897	1.2	.908
A25	0.07	311	157	0.52	97.1	2000	±19	2055.7	± 6.8	3	0.12692	0.39	6.367	1.2	0.3638	1.1	.943
A26	2.92	142	148	1.08	21.8	1032	±12	2031	±46	49	0.1251	2.6	2.996	2.9	0.1737	1.2	.427
A27	0.05	35	25	0.74	18.8	3120	±40	3136	±10	1	0.2424	0.65	20.81	1.7	0.623	1.6	.929
A28	0.03	183	132	0.74	62.8	2164	±21	2200.2	± 7.8	2	0.13784	0.45	7.582	1.2	0.399	1.2	.932
A29	0.90	233	203	0.90	60.7	1690	±17	2135	±15	21	0.1328	0.86	5.487	1.4	0.2997	1.1	.794
A31	0.03	235	87	0.38	81.1	2176	±21	2190.8	± 6.9	1	0.1371	0.4	7.588	1.2	0.4014	1.1	.943
A32	0.77	137	94	0.71	37.8	1788	±19	2129	±30	16	0.1323	1.7	5.83	2.1	0.3197	1.2	.582
A33	0.05	132	115	0.90	42.3	2046	±21	2083.5	± 9.8	2	0.12894	0.56	6.641	1.3	0.3735	1.2	.909
A35	--	68	20	0.30	22.5	2109	±25	2175	±13	3	0.13583	0.73	7.25	1.6	0.3869	1.4	.886
A36	0.04	148	74	0.51	50.2	2141	±22	2207.9	± 8.9	3	0.13845	0.51	7.519	1.3	0.3939	1.2	.919
A38	2.17	177	123	0.72	45.7	1657	±18	2076	±57	20	0.1284	3.2	5.19	3.5	0.2932	1.2	.349
A39	0.08	166	84	0.52	52.9	2034	±20	2089.8	± 9.4	3	0.1294	0.53	6.619	1.3	0.371	1.2	.910
B1	0.07	40	24	0.62	13.3	2110	±29	2141	±26	1	0.1333	1.5	7.11	2.2	0.3871	1.6	.729
B2	0.03	305	287	0.97	103	2141	±20	2119.9	± 6.6	-1	0.13164	0.38	7.151	1.2	0.394	1.1	.946
B3	0.65	415	234	0.58	110	1720	±16	1992	±12	14	0.1224	0.66	5.161	1.3	0.3058	1.1	.853
B4	0.14	121	86	0.74	38.3	2021	±22	2103	±12	4	0.13034	0.7	6.617	1.4	0.3682	1.2	.870
B5	0.06	120	77	0.66	41.7	2185	±23	2151	±11	-2	0.13399	0.61	7.45	1.4	0.4034	1.2	.900
B6	1.36	259	169	0.67	62.1	1567	±16	2139	±20	27	0.1331	1.1	5.051	1.6	0.2752	1.1	.704
B7	0.03	147	53	0.37	48.6	2094	±23	2150	±12	3	0.13395	0.66	7.09	1.5	0.3839	1.3	.892
B8	0.02	191	100	0.54	63.3	2102	±21	2163.4	± 8.7	3	0.13495	0.5	7.174	1.3	0.3855	1.2	.918
B11	1.15	286	361	1.31	66.8	1534	±15	2127	±18	28	0.1322	1	4.894	1.5	0.2686	1.1	.739
B12	2.34	348	396	1.18	98.2	1795	±18	2172	±36	17	0.1356	2	6	2.3	0.321	1.2	.497
B13	0.30	136	164	1.25	46	2131	±22	2147	±13	1	0.1337	0.75	7.22	1.4	0.3918	1.2	.852
B14	0.12	76	46	0.63	33.1	2638	±34	2727	±14	3	0.1883	0.82	13.12	1.8	0.5055	1.6	.884
B15	0.37	170	90	0.55	63.3	2315	±25	2807.2	± 7.9	18	0.19768	0.49	11.78	1.4	0.4321	1.3	.933
B16	4.64	907	551	0.63	119	876.1	± 9.2	1593	±60	45	0.0983	3.2	1.974	3.4	0.1456	1.1	.328

B17	0.05	123	89	0.75	52.7	2607	±27	2717.4	± 8.2	4	0.18717	0.5	12.86	1.3	0.4984	1.2	.929
B19	--	70	48	0.71	32.2	2754	±31	2716	±11	-1	0.187	0.68	13.74	1.6	0.5329	1.4	.900
B18	0.19	267	417	1.61	80.4	1933	±20	2041.7	± 9.3	5	0.12592	0.53	6.07	1.3	0.3496	1.2	.912
B20	0.03	206	112	0.56	68.5	2105	±21	2153	± 8.2	2	0.13415	0.47	7.143	1.3	0.3862	1.2	.926
B21	0.04	97	46	0.49	33.8	2187	±24	2196	±11	0	0.13754	0.66	7.66	1.5	0.4038	1.3	.895
B23	0.00	23	39	1.70	10.5	2700	±44	2700	±17	0	0.1852	1.1	13.28	2.3	0.52	2	.886
B24	0.15	121	82	0.70	40.4	2116	±23	2145	±12	1	0.13352	0.68	7.15	1.4	0.3886	1.3	.880
B25	0.18	107	52	0.50	42.5	2444	±27	2724	±11	10	0.1879	0.68	11.94	1.5	0.461	1.3	.887
B26	--	77	43	0.58	25.8	2130	±25	2204	±13	3	0.1381	0.77	7.46	1.6	0.3917	1.4	.878
B27	0.08	232	82	0.36	102	2669	±25	2833.5	± 5.7	6	0.2009	0.35	14.21	1.2	0.5128	1.2	.957
B29	0.05	72	60	0.86	32.4	2715	±31	2797	±10	3	0.1965	0.63	14.19	1.5	0.5238	1.4	.914
B30	0.65	234	157	0.69	91.6	2406	±23	2644	±18	9	0.179	1.1	11.17	1.6	0.4525	1.2	.734
B31	0.71	145	61	0.44	42.6	1887	±20	2176	±20	13	0.1359	1.1	6.37	1.7	0.3401	1.3	.738
B32	0.02	128	71	0.58	57.1	2696	±28	2790.1	± 7.3	3	0.19563	0.44	14.01	1.3	0.5193	1.3	.942
B33	0.33	261	67	0.27	81.2	1984	±19	2121	±10	6	0.13172	0.59	6.546	1.3	0.3604	1.1	.888
B34	0.02	140	90	0.66	64.1	2750	±28	2783	± 7.1	1	0.19479	0.43	14.29	1.3	0.532	1.2	.945
B35	--	164	75	0.47	57.5	2202	±23	2200.7	± 8.9	0	0.13788	0.51	7.74	1.3	0.4071	1.2	.922
B36	0.00	127	96	0.78	56.5	2686	±28	2715.6	± 9.4	1	0.187	0.57	13.33	1.4	0.517	1.3	.911
B37	0.06	108	129	1.24	36.1	2123	±24	2168	±11	2	0.13534	0.65	7.28	1.5	0.39	1.3	.896
B38	0.19	233	308	1.37	67.7	1878	±19	2005.4	± 9.9	6	0.12336	0.56	5.754	1.3	0.3383	1.1	.898
B40	0.01	115	57	0.51	39.3	2159	±23	2184.5	± 9.8	1	0.1366	0.56	7.49	1.4	0.3977	1.3	.912
C2	0.00	189	94	0.51	67.3	2233	±22	2221.5	± 7.4	-1	0.13954	0.43	7.966	1.2	0.414	1.1	.937
C4	0.01	119	71	0.62	42.6	2246	±23	2176.9	± 9.7	-3	0.136	0.56	7.81	1.3	0.4168	1.2	.910
C5	1.78	96	32	0.35	24.7	1668	±21	2305	± 28	28	0.1465	1.6	5.96	2.2	0.2953	1.4	.658
C7	0.05	60	27	0.46	26.5	2665	±31	2691	± 11	1	0.1842	0.66	13	1.6	0.5119	1.4	.907
C8	0.03	78	99	1.31	35.8	2762	±30	2759.8	± 8.9	0	0.192	0.54	14.16	1.4	0.5349	1.3	.926
C9	0.00	77	32	0.44	26.9	2214	±25	2168	± 13	-2	0.13534	0.72	7.65	1.5	0.4098	1.4	.883
C11	4.31	217	219	1.04	47.7	1410	±24	2111	±230	33	0.131	13	4.42	13	0.2446	1.9	.138
C12	0.10	179	121	0.70	60	2121	±21	2198.5	± 8.9	4	0.1377	0.51	7.396	1.3	0.3895	1.2	.916
C13	0.12	100	103	1.06	44.6	2684	±28	2710.7	± 9.2	1	0.1864	0.56	13.27	1.4	0.5163	1.3	.915
C14	0.03	186	158	0.88	60.4	2069	±21	2094.8	± 8.9	1	0.12976	0.51	6.772	1.3	0.3785	1.2	.917

Resumo dos dados de U-Pb da amostra PE-GO-39 (Formação Sopa-Brumadinho).

Spot number			Concordia 1					Age (Ma)							%	Conc.	
	$^{207}Pb/^{235}U$	±	$^{206}Pb/^{238}U$	±	Rho 1	$^{207}Pb/^{206}Pb$	±	$^{206}Pb/^{238}U$	±	$^{207}Pb/^{235}U$	±	$^{207}Pb/^{206}Pb$	±	$^{232}Th/^{238}U$	Disc.	age (Ma)	2σ
003 ZR208_A_I_01	7.35371	1.77	0.41326	0.26	0.15	0.12906	1.75	2230	6	2155	38	2085	37	0.52	-7	2085	37
004 ZR208_A_I_02	4.43137	4.31	0.30576	1.07	0.25	0.10511	4.17	1720	18	1718	74	1716	72	0.89	0	1716	72
005 ZR208_A_I_03	2.38382	6.78	0.20367	0.94	0.14	0.08489	6.71	1195	11	1238	84	1313	88	1.09	9	1313	88
006 ZR208_A_I_05	12.28625	9.37	0.48936	8.94	0.95	0.18209	2.81	2568	229	2627	246	2672	75	1.53	4	2672	75
007 ZR208_A_I_07	4.73757	2.52	0.31645	1.48	0.59	0.10858	2.03	1772	26	1774	45	1776	36	0.94	0	1776	36
008 ZR208_A_I_08	7.46139	1.71	0.43190	0.24	0.14	0.12530	1.70	2314	6	2168	37	2033	34	0.34	-14		
009 ZR208_A_I_09	4.48539	2.38	0.30719	0.78	0.33	0.10590	2.25	1727	13	1728	41	1730	39	1.08	0	1730	39
010 ZR208_A_I_10	7.75445	2.07	0.40640	0.65	0.32	0.13839	1.96	2198	14	2203	46	2207	43	0.36	0	2207	43
011 ZR208_A_I_11	10.27345	1.55	0.49328	0.59	0.38	0.15105	1.43	2585	15	2460	38	2358	34	0.44	-10	2358	34
012 ZR208_A_I_12	4.73236	2.19	0.31498	0.72	0.33	0.10897	2.07	1765	13	1773	39	1782	37	0.93	1	1782	37
015 ZR208_A_I_13	7.71325	1.85	0.40248	0.69	0.37	0.13899	1.71	2180	15	2198	41	2215	38	0.80	2	2215	38
016 ZR208_A_I_14	4.45896	2.49	0.30876	0.51	0.20	0.10474	2.44	1735	9	1723	43	1710	42	1.32	-1	1710	42
017 ZR208_A_I_16	6.95326	1.68	0.38372	0.73	0.44	0.13142	1.51	2094	15	2105	35	2117	32	0.58	1	2117	32
018 ZR208_A_I_17	4.51310	3.17	0.30842	0.90	0.28	0.10613	3.04	1733	16	1733	55	1734	53	1.09	0	1734	53
019 ZR208_A_I_18	4.94834	3.35	0.32194	1.64	0.49	0.11148	2.92	1799	29	1811	61	1824	53	1.43	1	1824	53
020 ZR208_A_I_19	4.51945	1.44	0.31062	0.37	0.26	0.10553	1.40	1744	6	1735	25	1723	24	1.14	-1	1723	24
021 ZR208_A_I_24	4.43351	2.36	0.30733	0.64	0.27	0.10462	2.28	1728	11	1719	41	1708	39	1.17	-1	1708	39
022 ZR208_A_I_26	7.05024	3.00	0.38915	0.93	0.31	0.13140	2.85	2119	20	2118	64	2117	60	0.37	0	2117	60
023 ZR208_A_I_20	7.19076	1.69	0.40072	0.58	0.35	0.13015	1.58	2172	13	2135	36	2100	33	0.72	-3	2100	33
024 ZR208_A_I_27	4.46077	3.04	0.30629	0.84	0.27	0.10563	2.92	1722	14	1724	52	1725	50	1.06	0	1725	50
027 ZR208_A_I_28	7.37735	2.62	0.39706	0.58	0.22	0.13475	2.55	2155	12	2158	56	2161	55	0.34	0	2161	55
028 ZR208_A_I_33	4.42266	1.91	0.30527	0.53	0.28	0.10507	1.83	1717	9	1717	33	1716	31	1.35	0	1716	31
029 ZR208_A_I_35	19.85295	0.84	0.61508	0.46	0.55	0.23409	0.70	3090	14	3084	26	3080	22	0.78	0	3080	22
030 ZR208_A_I_37	6.56328	3.01	0.37205	2.64	0.88	0.12794	1.45	2039	54	2054	62	2070	30	0.66	1	2070	30
032 ZR208_B_II_09	10.04106	4.15	0.45946	1.68	0.41	0.15850	3.80	2437	41	2439	101	2440	93	1.01	0	2440	93
033 ZR208_A_I_39	4.96920	3.91	0.31125	0.88	0.22	0.11579	3.81	1747	15	1814	71	1892	72	0.52	8	1892	72
034 ZR208_B_II_01	11.70916	2.57	0.49027	0.83	0.32	0.17322	2.43	2572	21	2581	66	2589	63	0.91	1	2589	63

035 ZR208_B_II_02	4.00758	5.94	0.25529	0.54	0.09	0.11385	5.92	1466	8	1636	97	1862	110	1.19	21		
036 ZR208_B_II_04	13.27455	1.77	0.52496	1.01	0.57	0.18340	1.46	2720	27	2699	48	2684	39	0.60	-1	2684	39
040 ZR208_B_II_13	9.19433	6.78	0.43808	0.53	0.08	0.15222	6.76	2342	13	2358	160	2371	160	0.73	1	2371	160
041 ZR208_B_II_22	5.31250	6.21	0.33135	1.32	0.21	0.11628	6.07	1845	24	1871	116	1900	115	1.90	3	1900	115
042 ZR208_B_II_25	8.36253	1.66	0.43569	0.73	0.44	0.13921	1.49	2331	17	2271	38	2217	33	0.78	-5	2217	33
043 ZR208_B_II_15	6.82199	1.62	0.32638	0.72	0.44	0.15160	1.46	1821	13	2089	34	2364	34	0.22	23		
044 ZR208_B_II_16	7.08671	1.75	0.39685	0.51	0.29	0.12952	1.67	2154	11	2122	37	2091	35	0.34	-3	2091	35
045 ZR208_B_II_17	14.54696	1.73	0.54925	0.74	0.43	0.19209	1.57	2822	21	2786	48	2760	43	0.90	-2	2760	43
046 ZR208_B_II_18	4.78386	2.96	0.31515	0.77	0.26	0.11009	2.86	1766	14	1782	53	1801	51	0.98	2	1801	51
047 ZR208_B_II_19	4.46063	2.17	0.30735	0.36	0.17	0.10526	2.14	1728	6	1724	37	1719	37	1.29	-1	1719	37
048 ZR208_B_II_20	7.59554	1.64	0.41113	0.32	0.20	0.13399	1.61	2220	7	2184	36	2151	35	0.66	-3	2151	35
051 ZR208_C_III_04	11.55279	5.58	0.43339	4.90	0.88	0.19333	2.68	2321	114	2569	143	2771	74	0.69	16		
052 ZR208_C_III_05	1.60813	9.26	0.10472	8.97	0.97	0.11138	2.33	642	58	973	90	1822	43	1.49	65		
053 ZR208_B_II_28	8.63210	2.89	0.43135	2.13	0.74	0.14514	1.95	2312	49	2300	66	2289	45	0.56	-1	2289	45
054 ZR208_B_II_29	6.06798	3.54	0.35462	1.45	0.41	0.12410	3.23	1957	28	1986	70	2016	65	0.42	3	2016	65
055 ZR208_B_II_30	4.52768	3.93	0.31177	0.94	0.24	0.10533	3.82	1749	16	1736	68	1720	66	1.16	-2	1720	66
057 ZR208_C_III_14	10.53102	5.73	0.46956	4.05	0.71	0.16266	4.06	2482	100	2483	142	2483	101	0.53	0	2483	101
058 ZR208_C_III_08	4.49724	2.40	0.30732	0.97	0.40	0.10614	2.20	1727	17	1730	42	1734	38	1.02	0	1734	38
047 ZR208_B_II_19	4.46623	2.51	0.30813	0.50	0.20	0.10512	2.47	1732	9	1725	43	1716	42	1.58	-1	1716	42
048 ZR208_B_II_20	8.45407	3.55	0.41578	0.65	0.18	0.14747	3.49	2241	15	2281	81	2317	81	0.81	3	2317	81

Resumo dos dados de U-Pb da amostra PE-GO-59 (Formação Sopa-Brumadinho).

Spot number			**Concordia 1**					**Age (Ma)**							**%**	**Conc.**	
	207Pb/^{235U}	**±**	**206Pb/^{238}U**	**±**	**Rho 1**	**207Pb/^{206Pb}**	**±**	**206Pb/^{238}U**	**±**	**^{207}Pb/^{235}U**	**±**	**^{207}Pb/^{206}Pb**	**±**	**232Th/^{238}U**	**Disc.**	**age (Ma)**	**2σ**
003 ZR240_E_V_03	16.48612	4.27	0.57250	3.91	0.91	0.20885	1.73	2918	114	2905	124	2897	50	0.42	-1	2897	50
004 ZR240_D_IV_04	3.80875	4.93	0.27945	2.87	0.58	0.09885	4.01	1589	46	1595	79	1603	64	0.23	1	1603	64
005 ZR240_D_IV_05	20.55477	3.17	0.63042	1.51	0.48	0.23647	2.78	3151	48	3118	99	3096	86	0.35	-2	3096	86
006 ZR240_D_IV_06	15.03348	1.88	0.54988	0.87	0.46	0.19828	1.67	2825	24	2817	53	2812	47	1.72	0	2812	47

007 ZR240_D_IV_07	15.66694	3.29	0.56483	2.68	0.82	0.20117	1.90	2887	77	2857	94	2836	54	0.52	-2	2836	54
008 ZR240_D_IV_09	6.41927	4.08	0.36422	1.11	0.27	0.12783	3.93	2002	22	2035	83	2068	81	0.61	3	2068	81
009 ZR240_D_IV_10	6.28047	3.44	0.36714	1.65	0.48	0.12407	3.02	2016	33	2016	69	2016	61	0.54	0	2016	61
010 ZR240_D_IV_11	2.40534	4.73	0.21160	0.78	0.16	0.08244	4.67	1237	10	1244	59	1256	59	0.54	1	1256	59
011 ZR240_D_IV_14	6.34695	11.55	0.36219	2.39	0.21	0.12710	11.30	1993	48	2025	234	2058	233	0.46	3	2058	233
012 ZR240_D_IV_15	6.86712	4.84	0.37920	2.06	0.43	0.13134	4.38	2073	43	2094	101	2116	93	0.40	2	2116	93
015 ZR240_D_IV_16	12.84548	3.21	0.50145	1.86	0.58	0.18579	2.61	2620	49	2668	86	2705	71	0.49	3	2705	71
016 ZR240_D_IV_17	11.47989	2.93	0.47284	0.85	0.29	0.17608	2.80	2496	21	2563	75	2616	73	0.56	5	2616	73
017 ZR240_D_IV_18	6.01898	3.66	0.34965	1.04	0.29	0.12485	3.51	1933	20	1979	72	2027	71	0.77	5	2027	71
018 ZR240_D_IV_19	11.48025	3.36	0.48311	2.09	0.62	0.17235	2.63	2541	53	2563	86	2581	68	0.76	2	2581	68
019 ZR240_D_IV_20	10.71851	2.97	0.45356	1.18	0.40	0.17140	2.73	2411	28	2499	74	2571	70	0.60	6	2571	70
020 ZR240_D_IV_22	13.11652	2.54	0.49940	0.58	0.23	0.19049	2.48	2611	15	2688	68	2746	68	0.61	5	2746	68
021 ZR240_D_IV_24	25.96827	5.84	0.66440	5.43	0.93	0.28347	2.16	3284	178	3345	195	3382	73	0.56	3	3382	73
022 ZR240_D_IV_25	15.03252	5.35	0.54631	4.54	0.85	0.19957	2.82	2810	128	2817	151	2823	80	0.29	0	2823	80
023 ZR240_D_IV_27	9.06502	5.97	0.39201	4.68	0.78	0.16771	3.70	2132	100	2345	140	2535	94	0.37	16		
024 ZR240_D_IV_30	3.09379	9.74	0.24739	4.95	0.51	0.09070	8.39	1425	71	1431	139	1440	121	0.95	1	1440	121
027 ZR240_D_IV_31	6.20591	4.42	0.36244	3.24	0.73	0.12419	3.00	1994	65	2005	89	2017	61	0.44	1	2017	61
028 ZR240_D_IV_32	12.50067	4.45	0.50729	4.24	0.95	0.17872	1.36	2645	112	2643	118	2641	36	0.95	0	2641	36
029 ZR240_D_IV_33	11.58324	3.57	0.49161	2.44	0.68	0.17089	2.61	2578	63	2571	92	2566	67	1.42	0	2566	67
030 ZR240_D_IV_36	7.63901	5.30	0.39940	3.27	0.62	0.13872	4.17	2166	71	2189	116	2211	92	1.36	2	2211	92
031 ZR240_D_IV_37	7.58849	3.24	0.40478	2.56	0.79	0.13597	1.99	2191	56	2184	71	2176	43	1.17	-1	2176	43
032 ZR240_D_IV_38	17.25115	6.56	0.58170	6.36	0.97	0.21509	1.59	2956	188	2949	193	2944	47	0.53	0	2944	47
033 ZR240_D_IV_39	6.31232	2.28	0.36862	1.25	0.55	0.12420	1.91	2023	25	2020	46	2017	38	1.47	0	2017	38
034 ZR240_D_IV_40	13.31595	3.41	0.53445	2.84	0.83	0.18070	1.88	2760	79	2702	92	2659	50	0.59	-4	2659	50
035 ZR240_E_V_01	13.41214	2.94	0.52204	1.72	0.58	0.18633	2.39	2708	47	2709	80	2710	65	0.60	0	2710	65
036 ZR240_E_V_02	6.44527	5.15	0.36636	4.32	0.84	0.12760	2.79	2012	87	2038	105	2065	58	0.55	3	2065	58
039 ZR240_E_V_05	15.42550	2.81	0.56077	2.00	0.71	0.19951	1.97	2870	57	2842	80	2822	56	0.48	-2	2822	56
040 ZR240_E_V_06	13.43687	4.92	0.53357	4.36	0.89	0.18264	2.27	2756	120	2711	133	2677	61	1.01	-3	2677	61
041 ZR240_E_V_07	2.88105	7.29	0.23883	3.39	0.46	0.08749	6.46	1381	47	1377	100	1371	89	0.97	-1	1371	89
042 ZR240_E_V_08	6.83766	5.88	0.38291	3.18	0.54	0.12951	4.95	2090	66	2091	123	2091	104	0.50	0	2091	104
043 ZR240_E_V_09	16.86812	2.96	0.58572	1.74	0.59	0.20887	2.39	2972	52	2927	87	2897	69	0.49	-3	2897	69
044 ZR240_E_V_11	11.99197	10.35	0.48476	7.46	0.72	0.17942	7.17	2548	190	2604	269	2647	190	1.39	4	2647	190
045 ZR240_E_V_14	13.27921	3.84	0.52191	2.36	0.62	0.18453	3.02	2707	64	2700	104	2694	81	1.23	0	2694	81

046 ZR240_E_V_15	12.92859	2.57	0.51882	1.10	0.43	0.18073	2.32	2694	30	2674	69	2660	62	0.58	-1	2660	62
047 ZR240_E_V_16	7.29208	5.20	0.39588	2.90	0.56	0.13359	4.32	2150	62	2148	112	2146	93	0.63	0	2146	93
048 ZR240_E_V_18	14.79206	2.36	0.54561	1.31	0.56	0.19663	1.96	2807	37	2802	66	2798	55	0.52	0	2798	55
051 ZR240_E_V_19	6.72086	7.43	0.38023	5.34	0.72	0.12820	5.16	2077	111	2075	154	2073	107	0.85	0	2073	107
052 ZR240_E_V_20	15.32889	3.23	0.54947	2.14	0.66	0.20233	2.42	2823	60	2836	92	2845	69	0.45	1	2845	69
053 ZR240_E_V_21	12.86278	5.11	0.51374	3.59	0.70	0.18159	3.63	2673	96	2670	136	2667	97	0.71	0	2667	97
054 ZR240_E_V_22	14.57338	4.02	0.53554	2.00	0.50	0.19736	3.49	2765	55	2788	112	2805	98	0.53	1	2805	98
055 ZR240_E_V_23	6.84464	3.85	0.38034	2.22	0.58	0.13052	3.14	2078	46	2092	80	2105	66	0.53	1	2105	66
056 ZR240_E_V_24	6.90320	4.84	0.38678	1.51	0.31	0.12944	4.60	2108	32	2099	102	2090	96	0.48	-1	2090	96
057 ZR240_E_V_26	8.03238	2.35	0.43135	1.22	0.52	0.13506	2.01	2312	28	2235	53	2165	44	0.66	-7	2165	44
058 ZR240_E_V_27	2.59964	6.10	0.20002	4.92	0.81	0.09426	3.60	1175	58	1301	79	1513	55	0.45	22		
059 ZR240_E_V_28	14.20672	3.26	0.57213	2.96	0.91	0.18009	1.35	2917	86	2764	90	2654	36	0.72	-10	2654	36
060 ZR240_E_V_29	5.36670	7.43	0.33887	6.91	0.93	0.11486	2.74	1881	130	1880	140	1878	51	0.87	0	1878	51
063 ZR240_E_V_31	13.39689	1.34	0.54515	0.79	0.59	0.17823	1.09	2805	22	2708	36	2636	29	0.80	-6	2636	29
064 ZR240_E_V_32	16.66287	1.57	0.60890	0.81	0.52	0.19847	1.34	3066	25	2916	46	2814	38	0.58	-9	2814	38
065 ZR240_E_V_34	7.14413	3.07	0.39784	1.75	0.57	0.13024	2.52	2159	38	2130	65	2101	53	0.44	-3	2101	53
066 ZR240_E_V_37	12.80187	2.83	0.51527	1.40	0.50	0.18019	2.45	2679	38	2665	75	2655	65	0.63	-1	2655	65
067 ZR240_E_V_39	4.26423	4.33	0.30037	1.50	0.35	0.10296	4.07	1693	25	1686	73	1678	68	0.71	-1	1678	68
068 ZR240_E_V_40	13.90507	1.96	0.53130	1.36	0.69	0.18981	1.42	2747	37	2743	54	2741	39	0.97	0	2741	39
069 ZR240_E_V_42	6.70872	3.54	0.37404	2.62	0.74	0.13008	2.38	2048	54	2074	73	2099	50	0.54	2	2099	50
070 ZR240_E_V_43	5.11585	2.90	0.32091	1.24	0.43	0.11562	2.62	1794	22	1839	53	1890	50	0.83	5	1890	50
071 ZR240_E_V_44	17.22619	2.33	0.61753	1.91	0.82	0.20232	1.34	3100	59	2948	69	2845	38	0.56	-9	2845	38
072 ZR240_E_V_12	17.88949	1.81	0.60763	1.38	0.76	0.21353	1.17	3061	42	2984	54	2933	34	0.36	-4	2933	34

Resumo dos dados de U-Pb da amostra PE-GO-61 (Formação Sopa-Brumadinho).

Grain.Spot	% $^{206}Pb_c$	ppm U	ppm Th	^{232}Th /^{238}U	ppm ^{206}Pb*	(1) ^{206}Pb /^{238}U Age		(1) ^{207}Pb /^{206}Pb Age		% Dis-cor-dant	(1) $^{207}Pb^*$ /$^{206}Pb^*$	%	(1) $^{207}Pb^*$ /^{235}U	%	(1) $^{206}Pb^*$ /^{238}U	%	err corr
B-1.1	0.14	410	156	0.39	142	2187	33	2189.2	8	0	0.13696	0.44	7.63	1.8	0.4038	1.8	.970
B-2.1	0.34	119	36	0.31	41.7	2198	35	2102	17	-5	0.1303	0.96	7.3	2.1	0.4063	1.9	.890
B-3.1	0.28	338	250	0.76	81.9	1599	25	2673.6	8	40	0.18227	0.51	7.07	1.8	0.2815	1.8	.962
B-4.1	0.24	108	41	0.39	37	2165	34	2133	16	-2	0.1327	0.9	7.3	2.1	0.399	1.9	.899
B-5.1	0.85	172	129	0.78	34.6	1346	23	2007	24	33	0.1235	1.4	3.953	2.3	0.2321	1.9	.806
B-6.1	0.14	255	163	0.66	80.6	2017	31	2049	10	2	0.12644	0.55	6.4	1.9	0.3673	1.8	.955
B-7.1	0.24	412	207	0.52	96.7	1555	24	2053.7	10	24	0.12678	0.55	4.768	1.8	0.2728	1.8	.954
B-8.1	0.20	435	127	0.30	94	1444	23	1977.8	10	27	0.12146	0.55	4.204	1.8	0.251	1.8	.955
B-10.1	0.46	72	39	0.56	32.6	2730	43	2667	15	-2	0.1815	0.92	13.19	2.2	0.527	2	.904
B-11.1	0.18	221	116	0.54	69.2	2003	31	2124	11	6	0.13196	0.62	6.63	1.9	0.3644	1.8	.945
B-12.1	0.13	283	138	0.51	107	2349	35	2484.3	8	5	0.16274	0.46	9.86	1.8	0.4395	1.8	.969
B-13.1	0.47	76	21	0.29	26.4	2182	35	2124	22	-3	0.1319	1.2	7.33	2.3	0.4027	1.9	.839
B-14.1	0.31	264	250	0.98	49.6	1272	22	2633	22	52	0.1779	1.3	5.35	2.3	0.2182	1.9	.820
B-15.1	0.26	210	91	0.44	72.9	2180	33	2110	11	-3	0.13092	0.64	7.26	1.9	0.4023	1.8	.942
B-16.1	0.74	865	496	0.59	121	969	16	1563	17	38	0.09679	0.88	2.164	2	0.1621	1.7	.891
B-17.1	0.19	146	96	0.68	49	2117	33	2121	13	0	0.1317	0.77	7.06	2	0.3886	1.8	.922
B-18.1	0.02	220	125	0.59	102	2768	40	2717.4	6	-2	0.18716	0.39	13.84	1.8	0.5363	1.8	.977
B-19.1	0.05	240	124	0.54	110	2766	40	2704.3	6	-2	0.18568	0.37	13.72	1.8	0.5358	1.8	.979
B-20.1	0.34	80	44	0.57	37.1	2770	42	2702	12	-3	0.1854	0.74	13.73	2	0.537	1.9	.930
B-21.1	0.06	317	177	0.58	141	2692	39	2680.9	6	0	0.18307	0.33	13.09	1.8	0.5184	1.8	.982
B-22.1	0.11	196	41	0.21	70.9	2261	34	2207	11	-2	0.13834	0.62	8.01	1.9	0.4201	1.8	.945
B-23.1	0.29	609	480	0.81	146	1580	25	1978	9	20	0.12147	0.49	4.653	1.8	0.2778	1.8	.962
B-24.1	0.53	625	242	0.40	103	1122	18	2469	12	55	0.1613	0.72	4.227	1.9	0.1901	1.8	.927
B-26.1	0.54	135	113	0.86	18.8	960	17	2522	24	62	0.1664	1.4	3.686	2.4	0.1606	1.9	.805
B-29.1	0.12	208	89	0.44	75.8	2278	35	2172	11	-5	0.13564	0.63	7.93	1.9	0.4239	1.8	.945
B-30.1	0.37	216	280	1.34	61	1827	29	2084	15	12	0.129	0.85	5.83	2	0.3277	1.8	.907

B-31.1	0.25	132	59	0.47	45.8	2185	35	2152	15	-2	0.1341	0.89	7.46	2.1	0.4036	1.9	.906
B-32.1	0.41	583	525	0.93	117	1352	22	1616	16	16	0.09959	0.84	3.203	2	0.2333	1.8	.903
B-34.1	0.06	380	246	0.67	161	2580	38	2748.3	9	6	0.1907	0.55	12.94	1.9	0.4923	1.8	.955
B-35.1	0.13	169	92	0.56	57.2	2140	34	2114	14	-1	0.1312	0.8	7.12	2	0.3938	1.9	.919
B-36.1	0.47	549	361	0.68	113	1380	23	2660.4	9	48	0.18082	0.52	5.95	1.9	0.2387	1.8	.961
B-38.1	0.19	238	111	0.48	82	2172	34	2154	12	-1	0.13426	0.66	7.42	1.9	0.4006	1.8	.940
B-39.1	0.37	83	43	0.54	28.8	2193	37	2123	26	-3	0.1319	1.5	7.37	2.5	0.4051	2	.808
B-40.1	0.48	91	101	1.14	42	2764	47	2710	17	-2	0.1863	1.1	13.75	2.4	0.535	2.1	.895
B-41.1	0.22	562	463	0.85	144	1685	26	2006.4	9	16	0.12343	0.5	5.082	1.8	0.2986	1.8	.962
B-43.1	0.28	116	69	0.62	39.5	2157	35	2108	17	-2	0.1307	0.96	7.16	2.1	0.3973	1.9	.893
B-47.1	0.12	445	189	0.44	174	2411	36	2662.2	6	9	0.18102	0.36	11.32	1.8	0.4536	1.8	.980
C-1.1	0.34	159	214	1.40	36.4	1522	25	2087	28	27	0.1292	1.6	4.74	2.5	0.2662	1.9	.761
C-2.1	0.16	121	81	0.69	43.1	2232	36	2166	15	-3	0.1351	0.89	7.71	2.1	0.4137	1.9	.905
C-3.1	0.03	388	479	1.27	140	2255	34	2215.4	7	-2	0.13905	0.41	8.03	1.8	0.4187	1.8	.974
C-4.1	0.28	158	72	0.47	53.5	2134	35	2173	16	2	0.1357	0.9	7.34	2.1	0.3923	1.9	.906
C-5.1	0.27	654	286	0.45	192	1892	29	2585.4	7	27	0.17284	0.43	8.13	1.8	0.3411	1.8	.972
C-6.1	0.26	660	548	0.86	172	1708	26	2549.7	7	33	0.1692	0.4	7.08	1.8	0.3035	1.8	.975
C-7.1	0.90	516	407	0.81	115	1472	23	1963	17	25	0.1205	0.94	4.262	2	0.2566	1.8	.883
C-8.1	0.55	844	246	0.30	150	1205	19	1971	11	39	0.12103	0.63	3.431	1.9	0.2056	1.8	.941
C-9.1	0.10	209	136	0.67	85.6	2516	38	2540.1	9	1	0.16823	0.53	11.07	1.9	0.4774	1.8	.960
C-10.1	0.08	159	60	0.39	57	2251	35	2187	12	-3	0.13679	0.68	7.88	2	0.4179	1.8	.939
C-11.1	0.31	704	323	0.47	144	1372	22	2438	18	44	0.1583	1.1	5.18	2.1	0.2371	1.8	.851
C-12.1	0.11	618	165	0.28	210	2145	32	2765.1	5	22	0.19268	0.32	10.49	1.8	0.3947	1.8	.984
C-13.1	0.47	551	281	0.53	102	1250	20	2033	13	39	0.1253	0.74	3.697	1.9	0.214	1.8	.922
C-14.1	0.11	256	42	0.17	91.2	2237	34	2170	10	-3	0.13546	0.59	7.75	1.9	0.4148	1.8	.951
C-15.1	0.31	538	357	0.69	145	1759	27	2490	8	29	0.16329	0.45	7.06	1.8	0.3137	1.8	.968
C-16.1	0.05	423	177	0.43	141	2108	32	2141.9	8	2	0.1333	0.45	7.11	1.8	0.3868	1.8	.969
C-17.1	0.35	93	155	1.72	31.2	2117	35	2062	25	-3	0.1274	1.4	6.83	2.4	0.3887	2	.812
C-18.1	0.30	395	500	1.31	89.7	1506	25	2673.5	9	44	0.18225	0.53	6.61	1.9	0.2632	1.8	.960
C-19.1	0.06	197	81	0.43	72.9	2308	36	2276.9	10	-1	0.14408	0.57	8.55	1.9	0.4306	1.8	.956
C-20.1	0.28	546	395	0.75	151	1791	28	2086.9	10	14	0.12919	0.55	5.7	1.9	0.3202	1.8	.955
C-21.1	0.06	265	23	0.09	93.2	2211	35	2183	9	-1	0.13648	0.54	7.7	1.9	0.4092	1.9	.960
C-22.1	0.27	296	66	0.23	103	2192	33	2203	11	0	0.13804	0.65	7.71	1.9	0.4051	1.8	.940

C-23.1	0.26	115	50	0.45	40	2194	35	2163	17	-1	0.1349	0.98	7.54	2.1	0.4055	1.9	.890
C-24.1	0.18	484	131	0.28	143	1906	29	2547	29	25	0.1689	1.8	8.01	2.5	0.344	1.8	.711
C-25.1	0.10	483	62	0.13	150	1985	30	1977.3	9	0	0.12143	0.49	6.04	1.8	0.3607	1.8	.965
C-26.1	0.28	174	89	0.53	56.7	2073	33	2132	17	3	0.1326	0.96	6.93	2.1	0.3793	1.9	.887
C-27.1	0.31	780	116	0.15	144	1247	20	1826	11	32	0.11161	0.61	3.285	1.9	0.2135	1.8	.945
C-28.1	0.10	329	162	0.51	105	2045	31	2161.4	9	5	0.13479	0.52	6.94	1.9	0.3733	1.8	.960
C-29.1	0.27	79	23	0.29	27.5	2182	37	2137	21	-2	0.1329	1.2	7.38	2.3	0.4029	2	.858
C-30.1	0.42	65	32	0.51	28	2619	44	2625	18	0	0.177	1.1	12.24	2.3	0.501	2	.880
C-31.1	0.62	138	129	0.97	31.9	1529	27	2368	36	35	0.1519	2.1	5.61	2.9	0.2677	2	.680
C-32.1	0.09	222	79	0.37	101	2733	41	2691.6	8	-2	0.18426	0.49	13.41	1.9	0.528	1.8	.966
C-33.1	0.13	376	345	0.95	147	2413	36	2799.3	6	14	0.19673	0.39	12.32	1.8	0.454	1.8	.977
C-34.1	--	116	59	0.52	37.9	2073	35	2151	14	4	0.134	0.78	7.01	2.1	0.3794	2	.930
C-35.1	0.42	86	62	0.74	29.4	2161	36	2067	23	-5	0.1277	1.3	7.01	2.4	0.3982	2	.841
C-36.1	0.99	230	187	0.84	37.4	1105	19	2037	25	46	0.1256	1.4	3.237	2.3	0.1869	1.8	.794
C-38.1	0.05	264	81	0.32	93.6	2227	34	2208.6	9	-1	0.1385	0.54	7.88	1.9	0.4126	1.8	.959
C-39.1	0.32	148	73	0.51	52	2199	35	2104	17	-5	0.1305	0.96	7.31	2.1	0.4066	1.9	.890
C-40.1	0.39	121	57	0.49	41.6	2157	35	2136	19	-1	0.1329	1.1	7.28	2.2	0.3974	1.9	.867
C-41.1	0.36	472	224	0.49	145	1967	30	2323.5	10	15	0.14805	0.57	7.28	1.9	0.3568	1.8	.952
C-42.1	0.33	504	395	0.81	165	2078	31	2520	8	18	0.16622	0.46	8.72	1.8	0.3804	1.8	.968
C-43.1	0.22	166	81	0.50	58.7	2221	35	2178	14	-2	0.1361	0.83	7.72	2	0.4114	1.9	.913
C-44.1	0.34	154	136	0.91	59.9	2401	37	2672	11	10	0.1821	0.68	11.33	2	0.4513	1.9	.938

Resumo dos dados de U-Pb da amostra PE-CM-14 (Formação Galho do Miguel).

Spot	**% $^{206}Pb_c$**	**ppm U**	**ppm Th**	**$^{232}Th/^{238}U$**	**ppm $^{206}Pb^*$**	**(1) $^{206}Pb/^{238}U$ Age**		**(1) $^{207}Pb/^{206}Pb$ Age**		**% Dis-cor-dant**	**(1) $^{207}Pb^*/^{206}Pb^*$**	**±%**	**(1) $^{207}Pb^*/^{235}U$**	**±%**	**(1) $^{206}Pb^*/^{238}U$**	**±%**	**err corr**	**Best estimated age (Ma)**	
A-1.1	0,23	87	22	0,3	27.9	2049	±24	2105	±15	3	0.1305	0.87	6.73	1.6	0.3741	1.4	,846	2105	15

A-2.1	1,89	358	41	0,1	69.5	1291	±15	1925	±34	33	0.118	1.9	3.608	2.3	0.2218	1.2	,550		
A-3.1	0,14	85	64	0,8	35.4	2549	±30	2708	±10	6	0.1861	0.63	12.45	1.5	0.4851	1.4	,912	2708	10
A-4.1	0,09	213	75	0,4	62.3	1891	±20	2098.7	± 9.5	10	0.13006	0.54	6.114	1.4	0.3409	1.2	,918	2098.7	9,5
A-5.1	0,47	119	66	0,6	33.1	1809	±21	2035	±20	11	0.1254	1.1	5.603	1.7	0.324	1.3	,769	2035	20
A-6.1	0,04	76	22	0,3	23.6	2000	±25	2140	±15	7	0.1332	0.83	6.68	1.7	0.3638	1.4	,866	2140	15
A-8.1	0,04	156	65	0,4	53.4	2167	±25	2178.6	± 9.7	1	0.13614	0.56	7.5	1.5	0.3996	1.4	,926	2178.6	9,7
A-9.1	0,33	303	199	0,7	60.8	1349	±15	1589	±17	15	0.09816	0.92	3.151	1.5	0.2328	1.2	,795	1589	17
A-10.1	0,25	77	85	1,1	25	2056	±25	2073	±19	1	0.1282	1.1	6.64	1.8	0.3756	1.4	,799	2073	19
A-11.1	0,07	49	25	0,5	23.8	2868	±40	2908	±12	1	0.2103	0.72	16.25	1.9	0.5604	1.7	,923	2908	12
A-12.1	0,26	63	44	0,7	19.5	1992	±26	2096	±22	5	0.1298	1.2	6.48	2	0.3621	1.5	,774	2096	22
A-13.1	0,26	44	20	0,5	14.3	2078	±33	2152	±23	3	0.134	1.3	7.03	2.3	0.3804	1.9	,817	2152	23
A-15.1	0,18	91	32	0,4	28.3	1993	±24	2113	±16	6	0.1312	0.92	6.55	1.7	0.3623	1.4	,834	2113	16
A-16.1	--	77	29	0,4	32.3	2574	±30	2802	±10	8	0.197	0.63	13.34	1.5	0.4908	1.4	,912	2802	10
A-17.1	3,56	468	89	0,2	78	1105	±13	1808	±72	39	0.1105	4	2.85	4.2	0.1869	1.2	,299		
A-18.1	0,04	257	116	0,5	97.9	2366	±24	2459.4	± 8.6	4	0.16035	0.51	9.8	1.3	0.4435	1.2	,923	2459.4	8,6
A-20.1	0,76	368	46	0,1	87	1559	±17	2157	±21	28	0.1345	1.2	5.071	1.7	0.2735	1.2	,706		
A-21.1	0,04	198	62	0,3	60.6	1962	±21	2076.5	± 9.1	6	0.12843	0.52	6.298	1.3	0.3557	1.2	,924	2076.5	9,1
A-22.1	0,36	291	81	0,3	78.1	1744	±18	2539	±11	31	0.1681	0.63	7.2	1.4	0.3106	1.2	,886		
A-23.1	0,04	316	90	0,3	95	1933	±20	2039.5	± 7.7	5	0.12576	0.44	6.064	1.3	0.3497	1.2	,939	2039.5	7,7
A-24.1	0,21	102	22	0,2	30.3	1920	±24	2102	±39	9	0.1303	2.2	6.23	2.7	0.3469	1.5	,549	2102	39
A-27.1	0,09	139	39	0,3	47	2140	±25	2190	±11	2	0.13704	0.6	7.44	1.5	0.3938	1.4	,916	2190	11
A-28.1	0,07	186	35	0,2	42.3	1513	±18	1604	±13	6	0.09893	0.69	3.609	1.5	0.2646	1.3	,889	1604	13
A-29.1	0,02	76	29	0,4	24	2006	±25	2131	±21	6	0.1325	1.2	6.67	1.9	0.3651	1.4	,770	2131	21
A-30.1	0,15	85	44	0,5	29.5	2182	±26	2205	±14	1	0.1382	0.8	7.67	1.6	0.4027	1.4	,867	2205	14
A-31.1	0,55	169	56	0,3	38.6	1512	±17	2023	±17	25	0.1246	0.98	4.543	1.6	0.2644	1.3	,793		
A-32.1	0,05	218	72	0,3	70.5	2058	±22	2145.3	± 9.1	4	0.13356	0.52	6.925	1.3	0.376	1.2	,922	2145.3	9,1
A-33.1	1,40	388	74	0,2	72	1246	±14	1827	±34	32	0.1117	1.9	3.284	2.2	0.2133	1.2	,536		
A-34.1	0,85	368	100	0,3	78.7	1421	±16	1927	±18	26	0.118	0.98	4.013	1.6	0.2466	1.2	,783		

A-35.1	0,70	301	104	0,4	74.2	1618	±17	2099	±14	23	0.1301	0.81	5.115	1.5	0.2852	1.2	,829		
A-36.1	0,51	211	76	0,4	63.1	1921	±21	2044	±23	6	0.1261	1.3	6.04	1.8	0.3472	1.2	,694	2044	23
A-37.1	0,09	145	72	0,5	50	2173	±25	2199.5	± 9.8	1	0.13778	0.56	7.61	1.5	0.4008	1.4	,924	2199.5	9,8
A-38.1	0,19	216	94	0,5	48.1	1480	±17	1583	±16	6	0.0978	0.84	3.481	1.5	0.2581	1.2	,828	1583	16
A-39.1	0,26	106	59	0,6	23.7	1484	±18	1599	±24	7	0.0987	1.3	3.521	1.9	0.2588	1.4	,720	1599	24
B-1.1	0,09	223	132	0,6	86.8	2404	±25	2684.9	± 6.7	10	0.18351	0.4	11.44	1.3	0.452	1.2	,951	2684.9	6,7
B-3.1	0,17	251	111	0,5	68.6	1780	±19	2103	± 16	15	0.1304	0.94	5.719	1.5	0.3181	1.2	,793	2103	16
B-4.1	0,14	90	46	0,5	33.4	2318	±27	2423	± 12	4	0.1569	0.74	9.36	1.6	0.4327	1.4	,883	2423	12
B-5.1	--	129	40	0,3	57.1	2681	±29	2887.7	± 7.3	7	0.2077	0.45	14.77	1.4	0.5158	1.3	,945	2887.7	7,3
B-7.1	0,18	86	113	1,4	27.1	2009	±24	2091	± 18	4	0.1295	1	6.53	1.7	0.3657	1.4	,814	2091	18
B-8.1	0,06	285	192	0,7	98.4	2180	±22	2413	± 11	10	0.156	0.67	8.65	1.4	0.4023	1.2	,873	2413	11
B-9.1	--	82	47	0,6	26.3	2044	±25	2101	± 14	3	0.1302	0.79	6.7	1.6	0.3732	1.4	,875	2101	14
B-10.1	0,07	136	54	0,4	42.7	2002	±24	2059	± 13	3	0.12715	0.72	6.38	1.6	0.3641	1.4	,889	2059	13
B-11.1	0,08	174	71	0,4	50.2	1865	±22	2088	± 12	11	0.1293	0.68	5.982	1.5	0.3356	1.3	,893	2088	12
B-14.1	0,31	67	18	0,3	21.2	2027	±26	2093	± 19	3	0.1296	1.1	6.6	1.9	0.3694	1.5	,802	2093	19
B-12.1	0,39	61	17	0,3	16.9	1789	±24	2167	± 25	17	0.1353	1.5	5.97	2.1	0.3199	1.5	,721	2167	25
B-15.1	0,08	121	57	0,5	38	2006	±23	2151	± 12	7	0.13399	0.68	6.74	1.5	0.3651	1.3	,889	2151	12
B-17.1	0,08	118	40	0,3	37	2005	±23	2077	± 13	3	0.12844	0.73	6.46	1.5	0.3648	1.3	,877	2077	13
B-18.1	0,45	172	59	0,4	42.5	1626	±18	2049	± 25	21	0.1265	1.4	5.001	1.9	0.2868	1.3	,678		
B-20.1	--	117	47	0,4	37.4	2040	±23	2118	± 11	4	0.13146	0.66	6.75	1.5	0.3724	1.3	,897	2118	11
B-21.1	0,06	122	33	0,3	39.8	2066	±25	2132	± 13	3	0.13252	0.73	6.9	1.6	0.3779	1.4	,890	2132	13
B-22.1	--	117	35	0,3	38.6	2093	±26	2192	± 12	5	0.13721	0.67	7.26	1.6	0.3835	1.5	,908	2192	12
B-23.1	0,24	122	47	0,4	32.8	1751	±20	2116	± 15	17	0.1313	0.85	5.653	1.6	0.3122	1.3	,843	2116	15
B-25.1	0,12	136	58	0,4	47.3	2184	±25	2321	± 14	6	0.1479	0.79	8.22	1.6	0.4032	1.4	,865	2321	14
B-26.1	1,24	459	92	0,2	79.1	1164	±13	1905	± 20	39	0.1166	1.1	3.183	1.7	0.1979	1.2	,730		
B-28.1	23,93	569	137	0,2	80.6	762	±18	1094	±490	30	0.076	25	1.31	25	0.1255	2.4	,099		
B-29.1	0,12	54	21	0,4	17.1	2015	±27	2119	± 20	5	0.1316	1.1	6.66	1.9	0.367	1.5	,811	2119	20
B-30.1	0,12	122	99	0,8	39.5	2054	±23	2070	± 13	1	0.12793	0.71	6.62	1.5	0.3753	1.3	,880	2070	13

B-31.1	0,34	289	95	0,3	84.2	1880	±20	2464	± 15	24	0.1608	0.88	7.5	1.5	0.3386	1.2	,818		
B-32.1	0,20	173	63	0,4	44.5	1689	±19	2062	± 13	18	0.12736	0.73	5.259	1.5	0.2995	1.3	,867	2062	13
B-34.1	0,17	101	54	0,6	24.1	1582	±21	1605	± 19	1	0.099	1	3.795	1.8	0.2781	1.5	,817	1605	19
B-35.1	0,25	175	35	0,2	50.3	1852	±20	2179	± 12	15	0.13615	0.67	6.247	1.4	0.3328	1.2	,880	2179	12
B-36.1	0,23	165	89	0,6	64	2400	±25	2803.1	± 8.6	14	0.1972	0.53	12.27	1.4	0.4512	1.3	,922	2803.1	8,6
B-37.1	0,03	42	14	0,3	11.5	1782	±25	2078	± 21	14	0.1285	1.2	5.64	2	0.3185	1.6	,811	2078	21
C-1.1	0,20	50	20	0,4	15.1	1951	±26	2094	±23	7	0.1297	1.3	6.32	2.1	0.3534	1.6	,763	2094	23
C-2.1	0,02	90	52	0,6	28.2	2001	±24	2057	±16	3	0.127	0.88	6.37	1.7	0.364	1.4	,847	2057	16
C-3.1	0,04	184	67	0,4	53.3	1873	±21	2079.5	±10	10	0.12864	0.57	5.981	1.4	0.3372	1.3	,912	2079.5	10
C-4.1	0,38	254	94	0,4	58.3	1519	±17	2088	±13	27	0.12928	0.75	4.736	1.5	0.2657	1.3	,864		
C-5.1	0,36	213	87	0,4	57.8	1764	±19	2045	±13	14	0.12618	0.76	5.475	1.5	0.3147	1.2	,854	2045	13
C-6.1	0,26	117	105	0,9	37	2017	±23	2201	±14	8	0.1379	0.82	6.99	1.6	0.3674	1.3	,852	2201	14
C-7.1	0,07	173	70	0,4	52.6	1952	±21	2098	±10	7	0.13	0.59	6.34	1.4	0.3537	1.3	,906	2098	10
C-8.1	0,08	80	46	0,6	23.2	1885	±23	2094	±17	10	0.1297	0.97	6.08	1.7	0.3398	1.4	,827	2094	17
C-9.1	0,47	313	97	0,3	65.7	1406	±15	2003	±14	30	0.1232	0.82	4.141	1.5	0.2437	1.2	,828		
C-10.1	0,04	144	60	0,4	46.8	2072	±24	2140	±10	3	0.13315	0.59	6.96	1.5	0.3791	1.4	,920	2140	10
C-11.1	--	111	59	0,5	34.5	1997	±23	2081	±12	4	0.12874	0.7	6.444	1.5	0.363	1.3	,888	2081	12
C-12.1	0,11	182	133	0,8	54.7	1936	±21	2095	±11	8	0.12976	0.63	6.266	1.4	0.3502	1.3	,896	2095	11
C-13.1	0,12	83	45	0,6	25.5	1972	±24	2157	±17	9	0.1344	0.97	6.63	1.7	0.3579	1.4	,826	2157	17
C-14.1	0,22	243	96	0,4	73	1932	±20	2475.6	± 9	22	0.1619	0.53	7.8	1.3	0.3495	1.2	,917		
C-15.1	0,04	85	70	0,8	18.1	1425	±20	1596	±20	11	0.0985	1.1	3.36	1.9	0.2475	1.6	,826	1596	20
C-16.1	0,14	257	197	0,8	56.1	1456	±17	1589	±19	8	0.09812	1	3.43	1.6	0.2535	1.3	,785	1589	19
C-18.1	1,27	127	40	0,3	20.4	1092	±14	1621	±59	33	0.0998	3.2	2.54	3.5	0.1846	1.4	,392		
C-19.1	0,12	66	37	0,6	14	1414	±19	1541	±26	8	0.0957	1.4	3.236	2	0.2453	1.5	,741	1541	26

Resumo dos dados de U-Pb da amostra PE-CM-15A (Formação Galho do Miguel).

Spot	% $^{206}Pb_c$	ppm U	ppm Th	^{232}Th / ^{238}U	ppm $^{206}Pb^*$	(1) ^{206}Pb / ^{238}U Age		(1) ^{207}Pb / ^{206}Pb Age		% Dis-cor-dant	(1) $^{207}Pb^*$ / $^{206}Pb^*$	±%	(1) $^{207}Pb^*$ / ^{235}U	±%	(1) $^{206}Pb^*$ / ^{238}U	±%	err corr	Best estimated age (Ma)	
D-2.1	0,23	72	27	0,4	22.2	1968	±27	2218	±16	11	0.1393	0.92	6.85	1.8	0.357	1.6	,865	2218	16
D-3.1	0,06	75	31	0,4	31.9	2590	±33	2805	±13	8	0.1975	0.81	13.46	1.7	0.4944	1.5	,887	2805	13
D-4.1	0,33	284	219	0,8	72.2	1665	±19	2100	±12	21	0.13016	0.67	5.288	1.4	0.2946	1.3	,884		
D-5.1	0,44	373	216	0,6	116	1981	±22	2117	±41	6	0.1314	2.3	6.52	2.7	0.3598	1.3	,480	2117	41
D-6.1	0,12	114	63	0,6	52.4	2755	±31	2697	±14	-2	0.1848	0.84	13.59	1.6	0.5333	1.4	,850	2697	14
D-7.1	0,27	201	324	1,7	47.5	1563	±17	1920	±14	19	0.1176	0.77	4.45	1.5	0.2744	1.2	,851		
D-8.1	0,16	217	132	0,6	50.3	1540	±18	2096	±11	27	0.12988	0.64	4.831	1.4	0.2698	1.3	,895		
D-9.1	0,19	99	49	0,5	28.7	1869	±24	2097	±15	11	0.1299	0.84	6.02	1.7	0.3363	1.5	,870	2097	15
D-10.1	0,14	119	83	0,7	29.8	1642	±19	2116	±13	22	0.1313	0.76	5.253	1.5	0.2902	1.3	,863		
D-11.1	0,05	202	76	0,4	56.3	1811	±19	2069.1	± 8.9	12	0.12788	0.5	5.72	1.3	0.3244	1.2	,925	2069,1	8,9
D-13.1	0,27	161	118	0,8	37	1525	±18	2135	±14	29	0.1328	0.8	4.886	1.5	0.2669	1.3	,855		
D-14.1	0,11	287	198	0,7	103	2246	±24	3173.2	± 4.8	29	0.24818	0.3	14.26	1.3	0.4167	1.2	,972		
D-15.1	--	94	44	0,5	35	2329	±27	2559	±60	9	0.1701	3.6	10.21	3.9	0.4352	1.4	,352	2559	60
D-17.1	0,42	457	409	0,9	56.4	862.8	± 9.5	1920	±34	55	0.1176	1.9	2.322	2.3	0.1432	1.2	,524		
D-18.1	0,17	130	87	0,7	30.5	1556	±18	2084	±25	25	0.129	1.4	4.854	1.9	0.273	1.3	,684		
D-20.1	0,92	456	184	0,4	65.5	989	±11	1766	±19	44	0.108	1	2.469	1.6	0.1658	1.2	,764		
E-2.1	0,10	179	111	0,6	48.8	1777	±19	2153	± 11	17	0.13416	0.65	5.87	1.4	0.3173	1.2	,887	2153	11
E-3.1	1,42	1688	912	0,6	57.2	245.9	± 2.8	723	± 49	66	0.0634	2.3	0.34	2.6	0.03888	1.2	,449		
E-4.1	0,19	510	391	0,8	71.2	970	±11	1999.7	± 9.3	52	0.12297	0.52	2.752	1.3	0.1623	1.2	,917		
E-5.1	0,03	212	80	0,4	68.5	2056	±22	2115.8	± 8.2	3	0.13133	0.47	6.801	1.3	0.3756	1.2	,935	2115,8	8,2
E-6.1	0,09	87	55	0,7	36.6	2567	±29	2763	± 25	7	0.1924	1.5	12.97	2.1	0.4891	1.4	,665	2763	25
E-7.1	0,15	90	29	0,3	28	1991	±25	2137	± 14	7	0.1329	0.82	6.63	1.7	0.3619	1.5	,875	2137	14
E-8.1	0,03	181	29	0,2	62.1	2170	±23	2475	± 13	12	0.1619	0.75	8.93	1.5	0.4003	1.2	,856	2475	13
E-9.1	0,18	238	126	0,5	57.2	1586	±18	2068	± 14	23	0.1278	0.79	4.914	1.5	0.2789	1.3	,848		

E-10.1	0,08	120	59	0,5	37.8	2010	±23	2087	± 13	4	0.12921	0.76	6.52	1.5	0.366	1.3	,866	2087	13
E-11.1	0,05	95	29	0,3	31.7	2108	±24	2179	± 13	3	0.1362	0.75	7.26	1.6	0.3867	1.4	,875	2179	13
E-12.1	0,12	55	90	1,7	17.2	2013	±26	2071	± 20	3	0.128	1.2	6.47	1.9	0.3665	1.5	,793	2071	20
E-13.1	0,05	236	82	0,4	74.4	2015	±21	2229.9	± 9.4	10	0.14022	0.54	7.093	1.3	0.3669	1.2	,913	2229,9	9,4
E-14.1	0,23	36	12	0,4	10.3	1863	±27	2065	± 21	10	0.1276	1.2	5.9	2.1	0.3352	1.7	,808	2065	21
E-15.1	11,24	413	272	0,7	122	1713	±27	2645	±140	35	0.179	8.7	7.52	8.8	0.3045	1.8	,199	2645	140
E-16.1	0,09	149	60	0,4	46.5	2001	±23	2176	± 13	8	0.136	0.75	6.82	1.5	0.3639	1.3	,874	2176	13
E-17.1	0,05	79	59	0,8	24.8	2000	±24	2059	± 13	3	0.12714	0.75	6.38	1.6	0.3637	1.4	,879	2059	13
E-19.1	0,03	164	84	0,5	47.2	1865	±20	1843	± 12	-1	0.1127	0.68	5.215	1.4	0.3356	1.3	,880	1843	12
E-20.1	0,29	422	205	0,5	68.9	1120	±12	2021	± 11	45	0.12442	0.62	3.254	1.3	0.1897	1.2	,885		
E-21.1	0,02	120	18	0,2	41.3	2167	±24	2151	± 10	-1	0.13401	0.59	7.38	1.4	0.3996	1.3	,911	2151	10
E-22.1	0,06	116	107	0,9	38.1	2080	±23	2142	± 11	3	0.13332	0.65	7	1.5	0.3809	1.3	,898	2142	11
E-23.1	0,08	134	33	0,3	44	2087	±24	2161	± 11	3	0.13475	0.61	7.1	1.5	0.3823	1.4	,913	2161	11
E-25.1	0,23	44	26	0,6	12.3	1803	±25	2095	± 23	14	0.1298	1.3	5.78	2.1	0.3228	1.6	,762	2095	23
E-26.1	0,20	122	34	0,3	33.7	1791	±20	2103	± 14	15	0.1303	0.8	5.758	1.5	0.3204	1.3	,853	2103	14
E-27.1	0,11	60	34	0,6	32.7	3178	±37	3273.8	± 8.4	3	0.2645	0.53	23.24	1.5	0.6372	1.5	,939	3273,8	8,4
E-28.1	0,64	275	203	0,8	62.3	1502	±16	1997	± 14	25	0.12277	0.8	4.443	1.4	0.2624	1.2	,832		
E-29.1	0,12	197	118	0,6	45	1521	±18	2094	± 10	27	0.12974	0.59	4.76	1.4	0.2661	1.3	,911		
E-30.1	1,79	984	716	0,8	58.4	422.7	± 4.8	1464	± 38	71	0.0918	2	0.858	2.3	0.06778	1.2	,512		
E-31.1	0,14	251	110	0,5	54.1	1444	±16	2000	± 11	28	0.12299	0.63	4.256	1.4	0.251	1.2	,888		
E-35.1	1,61	1063	643	0,6	48.4	327.7	± 3.7	1026	± 42	68	0.0734	2.1	0.528	2.4	0.05214	1.2	,487		
E-37.1	0,99	1464	702	0,5	57.2	283.9	± 3.2	912	± 39	69	0.0694	1.9	0.4311	2.2	0.04502	1.2	,528		
E-38.1	0,25	152	90	0,6	30.6	1353	±15	2058	± 15	34	0.1271	0.85	4.091	1.5	0.2335	1.3	,829		
E-39.1	0,04	208	113	0,6	52.9	1674	±19	2108.9	± 9.3	21	0.13081	0.53	5.348	1.4	0.2965	1.3	,923		

Resumo dos dados de U-Pb da amostra PE-CM-15B (Formação Galho do Miguel).

						Isotope ratios[b]							Ages (Ma)								
Spot number	f 206	Pb ppm	U ppm	Th ppm	Th/U[a]	$^{207}Pb/^{235}U$	1 s [%]	$^{206}Pb/^{238}U$	1 s [%]	Rho[c]	$^{207}Pb/^{206}Pb$[d]	1 s [%]	$^{206}Pb/^{238}U$	1 s abs	$^{207}Pb/^{235}U$	1 s abs	$^{207}Pb/^{206}Pb$	1 s abs	% Conc[e]	Best estimated age (Ma)	
Zr-222-A-I-01	0,0008	54	112	77	0,70	6,5213	1,68	0,3696	0,58	0,34	0,1280	1,58	2027	12	2049	34	2070	33	98	2070	33
Zr-222-A-I-02	0,0005	89	179	71	0,40	7,2714	2,11	0,3949	0,81	0,38	0,1335	1,95	2146	17	2145	45	2145	42	100	2145	42
Zr-222-A-I-05	0,0006	74	113	84	0,75	10,4680	1,69	0,4682	0,96	0,57	0,1622	1,38	2476	24	2477	42	2478	34	100	2478	34
Zr-222-A-I-07	0,0011	32	67	34	0,51	6,7569	2,21	0,3797	0,99	0,45	0,1290	1,97	2075	21	2080	46	2085	41	100	2085	41
Zr-222-A-I-08	0,0007	50	100	111	1,12	6,7455	2,27	0,3799	1,07	0,47	0,1288	2,00	2076	22	2079	47	2081	42	100	2081	42
Zr-222-A-I-09	0,0009	39	81	25	0,31	7,3040	2,10	0,3922	0,84	0,40	0,1351	1,92	2133	18	2149	45	2165	42	99	2165	42
Zr-222-A-I-12	0,0008	59	127	39	0,31	7,0192	1,70	0,3837	0,98	0,57	0,1327	1,39	2093	20	2114	36	2134	30	98	2134	30
Zr-222-A-I-14	0,0010	46	85	67	0,79	7,3863	2,21	0,3984	0,97	0,44	0,1345	1,99	2161	21	2159	48	2157	43	100	2157	43
Zr-222-A-I-15	0,0006	57	119	32	0,27	7,4482	1,80	0,3977	0,98	0,54	0,1358	1,52	2158	21	2167	39	2175	33	99	2175	33
Zr-222-A-I-18	0,0010	36	67	32	0,49	8,0916	2,37	0,4138	1,38	0,58	0,1418	1,93	2232	31	2241	53	2250	43	99	2250	43
Zr-222-A-I-19	0,0005	40	82	31	0,38	6,9783	1,94	0,3846	0,68	0,35	0,1316	1,82	2098	14	2109	41	2119	38	99	2119	38
Zr-222-A-I-20	0,0008	36	65	69	1,07	6,7786	2,07	0,3805	0,93	0,45	0,1292	1,85	2079	19	2083	43	2087	39	100	2087	39
Zr-222-A-I-39	0,0004	59	107	41	0,39	10,6879	1,91	0,4740	1,30	0,68	0,1635	1,40	2501	32	2496	48	2493	35	100	2493	35
Zr-222-A-I-22	0,0004	78	154	70	0,46	7,8985	1,62	0,4103	0,87	0,54	0,1396	1,36	2216	19	2220	36	2223	30	100	2223	30
Zr-222-A-I-23	0,0003	59	128	65	0,51	6,8682	1,75	0,3827	0,81	0,46	0,1302	1,56	2089	17	2095	37	2100	33	99	2100	33
Zr-222-A-I-26	0,0003	92	182	76	0,42	7,3578	1,58	0,3972	0,89	0,56	0,1343	1,30	2156	19	2156	34	2156	28	100	2156	28
Zr-222-A-I-27	0,0008	65	147	81	0,56	8,0610	1,18	0,4098	0,59	0,50	0,1427	1,03	2214	13	2238	27	2260	23	98	2260	23
Zr-222-A-I-30	0,0006	47	82	105	1,29	6,9222	2,18	0,3861	1,34	0,62	0,1300	1,72	2105	28	2102	46	2098	36	100	2098	36
Zr-222-A-I-32	0,0002	89	190	72	0,38	7,2964	1,73	0,3929	1,03	0,59	0,1347	1,39	2136	22	2148	37	2160	30	99	2160	30
Zr-222-A-I-35	0,0007	67	144	67	0,47	6,4863	1,82	0,3721	0,76	0,42	0,1264	1,66	2039	15	2044	37	2049	34	100	2049	34
Zr-222-B-II-03	0,0006	106	330	212	0,65	6,3674	1,06	0,3406	0,25	0,24	0,1356	1,03	1889	5	2028	21	2172	22	87	2172	22
Zr-222-B-II-04	0,0008	55	141	53	0,38	6,9221	1,47	0,3678	1,04	0,71	0,1365	1,04	2019	21	2101	31	2183	23	92	2183	23

Zr-222-B-II-06	0,0004	58	135	42	0,31	7,2614	1,76	0,3920	0,74	0,42	0,1344	1,59	2132	16	2144	38	2156	34	99	2156	34
Zr-222-B-II-07	0,0003	65	129	66	0,52	7,3991	1,60	0,3982	0,70	0,44	0,1348	1,44	2161	15	2161	35	2161	31	100	2161	31
Zr-222-B-II-08	0,0013	55	158	110	0,70	6,1229	4,06	0,3047	3,94	0,97	0,1457	1,01	1715	68	1994	81	2297	23	75		
Zr-222-B-II-09	0,0012	20	42	27	0,64	7,1073	3,09	0,3889	1,54	0,50	0,1325	2,68	2118	33	2125	66	2132	57	99	2132	57
Zr-222-B-II-10	0,0003	74	174	36	0,21	6,9271	1,88	0,3859	1,18	0,63	0,1302	1,46	2104	25	2102	40	2100	31	100	2100	31
Zr-222-B-II-11	0,0005	37	79	24	0,31	7,4647	2,04	0,3979	0,92	0,45	0,1360	1,82	2160	20	2169	44	2177	40	99	2177	40
Zr-222-B-II-13	0,0015	15	30	14	0,48	8,2471	4,01	0,4199	1,60	0,40	0,1424	3,67	2260	36	2259	91	2257	83	100	2257	83
Zr-222-B-II-16	0,0005	60	113	122	1,09	6,4238	2,14	0,3714	0,95	0,44	0,1254	1,92	2036	19	2036	44	2035	39	100	2035	39
Zr-222-B-II-18	0,0013	24	47	36	0,77	7,0463	3,57	0,3800	2,18	0,61	0,1345	2,82	2076	45	2117	75	2157	61	96	2157	61
Zr-222-B-II-19	0,0002	41	95	32	0,34	7,2271	1,94	0,3935	1,09	0,56	0,1332	1,60	2139	23	2140	41	2141	34	100	2141	34
Zr-222-B-II-24	0,0006	45	101	38	0,38	7,0598	2,33	0,3885	1,06	0,46	0,1318	2,08	2116	22	2119	49	2122	44	100	2122	44
Zr-222-B-II-25	0,0003	92	184	103	0,56	6,8248	2,11	0,3824	1,37	0,65	0,1294	1,61	2088	29	2089	44	2090	34	100	2090	34
Zr-222-B-II-26	0,0007	25	47	32	0,70	7,7056	3,36	0,4065	1,47	0,44	0,1375	3,02	2199	32	2197	74	2196	66	100	2196	66
Zr-222-B-II-27	0,0007	71	189	150	0,80	5,5117	1,78	0,3192	1,04	0,59	0,1253	1,44	1786	19	1902	34	2032	29	88	2032	29
Zr-222-B-II-32	0,0006	64	76	59	0,78	18,1646	1,76	0,5915	1,26	0,72	0,2227	1,22	2995	38	2998	53	3001	37	100	3001	37
Zr-222-B-II-33	0,0004	39	80	50	0,63	6,6006	2,01	0,3733	0,99	0,49	0,1282	1,76	2045	20	2059	41	2074	36	99	2074	36
Zr-222-B-II-35	0,0004	69	137	116	0,85	6,7390	1,88	0,3814	0,96	0,51	0,1282	1,62	2083	20	2078	39	2073	34	100	2073	34
Zr-222-B-II-37	0,0040	129	397	189	0,48	7,3317	1,52	0,3774	0,81	0,53	0,1409	1,29	2064	17	2153	33	2238	29	92	2238	29
Zr-222-C-III-01	0,0008	42	92	61	0,67	6,4516	1,93	0,3723	1,29	0,67	0,1257	1,43	2040	26	2039	39	2039	29	100	2039	29
Zr-222-C-III-02	0,0015	74	232	170	0,74	5,7541	1,76	0,3197	1,44	0,82	0,1306	1,01	1788	26	1940	34	2105	21	85	2105	21
Zr-222-C-III-03	0,0009	33	69	30	0,44	7,3193	1,84	0,3968	1,00	0,54	0,1338	1,54	2154	22	2151	40	2148	33	100	2148	33
Zr-222-C-III-04	0,0008	53	124	64	0,52	5,2284	3,84	0,2833	3,53	0,92	0,1338	1,52	1608	57	1857	71	2149	33	75		
Zr-222-C-III-05	0,0017	20	41	33	0,81	7,1072	2,24	0,3949	0,90	0,40	0,1305	2,06	2145	19	2125	48	2105	43	102	2105	43
Zr-222-C-III-07	0,0005	75	170	96	0,57	7,3592	1,67	0,3913	0,79	0,47	0,1364	1,47	2129	17	2156	36	2182	32	98	2182	32
Zr-222-C-III-08	0,0005	56	116	40	0,34	7,2786	1,69	0,3933	0,88	0,52	0,1342	1,44	2138	19	2146	36	2154	31	99	2154	31
Zr-222-C-III-09	0,0008	28	57	18	0,32	7,4735	1,80	0,3999	0,77	0,43	0,1355	1,63	2169	17	2170	39	2171	35	100	2171	35
Zr-222-C-III-11	0,0014	35	41	35	0,86	23,9302	2,48	0,6568	1,17	0,47	0,2642	2,19	3255	38	3266	81	3272	72	99	3272	72
Zr-222-C-III-12	0,0007	43	97	24	0,25	7,0734	2,70	0,3892	2,23	0,83	0,1318	1,52	2119	47	2121	57	2122	32	100	2122	32

Zr-222-C-III-17	0,0004	65	142	56	0,40	6,6478	1,79	0,3761	1,12	0,63	0,1282	1,39	2058	23	2066	37	2073	29	99	2073	29
Zr-222-C-III-18	0,0012	36	74	53	0,73	7,1536	2,05	0,3919	1,08	0,53	0,1324	1,74	2132	23	2131	44	2130	37	100	2130	37
Zr-222-C-III-19	0,0006	66	143	53	0,37	7,3574	1,77	0,3946	0,68	0,38	0,1352	1,64	2144	14	2156	38	2167	36	99	2167	36
Zr-222-C-III-20	0,0007	42	86	51	0,60	6,8624	2,33	0,3840	0,88	0,38	0,1296	2,15	2095	18	2094	49	2093	45	100	2093	45
Zr-222-C-III-23	0,0018	28	59	40	0,67	7,4184	3,40	0,3994	1,40	0,41	0,1347	3,10	2166	30	2163	73	2160	67	100	2160	67
Zr-222-C-III-26	0,0006	65	138	82	0,59	8,0287	1,62	0,4143	1,24	0,76	0,1405	1,05	2235	28	2234	36	2234	23	100	2234	23
Zr-222-C-III-28	0,0011	36	80	34	0,43	7,2973	2,46	0,3931	0,78	0,32	0,1346	2,33	2137	17	2148	53	2159	50	99	2159	50
Zr-222-C-III-30	0,0002	128	185	87	0,47	15,7805	1,27	0,5589	0,91	0,72	0,2048	0,88	2862	26	2864	36	2865	25	100	2865	25
Zr-222-C-III-33	0,0009	34	72	37	0,51	7,5923	1,94	0,4013	1,25	0,64	0,1372	1,48	2175	27	2184	42	2193	33	99	2193	33
Zr-222-C-III-35	0,0010	33	77	53	0,69	7,2723	3,26	0,3848	2,49	0,77	0,1371	2,09	2099	52	2145	70	2191	46	96	2191	46

Resumo dos dados de U-Pb da amostra PE-SC-43 (Formação Galho do Miguel)

						Isotope ratios[b]							**Ages (Ma)**								
Spot number	f 206	Pb ppm	U ppm	Th ppm	Th/U[a]	$^{207}Pb/^{235}U$	1 s [%]	$^{206}Pb/^{238}U$	1 s [%]	Rho[c]	$^{207}Pb/^{206}Pb^{d}$	1 s [%]	$^{206}Pb/^{238}U$	1 s abs	$^{207}Pb/^{235}U$	1 s abs	$^{207}Pb/^{206}Pb$	1 s abs	% Conc[e]	Best estimated age (Ma)	
Zr-206-A-I-04	0,0006	48,8	104,9	47,5	0,46	7,03651	1,38	0,38637	0,81	0,59	0,13208	1,11	2106	17	2116	29	2126	24	99	2126	24
Zr-206-A-I-06	0,0004	14,8	46,5	13,4	0,29	3,87628	1,69	0,28412	0,65	0,39	0,09895	1,56	1612	11	1609	27	1604	25	100	1604	25
Zr-206-A-I-07	0,0003	59,2	128,1	36,4	0,29	6,92109	1,32	0,38502	0,42	0,32	0,13037	1,25	2100	9	2101	28	2103	26	100	2103	26
Zr-206-A-I-08	0,0012	53,7	187,9	123,5	0,66	6,08459	2,65	0,35688	2,21	0,84	0,12365	1,45	1967	44	1988	53	2010	29	98	2010	29
Zr-206-A-I-09	0,0004	37,1	74,5	32,6	0,44	7,33992	1,60	0,39526	0,92	0,58	0,13468	1,30	2147	20	2154	34	2160	28	99	2160	28
Zr-206-A-I-11	0,0018	37,7	89,4	69,6	0,78	6,99149	1,36	0,38490	0,57	0,42	0,13174	1,23	2099	12	2110	29	2121	26	99	2121	26
Zr-206-A-I-12	0,0009	55,4	163,1	144,7	0,89	3,83477	1,74	0,28115	0,89	0,51	0,09892	1,49	1597	14	1600	28	1604	24	100	1604	24
Zr-206-A-I-13	0,0008	72,5	161,0	52,8	0,33	7,38648	1,68	0,39825	0,98	0,58	0,13452	1,37	2161	21	2159	36	2158	29	100	2158	29
Zr-206-A-I-14	0,0007	98,6	313,1	192,1	0,62	4,00422	4,03	0,28706	3,94	0,98	0,10117	0,87	1627	64	1635	66	1646	14	99	1646	14
Zr-206-A-I-15	0,0009	16,6	41,3	41,1	1,00	3,85870	1,60	0,28074	0,77	0,48	0,09969	1,40	1595	12	1605	26	1618	23	99	1618	23

Zr-206-A-I-16	0,0088	83,4	490,1	483,1	0,99	3,18262	1,84	0,24081	1,47	0,80	0,09585	1,11	1391	20	1453	27	1545	17	90	1545	17
Zr-206-A-I-17	0,0036	52,8	222,4	154,4	0,70	5,92999	2,32	0,34633	0,93	0,40	0,12418	2,13	1917	18	1966	46	2017	43	95	2017	43
Zr-206-A-I-19	0,0007	19,4	50,8	35,8	0,71	3,85566	2,05	0,28323	0,96	0,47	0,09873	1,81	1608	15	1604	33	1600	29	100	1600	29
Zr-206-A-I-20	0,0005	44,0	114,5	66,6	0,59	5,62870	1,64	0,34633	0,93	0,57	0,11787	1,35	1917	18	1921	31	1924	26	100	1924	26
Zr-206-A-I-21	0,0008	23,5	74,8	31,5	0,42	3,86756	1,72	0,28241	0,76	0,44	0,09933	1,54	1603	12	1607	28	1611	25	100	1611	25
Zr-206-A-I-23	0,0023	16,5	48,5	40,8	0,85	6,42933	1,21	0,35989	0,98	0,81	0,12957	0,71	1982	20	2036	25	2092	15	95	2092	15
Zr-206-A-I-24	0,0017	14,8	40,7	35,3	0,87	3,87111	1,91	0,28326	0,80	0,42	0,09912	1,73	1608	13	1608	31	1608	28	100	1608	28
Zr-206-A-I-25	0,0008	43,5	87,2	38,2	0,44	7,71959	1,34	0,40620	0,70	0,53	0,13783	1,14	2198	15	2199	29	2200	25	100	2200	25
Zr-206-A-I-26	0,0331	59,8	235,4	113,2	0,48	5,50889	4,33	0,34412	1,59	0,37	0,11610	4,03	1906	30	1902	82	1897	76	100	1897	76
Zr-206-A-I-27	0,0014	21,9	46,0	30,4	0,66	7,67792	1,87	0,40573	0,74	0,40	0,13725	1,71	2195	16	2194	41	2193	38	100	2193	38
Zr-206-A-I-28	0,0016	18,9	58,2	44,0	0,76	3,66559	2,46	0,26727	2,02	0,82	0,09947	1,41	1527	31	1564	39	1614	23	95	1614	23
Zr-206-A-I-30	0,0003	75,0	102,7	71,6	0,70	15,96041	1,32	0,55984	0,96	0,73	0,20676	0,91	2866	28	2874	38	2880	26	100	2880	26
Zr-206-A-I-31	0,0005	22,7	50,6	22,8	0,45	7,13007	1,72	0,38882	0,98	0,57	0,13300	1,42	2117	21	2128	37	2138	30	99	2138	30
Zr-206-A-I-34	0,0004	62,2	84,3	36,0	0,43	17,02578	1,41	0,57349	0,94	0,67	0,21532	1,05	2922	28	2936	41	2946	31	99	2946	31
Zr-206-A-I-35	0,0006	30,0	60,3	63,0	1,05	6,88477	1,39	0,38509	0,55	0,40	0,12967	1,28	2100	12	2097	29	2093	27	100	2093	27
Zr-206-A-I-36	0,0003	30,4	66,0	37,9	0,58	7,47621	2,30	0,40004	1,50	0,65	0,13554	1,74	2169	33	2170	50	2171	38	100	2171	38
Zr-206-B-II-01	0,0002	21,4	59,5	42,4	0,72	3,88928	1,72	0,28384	1,03	0,60	0,09938	1,37	1611	17	1611	28	1612	22	100	1612	22
Zr-206-B-II-02	0,0011	61,7	141,1	42,9	0,31	7,53362	1,30	0,40265	0,69	0,53	0,13570	1,10	2181	15	2177	28	2173	24	100	2173	24
Zr-206-B-II-03	0,0002	64,3	147,1	132,4	0,91	8,04047	1,07	0,41643	0,83	0,78	0,14004	0,67	2244	19	2236	24	2228	15	101	2228	15
Zr-206-B-II-04	0,0001	30,8	64,1	22,5	0,35	7,65906	1,09	0,40568	0,71	0,65	0,13693	0,82	2195	16	2192	24	2189	18	100	2189	18
Zr-206-B-II-10	0,0002	70,9	157,4	84,7	0,54	6,26049	1,15	0,36738	0,79	0,69	0,12359	0,83	2017	16	2013	23	2009	17	100	2009	17
Zr-206-B-II-11	0,0013	79,0	230,9	149,3	0,65	3,87447	1,83	0,28334	1,13	0,61	0,09917	1,45	1608	18	1608	29	1609	23	100	1609	23
Zr-206-B-II-12	0,0008	57,3	111,3	83,6	0,76	7,49660	1,47	0,40158	0,97	0,66	0,13539	1,11	2176	21	2173	32	2169	24	100	2169	24
Zr-206-B-II-14	0,0007	14,5	44,0	20,0	0,46	3,90036	2,12	0,28488	0,94	0,44	0,09930	1,90	1616	15	1614	34	1611	31	100	1611	31
Zr-206-B-II-16	0,0079	73,2	213,4	63,8	0,30	6,59211	4,45	0,37008	1,19	0,27	0,12919	4,29	2030	24	2058	92	2087	90	97	2087	90
Zr-206-B-II-19	0,0011	72,4	154,1	84,0	0,55	7,63398	1,57	0,40539	0,81	0,52	0,13658	1,35	2194	18	2189	34	2184	29	100	2184	29

Zr-206-B-II-21	0,0002	52,9	116,1	57,5	0,50	6,83366	1,18	0,38236	0,60	0,50	0,12962	1,02	2087	12	2090	25	2093	21	100	2093	21
Zr-206-B-II-24	0,0009	12,7	37,2	24,6	0,67	3,70451	2,17	0,27315	0,80	0,37	0,09836	2,02	1557	12	1572	34	1593	32	98	1593	32
Zr-206-B-II-26	0,0031	74,6	190,1	47,3	0,25	7,16287	1,06	0,39012	0,59	0,56	0,13317	0,88	2123	13	2132	23	2140	19	99	2140	19
Zr-206-B-II-29	0,0011	16,6	33,3	19,8	0,60	7,78630	2,01	0,40871	1,31	0,65	0,13817	1,52	2209	29	2207	44	2204	34	100	2204	34
Zr-206-B-II-31	0,0018	54,1	180,5	265,7	1,48	7,39488	1,53	0,39545	0,69	0,45	0,13562	1,36	2148	15	2160	33	2172	30	99	2172	30
Zr-206-B-II-34	0,0005	38,0	80,4	27,6	0,35	7,27247	1,30	0,39489	0,76	0,58	0,13357	1,06	2145	16	2145	28	2145	23	100	2145	23
Zr-206-B-II-36	0,0010	62,5	137,2	73,8	0,54	7,30823	1,91	0,39657	0,82	0,43	0,13366	1,73	2153	18	2150	41	2147	37	100	2147	37
Zr-206-B-II-41	0,0026	45,4	122,0	100,2	0,83	6,50207	2,06	0,37340	0,87	0,42	0,12629	1,87	2045	18	2046	42	2047	38	100	2047	38
Zr-206-C-III-01	0,0011	13,8	33,2	47,8	1,45	3,86974	2,50	0,28235	1,05	0,42	0,09940	2,27	1603	17	1607	40	1613	37	99	1613	37
Zr-206-C-III-02	0,0034	17,5	24,4	18,5	0,77	13,81939	1,43	0,52894	0,62	0,43	0,18949	1,29	2737	17	2737	39	2738	35	100	2738	35
Zr-206-C-III-03	0,0008	29,4	66,5	35,4	0,54	7,47518	1,72	0,40055	0,96	0,56	0,13535	1,43	2172	21	2170	37	2169	31	100	2169	31
Zr-206-C-III-05	0,0017	23,2	42,0	28,5	0,68	10,90949	3,12	0,46298	2,56	0,82	0,17090	1,78	2453	63	2515	78	2566	46	96	2566	46
Zr-206-C-III-07	0,0004	46,4	92,4	60,1	0,66	7,17513	1,31	0,39163	0,91	0,69	0,13288	0,94	2130	19	2133	28	2136	20	100	2136	20
Zr-206-C-III-08	0,0003	33,7	78,7	26,9	0,34	7,19465	1,24	0,39332	0,67	0,54	0,13267	1,05	2138	14	2136	27	2134	22	100	2134	22
Zr-206-C-III-09	0,0004	82,3	177,1	85,6	0,49	7,69191	1,56	0,40617	1,11	0,72	0,13735	1,09	2197	24	2196	34	2194	24	100	2194	24
Zr-206-C-III-10	0,0009	19,7	37,7	34,0	0,91	14,28501	1,43	0,53610	1,22	0,86	0,19326	0,74	2767	34	2769	40	2770	20	100	2770	20
Zr-206-C-III-11	0,0066	69,4	185,1	62,8	0,34	6,66978	1,61	0,37330	1,05	0,65	0,12958	1,22	2045	22	2069	33	2092	25	98	2092	25
Zr-206-C-III-14	0,0007	79,8	165,2	86,2	0,53	7,52405	1,96	0,40193	1,06	0,54	0,13577	1,64	2178	23	2176	43	2174	36	100	2174	36
Zr-206-C-III-15	0,0027	27,7	79,4	37,8	0,48	7,85478	1,47	0,40937	1,16	0,79	0,13916	0,90	2212	26	2215	33	2217	20	100	2217	20
Zr-206-C-III-16	0,0006	47,7	111,2	53,7	0,49	7,33117	2,10	0,39640	1,49	0,71	0,13413	1,47	2152	32	2153	45	2153	32	100	2153	32
Zr-206-C-III-19	0,0004	33,0	53,3	37,4	0,71	13,16720	1,79	0,51807	1,12	0,62	0,18433	1,40	2691	30	2692	48	2692	38	100	2692	38
Zr-206-C-III-20	0,0002	39,9	106,9	112,7	1,06	3,90681	1,33	0,28510	0,53	0,40	0,09938	1,22	1617	9	1615	22	1613	20	100	1613	20
Zr-206-C-III-22	0,0002	53,9	132,1	65,5	0,50	6,67895	1,20	0,36136	0,25	0,21	0,13405	1,17	1989	5	2070	25	2152	25	92	2152	25
Zr-206-C-III-23	0,0001	92,9	214,1	117,6	0,55	6,40977	1,54	0,37086	1,02	0,66	0,12535	1,15	2033	21	2034	31	2034	23	100	2034	23
Zr-206-C-III-24	0,0014	84,2	184,7	94,4	0,52	7,56226	2,31	0,40171	1,82	0,79	0,13653	1,43	2177	40	2180	50	2184	31	100	2184	31
Zr-206-C-III-26	0,0002	83,0	194,9	112,2	0,58	6,96610	1,86	0,38587	1,44	0,77	0,13093	1,17	2104	30	2107	39	2111	25	100	2111	25
Zr-206-C-III-27	0,0002	65,2	146,2	83,4	0,57	7,94154	2,67	0,41406	2,54	0,95	0,13910	0,83	2233	57	2224	59	2216	18	101	2216	18

Zr-206-C-III-28	0,0005	73,5	168,3	79,7	0,48	7,62666	1,54	0,40338	1,03	0,67	0,13712	1,14	2185	23	2188	34	2191	25	100	2191	25
Zr-206-C-III-29	0,0003	55,3	118,7	81,0	0,69	7,70951	1,73	0,40586	0,74	0,42	0,13777	1,57	2196	16	2198	38	2199	35	100	2199	35
Zr-206-C-III-30	0,0111	98,2	312,4	55,5	0,18	5,56088	1,35	0,31420	1,05	0,78	0,12836	0,85	1761	19	1910	26	2076	18	85	2076	18
Zr-206-C-III-32	0,0015	40,4	100,5	77,6	0,78	7,39449	3,11	0,37281	1,97	0,63	0,14385	2,41	2043	40	2160	67	2274	55	90	2274	55
Zr-206-C-III-33	0,0005	70,4	168,4	60,7	0,36	6,52453	1,42	0,37334	0,93	0,66	0,12675	1,07	2045	19	2049	29	2053	22	100	2053	22
Zr-206-C-III-38	0,0011	29,1	55,6	16,4	0,30	12,21319	1,90	0,49587	1,34	0,71	0,17863	1,34	2596	35	2621	50	2640	35	98	2640	35
Zr-206-C-III-39	0,0005	54,1	98,4	70,0	0,72	7,67414	2,00	0,40577	0,99	0,50	0,13717	1,73	2196	22	2194	44	2192	38	100	2192	38

Resumo dos dados de U-Pb da amostra PE-SC-45 (Formação Galho do Miguel).

						Isotope ratios[b]							**Ages (Ma)**								
Spot number	f 206	Pb ppm	U ppm	Th ppm	Th/U[a]	^{207}Pb/^{235}U	1 s [%]	^{206}Pb/^{238}U	1 s [%]	Rho[c]	^{207}Pb/^{206}Pb[d]	1 s [%]	^{206}Pb/^{238}U	1 s abs	^{207}Pb/^{235}U	1 s abs	^{207}Pb/^{206}Pb	1 s abs	% Conc[e]	Best estimated age (Ma)	
Zr-205-A-I-01	0,0003	49	117	38	0,32	6,1999	1,43	0,35553	0,70	0,49	0,1265	1,24	1961	14	2004	29	2050	25	96	2050	25
Zr-205-A-I-02	0,0005	24	47	19	0,41	7,8398	1,89	0,40619	0,68	0,36	0,1400	1,77	2197	15	2213	42	2227	39	99	2227	39
Zr-205-A-I-03	0,0006	65	135	81	0,61	0,2768	30,18	0,01596	30,15	1,00	0,1258	1,20	102	31	248	75	2040	25	5		
Zr-205-A-I-04	0,0005	67	249	100	0,41	3,4899	2,20	0,20390	1,88	0,86	0,1241	1,13	1196	23	1525	34	2016	23	59		
Zr-205-A-I-05	0,0002	24	42	17	0,41	13,1016	2,16	0,50150	0,91	0,42	0,1895	1,96	2620	24	2687	58	2738	54	96	2738	54
Zr-205-A-I-06	0,0001	53	112	38	0,34	7,4577	1,67	0,40059	0,71	0,43	0,1350	1,51	2172	15	2168	36	2164	33	100	2164	33
Zr-205-A-I-07	0,0000	51	122	68	0,56	5,7484	1,49	0,32332	0,98	0,65	0,1289	1,13	1806	18	1939	29	2084	23	87		
Zr-205-A-I-08	0,0000	102	170	74	0,44	13,1093	1,41	0,52025	1,24	0,88	0,1828	0,67	2700	33	2688	38	2678	18	101	2678	18
Zr-205-A-I-09	0,0000	55	84	36	0,43	12,5620	1,71	0,49662	1,29	0,75	0,1835	1,13	2599	34	2647	45	2684	30	97	2684	30
Zr-205-A-I-10	0,0001	60	94	44	0,48	12,9986	1,20	0,51454	0,57	0,48	0,1832	1,05	2676	15	2680	32	2682	28	100	2682	28
Zr-205-A-I-11	0,0052	67	76	53	0,70	19,8692	2,40	0,61074	1,14	0,47	0,2360	2,11	3073	35	3085	74	3093	65	99	3093	65
Zr-205-A-I-12	0,0005	80	156	51	0,33	11,3617	1,94	0,46426	0,62	0,32	0,1775	1,84	2458	15	2553	49	2630	48	93	2630	48
Zr-205-A-I-13	0,0008	80	213	100	0,47	5,8613	1,92	0,35058	1,03	0,54	0,1213	1,61	1937	20	1956	37	1975	32	98	1975	32

Zr-205-A-I-14	0,0016	80	104	104	1,00	13,5532	1,63	0,52758	0,75	0,46	0,1863	1,44	2731	21	2719	44	2710	39	101	2710	39
Zr-205-A-I-15	0,0005	36	80	53	0,67	6,2590	1,48	0,36907	0,68	0,46	0,1230	1,31	2025	14	2013	30	2000	26	101	2000	26
Zr-205-A-I-16	0,0002	150	259	105	0,41	12,7139	1,96	0,50278	1,62	0,82	0,1834	1,11	2626	42	2659	52	2684	30	98	2684	30
Zr-205-A-I-17	0,0021	57	161	55	0,34	6,6515	1,87	0,37221	1,17	0,62	0,1296	1,46	2040	24	2066	39	2093	31	97	2093	31
Zr-205-A-I-18	0,0192	167	924	408	0,45	1,6533	2,08	0,13781	1,32	0,63	0,0870	1,61	832	11	991	21	1361	22	61		
Zr-205-A-I-19	0,0015	66	184	105	0,57	6,3064	1,51	0,36440	1,26	0,84	0,1255	0,82	2003	25	2019	30	2036	17	98	2036	17
Zr-205-A-I-20	0,0010	78	181	76	0,43	8,4237	4,08	0,34138	3,89	0,95	0,1790	1,25	1893	74	2278	93	2643	33	72		
Zr-205-A-I-21	0,0002	103	171	82	0,48	12,6089	1,30	0,50719	0,85	0,65	0,1803	0,99	2645	22	2651	35	2656	26	100	2656	26
Zr-205-A-I-22	0,0006	72	166	104	0,63	6,6177	2,19	0,37262	1,24	0,57	0,1288	1,81	2042	25	2062	45	2082	38	98	2082	38
Zr-205-A-I-23	0,0146	39	93	103	1,12	4,0091	2,94	0,28254	1,45	0,49	0,1029	2,56	1604	23	1636	48	1677	43	96	1677	43
Zr-205-A-I-24	0,0039	91	394	166	0,43	6,1576	1,72	0,35097	1,43	0,83	0,1272	0,96	1939	28	1998	34	2060	20	94	2060	20
Zr-205-A-I-25	0,0009	103	279	98	0,36	5,7553	1,58	0,33242	0,89	0,56	0,1256	1,30	1850	17	1940	31	2037	27	91	2037	27
Zr-205-A-I-26	0,0013	75	231	127	0,55	5,8226	2,75	0,35143	1,12	0,40	0,1202	2,52	1941	22	1950	54	1959	49	99	1959	49
Zr-205-A-I-28	0,0011	19	36	16	0,45	7,8882	2,45	0,41398	1,05	0,43	0,1382	2,22	2233	23	2218	54	2205	49	101	2205	49
Zr-205-A-I-30	0,0005	46	91	60	0,66	6,9800	1,68	0,38644	0,51	0,30	0,1310	1,60	2106	11	2109	35	2111	34	100	2111	34
Zr-205-A-I-31	0,0005	31	59	29	0,50	7,9896	1,86	0,41596	0,57	0,31	0,1393	1,77	2242	13	2230	42	2219	39	101	2219	39
Zr-205-A-I-32	0,0004	45	101	42	0,42	6,9954	1,91	0,38913	1,38	0,72	0,1304	1,32	2119	29	2111	40	2103	28	101	2103	28
Zr-205-A-I-34	0,0003	68	108	44	0,41	13,2587	1,03	0,51769	0,64	0,63	0,1857	0,80	2689	17	2698	28	2705	22	99	2705	22
Zr-205-A-I-36	0,0004	53	123	77	0,63	6,1032	1,50	0,36245	0,75	0,50	0,1221	1,30	1994	15	1991	30	1988	26	100	1988	26
Zr-205-A-I-37	0,0017	33	86	91	1,07	4,0551	2,57	0,28344	1,16	0,45	0,1038	2,29	1609	19	1645	42	1692	39	95	1692	39
Zr-205-A-I-38	0,0002	83	130	60	0,47	13,2510	1,02	0,52172	0,50	0,50	0,1842	0,88	2706	14	2698	27	2691	24	101	2691	24
Zr-205-A-I-39	0,0009	31	44	54	1,24	13,0663	1,63	0,50777	0,80	0,49	0,1866	1,42	2647	21	2684	44	2713	39	98	2713	39
Zr-205-A-I-40	0,0006	27	40	26	0,67	12,6804	1,60	0,48761	0,87	0,54	0,1886	1,34	2560	22	2656	42	2730	37	94	2730	37
Zr-205-B-II-01	0,0003	79	119	60	0,51	13,2195	0,88	0,51809	0,59	0,66	0,1851	0,66	2691	16	2695	24	2699	18	100	2699	18
Zr-205-B-II-03	0,0027	17	39	26	0,67	6,8451	2,25	0,37739	0,95	0,42	0,1315	2,03	2064	20	2092	47	2119	43	97	2119	43
Zr-205-B-II-05	0,0002	64	113	46	0,41	12,1449	1,26	0,48033	0,87	0,68	0,1834	0,92	2529	22	2616	33	2684	25	94	2684	25
Zr-205-B-II-06	0,0017	4	5	20	3,76	7,2804	6,09	0,38866	1,73	0,29	0,1359	5,83	2117	37	2146	131	2175	127	97	2175	127

Zr-205-B-II-07	0,0005	33	63	25	0,39	8,6789	1,17	0,42734	0,66	0,56	0,1473	0,97	2294	15	2305	27	2315	22	99	2315	22
Zr-205-B-II-08	0,0002	121	163	52	0,32	19,7223	0,85	0,60730	0,67	0,79	0,2355	0,52	3059	20	3078	26	3090	16	99	3090	16
Zr-205-B-II-09	0,0009	22	50	34	0,68	5,9758	1,75	0,35377	0,62	0,35	0,1225	1,63	1953	12	1972	34	1993	33	98	1993	33
Zr-205-B-II-10	0,0003	47	114	27	0,24	7,2504	1,40	0,39583	0,59	0,42	0,1328	1,27	2150	13	2143	30	2136	27	101	2136	27
Zr-205-B-II-11	0,0004	53	71	20	0,28	23,6369	1,33	0,63846	0,57	0,43	0,2685	1,20	3183	18	3254	43	3297	40	97	3297	40
Zr-205-B-II-12	0,0008	27	53	49	0,93	6,6230	1,40	0,37790	0,48	0,34	0,1271	1,32	2066	10	2062	29	2058	27	100	2058	27
Zr-205-B-II-13	0,0002	82	177	107	0,61	6,7712	1,17	0,38314	0,58	0,49	0,1282	1,02	2091	12	2082	24	2073	21	101	2073	21
Zr-205-B-II-14	0,0049	79	273	113	0,42	12,3608	0,91	0,47682	0,66	0,73	0,1880	0,63	2513	17	2632	24	2725	17	92	2725	17
Zr-205-B-II-16	0,0003	104	133	103	0,78	18,4994	0,74	0,59494	0,34	0,47	0,2255	0,65	3009	10	3016	22	3021	20	100	3021	20
Zr-205-B-II-17	0,0020	50	116	56	0,49	6,6359	1,64	0,36402	1,36	0,83	0,1322	0,91	2001	27	2064	34	2128	19	94	2128	19
Zr-205-B-II-18	0,0014	37	47	39	0,83	12,8164	1,54	0,49742	0,80	0,52	0,1869	1,32	2603	21	2666	41	2715	36	96	2715	36
Zr-205-B-II-20	0,0012	19	37	22	0,58	7,7880	1,55	0,40207	0,64	0,41	0,1405	1,41	2179	14	2207	34	2233	31	98	2233	31
Zr-205-B-II-21	0,0018	37	95	44	0,46	6,8671	1,62	0,37398	0,65	0,40	0,1332	1,49	2048	13	2094	34	2140	32	96	2140	32
Zr-205-B-II-22	0,0007	43	55	26	0,47	20,5438	1,18	0,61926	0,68	0,58	0,2406	0,96	3107	21	3117	37	3124	30	99	3124	30
Zr-205-B-II-25	0,0031	58	98	35	0,36	14,6289	1,81	0,54017	1,69	0,94	0,1964	0,64	2784	47	2791	50	2797	18	100	2797	18
Zr-205-B-II-26	0,0016	58	278	146	0,53	4,9686	1,53	0,31098	0,82	0,53	0,1159	1,29	1746	14	1814	28	1894	24	92	1894	24
Zr-205-B-II-27	0,0002	90	130	25	0,19	23,2666	0,90	0,64966	0,74	0,82	0,2597	0,51	3227	24	3238	29	3245	17	99	3245	17
Zr-205-B-II-29	0,0008	77	139	56	0,40	11,9916	2,20	0,48575	0,89	0,40	0,1790	2,01	2552	23	2604	57	2644	53	97	2644	53
Zr-205-B-II-30	0,0005	95	156	69	0,45	12,8660	1,29	0,50529	0,92	0,71	0,1847	0,91	2636	24	2670	35	2695	24	98	2695	24
Zr-205-B-II-31	0,0101	64	100	43	0,43	13,1949	1,50	0,51978	0,92	0,61	0,1841	1,18	2698	25	2694	40	2690	32	100	2690	32
Zr-205-B-II-33	0,0009	96	270	106	0,40	5,8371	1,58	0,33603	0,45	0,28	0,1260	1,51	1868	8	1952	31	2043	31	91	2043	31
Zr-205-B-II-34	0,0005	77	167	130	0,78	6,7257	1,30	0,37700	0,65	0,50	0,1294	1,12	2062	13	2076	27	2090	24	99	2090	24
Zr-205-B-II-36	0,0004	72	151	76	0,51	7,3128	1,25	0,39500	0,67	0,53	0,1343	1,06	2146	14	2150	27	2155	23	100	2155	23
Zr-205-B-II-37	0,0008	83	207	167	0,81	6,2673	1,38	0,35841	1,06	0,76	0,1268	0,89	1975	21	2014	28	2054	18	96	2054	18
Zr-205-B-II-38	0,0013	34	75	29	0,40	7,2630	1,64	0,39216	1,00	0,61	0,1343	1,30	2133	21	2144	35	2155	28	99	2155	28
Zr-205-C-III-01	0,0023	16	22	43	1,93	9,4040	1,85	0,40951	0,78	0,42	0,1666	1,68	2213	17	2378	44	2523	42	88		
Zr-205-C-III-02	0,0011	60	151	109	0,73	6,0291	1,24	0,34062	0,94	0,76	0,12838	0,81	1890	18	1980	25	2076	17	91	2076	17
Zr-205-C-III-03	0,0024	90	105	54	0,51	25,2483	1,17	0,67651	0,47	0,40	0,2707	1,07	3331	16	3318	39	3310	35	101	3310	35

Zr-205-C-III-04	0,0009	45	108	75	0,70	5,3142	1,54	0,30786	1,12	0,72	0,1252	1,07	1730	19	1871	29	2032	22	85		
Zr-205-C-III-05	0,0005	60	93	48	0,51	13,4069	0,99	0,52072	0,58	0,58	0,1867	0,81	2702	16	2709	27	2714	22	100	2714	22
Zr-205-C-III-06	0,0004	105	203	301	1,49	6,5918	1,67	0,37796	0,97	0,58	0,1265	1,36	2067	20	2058	34	2050	28	101	2050	28
Zr-205-C-III-07	0,0007	45	92	22	0,24	10,3939	1,47	0,46504	0,56	0,38	0,1621	1,36	2462	14	2471	36	2478	34	99	2478	34
Zr-205-C-III-08	0,0018	38	119	77	0,65	6,5469	1,08	0,36285	0,21	0,19	0,1309	1,06	1996	4	2052	22	2110	22	95	2110	22
Zr-205-C-III-09	0,0011	35	76	46	0,61	7,1747	1,96	0,38965	1,12	0,57	0,1335	1,61	2121	24	2133	42	2145	35	99	2145	35
Zr-205-C-III-11	0,0044	151	383	319	0,84	17,1187	4,99	0,56462	4,68	0,94	0,2199	1,74	2886	135	2942	147	2980	52	97	2980	52
Zr-205-C-III-12	0,0003	52	111	45	0,41	7,4136	1,25	0,39417	0,57	0,46	0,1364	1,11	2142	12	2163	27	2182	24	98	2182	24
Zr-205-C-III-13	0,0004	59	89	49	0,55	15,6571	1,51	0,55093	1,02	0,68	0,2061	1,11	2829	29	2856	43	2875	32	98	2875	32
Zr-205-C-III-14	0,0030	54	153	78	0,52	5,1842	1,68	0,29387	1,20	0,71	0,1279	1,18	1661	20	1850	31	2070	24	80		
Zr-205-C-III-15	0,0005	37	83	77	0,94	5,9155	1,83	0,35092	1,03	0,56	0,1223	1,52	1939	20	1964	36	1989	30	97	1989	30
Zr-205-C-III-16	0,0002	65	115	46	0,41	11,8384	1,03	0,46793	0,77	0,75	0,1835	0,68	2474	19	2592	27	2685	18	92	2685	18
Zr-205-C-III-17	0,0008	37	99	42	0,42	6,9139	1,25	0,37072	0,60	0,48	0,1353	1,10	2033	12	2100	26	2167	24	94	2167	24
Zr-205-C-III-19	0,0008	49	86	34	0,39	12,9129	1,53	0,50044	0,96	0,63	0,1871	1,19	2616	25	2673	41	2717	32	96	2717	32
Zr-205-C-III-21	0,0036	117	410	239	0,59	6,3948	1,18	0,36965	0,85	0,72	0,1255	0,82	2028	17	2032	24	2035	17	100	2035	17
Zr-205-C-III-22	0,0022	15	36	17	0,47	7,8768	2,58	0,41055	1,61	0,62	0,1391	2,02	2217	36	2217	57	2217	45	100	2217	45
Zr-205-C-III-23	0,0008	64	120	144	1,20	7,8055	2,33	0,40523	0,91	0,39	0,1397	2,15	2193	20	2209	52	2224	48	99	2224	48
Zr-205-C-III-25	0,0054	53	251	102	0,41	4,1695	2,36	0,29101	1,34	0,57	0,1039	1,94	1647	22	1668	39	1695	33	97	1695	33
Zr-205-C-III-27	0,0011	51	103	43	0,42	11,5560	2,25	0,47648	1,36	0,60	0,1759	1,79	2512	34	2569	58	2615	47	96	2615	47
Zr-205-C-III-28	0,0022	73	151	75	0,50	14,2098	1,39	0,52815	1,28	0,92	0,1951	0,55	2734	35	2764	38	2786	15	98	2786	15
Zr-205-C-III-29	0,0050	94	235	119	0,51	12,4872	0,64	0,47944	0,35	0,54	0,1889	0,54	2525	9	2642	17	2733	15	92	2733	15
Zr-205-C-III-30	0,0006	51	101	121	1,21	6,6368	1,86	0,37427	0,87	0,47	0,1286	1,65	2049	18	2064	38	2079	34	99	2079	34

Resumo dos dados de U-Pb da amostra PE-SC-48 (Formação Galho do Miguel).

Spot number	f 206	Pb ppm	U ppm	Th ppm	Th/U[a]	Isotope ratios[b] $^{207}Pb/^{235}U$	1 s [%]	$^{206}Pb/^{238}U$	1 s [%]	Rho[c]	$^{207}Pb/^{206}Pb$[d]	1 s [%]	Ages (Ma) $^{206}Pb/^{238}U$	1 s abs	$^{207}Pb/^{235}U$	1 s abs	$^{207}Pb/^{206}Pb$	1 s abs	% Conc[e]	Best estimated age (Ma)	
003 ZR210_D_IV_01	0,0006	23,8	56,8	44,1	0,78	7,76898	3,34	0,41042	1,77	0,53	0,13729	2,83	2217	39	2205	74	2193	62	101	2193	62
004 ZR210_D_IV_02	0,0015	45,2	103,8	84,5	0,82	6,98576	4,25	0,40338	2,49	0,59	0,12560	3,45	2185	54	2110	90	2037	70	107	2037	70
005 ZR210_D_IV_03	0,0006	54,3	133,7	71,9	0,54	6,18872	6,02	0,35962	5,25	0,87	0,12481	2,95	1980	104	2003	121	2026	60	98	2026	60
006 ZR210_D_IV_04	0,0010	34,5	77,3	50,8	0,66	6,88483	4,77	0,38168	3,18	0,67	0,13082	3,55	2084	66	2097	100	2109	75	99	2109	75
007 ZR210_D_IV_05	0,0013	48,5	122,7	55,6	0,46	7,09737	3,48	0,39541	1,57	0,45	0,13018	3,11	2148	34	2124	74	2100	65	102	2100	65
008 ZR210_D_IV_07	0,0015	35,0	80,8	57,4	0,72	7,69193	4,27	0,41342	1,84	0,43	0,13494	3,86	2231	41	2196	94	2163	83	103	2163	83
009 ZR210_D_IV_08	0,0025	112,7	288,8	95,1	0,33	7,46002	3,45	0,41684	2,61	0,75	0,12980	2,26	2246	59	2168	75	2095	47	107	2095	47
010 ZR210_D_IV_10	0,0008	28,6	67,1	29,5	0,44	7,73462	3,54	0,40973	1,66	0,47	0,13691	3,12	2214	37	2201	78	2188	68	101	2188	68
011 ZR210_D_IV_11	0,0006	34,9	85,0	37,8	0,45	6,54682	3,72	0,37377	2,16	0,58	0,12704	3,03	2047	44	2052	76	2057	62	100	2057	62
012 ZR210_D_IV_12	0,0002	53,8	121,8	90,3	0,75	7,56541	3,21	0,40929	2,16	0,67	0,13406	2,37	2212	48	2181	70	2152	51	103	2152	51
015 ZR210_D_IV_13	0,0007	41,3	104,4	53,4	0,52	7,48514	2,76	0,40262	1,79	0,65	0,13483	2,09	2181	39	2171	60	2162	45	101	2162	45
016 ZR210_D_IV_14	0,0007	28,3	73,4	51,3	0,70	7,41740	3,34	0,39915	1,33	0,40	0,13478	3,06	2165	29	2163	72	2161	66	100	2161	66
017 ZR210_D_IV_15	0,0019	19,4	47,9	48,3	1,02	7,26607	4,92	0,39156	2,14	0,44	0,13459	4,43	2130	46	2145	106	2159	96	99	2159	96
018 ZR210_D_IV_16	0,0011	42,2	101,4	42,6	0,42	7,24224	3,46	0,39671	1,48	0,43	0,13240	3,13	2154	32	2142	74	2130	67	101	2130	67
019 ZR210_D_IV_17	0,0008	39,2	102,6	71,2	0,70	6,71289	3,20	0,38047	1,51	0,47	0,12796	2,82	2078	31	2074	66	2070	58	100	2070	58
020 ZR210_D_IV_19	0,0009	37,2	97,0	46,0	0,48	7,45114	4,48	0,40288	3,39	0,76	0,13414	2,92	2182	74	2167	97	2153	63	101	2153	63
021 ZR210_D_IV_22	0,0021	20,9	57,7	28,5	0,50	6,81793	6,42	0,38266	1,98	0,31	0,12922	6,11	2089	41	2088	134	2087	128	100	2087	128
022 ZR210_D_IV_24	0,0029	53,8	95,4	76,5	0,81	23,48970	1,80	0,55266	1,13	0,63	0,30826	1,40	2836	32	3247	58	3512	49	81		
023 ZR210_D_IV_25	0,0038	30,6	52,6	5,7	0,11	17,49589	4,37	0,58465	1,65	0,38	0,21704	4,05	2968	49	2962	129	2959	120	100	2959	120
024 ZR210_D_IV_26	0,0053	46,9	222,0	215,2	0,98	3,80754	3,04	0,27284	1,45	0,48	0,10121	2,68	1555	22	1594	48	1646	44	94	1646	44
027 ZR210_E_V_01	0,0014	78,8	203,1	87,8	0,44	7,82347	2,08	0,40153	1,11	0,53	0,14131	1,76	2176	24	2211	46	2243	39	97	2243	39
028 ZR210_E_V_02	0,0012	68,4	163,2	162,4	1,00	9,44190	6,99	0,44855	6,40	0,92	0,15267	2,81	2389	153	2382	166	2376	67	101	2376	67

029 ZR210_E_V_03	0,0006	78,1	192,6	142,4	0,74	7,21756	1,76	0,39504	0,88	0,50	0,13251	1,52	2146	19	2139	38	2131	33	101	2131	33
030 ZR210_E_V_04	0,0008	84,8	226,9	105,3	0,47	6,56037	4,16	0,37918	2,63	0,63	0,12548	3,22	2072	54	2054	85	2036	66	102	2036	66
031 ZR210_E_V_05	0,0003	37,4	89,5	29,8	0,34	6,83897	2,52	0,38328	1,62	0,64	0,12941	1,93	2092	34	2091	53	2090	40	100	2090	40
032 ZR210_E_V_07	0,0002	117,3	298,6	96,0	0,32	6,60822	1,95	0,38708	0,89	0,45	0,12382	1,74	2109	19	2060	40	2012	35	105	2012	35
033 ZR210_E_V_10	0,0001	56,0	145,1	43,7	0,30	6,81627	1,92	0,37685	1,15	0,60	0,13118	1,53	2062	24	2088	40	2114	32	98	2114	32
034 ZR210_E_V_11	0,0007	36,9	99,5	41,1	0,42	6,96161	3,71	0,38549	1,53	0,41	0,13098	3,38	2102	32	2107	78	2111	71	100	2111	71
035 ZR210_E_V_12	0,0007	41,0	122,8	115,0	0,94	5,74104	3,80	0,35071	1,12	0,30	0,11873	3,63	1938	22	1938	74	1937	70	100	1937	70
036 ZR210_E_V_13	0,0004	32,6	84,2	36,5	0,44	7,28515	2,98	0,39489	1,52	0,51	0,13380	2,56	2145	33	2147	64	2148	55	100	2148	55
039 ZR210_E_V_14	0,0008	51,8	89,7	51,3	0,58	18,74298	4,24	0,59770	4,01	0,94	0,22743	1,39	3021	121	3029	128	3034	42	100	3034	42
040 ZR210_E_V_16	0,0005	33,8	103,4	60,6	0,59	5,93020	2,93	0,35587	1,07	0,36	0,12086	2,73	1963	21	1966	58	1969	54	100	1969	54
041 ZR210_E_V_17	0,0011	12,5	33,9	17,1	0,51	7,17778	6,41	0,39170	3,52	0,55	0,13290	5,36	2131	75	2134	137	2137	114	100	2137	114
042 ZR210_E_V_18	0,0019	16,2	44,5	16,3	0,37	6,82409	7,15	0,38081	2,76	0,39	0,12997	6,60	2080	57	2089	149	2098	138	99	2098	138
043 ZR210_E_V_19	0,0008	17,8	47,9	36,5	0,77	7,84797	4,99	0,41088	3,52	0,71	0,13853	3,54	2219	78	2214	110	2209	78	100	2209	78
044 ZR210_E_V_21	0,0015	20,9	58,7	64,7	1,11	6,34175	7,52	0,36614	4,96	0,66	0,12562	5,65	2011	100	2024	152	2038	115	99	2038	115
045 ZR210_E_V_22	0,0014	23,8	64,7	36,7	0,57	6,39906	4,30	0,37030	1,02	0,24	0,12533	4,18	2031	21	2032	87	2033	85	100	2033	85
046 ZR210_E_V_23	0,0013	13,4	37,6	24,6	0,66	6,90384	6,49	0,38519	3,69	0,57	0,12999	5,35	2101	77	2099	136	2098	112	100	2098	112
047 ZR210_E_V_25	0,0007	35,6	94,6	37,5	0,40	6,81487	3,33	0,38013	1,40	0,42	0,13003	3,02	2077	29	2088	70	2098	63	99	2098	63
048 ZR210_E_V_26	0,0010	32,6	88,7	36,7	0,42	6,28993	3,85	0,36645	1,33	0,34	0,12449	3,61	2013	27	2017	78	2022	73	100	2022	73
051 ZR210_F_VI_01	0,0002	127,9	245,5	131,0	0,54	8,78561	1,76	0,43038	1,26	0,71	0,14805	1,24	2307	29	2316	41	2324	29	99	2324	29
052 ZR210_F_VI_02	0,0006	54,2	118,2	43,5	0,37	7,26591	2,35	0,39552	1,31	0,56	0,13324	1,95	2148	28	2145	50	2141	42	100	2141	42
053 ZR210_F_VI_03	0,0005	107,0	175,1	130,6	0,75	12,11900	2,09	0,50004	1,36	0,65	0,17578	1,58	2614	36	2614	55	2613	41	100	2613	41
054 ZR210_F_VI_04	0,0005	107,5	207,0	244,5	1,19	8,52609	2,23	0,42813	1,33	0,60	0,14444	1,79	2297	31	2289	51	2281	41	101	2281	41
055 ZR210_F_VI_05	0,0005	120,8	160,3	121,5	0,76	18,26361	2,39	0,60421	2,01	0,84	0,21923	1,30	3047	61	3004	72	2975	39	102	2975	39
056 ZR210_F_VI_06	0,0009	64,5	137,5	118,5	0,87	6,40554	2,71	0,37260	1,41	0,52	0,12468	2,32	2042	29	2033	55	2024	47	101	2024	47
057 ZR210_F_VI_07	0,0003	118,6	247,8	132,6	0,54	6,88103	1,57	0,39222	0,96	0,61	0,12724	1,24	2133	21	2096	33	2060	26	104	2060	26
058 ZR210_F_VI_08	0,0016	53,2	131,6	174,0	1,33	5,34337	2,41	0,34239	0,87	0,36	0,11318	2,24	1898	17	1876	45	1851	42	103	1851	42
059 ZR210_F_VI_09	0,0011	79,0	181,1	98,3	0,55	7,44737	1,70	0,39829	0,99	0,59	0,13561	1,37	2161	21	2167	37	2172	30	100	2172	30
060 ZR210_F_VI_10	0,0003	46,9	112,8	62,1	0,55	6,41160	2,16	0,37071	0,93	0,43	0,12544	1,95	2033	19	2034	44	2035	40	100	2035	40

063 ZR210_F_VI_11	0,0006	43,3	110,1	197,3	1,81	6,96178	2,31	0,38373	0,93	0,40	0,13158	2,11	2094	20	2107	49	2119	45	99	2119	45
064 ZR210_F_VI_13	0,0011	31,1	76,5	32,5	0,43	7,09079	3,91	0,39217	1,07	0,27	0,13114	3,76	2133	23	2123	83	2113	80	101	2113	80
065 ZR210_F_VI_14	0,0020	16,3	43,6	17,1	0,39	6,48309	6,71	0,37023	1,70	0,25	0,12700	6,49	2030	35	2044	137	2057	133	99	2057	133
066 ZR210_F_VI_15	0,0032	25,3	48,0	19,7	0,41	12,28242	6,87	0,50273	1,78	0,26	0,17719	6,63	2626	47	2626	180	2627	174	100	2627	174
067 ZR210_F_VI_16	0,0016	18,7	44,8	40,0	0,90	6,28538	6,00	0,36740	1,77	0,30	0,12408	5,73	2017	36	2016	121	2016	116	100	2016	116
068 ZR210_F_VI_17	0,0029	11,0	27,4	17,2	0,63	7,09580	8,96	0,39006	2,89	0,32	0,13194	8,48	2123	61	2124	190	2124	180	100	2124	180
069 ZR210_F_VI_20	0,0016	22,9	57,1	43,9	0,78	7,95521	5,16	0,41127	1,61	0,31	0,14029	4,90	2221	36	2226	115	2231	109	100	2231	109
070 ZR210_F_VI_21	0,0014	36,6	68,7	25,4	0,37	12,67693	2,62	0,51264	1,35	0,51	0,17935	2,25	2668	36	2656	70	2647	60	101	2647	60
071 ZR210_F_VI_23	0,0020	25,0	67,0	29,9	0,45	6,32987	5,30	0,36897	1,11	0,21	0,12442	5,18	2025	22	2023	107	2021	105	100	2021	105
072 ZR210_F_VI_26	0,0008	86,7	132,7	152,6	1,16	18,70030	1,40	0,60642	1,24	0,89	0,22365	0,65	3056	38	3026	42	3007	20	102	3007	20

Resumo dos dados de U-Pb da amostra PE-FM-71 (Formação Galho do Miguel).

Grain.Spot	% $^{206}Pb_c$	ppm U	ppm Th	$^{232}Th/^{238}U$	ppm $^{206}Pb^*$	(1) $^{206}Pb/^{238}U$ Age		(1) $^{207}Pb/^{206}Pb$ Age		% Dis-cor-dant	(1) $^{207}Pb^*/^{206}Pb^*$	±%	(1) $^{207}Pb^*/^{235}U$	±%	(1) $^{206}Pb^*/^{238}U$	±%	err corr	Best estimated age (Ma)	
D-1.1	3,19	487	124	0,26	120	1582	±19	1713	± 78	8	0.1049	4.2	4.02	4.4	0.2782	1.4	,311	1582	19
D-2.1	0,08	93	74	0,83	30.3	2075	±29	2156	± 18	4	0.1344	1	7.03	1.9	0.3796	1.6	,846	2075	29
D-4.1	0,33	154	61	0,41	42.3	1788	±22	2102	± 19	15	0.1303	1.1	5.74	1.8	0.3197	1.4	,800		
D-5.1	0,02	210	108	0,53	71.6	2154	±24	2151	± 10	0	0.13398	0.6	7.33	1.4	0.3968	1.3	,908	2154	24
D-6.1	0,16	199	163	0,85	67.6	2145	±25	2208	± 14	3	0.1385	0.8	7.54	1.6	0.3948	1.4	,861	2145	25
D-7.1	0,49	245	195	0,82	74.3	1944	±21	2073	± 16	6	0.1282	0.93	6.222	1.6	0.352	1.3	,806	1944	21
D-8.1	0,00	215	129	0,62	74.9	2198	±24	2208.3	± 7.9	#VALOR!	0.13848	0.46	7.76	1.3	0.4063	1.3	,940	2198	24
D-10.1	0,00	180	90	0,52	62.7	2198	±23	2204	± 8.7	0	0.13814	0.5	7.74	1.3	0.4063	1.2	,927	2198	23
D-11.1	0,29	102	79	0,80	32.8	2048	±23	2164	± 16	5	0.135	0.92	6.96	1.6	0.374	1.3	,823	2048	23

D-12.1	15,83	528	745	1,46	155	1634	±38	2266	±390	28	0.143	23	5.7	23	0.2885	2.6	,114		
D-13.1	27,03	232	303	1,35	71.8	1503	±39	2080	±330	28	0.129	19	4.66	19	0.2626	2.9	,153		
D-14.1	1,62	183	204	1,15	81.5	2653	±29	2720	± 30	2	0.1874	1.8	13.16	2.3	0.5092	1.3	,589	2653	29
D-15.1	0,91	351	171	0,50	118	2110	±22	2646	± 10	20	0.1792	0.63	9.57	1.3	0.3872	1.2	,885		
E-1.1	0,02	192	178	0,96	62.6	2074	±24	2080	± 9.2	0	0.12868	0.52	6.732	1.4	0.3794	1.3	,932	2074	24
E-2.1	2,75	572	188	0,34	148	1659	±18	2682	± 23	38	0.1832	1.4	7.41	1.9	0.2935	1.3	,676		
E-3.1	0,16	332	265	0,82	74.7	1497	±17	1601	± 13	6	0.09879	0.68	3.562	1.5	0.2615	1.3	,884	1497	17
E-4.1	0,28	221	172	0,80	56.1	1662	±19	2060	± 14	19	0.12722	0.78	5.16	1.5	0.2942	1.3	,862		
E-5.1	--	147	133	0,93	49	2117	±25	2169	± 10	2	0.13538	0.57	7.25	1.5	0.3887	1.4	,924	2117	25
E-6.1	0,03	141	59	0,43	48	2154	±25	2196	± 11	2	0.13751	0.63	7.52	1.5	0.3967	1.4	,912	2154	25
E-7.1	8,52	949	269	0,29	161	1068	±14	1668	±110	36	0.1024	6	2.54	6.2	0.1802	1.4	,227		
E-8.1	3,76	532	505	0,98	133	1597	±19	2629	± 47	39	0.1774	2.8	6.88	3.1	0.2811	1.3	,428		
E-9.1	--	182	14	0,08	57	2008	±23	2022	± 10	1	0.12455	0.57	6.277	1.5	0.3655	1.4	,922	2008	23
E-10.1	0,06	119	62	0,54	38.6	2064	±25	2120	± 13	3	0.13161	0.74	6.85	1.6	0.3774	1.4	,889	2064	25
E-12.1	0,05	179	122	0,71	57.9	2055	±24	2083	± 11	1	0.12893	0.63	6.67	1.5	0.3755	1.4	,909	2055	24
E-15.1	0,81	142	143	1,05	57.7	2482	±31	2457	± 55	-1	0.1601	3.2	10.37	3.6	0.4697	1.5	,417	2482	31
E-16.1	7,49	868	295	0,35	130	964	±12	1732	±100	44	0.106	5.5	2.36	5.7	0.1614	1.4	,239		
E-17.1	0,41	269	172	0,66	74.7	1796	±20	2040	± 13	12	0.1258	0.73	5.574	1.5	0.3213	1.3	,874	1796	20
E-18.1	0,58	130	92	0,73	35.7	1783	±24	2080	± 21	14	0.1287	1.2	5.65	2	0.3186	1.5	,786	1783	24
E-19.1	0,01	145	98	0,70	48.4	2123	±25	2198	± 10	3	0.13769	0.59	7.4	1.5	0.39	1.4	,920	2123	25
E-20.1	--	182	76	0,43	58.8	2062	±24	2080	± 10	1	0.12867	0.57	6.687	1.5	0.3769	1.4	,922	2062	24
E-24.1	0,11	36	42	1,22	11.7	2082	±35	2071	± 27	-1	0.128	1.5	6.73	2.5	0.3813	1.9	,785	2082	35
E-26.1	0,37	122	97	0,83	29.2	1579	±20	1553	± 24	-2	0.0963	1.3	3.684	1.9	0.2775	1.5	,751	1579	20
E-28.1	0,04	91	73	0,83	32.1	2212	±29	2187	± 14	-1	0.1368	0.81	7.72	1.7	0.4094	1.5	,884	2212	29
E-29.1	0,67	180	85	0,49	43.5	1590	±19	2049	± 22	22	0.1264	1.2	4.878	1.9	0.2798	1.4	,746		
E-30.1	0,07	108	23	0,22	31.6	1892	±24	2022	± 15	6	0.1245	0.82	5.857	1.7	0.3412	1.5	,875	1892	24
E-31.1	2,76	364	240	0,68	92.4	1629	±19	1939	± 41	16	0.1188	2.3	4.71	2.6	0.2875	1.3	,502		
E-32.1	0,08	197	181	0,95	63.2	2047	±24	2096	± 11	2	0.12982	0.61	6.69	1.5	0.3737	1.4	,914	2047	24

E-33.1	0,18	131	108	0,85	34.1	1700	±22	1727	± 24	2	0.1057	1.3	4.4	2	0.3018	1.5	,748	1700	22
E-34.1	13,50	771	397	0,53	87	693	±11	1297	±210	47	0.0842	11	1.32	11	0.1136	1.6	,149		
E-36.1	3,74	462	197	0,44	84.4	1201	±14	1883	± 70	36	0.1152	3.9	3.25	4.1	0.2048	1.3	,321		
E-37.1	0,07	91	123	1,40	21.3	1559	±22	1562	± 32	0	0.0967	1.7	3.647	2.3	0.2735	1.6	,676	1559	22
E-38.1	0,71	164	157	0,99	50.6	1963	±24	2102	± 25	7	0.1303	1.4	6.39	2	0.3559	1.4	,705	1963	24
E-39.1	5,57	581	363	0,65	110	1223	±15	1826	± 76	33	0.1116	4.2	3.22	4.4	0.2089	1.4	,311		
E-40.1	2,56	137	138	1,04	42.4	1944	±28	2108	±120	8	0.1307	7	6.34	7.2	0.3519	1.7	,231	1944	28
E-41.1	0,04	77	31	0,41	26.8	2191	±30	2161	± 16	-1	0.1348	0.91	7.52	1.9	0.4047	1.6	,874	2191	30
E-42.1	0,18	121	60	0,51	39.2	2060	±29	2163	± 19	5	0.135	1.1	7	2	0.3764	1.6	,839	2060	29
E-43.1	11,63	604	232	0,40	116	1158	±16	1755	±140	34	0.1074	7.6	2.91	7.8	0.1969	1.5	,199		

Resumo dos dados de U-Pb da amostra PE-CM-16 (Formação Santa Rita).

						Isotope ratios[b]							Ages (Ma)								
Spot number	f 206	Pb ppm	U ppm	Th ppm	Th/U[a]	$^{207}Pb/^{235}U$	1 s [%]	$^{206}Pb/^{238}U$	1 s [%]	Rho[c]	$^{207}Pb/^{206}Pb^{d}$	1 s [%]	$^{206}Pb/^{238}U$	1 s abs	$^{207}Pb/^{235}U$	1 s abs	$^{207}Pb/^{206}Pb$	1 s abs	% Conc[e]	Best estimated age (Ma)	
Zr-222-D-IV-01	0,0006	32	56	36	0,65	6,673	2,12	0,377	0,94	0,45	0,128	1,89	2062	19	2069	44	2076	39	99	2076	39
Zr-222-D-IV-02	0,0019	32	72	38	0,53	6,748	2,50	0,377	1,66	0,67	0,130	1,86	2064	34	2079	52	2094	39	99	2094	39
Zr-222-D-IV-03	0,0002	81	170	84	0,50	6,621	1,46	0,377	0,55	0,37	0,127	1,35	2064	11	2062	30	2061	28	100	2061	28
Zr-222-D-IV-05	0,0016	94	168	240	1,44	6,919	1,71	0,385	0,66	0,39	0,130	1,57	2098	14	2101	36	2104	33	100	2104	33
Zr-222-D-IV-07	0,0005	93	172	82	0,48	11,959	1,13	0,483	0,80	0,71	0,179	0,79	2542	20	2601	29	2648	21	96	2648	21
Zr-222-D-IV-08	0,0002	84	92	51	0,56	25,471	0,97	0,675	0,52	0,54	0,274	0,82	3324	17	3326	32	3328	27	100	3328	27
Zr-222-D-IV-09	0,0009	34	70	60	0,85	6,416	1,68	0,360	0,76	0,45	0,129	1,50	1981	15	2034	34	2089	31	95	2089	31
Zr-222-D-IV-10	0,0016	48	95	79	0,84	7,162	1,93	0,391	0,77	0,40	0,133	1,77	2129	16	2132	41	2134	38	100	2134	38
Zr-222-D-IV-12	0,0002	155	148	107	0,73	31,595	0,97	0,728	0,44	0,46	0,315	0,86	3524	16	3538	34	3545	30	99	3545	30
Zr-222-D-IV-13	0,0010	27	55	85	1,56	6,056	2,60	0,338	1,96	0,75	0,130	1,71	1878	37	1984	52	2096	36	90	2096	36

Zr-222-D-IV-16	0,0006	45	88	51	0,58	6,839	1,62	0,382	1,26	0,78	0,130	1,02	2086	26	2091	34	2095	21	100	2095	21
Zr-222-D-IV-20	0,0008	76	127	63	0,50	12,219	1,64	0,500	0,80	0,49	0,177	1,43	2612	21	2621	43	2629	38	99	2629	38
Zr-222-D-IV-22	0,0004	93	202	154	0,77	6,387	1,74	0,368	0,98	0,56	0,126	1,44	2021	20	2030	35	2040	29	99	2040	29
Zr-222-D-IV-28	0,0007	39	79	67	0,85	6,489	2,96	0,373	2,41	0,81	0,126	1,72	2046	49	2044	61	2043	35	100	2043	35
Zr-222-D-IV-29	0,0007	110	237	103	0,44	7,346	1,40	0,397	1,04	0,74	0,134	0,94	2157	22	2154	30	2152	20	100	2152	20
Zr-222-D-IV-32	0,0002	85	122	58	0,48	13,499	1,05	0,525	0,67	0,64	0,187	0,81	2719	18	2715	29	2713	22	100	2713	22
Zr-222-D-IV-34	0,0097	161	379	94	0,25	14,838	1,90	0,525	1,72	0,91	0,205	0,81	2722	47	2805	53	2865	23	95	2865	23
Zr-222-D-IV-35	0,0005	47	63	43	0,68	15,270	1,42	0,551	0,78	0,54	0,201	1,19	2829	22	2832	40	2834	34	100	2834	34
Zr-222-D-IV-36	0,0006	26	49	26	0,52	7,984	2,18	0,414	1,11	0,51	0,140	1,87	2232	25	2229	49	2227	42	100	2227	42
Zr-222-D-IV-37	0,0003	52	63	32	0,52	15,379	1,29	0,522	1,10	0,85	0,214	0,67	2707	30	2839	37	2934	20	92	2934	20
Zr-222-E-V-01	0,0010	77	121	71	0,59	12,981	1,38	0,515	1,05	0,76	0,183	0,89	2679	28	2678	37	2678	24	100	2678	24
Zr-222-E-V-02	0,0002	89	181	127	0,70	6,488	1,26	0,373	0,59	0,46	0,126	1,12	2046	12	2044	26	2043	23	100	2043	23
Zr-222-E-V-04	0,0006	76	125	63	0,51	11,925	1,11	0,496	0,82	0,74	0,174	0,74	2596	21	2599	29	2600	19	100	2600	19
Zr-222-E-V-05	0,0002	83	174	85	0,49	6,470	1,27	0,372	0,58	0,46	0,126	1,13	2041	12	2042	26	2043	23	100	2043	23
Zr-222-E-V-08	0,0004	44	90	53	0,59	6,850	1,45	0,384	0,89	0,61	0,129	1,14	2096	19	2092	30	2089	24	100	2089	24
Zr-222-E-V-09	0,0004	27	51	54	1,06	6,564	2,26	0,374	0,71	0,31	0,127	2,15	2048	15	2055	46	2061	44	99	2061	44
Zr-222-E-V-12	0,0008	66	155	75	0,49	6,240	1,38	0,359	0,77	0,55	0,126	1,15	1977	15	2010	28	2044	24	97	2044	24
Zr-222-E-V-13	0,0005	62	98	49	0,50	13,029	1,47	0,515	0,98	0,67	0,183	1,09	2678	26	2682	39	2684	29	100	2684	29
Zr-222-E-V-14	0,0002	106	165	84	0,52	12,918	1,25	0,515	1,00	0,80	0,182	0,76	2676	27	2674	34	2672	20	100	2672	20
Zr-222-E-V-15	0,0003	37	72	47	0,65	7,277	1,69	0,394	0,91	0,54	0,134	1,43	2142	19	2146	36	2150	31	100	2150	31
Zr-222-E-V-19	0,0001	23	43	23	0,55	7,901	1,80	0,411	0,75	0,42	0,139	1,64	2219	17	2220	40	2221	36	100	2221	36
Zr-222-E-V-20	0,0024	33	73	65	0,90	6,636	2,26	0,378	1,20	0,53	0,127	1,92	2069	25	2064	47	2060	40	100	2060	40
Zr-222-E-V-21	0,0003	44	59	34	0,58	16,463	1,51	0,564	1,24	0,82	0,212	0,86	2882	36	2904	44	2919	25	99	2919	25
Zr-222-E-V-26	0,0001	30	56	40	0,72	7,307	1,60	0,393	0,74	0,46	0,135	1,42	2138	16	2150	34	2161	31	99	2161	31
Zr-222-E-V-27	0,0002	61	104	140	1,36	6,607	1,59	0,378	0,86	0,54	0,127	1,33	2065	18	2060	33	2055	27	100	2055	27
Zr-222-E-V-29	0,0001	52	105	40	0,38	7,475	1,42	0,400	0,65	0,46	0,135	1,27	2170	14	2170	31	2170	28	100	2170	28
Zr-222-E-V-30	0,0002	23	43	23	0,55	7,993	1,76	0,413	0,61	0,34	0,140	1,65	2228	13	2230	39	2233	37	100	2233	37
Zr-222-E-V-31	0,0001	98	160	71	0,45	12,537	1,66	0,499	1,16	0,69	0,182	1,20	2611	30	2646	44	2672	32	98	2672	32

Zr-222-E-V-33	0,0002	60	122	68	0,56	6,780	1,10	0,381	0,47	0,42	0,129	0,99	2082	10	2083	23	2084	21	100	2084	21
Zr-222-E-V-40	0,0016	36	66	62	0,95	6,629	2,21	0,378	1,07	0,49	0,127	1,93	2065	22	2063	46	2062	40	100	2062	40
Zr-222-F-VI-02	0,0005	29	56	35	0,63	7,387	1,43	0,399	0,64	0,45	0,134	1,28	2162	14	2159	31	2157	28	100	2157	28
Zr-222-F-VI-03	0,0001	101	234	114	0,49	6,376	1,35	0,369	0,72	0,53	0,125	1,14	2026	15	2029	27	2032	23	100	2032	23
Zr-222-F-VI-04	0,0018	81	216	172	0,80	5,599	1,34	0,334	0,64	0,48	0,122	1,18	1856	12	1916	26	1982	23	94	1982	23
Zr-222-F-VI-06	0,0003	32	65	44	0,67	6,410	1,69	0,371	0,64	0,38	0,125	1,57	2035	13	2034	34	2032	32	100	2032	32
Zr-222-F-VI-09	0,0015	66	96	42	0,44	12,973	1,20	0,515	0,83	0,69	0,183	0,86	2679	22	2678	32	2677	23	100	2677	23
Zr-222-F-VI-10	0,0003	81	126	56	0,44	12,741	0,99	0,509	0,38	0,38	0,181	0,92	2653	10	2661	26	2666	24	100	2666	24
Zr-222-F-VI-13	0,0003	51	85	160	1,90	6,603	1,66	0,377	0,82	0,49	0,127	1,45	2062	17	2060	34	2058	30	100	2058	30
Zr-222-F-VI-14	0,0014	59	93	41	0,44	12,055	1,63	0,498	0,90	0,55	0,175	1,36	2606	23	2609	43	2611	36	100	2611	36
Zr-222-F-VI-15	0,0004	73	117	53	0,45	12,907	1,16	0,515	0,65	0,56	0,182	0,96	2677	17	2673	31	2670	26	100	2670	26
Zr-222-F-VI-17	0,0003	61	61	69	1,14	22,202	1,28	0,641	0,81	0,63	0,251	1,00	3193	26	3193	41	3192	32	100	3192	32

Resumo dos dados de U-Pb da amostra PE-CM-17 (Formação Santa Rita).

						Isotope ratios[b]							**Ages (Ma)**								
Spot number	f 206	Pb ppm	U ppm	Th ppm	Th/U[a]	$^{207}Pb/^{235}U$	1 s [%]	$^{206}Pb/^{238}U$	1 s [%]	Rho[c]	$^{207}Pb/^{206}Pb^{d}$	1 s [%]	$^{206}Pb/^{238}U$	1 s abs	$^{207}Pb/^{235}U$	1 s abs	$^{207}Pb/^{206}Pb$	1 s abs	% Conc[e]	Best estimated age (Ma)	
Zr-217-D-IV-01	0,0003	21	65	47	0,72	3,56034	2,44	0,26499	1,93	0,79	0,0974	1,49	1515	29	1541	38	1576	24	96	1576	24
Zr-217-D-IV-02	0,0007	51	165	107	0,65	3,27901	3,26	0,25094	2,48	0,76	0,0948	2,12	1443	36	1476	48	1524	32	95	1524	32
Zr-217-D-IV-03	0,0002	25	83	40	0,49	3,50148	2,70	0,26408	1,89	0,70	0,0962	1,94	1511	28	1528	41	1551	30	97	1551	30
Zr-217-D-IV-04	0,0021	78	217	141	0,65	5,06826	1,96	0,30846	1,19	0,61	0,1192	1,56	1733	21	1831	36	1944	30	89	1944	30
Zr-217-D-IV-05	0,0002	70	126	48	0,39	12,61949	2,05	0,48923	1,55	0,76	0,1871	1,34	2567	40	2652	54	2717	36	95	2717	36
Zr-217-D-IV-06	0,0004	46	100	46	0,46	7,12915	1,64	0,39207	0,96	0,59	0,1319	1,33	2132	20	2128	35	2123	28	100	2123	28
Zr-217-D-IV-07	0,0005	30	101	52	0,52	3,27760	3,73	0,24884	3,04	0,81	0,0955	2,16	1433	43	1476	55	1538	33	93	1538	33
Zr-217-D-IV-08	0,0005	63	153	20	0,13	6,65297	1,61	0,36814	0,61	0,38	0,1311	1,49	2021	12	2066	33	2112	31	96	2112	31

Zr-217-D-IV-09	0,0009	53	146	115	0,79	5,22415	1,58	0,30360	1,05	0,66	0,1248	1,18	1709	18	1857	29	2026	24	84		
Zr-217-D-IV-10	0,0023	24	75	43	0,58	3,37172	4,20	0,24492	3,36	0,80	0,0998	2,52	1412	48	1498	63	1621	41	87	1621	41
Zr-217-D-IV-11	0,0008	39	93	38	0,41	6,74729	2,04	0,36952	1,29	0,63	0,1324	1,58	2027	26	2079	42	2130	34	95	2130	34
Zr-217-D-IV-13	0,0008	19	58	45	0,78	3,51781	3,46	0,26628	2,62	0,76	0,0958	2,26	1522	40	1531	53	1544	35	99	1544	35
Zr-217-D-IV-14	0,0003	43	135	64	0,47	3,57459	2,60	0,27142	1,80	0,69	0,0955	1,87	1548	28	1544	40	1538	29	101	1538	29
Zr-217-D-IV-15	0,0002	68	107	43	0,40	11,98850	2,93	0,49276	2,61	0,89	0,1765	1,32	2583	68	2604	76	2620	35	99	2620	35
Zr-217-D-IV-16	0,0009	50	184	163	0,89	3,12403	2,67	0,24172	1,19	0,45	0,0937	2,39	1396	17	1439	38	1503	36	93	1503	36
Zr-217-D-IV-18	0,0010	69	113	119	1,06	12,19908	1,91	0,50117	1,01	0,53	0,1765	1,63	2619	26	2620	50	2621	43	100	2621	43
Zr-217-D-IV-19	0,0006	60	149	68	0,46	7,14958	1,89	0,38787	1,13	0,59	0,1337	1,52	2113	24	2130	40	2147	33	98	2147	33
Zr-217-D-IV-22	0,0145	58	128	90	0,70	12,50720	5,37	0,49054	1,18	0,22	0,1849	5,24	2573	30	2643	142	2698	141	95	2698	141
Zr-217-D-IV-23	0,0003	91	140	80	0,57	11,98529	1,39	0,49922	0,94	0,67	0,1741	1,03	2610	24	2603	36	2598	27	100	2598	27
Zr-217-D-IV-24	0,0009	47	108	74	0,69	5,87527	1,77	0,35217	1,17	0,66	0,1210	1,32	1945	23	1958	35	1971	26	99	1971	26
Zr-217-D-IV-25	0,0014	25	84	63	0,75	3,27434	3,79	0,25517	3,27	0,86	0,0931	1,92	1465	48	1475	56	1489	29	98	1489	29
Zr-217-D-IV-27	0,0001	27	102	44	0,43	3,04741	2,91	0,22870	2,01	0,69	0,0966	2,11	1328	27	1420	41	1560	33	85	1560	33
Zr-217-D-IV-30	0,0003	66	166	98	0,59	6,75273	2,45	0,38067	1,26	0,51	0,1287	2,10	2079	26	2080	51	2080	44	100	2080	44
Zr-217-D-IV-31	0,0003	62	143	74	0,52	6,88986	3,65	0,38320	2,99	0,82	0,1304	2,09	2091	63	2097	77	2103	44	99	2103	44
Zr-217-D-IV-32	0,0006	58	141	69	0,50	6,18835	4,87	0,36740	4,55	0,93	0,1222	1,73	2017	92	2003	97	1988	34	101	1988	34
Zr-217-D-IV-33	0,0005	25	63	45	0,71	4,97312	5,24	0,32515	4,60	0,88	0,1109	2,51	1815	84	1815	95	1815	45	100	1815	45
Zr-217-D-IV-34	0,0006	28	97	58	0,60	3,33052	4,95	0,25426	4,42	0,89	0,0950	2,22	1460	65	1488	74	1528	34	96	1528	34
Zr-217-D-IV-36	0,0006	31	114	69	0,61	3,30317	4,29	0,25374	4,12	0,96	0,0944	1,21	1458	60	1482	64	1516	18	96	1516	18
Zr-217-D-IV-37	0,0795	178	635	316	0,50	3,89651	23,11	0,28364	14,90	0,64	0,0996	17,67	1610	240	1613	373	1617	286	100	1617	286
Zr-217-E-V-01	0,0006	35	124	54	0,44	3,15883	2,53	0,24137	2,28	0,90	0,0949	1,12	1394	32	1447	37	1526	17	91	1526	17
Zr-217-E-V-02	0,0001	39	126	63	0,50	3,48469	3,91	0,26618	3,70	0,95	0,0949	1,27	1521	56	1524	60	1527	19	100	1527	19
Zr-217-E-V-03	0,0087	54	170	55	0,32	3,65124	4,61	0,27349	3,95	0,86	0,0968	2,37	1558	62	1561	72	1564	37	100	1564	37
Zr-217-E-V-05	0,0011	24	82	54	0,67	3,54168	3,43	0,27392	2,96	0,86	0,0938	1,72	1561	46	1537	53	1504	26	104	1504	26
Zr-217-E-V-06	0,0006	91	182	263	1,46	6,58527	3,63	0,37184	3,37	0,93	0,1284	1,35	2038	69	2057	75	2077	28	98	2077	28
Zr-217-E-V-09	0,0004	31	49	28	0,56	12,28739	4,71	0,50006	4,62	0,98	0,1782	0,94	2614	121	2627	124	2636	25	99	2636	25

Zr-217-E-V-10	0,0004	31	106	49	0,47	3,52589	4,16	0,27015	3,54	0,85	0,0947	2,20	1542	55	1533	64	1521	33	101	1521	33
Zr-217-E-V-11	0,0005	36	82	36	0,44	7,02276	3,40	0,38532	3,02	0,89	0,1322	1,55	2101	64	2114	72	2127	33	99	2127	33
Zr-217-E-V-12	0,0001	51	164	76	0,47	3,49898	3,81	0,26747	3,50	0,92	0,0949	1,51	1528	53	1527	58	1526	23	100	1526	23
Zr-217-E-V-14	0,0005	11	26	47	1,83	3,66839	4,57	0,27313	3,88	0,85	0,0974	2,42	1557	60	1565	72	1575	38	99	1575	38
Zr-217-E-V-15	0,0022	95	273	219	0,81	9,58064	2,90	0,42063	2,05	0,71	0,1652	2,04	2263	46	2395	69	2510	51	90	2510	51
Zr-217-E-V-16	0,0005	38	62	33	0,54	11,39739	2,44	0,47775	1,93	0,79	0,1730	1,50	2517	49	2556	62	2587	39	97	2587	39
Zr-217-E-V-17	0,0004	34	76	50	0,66	6,97619	2,25	0,38376	1,75	0,78	0,1318	1,42	2094	37	2108	48	2123	30	99	2123	30
Zr-217-E-V-18	0,0002	40	84	42	0,50	7,29268	2,36	0,40124	1,97	0,83	0,1318	1,31	2175	43	2148	51	2122	28	102	2122	28
Zr-217-E-V-19	0,0004	25	54	20	0,38	7,30037	2,80	0,40333	2,20	0,79	0,1313	1,73	2184	48	2149	60	2115	37	103	2115	37
Zr-217-E-V-21	0,0003	40	68	35	0,51	11,80344	2,08	0,48656	1,75	0,84	0,1759	1,12	2556	45	2589	54	2615	29	98	2615	29
Zr-217-E-V-22	0,0003	72	240	103	0,43	3,38906	2,56	0,26036	2,26	0,88	0,0944	1,20	1492	34	1502	38	1516	18	98	1516	18
Zr-217-E-V-25	0,0005	25	51	12	0,23	6,58207	3,25	0,36992	2,82	0,87	0,1290	1,62	2029	57	2057	67	2085	34	97	2085	34
Zr-217-E-V-26	0,0002	77	178	103	0,58	6,04174	2,03	0,36472	1,74	0,86	0,1201	1,05	2004	35	1982	40	1958	21	102	1958	21
Zr-217-E-V-27	0,0004	41	128	75	0,59	3,62362	3,23	0,27171	2,74	0,85	0,0967	1,72	1549	42	1555	50	1562	27	99	1562	27
Zr-217-E-V-35	0,0006	25	56	26	0,48	7,28152	3,19	0,39424	2,59	0,81	0,1340	1,86	2142	55	2147	68	2150	40	100	2150	40
Zr-217-F-VI-01	0,0003	46	87	79	0,91	6,92279	2,62	0,37648	2,37	0,91	0,1334	1,10	2060	49	2102	55	2143	24	96	2143	24
Zr-217-F-VI-02	0,0011	41	94	28	0,30	6,96784	1,96	0,37596	1,51	0,77	0,1344	1,25	2057	31	2107	41	2156	27	95	2156	27
Zr-217-F-VI-05	0,0011	50	82	40	0,49	13,52232	3,52	0,52699	1,36	0,39	0,1861	3,25	2729	37	2717	96	2708	88	101	2708	88
Zr-217-F-VI-08	0,0013	108	220	131	0,60	11,93480	1,89	0,44673	1,55	0,82	0,1938	1,07	2381	37	2599	49	2774	30	86	2774	30
Zr-217-F-VI-10	0,0001	70	150	133	0,89	6,32678	4,75	0,34723	4,59	0,97	0,1322	1,21	1921	88	2022	96	2127	26	90	2127	26
Zr-217-F-VI-11	0,0002	44	96	30	0,31	7,52495	2,93	0,40117	2,66	0,91	0,1360	1,23	2174	58	2176	64	2177	27	100	2177	27
Zr-217-F-VI-12	0,0003	51	159	81	0,51	3,71293	2,83	0,27636	2,56	0,91	0,0974	1,20	1573	40	1574	44	1576	19	100	1576	19
Zr-217-F-VI-13	0,0001	73	153	95	0,62	7,19039	2,71	0,39335	2,41	0,89	0,1326	1,25	2138	52	2135	58	2132	27	100	2132	27
Zr-217-F-VI-14	0,0006	16	36	10	0,27	7,19149	3,94	0,37679	3,16	0,80	0,1384	2,35	2061	65	2135	84	2208	52	93	2208	52
Zr-217-F-VI-15	0,0002	58	120	64	0,54	7,55268	1,83	0,39628	1,33	0,73	0,1382	1,25	2152	29	2179	40	2205	28	98	2205	28
Zr-217-F-VI-17	0,0001	84	137	68	0,50	12,06388	3,03	0,49846	2,49	0,82	0,1755	1,73	2607	65	2609	79	2611	45	100	2611	45
Zr-217-F-VI-20	0,0004	28	38	37	0,98	14,12148	4,04	0,52249	3,31	0,82	0,1960	2,31	2710	90	2758	111	2793	65	97	2793	65
Zr-217-F-VI-23	0,0003	41	91	36	0,40	7,08181	2,99	0,39182	2,38	0,80	0,1311	1,81	2131	51	2122	64	2113	38	101	2113	38

Zr-217-F-VI-24	0,0008	26	54	52	0,97	7,36906	4,42	0,39340	3,63	0,82	0,1359	2,53	2139	78	2157	95	2175	55	98	2175	55
Zr-217-F-VI-28	0,0002	73	86	36	0,43	21,72988	3,14	0,63295	2,78	0,88	0,2490	1,47	3161	88	3172	100	3178	47	99	3178	47
Zr-217-F-VI-34b	0,0005	83	209	124	0,60	5,62080	4,82	0,31193	4,43	0,92	0,1307	1,91	1750	77	1919	93	2107	40	83		
Zr-217-F-VI-36	0,0002	58	107	50	0,47	10,08607	4,44	0,46007	3,62	0,81	0,1590	2,59	2440	88	2443	109	2445	63	100	2445	63
Zr-217-F-VI-37	0,0005	44	85	103	1,21	6,96174	2,75	0,37900	1,78	0,65	0,1332	2,10	2072	37	2107	58	2141	45	97	2141	45
Zr-217-F-VI-38	0,0002	60	194	90	0,46	3,50876	2,86	0,26973	1,47	0,51	0,0943	2,46	1539	23	1529	44	1515	37	102	1515	37

Resumo dos dados de U-Pb da amostra PE-CM-20 (Formação Córrego dos Borges).

						Isotope ratios[b]							**Ages (Ma)**								
Spot number	f 206	Pb ppm	U ppm	Th ppm	Th/U[a]	^{207}Pb/^{235}U	1 s [%]	^{206}Pb/^{238}U	1 s [%]	Rho[c]	^{207}Pb/^{206}Pb[d]	1 s [%]	^{206}Pb/^{238}U	1 s abs	^{207}Pb/^{235}U	1 s abs	^{207}Pb/^{206}Pb	1 s abs	% Conc[e]	Best estimated age (Ma)	
003 ZR216_D_IV_01	0,0005	86,4	147,1	30,4	0,21	15,89581	1,60	0,56268	0,93	0,58	0,20489	1,31	2878	27	2871	46	2866	37	100	2866	37
004 ZR216_D_IV_03	0,0017	38,2	155,4	54,8	0,35	8,57714	2,38	0,41259	0,78	0,33	0,15077	2,25	2227	17	2294	55	2355	53	95	2355	53
005 ZR216_D_IV_05	0,0009	125,9	269,1	123,7	0,46	10,85077	2,28	0,49469	0,67	0,29	0,15908	2,18	2591	17	2510	57	2446	53	106	2446	53
006 ZR216_D_IV_06	0,0004	49,7	126,7	73,5	0,58	6,28003	2,74	0,37257	1,16	0,42	0,12225	2,48	2041	24	2016	55	1989	49	103	1989	49
007 ZR216_D_IV_08	0,0013	34,4	168,7	81,0	0,48	27,74193	2,83	0,69675	2,28	0,80	0,28877	1,68	3408	78	3410	96	3411	57	100	3411	57
008 ZR216_D_IV_11	0,0008	52,2	247,0	99,9	0,41	3,74722	4,10	0,23650	3,21	0,78	0,11491	2,56	1368	44	1582	65	1879	48	73		
009 ZR216_D_IV_12	0,0039	44,6	114,9	66,9	0,59	5,99015	13,10	0,35963	2,80	0,21	0,12080	12,80	1980	55	1974	259	1968	252	101	1968	252
010 ZR216_D_IV_13	0,0007	56,6	188,9	38,5	0,21	6,67340	4,03	0,37886	1,68	0,42	0,12775	3,66	2071	35	2069	83	2067	76	100	2067	76
011 ZR216_D_IV_15	0,0004	51,9	111,6	70,2	0,63	12,15293	2,08	0,51190	0,75	0,36	0,17218	1,94	2665	20	2616	54	2579	50	103	2579	50
012 ZR216_D_IV_18	0,0003	76,1	164,9	136,0	0,83	11,98600	2,35	0,50941	1,52	0,65	0,17065	1,80	2654	40	2603	61	2564	46	104	2564	46
015 ZR216_D_IV_19	0,0013	36,4	109,9	73,5	0,67	6,24793	3,50	0,35756	2,49	0,71	0,12673	2,47	1971	49	2011	70	2053	51	96	2053	51

016 ZR216_D_IV_21	0,0012	31,0	143,9	75,7	0,53	12,41383	2,51	0,49525	2,03	0,81	0,18180	1,48	2593	53	2636	66	2669	39	97	2669	39
017 ZR216_E_V_01	0,0009	41,2	121,6	97,9	0,81	6,24621	6,03	0,36552	4,97	0,82	0,12394	3,41	2008	100	2011	121	2014	69	100	2014	69
018 ZR216_E_V_02	0,0008	22,7	81,9	72,3	0,89	3,50217	3,90	0,26702	0,92	0,24	0,09513	3,79	1526	14	1528	60	1531	58	100	1531	58
019 ZR216_E_V_04	0,0007	58,4	137,5	75,5	0,55	7,28016	1,19	0,39415	0,53	0,45	0,13396	1,07	2142	11	2146	26	2151	23	100	2151	23
020 ZR216_E_V_05	0,0021	36,3	159,6	67,8	0,43	6,87072	3,19	0,38359	2,31	0,72	0,12991	2,20	2093	48	2095	67	2097	46	100	2097	46
021 ZR216_E_V_06	0,0005	61,2	116,4	66,9	0,58	12,56868	1,13	0,51327	0,79	0,70	0,17760	0,80	2671	21	2648	30	2631	21	102	2631	21
022 ZR216_E_V_07	0,0004	56,8	360,0	161,1	0,45	4,76348	5,03	0,31625	1,33	0,26	0,10924	4,86	1771	23	1778	90	1787	87	99	1787	87
023 ZR216_E_V_08	0,0004	91,6	177,0	78,7	0,45	11,78501	1,03	0,50561	0,64	0,62	0,16905	0,81	2638	17	2587	27	2548	21	104	2548	21
024 ZR216_E_V_10	0,0014	6,5	26,2	17,0	0,65	3,20136	9,16	0,25112	2,31	0,25	0,09246	8,87	1444	33	1457	134	1477	131	98	1477	131
027 ZR216_E_V_12	0,0008	23,3	72,9	72,9	1,01	5,92839	4,64	0,35093	3,43	0,74	0,12252	3,12	1939	66	1965	91	1993	62	97	1993	62
028 ZR216_E_V_14	0,0021	16,7	39,8	44,6	1,13	10,11835	6,79	0,45357	4,72	0,69	0,16179	4,88	2411	114	2446	166	2474	121	97	2474	121
029 ZR216_E_V_17	0,0009	36,7	76,9	43,9	0,58	13,20133	4,39	0,51743	3,86	0,88	0,18504	2,08	2688	104	2694	118	2699	56	100	2699	56
030 ZR216_E_V_20	0,0030	8,3	19,8	15,2	0,77	11,63046	6,79	0,47771	2,35	0,35	0,17658	6,37	2517	59	2575	175	2621	167	96	2621	167
031 ZR216_E_V_21	0,0004	45,3	153,0	92,2	0,61	5,67311	2,83	0,34913	1,07	0,38	0,11785	2,63	1930	21	1927	55	1924	51	100	1924	51
032 ZR216_E_V_23	0,0003	47,9	141,4	125,8	0,90	5,90686	2,17	0,36031	0,87	0,40	0,11890	1,98	1984	17	1962	43	1940	39	102	1940	39
033 ZR216_E_V_25	0,0010	20,6	56,4	89,3	1,59	6,20517	3,92	0,35914	1,24	0,32	0,12531	3,71	1978	25	2005	79	2033	75	97	2033	75
034 ZR216_E_V_27	0,0005	55,1	141,2	94,1	0,67	6,39071	2,73	0,36452	1,24	0,45	0,12715	2,44	2004	25	2031	56	2059	50	97	2059	50
035 ZR216_E_V_28	0,0018	55,1	370,3	110,1	0,30	4,84189	3,86	0,31724	3,22	0,84	0,11069	2,12	1776	57	1792	69	1811	38	98	1811	38
036 ZR216_E_V_29	0,0017	18,8	47,5	50,3	1,07	6,60029	5,68	0,37701	0,90	0,16	0,12697	5,61	2062	19	2059	117	2056	115	100	2056	115
039 ZR216_E_V_30	0,0010	47,1	180,5	86,9	0,48	11,16230	2,23	0,47619	1,54	0,69	0,17001	1,61	2511	39	2537	56	2558	41	98	2558	41
040 ZR216_F_VI_13	0,0005	27,9	114,7	61,2	0,54	3,42218	4,97	0,26240	2,86	0,57	0,09459	4,07	1502	43	1510	75	1520	62	99	1520	62
041 ZR216_F_VI_14	0,0005	51,5	114,1	55,4	0,49	11,66444	2,77	0,48797	2,19	0,79	0,17337	1,69	2562	56	2578	71	2590	44	99	2590	44
042 ZR216_F_VI_01	0,0023	5,8	14,9	9,7	0,66	7,02425	7,97	0,38777	3,85	0,48	0,13138	6,98	2112	81	2115	169	2116	148	100	2116	148
043 ZR216_F_VI_03	0,0005	66,7	161,5	97,3	0,61	6,71666	2,18	0,38729	0,65	0,30	0,12578	2,08	2110	14	2075	45	2040	42	103	2040	42
044 ZR216_F_VI_04	0,0004	88,9	157,3	83,5	0,53	11,91860	1,38	0,51391	0,54	0,39	0,16820	1,27	2673	14	2598	36	2540	32	105	2540	32
045 ZR216_F_VI_09	0,0007	53,1	108,7	64,0	0,59	11,44758	1,81	0,47820	0,88	0,48	0,17362	1,58	2519	22	2560	46	2593	41	97	2593	41
046 ZR216_F_VI_10	0,0004	47,2	192,4	127,0	0,66	6,53674	2,60	0,37681	1,93	0,74	0,12582	1,75	2061	40	2051	53	2040	36	101	2040	36
047 ZR216_F_VI_12	0,0008	34,0	184,1	94,3	0,52	8,36676	3,38	0,42367	2,44	0,72	0,14323	2,34	2277	56	2272	77	2267	53	100	2267	53

048 ZR216_F_VI_16	0,0008	24,3	133,5	67,0	0,51	6,26482	4,84	0,36781	2,83	0,59	0,12353	3,92	2019	57	2014	97	2008	79	101	2008	79
051 ZR216_F_VI_17	0,0009	21,2	59,0	23,5	0,40	7,13682	3,50	0,38762	1,29	0,37	0,13354	3,26	2112	27	2129	75	2145	70	98	2145	70
052 ZR216_F_VI_19	0,0014	18,2	48,6	33,3	0,69	7,02446	4,73	0,37827	1,61	0,34	0,13468	4,45	2068	33	2115	100	2160	96	96	2160	96
053 ZR216_F_VI_20	0,0017	5,0	12,6	7,0	0,56	7,24877	7,13	0,39401	4,29	0,60	0,13343	5,70	2141	92	2143	153	2144	122	100	2144	122
054 ZR216_F_VI_22	0,0007	22,4	62,2	38,3	0,62	7,27749	3,20	0,39066	1,06	0,33	0,13511	3,02	2126	23	2146	69	2165	65	98	2165	65
055 ZR216_F_VI_23	0,0020	60,0	660,9	269,2	0,41	2,23199	2,82	0,17555	1,68	0,60	0,09221	2,26	1043	18	1191	34	1472	33	71		
056 ZR216_F_VI_24	0,0003	41,5	111,2	81,9	0,74	6,82448	1,92	0,38082	0,51	0,27	0,12997	1,85	2080	11	2089	40	2098	39	99	2098	39
057 ZR216_F_VI_25	0,0009	30,6	87,7	43,2	0,50	5,72502	3,01	0,34776	1,18	0,39	0,11940	2,77	1924	23	1935	58	1947	54	99	1947	54
058 ZR216_F_VI_26	0,0010	65,1	121,8	57,4	0,47	11,15964	3,05	0,48496	2,42	0,79	0,16689	1,85	2549	62	2537	77	2527	47	101	2527	47
059 ZR216_F_VI_27	0,0009	36,4	85,8	53,3	0,63	6,99458	2,87	0,38924	0,76	0,27	0,13033	2,76	2119	16	2111	61	2102	58	101	2102	58
060ZR216_F_VI_29	0,0006	56,5	149,2	54,5	0,37	5,87569	2,10	0,36336	0,45	0,22	0,11728	2,05	1998	9	1958	41	1915	39	104	1915	39
063 ZR216_F_VI_30	0,0009	92,0	231,1	163,6	0,71	7,60701	2,16	0,40815	1,88	0,87	0,13517	1,05	2206	42	2186	47	2166	23	102	2166	23
064 ZR216_F_VI_31	0,0004	81,7	238,9	116,3	0,49	6,61239	2,21	0,38898	0,91	0,41	0,12329	2,02	2118	19	2061	46	2004	40	106	2004	40
065 ZR216_F_VI_37	0,0004	124,6	227,4	139,1	0,62	12,68649	1,48	0,52883	1,04	0,70	0,17399	1,05	2737	28	2657	39	2596	27	105	2596	27

Resumo dos dados de U-Pb da amostra PE-SC-42 (Formação Córrego dos Borges).

						Isotope ratios[b]							**Ages (Ma)**								
Spot number	f 206	Pb ppm	U ppm	Th ppm	Th/U[a]	^{207}Pb/^{235}U	1 s [%]	^{206}Pb/^{238}U	1 s [%]	Rho[c]	^{207}Pb/^{206}Pb[d]	1 s [%]	^{206}Pb/^{238}U	1 s abs	^{207}Pb/^{235}U	1 s abs	^{207}Pb/^{206}Pb	1 s abs	% Conc[e]	Best estimated age (Ma)	
Zr-206-D-IV-02	0,0010	25,6	70,1	47,6	0,68	4,76662	2,38	0,31847	1,56	0,66	0,10855	1,79	1782	28	1779	42	1775	32	100	1775	32
Zr-206-D-IV-03	0,0008	35,5	88,7	30,0	0,34	4,74593	1,87	0,31773	0,75	0,40	0,10833	1,71	1779	13	1775	33	1772	30	100	1772	30
Zr-206-D-IV-05	0,0010	52,5	150,4	63,6	0,43	4,69022	1,52	0,31466	0,68	0,45	0,10811	1,36	1764	12	1765	27	1768	24	100	1768	24
Zr-206-D-IV-06	0,0010	30,1	64,1	43,9	0,69	6,33743	1,65	0,36955	0,89	0,54	0,12438	1,38	2027	18	2024	33	2020	28	100	2020	28
Zr-206-D-IV-07	0,0004	57,9	158,2	87,0	0,55	4,81556	1,62	0,31979	1,01	0,62	0,10922	1,26	1789	18	1788	29	1786	23	100	1786	23
Zr-206-D-IV-08	0,0004	30,4	99,6	48,8	0,49	3,54112	1,81	0,26876	0,85	0,47	0,09556	1,60	1535	13	1536	28	1539	25	100	1539	25

Zr-206-D-IV-09	0,0003	33,5	83,9	76,1	0,91	4,99926	3,12	0,31069	2,54	0,81	0,11670	1,81	1744	44	1819	57	1906	35	91	1906	35
Zr-206-D-IV-10	0,0003	72,8	182,4	142,0	0,78	4,76889	1,44	0,31993	0,69	0,48	0,10811	1,26	1789	12	1779	26	1768	22	101	1768	22
Zr-206-D-IV-12	0,0003	61,1	212,3	139,5	0,66	3,15290	1,67	0,25368	0,89	0,53	0,09014	1,42	1457	13	1446	24	1429	20	102	1429	20
Zr-206-D-IV-13	0,0006	44,2	101,6	90,3	0,90	4,87209	1,91	0,31908	1,16	0,61	0,11074	1,52	1785	21	1797	34	1812	27	99	1812	27
Zr-206-D-IV-14	0,0047	110,5	191,7	117,4	0,62	12,26502	3,85	0,50310	1,13	0,29	0,17681	3,68	2627	30	2625	101	2623	97	100	2623	97
Zr-206-D-IV-15	0,0013	76,5	171,1	82,1	0,48	6,69256	1,78	0,37907	1,02	0,58	0,12805	1,45	2072	21	2072	37	2071	30	100	2071	30
Zr-206-D-IV-16	0,0048	118,4	324,9	217,3	0,67	4,66757	1,63	0,31218	1,02	0,63	0,10844	1,27	1751	18	1761	29	1773	22	99	1773	22
Zr-206-D-IV-17	0,0003	57,8	155,1	91,4	0,59	4,80673	1,52	0,31916	0,90	0,59	0,10923	1,22	1786	16	1786	27	1787	22	100	1787	22
Zr-206-D-IV-18	0,0005	61,2	133,7	149,1	1,12	4,96982	1,93	0,32462	1,38	0,72	0,11103	1,35	1812	25	1814	35	1816	24	100	1816	24
Zr-206-D-IV-19	0,0004	70,3	196,8	93,9	0,48	4,81315	2,08	0,32003	1,17	0,56	0,10908	1,72	1790	21	1787	37	1784	31	100	1784	31
Zr-206-D-IV-20	0,0009	27,7	44,6	34,1	0,77	10,27806	1,94	0,46348	1,36	0,70	0,16083	1,38	2455	33	2460	48	2464	34	100	2464	34
Zr-206-D-IV-21	0,0003	45,9	120,7	119,6	1,00	4,75054	5,21	0,31373	4,93	0,95	0,10982	1,66	1759	87	1776	92	1796	30	98	1796	30
Zr-206-D-IV-22	0,0013	107,1	181,1	85,0	0,47	13,01495	1,77	0,51404	1,12	0,63	0,18363	1,37	2674	30	2681	47	2686	37	100	2686	37
Zr-206-D-IV-23	0,0005	40,9	105,7	62,8	0,60	4,74646	1,74	0,31661	1,09	0,63	0,10873	1,36	1773	19	1775	31	1778	24	100	1778	24
Zr-206-D-IV-24	0,0011	35,1	65,8	27,2	0,42	7,35573	2,00	0,39779	1,08	0,54	0,13411	1,68	2159	23	2156	43	2153	36	100	2153	36
Zr-206-D-IV-25	0,0006	69,6	174,6	54,1	0,31	6,78429	1,55	0,38270	0,77	0,50	0,12857	1,35	2089	16	2084	32	2079	28	100	2079	28
Zr-206-D-IV-26	0,0024	110,8	327,0	320,4	0,99	4,90584	2,04	0,32219	1,46	0,71	0,11043	1,43	1800	26	1803	37	1807	26	100	1807	26
Zr-206-D-IV-27	0,0023	37,5	56,8	47,8	0,85	15,69181	2,89	0,55496	2,23	0,77	0,20507	1,83	2846	64	2858	83	2867	53	99	2867	53
Zr-206-D-IV-28	0,0014	125,7	169,6	60,5	0,36	19,98681	1,21	0,61642	0,81	0,66	0,23516	0,91	3096	25	3091	38	3088	28	100	3088	28
Zr-206-D-IV-29	0,0030	111,5	266,3	471,1	1,78	4,84683	1,81	0,31994	0,89	0,49	0,10987	1,58	1789	16	1793	33	1797	28	100	1797	28
Zr-206-D-IV-30	0,0003	47,1	126,4	72,6	0,58	4,90969	1,70	0,32245	0,80	0,47	0,11043	1,50	1802	14	1804	31	1807	27	100	1807	27
Zr-206-D-IV-32	0,0009	131,3	234,2	173,1	0,74	11,55017	2,09	0,49068	1,54	0,74	0,17072	1,41	2574	40	2569	54	2565	36	100	2565	36
Zr-206-D-IV-33	0,0029	192,4	289,9	225,0	0,78	12,36426	2,31	0,50496	1,64	0,71	0,17759	1,63	2635	43	2632	61	2630	43	100	2630	43
Zr-206-E-V-01	0,0003	66,9	127,7	117,3	0,92	6,65500	1,40	0,37839	0,89	0,64	0,12756	1,08	2069	19	2067	29	2065	22	100	2065	22
Zr-206-E-V-02	0,0013	59,6	156,0	93,0	0,60	4,65827	1,89	0,31415	1,02	0,54	0,10754	1,59	1761	18	1760	33	1758	28	100	1758	28
Zr-206-E-V-03	0,0014	16,3	36,3	35,8	0,99	4,77890	2,61	0,31583	1,31	0,50	0,10974	2,25	1769	23	1781	46	1795	40	99	1795	40

Zr-206-E-V-04	0,0010	27,3	47,5	49,3	1,04	7,32896	2,24	0,39576	1,50	0,67	0,13431	1,66	2149	32	2152	48	2155	36	100	2155	36
Zr-206-E-V-05	0,0005	67,1	104,6	68,3	0,66	12,43089	1,88	0,50613	1,50	0,80	0,17813	1,14	2640	40	2638	50	2636	30	100	2636	30
Zr-206-E-V-06	0,0003	43,1	84,6	44,1	0,53	6,77454	1,65	0,38022	1,01	0,61	0,12923	1,30	2077	21	2082	34	2087	27	100	2087	27
Zr-206-E-V-07	0,0027	126,7	295,0	523,7	1,79	4,93227	2,37	0,32356	1,81	0,77	0,11056	1,52	1807	33	1808	43	1809	28	100	1809	28
Zr-206-E-V-08	0,0394	104,1	226,0	301,1	1,34	6,64790	1,72	0,36678	0,57	0,33	0,13145	1,62	2014	12	2066	35	2117	34	95	2117	34
Zr-206-E-V-09	0,0004	33,9	68,8	33,7	0,49	7,20931	1,62	0,39275	0,98	0,60	0,13313	1,29	2136	21	2138	35	2140	28	100	2140	28
Zr-206-E-V-10	0,0008	22,2	65,7	38,1	0,58	4,07099	2,81	0,28931	2,26	0,81	0,10205	1,66	1638	37	1649	46	1662	28	99	1662	28
Zr-206-E-V-11	0,0017	40,9	98,1	125,7	1,29	4,94549	2,11	0,32437	1,02	0,48	0,11058	1,84	1811	18	1810	38	1809	33	100	1809	33
Zr-206-E-V-12	0,0008	21,6	57,5	34,4	0,60	4,77072	2,12	0,31816	0,95	0,45	0,10875	1,89	1781	17	1780	38	1779	34	100	1779	34
Zr-206-E-V-13	0,0007	20,9	58,9	27,3	0,47	4,73556	2,79	0,31667	1,76	0,63	0,10846	2,16	1773	31	1774	49	1774	38	100	1774	38
Zr-206-E-V-14	0,0020	36,8	105,1	71,0	0,68	7,09276	1,86	0,38905	0,82	0,44	0,13222	1,66	2118	17	2123	39	2128	35	100	2128	35
Zr-206-E-V-15	0,0007	44,1	94,2	41,0	0,44	7,59411	1,47	0,40324	0,79	0,54	0,13659	1,24	2184	17	2184	32	2184	27	100	2184	27
Zr-206-E-V-17	0,0004	76,4	180,3	191,8	1,07	4,88745	1,80	0,32137	0,76	0,42	0,11030	1,63	1796	14	1800	32	1804	29	100	1804	29
Zr-206-E-V-18	0,0008	62,9	155,9	118,6	0,77	4,68704	1,99	0,31500	1,40	0,70	0,10792	1,41	1765	25	1765	35	1765	25	100	1765	25
Zr-206-E-V-21	0,0009	68,3	111,8	38,8	0,35	12,73698	1,39	0,51253	0,75	0,54	0,18024	1,17	2667	20	2660	37	2655	31	100	2655	31
Zr-206-E-V-22	0,0015	62,7	118,9	97,9	0,83	7,83144	1,90	0,40941	0,92	0,48	0,13873	1,66	2212	20	2212	42	2211	37	100	2211	37
Zr-206-E-V-23	0,0006	44,7	108,4	63,3	0,59	4,89875	1,58	0,32305	0,76	0,48	0,10998	1,39	1805	14	1802	29	1799	25	100	1799	25
Zr-206-F-VI-01	0,0003	115,1	251,6	73,2	0,29	7,00054	1,48	0,39242	0,49	0,33	0,12938	1,39	2134	10	2111	31	2090	29	102	2090	29
Zr-206-F-VI-02	0,0004	87,7	103,7	141,6	1,38	13,83606	1,47	0,52930	0,80	0,54	0,18959	1,24	2739	22	2739	40	2739	34	100	2739	34
Zr-206-F-VI-03	0,0006	40,1	80,7	65,1	0,81	7,34371	1,83	0,39791	0,94	0,51	0,13385	1,57	2159	20	2154	39	2149	34	100	2149	34
Zr-206-F-VI-04	0,0007	29,8	54,5	15,5	0,29	11,00219	1,75	0,47933	1,05	0,60	0,16647	1,40	2524	27	2523	44	2522	35	100	2522	35
Zr-206-F-VI-05	0,0005	49,1	108,7	55,4	0,51	6,92865	1,63	0,38637	0,92	0,56	0,13006	1,34	2106	19	2102	34	2099	28	100	2099	28
Zr-206-F-VI-06	0,0006	45,0	105,9	64,6	0,61	5,99417	1,93	0,35891	1,07	0,56	0,12113	1,60	1977	21	1975	38	1973	32	100	1973	32
Zr-206-F-VI-07	0,0009	75,6	132,5	55,4	0,42	12,87103	1,77	0,51217	1,33	0,75	0,18226	1,17	2666	35	2670	47	2674	31	100	2674	31
Zr-206-F-VI-08	0,0012	132,9	201,6	193,2	0,97	12,88838	1,34	0,51319	0,81	0,61	0,18214	1,07	2670	22	2672	36	2672	28	100	2672	28
Zr-206-F-VI-09	0,0016	16,5	36,1	22,1	0,62	6,99288	2,33	0,38716	1,08	0,47	0,13100	2,06	2110	23	2111	49	2111	43	100	2111	43
Zr-206-F-VI-10	0,0008	40,0	82,1	40,3	0,49	7,59982	1,86	0,40449	0,93	0,50	0,13627	1,62	2190	20	2185	41	2180	35	100	2180	35

Zr-206-F-VI-11	0,0014	32,1	66,2	33,2	0,50	7,25702	2,92	0,39396	1,94	0,67	0,13360	2,18	2141	42	2144	63	2146	47	100	2146	47
Zr-206-F-VI-12	0,0011	48,0	60,5	168,2	2,80	9,47762	2,71	0,44646	2,07	0,76	0,15396	1,75	2379	49	2385	65	2390	42	100	2390	42
Zr-206-F-VI-13	0,0013	28,0	58,4	31,3	0,54	7,13610	2,25	0,39239	1,06	0,47	0,13190	1,99	2134	23	2129	48	2123	42	100	2123	42
Zr-206-F-VI-14	0,0010	86,7	184,5	142,5	0,78	5,81015	1,98	0,35226	1,01	0,51	0,11963	1,71	1945	20	1948	39	1951	33	100	1951	33
Zr-206-F-VI-15	0,0007	41,8	103,2	40,2	0,39	6,95267	2,53	0,38517	1,78	0,70	0,13092	1,80	2100	37	2105	53	2110	38	100	2110	38
Zr-206-F-VI-16	0,0007	50,9	103,8	36,8	0,36	7,10129	2,00	0,39094	0,67	0,33	0,13174	1,88	2127	14	2124	42	2121	40	100	2121	40
Zr-206-F-VI-17	0,0006	69,2	138,7	89,8	0,65	6,82492	1,87	0,38327	0,80	0,43	0,12915	1,69	2092	17	2089	39	2086	35	100	2086	35
Zr-206-F-VI-18	0,0014	24,5	76,1	38,4	0,51	3,44623	3,59	0,26527	0,99	0,28	0,09422	3,45	1517	15	1515	54	1513	52	100	1513	52
Zr-206-F-VI-19	0,0016	59,2	157,8	82,1	0,52	4,53084	2,72	0,30956	1,10	0,40	0,10615	2,49	1739	19	1737	47	1734	43	100	1734	43
Zr-206-F-VI-20	0,0078	44,7	149,8	70,6	0,47	3,34248	3,48	0,26012	2,37	0,68	0,09319	2,55	1490	35	1491	52	1492	38	100	1492	38

Resumo dos dados de U-Pb da amostra PE-JQ-52 (Formação Córrego dos Borges).

Grain.Spot	**% $^{206}Pb_c$**	**ppm U**	**ppm Th**	**$^{232}Th/^{238}U$**	**ppm $^{206}Pb^*$**	**(1) $^{206}Pb/^{238}U$ Age**		**(1) $^{207}Pb/^{206}Pb$ Age**		**% Dis-cor-dant**	**(1) $^{207}Pb^*/^{206}Pb^*$**	**±%**	**(1) $^{207}Pb^*/^{235}U$**	**±%**	**(1) $^{206}Pb^*/^{238}U$**	**±%**	**err corr**	**Best estimated age (Ma)**	
1	0,11	65	26	0,41	26.5	2489	±48	2458	± 13	-1	0.1602	0.75	10.41	2.4	0.471	2.3	,951	2458	13
3	0,02	119	48	0,42	49.1	2521	±46	2485,8	± 9.1	-1	0.16288	0.54	10.75	2.2	0.479	2.2	,971	2485,8	9,1
4	3,54	327	272	0,86	71.4	1413	±27	1705	± 48	17	0.1045	2.6	3.53	3.4	0.245	2.1	,635		
5	0,32	76	39	0,53	16.2	1434	±29	1417	± 36	-1	0.0896	1.9	3.079	3	0.2492	2.3	,768	1417	36
6	0,76	102	41	0,42	21.9	1432	±29	1402	± 33	-2	0.0889	1.7	3.048	2.8	0.2487	2.2	,789	1402	33
7	0,17	198	73	0,38	61.7	1989	±36	2017	± 10	1	0.1242	0.59	6.19	2.2	0.3614	2.1	,964	2017	10
8	9,21	180	77	0,44	64.4	2068	±40	1967	± 99	-5	0.1207	5.6	6.3	6	0.3783	2.3	,376	1967	99
9	0,17	105	55	0,54	30	1856	±36	1794	± 16	-4	0.10965	0.9	5.04	2.4	0.3337	2.2	,926	1794	16
10	0,55	126	75	0,61	36.6	1863	±35	1810	± 19	-3	0.1107	1.1	5.11	2.4	0.335	2.2	,899	1810	19

11	5,34	338	328	1,00	79.1	1480	±29	1754	± 68	16	0.1073	3.7	3.82	4.3	0.2581	2.2	,505		
12	0,09	148	76	0,53	35.2	1577	±30	1556	± 15	-1	0.09641	0.78	3.685	2.3	0.2772	2.2	,940	1556	15
13	0,32	196	83	0,44	41.8	1425	±27	1361	± 19	-5	0.08704	10	2.97	2.4	0.2474	2.1	,906	1361	19
14	1,67	280	259	0,96	79.2	1810	±33	1962	± 23	8	0.1204	1.3	5.38	2.5	0.3242	2.1	,858	1962	23
15	0,24	71	56	0,82	24	2139	±41	2132	± 16	0	0.1326	0.94	7.19	2.4	0.3936	2.3	,924	2132	16
16	6,87	227	234	1,07	58	1577	±31	1978	± 78	20	0.1215	4.4	4.64	4.9	0.2772	2.2	,448		
17	0,32	96	34	0,36	32.3	2133	±40	2125	± 15	0	0.1321	0.83	7.14	2.4	0.3922	2.2	,935	2125	15
18	1,50	122	160	1,35	36.1	1877	±35	2019	± 27	7	0.1243	1.5	5.79	2.6	0.3379	2.2	,823	2019	27
19	1,00	35	37	1,09	10.4	1889	±41	1913	± 43	1	0.1171	2.4	5.5	3.5	0.3404	2.5	,717	1913	43
21	0,80	198	165	0,86	48.4	1600	±30	1683	± 21	5	0.1032	1.2	4.01	2.4	0.2816	2.1	,880	1683	21
22	2,06	293	424	1,49	63.6	1426	±27	2037	± 26	30	0.1256	1.5	4.28	2.6	0.2475	2.1	,823		
23	0,52	116	110	0,98	31.8	1772	±34	1857	± 20	5	0.1136	1.1	4.95	2.4	0.3165	2.2	,894	1857	20
24	--	52	37	0,73	11	1413	±30	1460	± 24	3	0.0917	1.3	3.097	2.7	0.2451	2.4	,882	1460	24
25	1,94	102	36	0,36	33.5	2047	±39	2085	± 31	2	0.1291	1.8	6.65	2.8	0.3736	2.2	,782	2085	31
26	3,91	133	100	0,78	38.3	1807	±35	2142	± 47	16	0.1333	2.7	5.94	3.5	0.3235	2.2	,633		
27	2,27	335	177	0,55	71.7	1403	±27	1941	± 29	28	0.119	1.6	3.99	2.7	0.2431	2.1	,794		
29	2,69	270	143	0,55	84.8	1965	±36	2160	± 64	9	0.1347	3.7	6.62	4.2	0.3563	2.1	,504	2160	64
31	0,08	140	55	0,41	63.2	2717	±48	2695,1	± 7.3	-1	0.18465	0.44	13.35	2.2	0.524	2.2	,980	2695,1	7,3
32	0,09	103	43	0,43	21.8	1422	±28	1395	± 21	-2	0.08857	1.1	3.014	2.5	0.2468	2.2	,897	1395	21
33	0,33	64	51	0,83	22.1	2163	±42	2103	± 18	-3	0.1304	1	7.17	2.5	0.3987	2.3	,916	2103	18
34	0,32	96	69	0,74	19.5	1364	±27	1377	± 28	1	0.0878	1.5	2.851	2.7	0.2356	2.2	,835	1377	28
36	0,03	173	79	0,48	36.1	1406	±27	1415	± 15	1	0.08951	0.76	3.009	2.3	0.2438	2.1	,943	1415	15
37	0,03	147	67	0,47	29.5	1348	±26	1409	± 15	4	0.08922	0.79	2.862	2.3	0.2327	2.2	,939	1409	15
38	0,85	368	225	0,63	82.8	1491	±28	1713	± 18	13	0.1049	0.95	3.763	2.3	0.2601	2.1	,911		
39	5,16	285	166	0,60	63.5	1418	±27	1449	± 80	2	0.0911	4.2	3.09	4.7	0.246	2.2	,455	1449	80
40	0,10	208	94	0,47	71	2156	±39	2106,1	± 8.5	-2	0.1306	0.48	7.15	2.2	0.3973	2.1	,975	2106,1	8,5
41	9,99	1475	1275	0,89	129	564	±12	955	±170	41	0.0709	8.5	0.894	8.8	0.0914	2.2	,249		
43	0,13	170	100	0,61	54.2	2038	±38	1962	± 11	-4	0.1204	0.61	6.17	2.2	0.3717	2.1	,962	1962	11

44	0,16	149	134	0,93	74.2	2945	±51	2971,3	± 6.7	1	0.21873	0.42	17.46	2.2	0.579	2.2	,982	2971,3	6,7
47	0,09	101	47	0,49	39.6	2426	±44	2399	± 10	-1	0.15477	0.59	9.75	2.3	0.457	2.2	,966	2399	10
48	0,09	174	54	0,32	60.9	2204	±40	2172	± 13	-1	0.1356	0.74	7.62	2.3	0.4075	2.1	,945	2172	13
50	0,13	199	144	0,75	55.9	1822	±34	1811	± 11	-1	0.11071	0.6	4.99	2.2	0.3267	2.1	,963	1811	11
51	0,63	64	30	0,49	22.8	2221	±43	2143	± 21	-4	0.1334	1.2	7.57	2.6	0.4113	2.3	,886	2143	21
52	0,22	132	65	0,51	41.3	1997	±37	1977	± 13	-1	0.12142	0.73	6.08	2.3	0.3631	2.2	,947	1977	13
53	0,21	106	52	0,51	36	2144	±40	2151	± 12	0	0.13403	0.71	7.29	2.3	0.3946	2.2	,951	2151	12
56	2,81	30	50	1,69	12.2	2418	±80	2769	± 95	13	0.193	5.8	12.12	7	0.455	4	,567		
57	3,82	140	113	0,84	40.4	1806	±45	2091	± 75	14	0.1295	4.3	5.77	5.1	0.3233	2.8	,555		
1	0,90	79	71	0,93	23.5	1897	±47	1939	± 54	2	0.1189	3	5.61	4.2	0.3422	2.8	,683	1939	54
2	5,27	190	134	0,73	42.7	1429	±32	1687	±110	18	0.1035	5.9	3.54	6.4	0.2482	2.5	,389		
4	5,06	240	226	0,97	64.7	1678	±35	1973	± 76	18	0.1211	4.3	4.97	4.9	0.2974	2.4	,490		
5	0,92	168	109	0,67	52.7	1989	±41	2108	± 30	6	0.1307	1.7	6.51	3	0.3614	2.4	,820	2108	30
6	0,68	246	684	2,87	51.9	1407	±30	1843	± 33	31	0.1127	1.8	3.79	3	0.2439	2.3	,790		
7	8,17	552	765	1,43	78.5	911	±19	1890	±100	107	0.1156	5.7	2.42	6.1	0.1518	2.3	,374	1890	100
8	10,60	251	221	0,91	65.8	1552	±34	1962	±160	26	0.12	8.9	4.52	9.3	0.2721	2.5	,269	1962	160
9	1,78	214	103	0,50	61.2	1824	±35	2067	± 32	13	0.1277	1.8	5.76	2.9	0.327	2.2	,779		
10	1,71	179	218	1,26	36.5	1354	±27	1722	± 37	27	0.1055	2	3.4	3	0.2337	2.2	,737		
11	3,71	225	119	0,55	59.8	1683	±32	1876	± 66	11	0.1148	3.6	4.72	4.3	0.2983	2.2	,516		
12	1,17	195	47	0,25	56.7	1856	±35	2026	± 26	9	0.1248	1.4	5.74	2.6	0.3337	2.2	,832	2026	26
13	4,28	240	235	1,01	66.2	1731	±33	2022	± 51	17	0.1245	2.9	5.29	3.6	0.308	2.2	,605		
14	21,21	241	245	1,05	58.8	1303	±35	2140	±270	64	0.133	16	4.11	16	0.2241	3	,187		
15	0,56	73	51	0,72	23.4	2034	±41	2052	± 24	1	0.1266	1.4	6.48	2.7	0.3709	2.4	,862	2052	24
16	4,10	303	290	0,99	46.7	1025	±21	1615	± 75	58	0.0995	4	2.37	4.6	0.1724	2.2	,476		
17	0,64	117	103	0,91	34.8	1908	±37	1987	± 24	4	0.1221	1.3	5.8	2.6	0.3445	2.2	,861	1987	24
18	0,72	76	38	0,51	23.6	1978	±40	1941	± 30	-2	0.119	1.7	5.89	2.9	0.359	2.3	,809	1941	30
19	2,72	88	107	1,26	19.1	1426	±31	1804	± 63	27	0.1103	3.5	3.76	4.2	0.2476	2.4	,574		
20	5,76	81	88	1,13	21.4	1647	±35	2077	± 79	26	0.1284	4.5	5.15	5.1	0.291	2.4	,469		

Resumo dos dados de U-Pb da amostra PE-CM-18 (Formação Córrego Pereira).

						Isotope ratios[b]							Ages (Ma)								
Spot number	f 206	Pb ppm	U ppm	Th ppm	Th/U[a]	$^{207}Pb/^{235}U$	1 s [%]	$^{206}Pb/^{238}U$	1 s [%]	Rho[c]	$^{207}Pb/^{206}Pb$[d]	1 s [%]	$^{206}Pb/^{238}U$	1 s abs	$^{207}Pb/^{235}U$	1 s abs	$^{207}Pb/^{206}Pb$	1 s abs	% Conc[e]	Best estimated age (Ma)	
Zr-218-D-IV-01	0,0002	46,8	110,2	15,2	0,14	6,36111	1,77	0,36916	0,88	0,50	0,12497	1,54	2025	18	2027	36	2028	31	100	2028	31
Zr-218-D-IV-02	0,0012	140,9	362,6	64,0	0,18	6,04840	1,38	0,36115	0,73	0,52	0,12147	1,18	1988	14	1983	27	1978	23	100	1978	23
Zr-218-D-IV-03	0,0002	77,8	124,8	48,8	0,39	12,28930	2,21	0,49834	1,95	0,88	0,17886	1,03	2607	51	2627	58	2642	27	99	2642	27
Zr-218-D-IV-04	0,0006	40,0	86,9	46,7	0,54	5,84996	2,78	0,35108	2,21	0,80	0,12085	1,68	1940	43	1954	54	1969	33	99	1969	33
Zr-218-D-IV-05	0,0018	81,5	175,0	129,6	0,75	6,05152	1,64	0,36073	0,85	0,52	0,12167	1,41	1986	17	1983	33	1981	28	100	1981	28
Zr-218-D-IV-07	0,0005	40,5	79,0	23,3	0,30	10,31436	1,85	0,46582	1,04	0,56	0,16059	1,53	2465	26	2463	46	2462	38	100	2462	38
Zr-218-D-IV-08	0,0005	35,4	75,0	64,6	0,87	6,09373	1,90	0,36104	1,06	0,56	0,12241	1,57	1987	21	1989	38	1992	31	100	1992	31
Zr-218-D-IV-09	0,0003	58,4	136,9	63,7	0,47	5,58975	1,74	0,34579	0,84	0,48	0,11724	1,52	1914	16	1915	33	1915	29	100	1915	29
Zr-218-D-IV-10	0,0007	35,4	80,9	37,1	0,46	5,56291	2,17	0,34476	1,04	0,48	0,11703	1,91	1910	20	1910	42	1911	36	100	1911	36
Zr-218-D-IV-11	0,0351	122,9	355,5	286,3	0,81	7,80148	2,58	0,40131	2,40	0,93	0,14099	0,95	2175	52	2208	57	2239	21	97	2239	21
Zr-218-D-IV-12	0,0004	69,1	137,8	153,8	1,12	5,78418	1,90	0,35295	1,07	0,57	0,11886	1,57	1949	21	1944	37	1939	30	100	1939	30
Zr-218-D-IV-13	0,0008	31,1	65,2	47,2	0,73	7,42356	2,23	0,39629	1,13	0,51	0,13586	1,92	2152	24	2164	48	2175	42	99	2175	42
Zr-218-D-IV-14	0,0005	55,4	99,5	26,7	0,27	10,19322	1,76	0,46081	1,19	0,67	0,16043	1,30	2443	29	2452	43	2460	32	99	2460	32
Zr-218-D-IV-15	0,0005	78,1	176,4	70,0	0,40	5,96272	1,70	0,35594	0,83	0,49	0,12150	1,48	1963	16	1970	33	1978	29	99	1978	29
Zr-218-D-IV-18	0,0005	54,6	194,7	95,0	0,49	2,66179	2,14	0,21618	0,90	0,42	0,08930	1,95	1262	11	1318	28	1411	27	89	1411	27
Zr-218-D-IV-19	0,0009	22,0	46,6	10,5	0,23	7,26699	2,20	0,39354	0,86	0,39	0,13393	2,02	2139	18	2145	47	2150	43	99	2150	43
Zr-218-D-IV-20	0,0010	48,9	99,0	81,9	0,83	5,93877	1,89	0,35702	0,83	0,44	0,12064	1,70	1968	16	1967	37	1966	33	100	1966	33
Zr-218-D-IV-21	0,0006	28,7	103,4	44,1	0,43	2,96310	2,41	0,24154	0,79	0,33	0,08897	2,28	1395	11	1398	34	1404	32	99	1404	32
Zr-218-D-IV-22	0,0004	47,7	101,1	51,6	0,51	6,53439	2,00	0,37438	1,22	0,61	0,12659	1,59	2050	25	2051	41	2051	33	100	2051	33
Zr-218-D-IV-23	0,0010	42,6	108,4	61,5	0,57	4,86383	2,34	0,32124	1,02	0,44	0,10981	2,11	1796	18	1796	42	1796	38	100	1796	38

Zr-218-E-V-01	0,0003	46,8	82,8	31,8	0,39	10,10127	1,51	0,45754	0,64	0,42	0,16012	1,37	2429	15	2444	37	2457	34	99	2457	34
Zr-218-E-V-02	0,0003	57,3	136,7	62,9	0,46	5,32994	1,61	0,32741	0,66	0,41	0,11807	1,47	1826	12	1874	30	1927	28	95	1927	28
Zr-218-E-V-03	0,0007	22,4	81,4	32,1	0,40	3,08912	3,03	0,24637	1,18	0,39	0,09094	2,79	1420	17	1430	43	1445	40	98	1445	40
Zr-218-E-V-04	0,0006	33,9	78,0	32,9	0,42	5,79304	2,10	0,34555	0,81	0,38	0,12159	1,94	1913	15	1945	41	1980	38	97	1980	38
Zr-218-E-V-05	0,0002	79,2	172,2	71,9	0,42	6,65642	1,41	0,37696	0,69	0,49	0,12807	1,23	2062	14	2067	29	2072	25	100	2072	25
Zr-218-E-V-06	0,0008	28,2	62,1	82,4	1,33	4,90506	2,43	0,32206	1,19	0,49	0,11046	2,12	1800	21	1803	44	1807	38	100	1807	38
Zr-218-E-V-07	0,0006	38,7	95,7	44,0	0,46	5,77643	1,75	0,34891	0,87	0,49	0,12007	1,53	1929	17	1943	34	1957	30	99	1957	30
Zr-218-E-V-08	0,0004	41,4	92,0	54,2	0,59	6,04157	2,00	0,36086	1,38	0,69	0,12143	1,45	1986	27	1982	40	1977	29	100	1977	29
Zr-218-E-V-10	0,0005	29,3	74,8	26,8	0,36	6,01191	2,29	0,35856	1,26	0,55	0,12160	1,91	1975	25	1978	45	1980	38	100	1980	38
Zr-218-E-V-12	0,0004	48,9	115,6	58,7	0,51	6,00376	1,90	0,35973	0,98	0,51	0,12105	1,63	1981	19	1976	38	1972	32	100	1972	32
Zr-218-E-V-13	0,0010	17,7	56,0	22,6	0,41	4,45365	2,96	0,30203	1,65	0,56	0,10695	2,46	1701	28	1722	51	1748	43	97	1748	43
Zr-218-E-V-14	0,0004	77,7	133,3	54,1	0,41	10,27396	1,92	0,46561	1,60	0,83	0,16004	1,06	2464	39	2460	47	2456	26	100	2456	26
Zr-218-E-V-15	0,0003	112,1	163,1	101,0	0,62	12,72553	1,00	0,51137	0,48	0,48	0,18048	0,88	2662	13	2660	27	2657	23	100	2657	23
Zr-218-E-V-16	0,0006	61,9	153,4	62,6	0,41	5,78570	1,45	0,34777	0,76	0,53	0,12066	1,23	1924	15	1944	28	1966	24	98	1966	24
Zr-218-E-V-17	0,0003	73,7	181,6	76,3	0,42	5,40497	1,63	0,34011	0,94	0,58	0,11526	1,33	1887	18	1886	31	1884	25	100	1884	25
Zr-218-E-V-18	0,0049	96,9	256,2	54,7	0,22	6,15976	2,30	0,35073	1,20	0,52	0,12738	1,97	1938	23	1999	46	2062	41	94	2062	41
Zr-218-E-V-19	0,0011	22,1	54,0	9,8	0,18	5,85768	2,18	0,35272	1,05	0,48	0,12045	1,91	1948	20	1955	43	1963	37	99	1963	37
Zr-218-E-V-20	0,0007	28,2	59,0	55,0	0,94	5,66734	2,13	0,34901	1,33	0,62	0,11777	1,66	1930	26	1926	41	1923	32	100	1923	32
Zr-218-E-V-21	0,0004	60,6	144,2	54,9	0,38	5,69046	1,91	0,34150	1,55	0,81	0,12085	1,12	1894	29	1930	37	1969	22	96	1969	22
Zr-218-E-V-22	0,0007	82,0	179,7	124,0	0,69	6,27744	1,54	0,36640	0,83	0,54	0,12426	1,29	2012	17	2015	31	2018	26	100	2018	26
Zr-218-E-V-23	0,0006	16,0	49,1	28,1	0,58	3,83168	2,86	0,28128	1,33	0,46	0,09880	2,53	1598	21	1599	46	1602	41	100	1602	41
Zr-218-E-V-24	0,0009	67,3	161,1	72,7	0,45	5,93572	1,83	0,35712	1,05	0,58	0,12055	1,49	1969	21	1966	36	1964	29	100	1964	29
Zr-218-E-V-30	0,0005	51,0	112,0	95,1	0,86	6,11382	1,99	0,36148	0,98	0,49	0,12267	1,74	1989	19	1992	40	1995	35	100	1995	35
Zr-218-E-V-38	0,0004	42,2	89,2	128,7	1,45	5,81509	2,21	0,35349	1,59	0,72	0,11931	1,54	1951	31	1949	43	1946	30	100	1946	30
Zr-218-E-V-40	0,0006	43,2	101,8	76,4	0,76	5,41880	1,71	0,33867	0,96	0,56	0,11604	1,41	1880	18	1888	32	1896	27	99	1896	27
Zr-218-F-VI-02	0,0008	46,5	105,8	65,9	0,63	5,64071	2,39	0,34256	1,08	0,45	0,11942	2,13	1899	20	1922	46	1948	42	98	1948	42
Zr-218-F-VI-03	0,0001	138,8	213,8	58,7	0,28	12,70993	1,64	0,50659	1,34	0,82	0,18197	0,95	2642	35	2658	44	2671	25	99	2671	25

Zr-218-F-VI-04	0,0008	52,1	139,5	97,8	0,71	4,59283	2,37	0,30889	1,40	0,59	0,10784	1,92	1735	24	1748	42	1763	34	98	1763	34
Zr-218-F-VI-06	0,0008	36,9	93,5	44,7	0,48	4,84914	1,96	0,32124	0,88	0,45	0,10948	1,76	1796	16	1793	35	1791	31	100	1791	31
Zr-218-F-VI-07	0,0004	47,7	111,3	39,9	0,36	5,79416	2,14	0,35163	1,48	0,69	0,11951	1,55	1942	29	1946	42	1949	30	100	1949	30
Zr-218-F-VI-09	0,0005	62,9	149,5	73,5	0,49	5,54295	1,69	0,34200	0,79	0,47	0,11755	1,50	1896	15	1907	32	1919	29	99	1919	29
Zr-218-F-VI-12	0,0003	86,0	151,4	57,3	0,38	10,13634	1,40	0,46121	0,76	0,54	0,15940	1,17	2445	18	2447	34	2449	29	100	2449	29
Zr-218-F-VI-13	0,0007	29,6	77,3	19,2	0,25	5,61521	2,17	0,34449	1,29	0,59	0,11822	1,74	1908	25	1918	42	1929	34	99	1929	34
Zr-218-F-VI-15	0,0006	54,3	126,4	62,4	0,50	5,35098	1,83	0,33718	1,07	0,59	0,11510	1,48	1873	20	1877	34	1881	28	100	1881	28
Zr-218-F-VI-17	0,0004	59,3	169,5	93,5	0,56	3,99253	1,63	0,28884	0,98	0,60	0,10025	1,30	1636	16	1633	27	1629	21	100	1629	21
Zr-218-F-VI-18	0,0003	104,7	151,5	112,1	0,75	13,71533	1,38	0,52871	0,95	0,69	0,18814	1,00	2736	26	2730	38	2726	27	100	2726	27
Zr-218-F-VI-19	0,0005	48,0	121,1	78,9	0,66	4,88388	2,05	0,32275	1,08	0,53	0,10975	1,74	1803	20	1799	37	1795	31	100	1795	31
Zr-218-F-VI-22	0,0006	58,7	88,5	50,5	0,57	12,99026	1,45	0,51682	1,04	0,72	0,18229	1,00	2686	28	2679	39	2674	27	100	2674	27
Zr-218-F-VI-24	0,0003	114,9	139,0	166,3	1,21	15,19012	1,26	0,54250	0,88	0,70	0,20308	0,90	2794	25	2827	36	2851	26	98	2851	26
Zr-218-F-VI-25	0,0006	39,9	81,7	52,2	0,64	6,94542	1,92	0,38705	1,06	0,55	0,13014	1,60	2109	22	2104	40	2100	34	100	2100	34
Zr-218-F-VI-26	0,0006	41,9	110,6	27,6	0,25	5,36733	1,76	0,33931	0,98	0,56	0,11473	1,46	1883	18	1880	33	1876	27	100	1876	27
Zr-218-F-VI-28	0,0005	33,7	77,3	31,9	0,42	6,31314	2,05	0,36793	1,08	0,52	0,12445	1,75	2020	22	2020	41	2021	35	100	2021	35
Zr-218-F-VI-30	0,0023	50,1	115,0	80,5	0,70	6,00033	2,00	0,35792	1,15	0,58	0,12159	1,64	1972	23	1976	40	1980	32	100	1980	32
Zr-218-F-VI-31	0,0004	42,8	87,2	48,6	0,56	7,11767	1,63	0,39189	0,90	0,55	0,13173	1,36	2132	19	2126	35	2121	29	100	2121	29
Zr-218-F-VI-33	0,0005	32,3	69,3	60,8	0,88	6,02269	2,16	0,35847	1,20	0,55	0,12185	1,80	1975	24	1979	43	1984	36	100	1984	36
Zr-218-F-VI-35	0,0003	53,9	143,9	62,8	0,44	4,86105	1,79	0,32100	0,84	0,47	0,10983	1,59	1795	15	1796	32	1797	29	100	1797	29
Zr-218-F-VI-36	0,0006	34,2	77,2	25,2	0,33	6,66386	2,38	0,37758	1,35	0,57	0,12800	1,96	2065	28	2068	49	2071	41	100	2071	41
Zr-218-F-VI-37	0,0004	66,9	167,5	109,5	0,66	4,87350	1,83	0,32096	1,13	0,62	0,11013	1,44	1794	20	1798	33	1802	26	100	1802	26
Zr-218-F-VI-39	0,0005	56,2	105,4	151,1	1,44	5,77567	1,87	0,35158	1,13	0,60	0,11915	1,49	1942	22	1943	36	1943	29	100	1943	29

Resumo dos dados de U-Pb da amostra PE-CM-54 (Formação Rio Pardo Grande).

						Isotope ratios[b]							**Ages (Ma)**								
Spot number	f 206	Pb ppm	U ppm	Th ppm	Th/U[a]	^{207}Pb/^{235}U	1 s [%]	^{206}Pb/^{238}U	1 s [%]	Rho[c]	^{207}Pb/^{206}Pb[d]	1 s [%]	^{206}Pb/^{238}U	1 s abs	^{207}Pb/^{235}U	1 s abs	^{207}Pb/^{206}Pb	1 s abs	% Conc[e]	Best estimated age (Ma)	
003 ZR236_C_III_03.static.exp	0,0009	16,5	42,6	31,7	0,75	5,96329	4,04	0,35654	1,70	0,42	0,12131	3,67	1966	33	1971	80	1976	72	100	1976	72
004 ZR236_C_III_04.static.exp	0,0013	46,9	112,6	62,6	0,56	6,70855	4,22	0,38078	2,10	0,50	0,12778	3,66	2080	44	2074	88	2068	76	101	2068	76
005 ZR236_C_III_05.static.exp	0,0013	24,7	72,3	56,5	0,79	4,76411	5,19	0,31957	1,59	0,31	0,10812	4,94	1788	28	1779	92	1768	87	101	1768	87
006 ZR236_C_III_07.static.exp	0,0023	30,0	86,4	52,7	0,61	5,66576	7,49	0,34638	1,56	0,21	0,11863	7,33	1917	30	1926	144	1936	142	99	1936	142
007 ZR236_C_III_01.static.exp	0,0010	39,9	108,4	43,8	0,41	5,46344	4,32	0,34016	1,85	0,43	0,11649	3,91	1887	35	1895	82	1903	74	99	1903	74
008 ZR236_C_III_02.static.exp	0,0004	78,7	153,2	43,3	0,28	10,00196	2,26	0,45924	1,52	0,67	0,15796	1,67	2436	37	2435	55	2434	41	100	2434	41
009 ZR236_C_III_08.static.exp	0,0018	25,0	65,9	43,6	0,67	5,64160	5,75	0,34711	1,62	0,28	0,11788	5,52	1921	31	1922	111	1924	106	100	1924	106
010 ZR236_C_III_09.static.exp	0,0025	18,4	48,0	32,3	0,68	6,10038	7,42	0,36142	1,70	0,23	0,12242	7,23	1989	34	1990	148	1992	144	100	1992	144
011 ZR236_C_III_10.static.exp	0,0024	17,1	48,3	21,1	0,44	5,53112	7,78	0,34131	2,10	0,27	0,11753	7,49	1893	40	1905	148	1919	144	99	1919	144
012 ZR236_C_III_11.static.exp	0,0017	31,0	89,3	56,6	0,64	5,40682	5,60	0,33923	1,73	0,31	0,11560	5,32	1883	33	1886	106	1889	101	100	1889	101
015 ZR236_C_III_13.static.exp	0,0004	27,5	80,1	47,5	0,60	6,17595	3,56	0,36287	2,50	0,70	0,12344	2,53	1996	50	2001	71	2007	51	99	2007	51
016 ZR236_C_III_15.static.exp	0,0006	39,4	117,4	89,3	0,77	5,14688	2,46	0,33119	1,58	0,64	0,11271	1,88	1844	29	1844	45	1844	35	100	1844	35
017 ZR236_C_III_16.static.exp	0,0012	15,4	40,2	45,2	1,13	5,87085	5,43	0,35416	1,55	0,29	0,12023	5,20	1954	30	1957	106	1960	102	100	1960	102
018 ZR236_C_III_19.static.exp	0,0019	26,6	77,0	43,7	0,57	6,33247	6,84	0,36869	2,34	0,34	0,12457	6,42	2023	47	2023	138	2023	130	100	2023	130
020 ZR236_C_III_20N.static.exp	0,0005	31,8	92,3	46,2	0,50	5,95871	2,73	0,35555	1,00	0,37	0,12155	2,54	1961	20	1970	54	1979	50	99	1979	50
021 ZR236_C_III_21.static.exp	0,0022	10,9	35,3	26,2	0,75	5,24012	11,59	0,33482	4,69	0,40	0,11351	10,60	1862	87	1859	216	1856	197	100	1856	197
022 ZR236_C_III_22.static.exp	0,0013	12,3	35,6	31,3	0,88	5,77009	6,62	0,35080	2,27	0,34	0,11930	6,22	1938	44	1942	129	1946	121	100	1946	121
023 ZR236_C_III_25.static.exp	0,0005	43,5	125,6	105,5	0,85	5,27446	3,35	0,33492	1,91	0,57	0,11422	2,76	1862	36	1865	63	1868	51	100	1868	51
024 ZR236_C_III_26.static.exp	0,0003	48,1	126,8	56,5	0,45	6,12654	2,86	0,36215	1,40	0,49	0,12269	2,50	1992	28	1994	57	1996	50	100	1996	50
027 ZR236_C_III_27.static.exp	0,0021	32,6	87,8	48,1	0,55	5,64414	6,05	0,34730	2,61	0,43	0,11787	5,46	1922	50	1923	116	1924	105	100	1924	105

028 ZR236_C_III_28.static.exp	0,0002	32,4	95,0	54,2	0,57	4,96179	2,62	0,32538	1,45	0,56	0,11060	2,18	1816	26	1813	47	1809	39	100	1809	39
029 ZR236_D_IV_01t.static.exp	0,0019	19,8	54,9	43,2	0,79	5,71903	6,50	0,34969	1,39	0,21	0,11861	6,35	1933	27	1934	126	1935	123	100	1935	123
030 ZR236_D_IV_02.static.exp	0,0014	14,5	41,6	25,3	0,61	5,70949	7,06	0,34768	1,76	0,25	0,11910	6,84	1924	34	1933	136	1943	133	99	1943	133
031 ZR236_D_IV_03.static.exp	0,0007	25,9	76,2	51,6	0,68	5,29874	4,41	0,33557	1,24	0,28	0,11452	4,23	1865	23	1869	82	1872	79	100	1872	79
032 ZR236_D_IV_05.static.exp	0,0004	37,1	105,6	43,9	0,42	5,53378	3,17	0,34317	1,41	0,44	0,11695	2,84	1902	27	1906	60	1910	54	100	1910	54
033 ZR236_D_IV_06.static.exp	0,0012	112,1	204,5	202,2	1,00	15,94359	1,30	0,56024	0,83	0,64	0,20640	1,00	2868	24	2873	37	2878	29	100	2878	29
034 ZR236_D_IV_07.static.exp	0,0019	21,6	47,7	34,0	0,72	9,87688	4,96	0,45581	1,74	0,35	0,15716	4,64	2421	42	2423	120	2425	113	100	2425	113
035 ZR236_D_IV_08.static.exp	0,0010	35,5	99,2	60,5	0,61	5,71337	3,82	0,34868	1,10	0,29	0,11884	3,66	1928	21	1933	74	1939	71	99	1939	71
036 ZR236_D_IV_09.static.exp	0,0007	47,1	142,5	65,0	0,46	5,71071	3,38	0,34973	1,41	0,42	0,11843	3,08	1933	27	1933	65	1933	59	100	1933	59
039 ZR236_D_IV_11.static.exp	0,0005	50,2	149,7	154,1	1,04	5,52031	3,21	0,34290	0,81	0,25	0,11676	3,11	1901	15	1904	61	1907	59	100	1907	59
040 ZR236_D_IV_13.static.exp	0,0003	7,0	30,4	12,5	0,41	3,56763	5,29	0,26959	3,66	0,69	0,09598	3,82	1539	56	1542	82	1547	59	99	1547	59
041 ZR236_D_IV_14.static.exp	0,0013	19,8	59,2	25,2	0,43	5,68141	8,77	0,34717	6,55	0,75	0,11869	5,83	1921	126	1929	169	1937	113	99	1937	113
042 ZR236_D_IV_15.static.exp	0,0048	33,2	119,8	67,6	0,57	4,26196	8,56	0,29516	3,16	0,37	0,10473	7,96	1667	53	1686	144	1709	136	98	1709	136
043 ZR236_D_IV_17.static.exp	0,0014	11,7	37,6	14,4	0,39	5,48532	7,08	0,34179	2,53	0,36	0,11640	6,61	1895	48	1898	134	1902	126	100	1902	126
044 ZR236_D_IV_18.static.exp	0,0008	40,9	113,9	78,5	0,69	6,61749	3,15	0,37714	1,14	0,36	0,12726	2,94	2063	23	2062	65	2060	61	100	2060	61
045 ZR236_D_IV_20.static.exp	0,0022	14,2	40,4	9,1	0,23	6,09815	10,31	0,36151	6,29	0,61	0,12234	8,17	1989	125	1990	205	1991	163	100	1991	163
046 ZR236_D_IV_22.static.exp	0,0007	37,0	141,3	78,3	0,56	2,97381	4,87	0,24285	1,42	0,29	0,08881	4,66	1401	20	1401	68	1400	65	100	1400	65
048 ZR236_D_IV_25.static.exp	0,0009	30,0	79,3	62,4	0,79	5,71407	4,05	0,34800	2,05	0,51	0,11909	3,49	1925	39	1933	78	1943	68	99	1943	68
051 ZR236_D_IV_27.static.exp	0,0005	31,6	74,7	30,3	0,41	7,09683	2,93	0,38968	1,99	0,68	0,13209	2,15	2121	42	2124	62	2126	46	100	2126	46
052 ZR236_D_IV_28.static.exp	0,0006	53,1	140,8	117,4	0,84	5,79861	3,00	0,35186	1,27	0,42	0,11952	2,72	1943	25	1946	58	1949	53	100	1949	53
041 ZR236_D_IV_14.static.exp	0,0005	19,4	57,8	26,4	0,46	6,11544	3,50	0,36171	2,16	0,62	0,12262	2,76	1990	43	1992	70	1995	55	100	1995	55
042 ZR236_D_IV_15.static.exp	0,0050	32,3	116,6	69,9	0,60	4,26083	8,52	0,29622	5,59	0,66	0,10432	6,44	1673	93	1686	144	1702	110	98	1702	110
043 ZR236_D_IV_17.static.exp	0,0020	11,3	36,0	15,6	0,44	5,27155	9,40	0,33582	1,93	0,20	0,11385	9,21	1867	36	1864	175	1862	171	100	1862	171
044 ZR236_D_IV_18.static.exp	0,0008	39,5	111,4	80,5	0,73	6,56266	5,27	0,37396	4,13	0,78	0,12728	3,28	2048	85	2054	108	2061	68	99	2061	68
045 ZR236_D_IV_20.static.exp	0,0019	13,8	39,5	10,0	0,25	6,33961	9,37	0,37119	6,91	0,74	0,12387	6,33	2035	141	2024	190	2013	127	101	2013	127
046 ZR236_D_IV_22.static.exp	0,0001	37,3	145,0	84,6	0,59	3,23673	3,14	0,25600	1,15	0,37	0,09170	2,92	1469	17	1466	46	1461	43	101	1461	43
048 ZR236_D_IV_25.static.exp	0,0008	29,1	77,1	65,2	0,85	5,83071	3,39	0,35310	1,98	0,58	0,11976	2,75	1949	39	1951	66	1953	54	100	1953	54

[a] Th/U ratios are calculated relative to GJ-1 reference zircon

[b] Corrected for background and within-run Pb/U fractionation and normalised to reference zircon GJ-1 (ID-TIMS values/measured value); 207Pb/235U calculated using ($^{207}Pb/^{206}Pb$)/($^{238}U/^{206}Pb$ * 1/137.88)

[c]Rho is the error correlation defined as the quotient of the propagated errors of the $^{206}Pb/^{238}U$ and the $^{207}/^{235}U$ ratio
[d]Corrected for mass-bias by normalising to GJ-1 reference zircon and common Pb using the model Pb composition of Stacey and Kramers (1975)

[e]Degree of concordance = ($^{206}Pb/^{238}U$ age * 100/$^{207}Pb/^{206}U$ age)

Errors are 1-sigma; Pb_c and Pb^* indicate the common and radiogenic portions, respectively.

Error in Standard calibration was 0.37%(not included in above errors but required when comparing data from different mounts).

(1) Common Pb corrected using measured ^{204}Pb.

Apêndice E

Resumo dos dados de Lu-Hf das amostras analisadas.

Sample	U/Pb Age		Sample (Present day ratios)				Sample Initial Ratios				DM Model Ages (Ga)		SigHf b
	(Ma)	±2σ	$^{176}Hf/^{177}Hf$	±2S	$^{176}Lu/^{177}Hf$	±2S	$^{176}Hf/^{177}Hf$ (t)	eHf(0)	eHf(t)	±2SE	T DM	T DM Crustal[d]	(V)
Schist GO-1													
Barão de Guacuí													
D-6.1	2933	85	0.280904	16	0.00104	9	0.280846	-66.51	-1.72	0.07	3.23	3.43	18
D-10.1	2806	9	0.280934	17	0.00249	22	0.280801	-65.44	-6.31	0.08	3.31	3.62	15
D-15.1	2692	9	0.281026	14	0.00168	12	0.280939	-62.21	-4.06	0.04	3.12	3.39	23
D-18.1	2714	10	0.281045	18	0.00214	18	0.280933	-61.55	-3.74	0.05	3.13	3.38	10
D-22.1	2726	18	0.280931	16	0.00058	6	0.280900	-65.58	-4.65	0.08	3.16	3.45	12
D-23.1	2815	8	0.280829	169	0.00095	14	0.280777	-69.18	-6.92	0.13	3.32	3.66	4
D-33.1	2114	13	0.280991	15	0.00211	13	0.280907	-63.43	-18.68	0.23	3.20	3.84	18
D-34.1	2884	14	0.280822	17	0.00412	37	0.280595	-69.40	-11.80	0.16	3.62	4.02	21
E-1.1	2711	21	0.280943	11	0.00096	6	0.280894	-65.12	-5.22	0.07	3.17	3.47	24
E-3.1	3131	7	0.280794	18	0.00323	50	0.280600	-70.39	-5.78	0.10	3.58	3.83	15
F-1.1	2946	10	0.280846	14	0.00079	5	0.280801	-68.58	-3.00	0.03	3.29	3.52	21
F-2.1	2124	12	0.281518	15	0.00153	19	0.281456	-44.80	1.08	0.02	2.43	2.63	24
F-7.1	2933	13	0.281319	18	0.00444	30	0.281069	-51.84	6.24	0.07	2.93	2.93	17
E-8.1	2726	16	0.281003	19	0.00224	17	0.280886	-63.02	-5.15	0.07	3.19	3.48	22
E-18.1	2899	8	0.280840	13	0.00040	2	0.280817	-68.80	-3.53	0.03	3.26	3.51	21
Gneiss GO-65													
Gouveia Complex													
A-2.1	2828	43	0.281040	16	0.00149	9	0.280959	-61.72	-0.15	0.01	3.08	3.25	14
A-4.1	2828	43	0.281028	17	0.00171	11	0.280935	-62.15	-1.02	0.08	3.12	3.30	13

A-6.1	2828	43	0.281018	17	0.00134	8	0.280946	-62.47	-0.63	0.05	3.10	3.28	16
A-8.1	2828	43	0.281120	17	0.00222	13	0.280999	-58.88	1.28	0.10	3.03	3.16	15
A-10.1	2828	43	0.281051	16	0.00169	11	0.280959	-61.32	-0.15	0.01	3.08	3.25	16
A-14.1	2828	43	0.281116	17	0.00276	18	0.280966	-59.02	0.10	0.01	3.08	3.23	18
A-18.1	2828	43	0.281071	12	0.00168	11	0.280980	-60.62	0.59	0.05	3.06	3.20	18
PE-GO-30 A													
Bandeirinha Fm													
A-1.1	2675	8	0.280964	12	0.00116	16	0.280904	-64.41	-5.69	0.10	3.16	3.48	18
A-4.1	2660	8	0.280882	16	0.00066	4	0.280848	-67.29	-8.04	0.07	3.23	3.61	17
A-5.1	2858	7	0.280918	16	0.00077	10	0.280876	-66.01	-2.41	0.04	3.19	3.41	17
A-11.1	1787	18	0.281250	20	0.00047	3	0.281234	-54.29	-14.60	0.25	2.72	3.34	15
A-12.1	3306	5	0.280777	18	0.00190	11	0.280656	-71.02	0.36	0.00	3.47	3.58	13
A-13.1	1773	20	0.281257	13	0.00043	3	0.281243	-54.02	-14.60	0.27	2.71	3.33	15
A-16.1	1777	27	0.281201	21	0.00077	5	0.281175	-56.02	-16.93	0.36	2.81	3.47	10
A-19.1	2660	6	0.280932	14	0.00087	5	0.280888	-65.53	-6.63	0.06	3.18	3.52	17
A-21.1	2686	6	0.280988	16	0.00082	7	0.280946	-63.56	-3.97	0.04	3.10	3.38	15
A-22.1	2680	6	0.280903	14	0.00059	4	0.280873	-66.55	-6.70	0.06	3.19	3.54	16
A-24.1	2650	5	0.281331	13	0.00042	3	0.281310	-51.41	8.15	0.07	2.61	2.59	18
B-28.1	2839	6	0.280914	19	0.00097	6	0.280862	-66.15	-3.36	0.03	3.21	3.46	10
B-11.1	2131	9	0.281548	18	0.00073	4	0.281518	-43.76	3.44	0.04	2.34	2.48	11
B-4.1	1745	17	0.281752	16	0.00168	11	0.281696	-36.55	0.84	0.01	2.12	2.35	13
B-2.1	1756	21	0.281246	15	0.00052	3	0.281228	-54.43	-15.51	0.28	2.73	3.37	12
B-1.1	2670	9	0.280979	16	0.00056	3	0.280950	-63.87	-4.18	0.04	3.09	3.38	15
C-33.1	2420	7	0.281257	17	0.00052	4	0.281233	-54.05	0.02	0.00	2.72	2.92	11
C-26.1	2416	12	0.281348	20	0.00070	4	0.281316	-50.82	2.87	0.03	2.61	2.74	11
C-24.1	2115	10	0.281079	24	0.00072	6	0.281050	-60.33	-13.56	0.17	2.97	3.53	11
PE-GO-28													
Bandeirinha Fm													
D-26.1	2508	6	0.281299	16	0.00088	14	0.281257	-52.54	2.95	0.05	2.69	2.81	15
D-8.1	2717	6	0.280993	22	0.00110	9	0.280936	-63.37	-3.60	0.04	3.11	3.38	11

D-7.1	2473	8	0.281341	14	0.00036	3	0.281324	-51.08	4.49	0.05	2.60	2.68	18
D-3.1	2088	22	0.281300	15	0.00192	13	0.281224	-52.52	-8.02	0.14	2.76	3.17	17
D-1.1	2089	9	0.281415	18	0.00109	7	0.281371	-48.46	-2.74	0.03	2.55	2.84	12
E-4.1	2699	6	0.280914	17	0.00096	6	0.280865	-66.16	-6.54	0.06	3.21	3.55	18
E-18.1	2715	6	0.281007	17	0.00108	11	0.280951	-62.87	-3.09	0.04	3.09	3.34	18
E-23.1	2112	47	0.281513	16	0.00102	7	0.281472	-44.98	1.37	0.04	2.41	2.60	16
E-39	2075	14	0.281477	18	0.00336	40	0.281344	-46.27	-4.05	0.08	2.62	2.91	16
E-33.1	2451	8	0.281145	17	0.00362	38	0.280975	-58.01	-8.41	0.12	3.11	3.47	19
F-40.1	3271	5	0.280604	17	0.00070	4	0.280560	-77.12	-3.90	0.03	3.60	3.82	16
F-35.1	2015	9	0.281090	21	0.00071	5	0.281063	-59.94	-15.43	0.17	2.95	3.57	14
F-29.1	2197	13	0.281426	15	0.00045	3	0.281407	-48.06	1.03	0.01	2.49	2.69	14
F-19.1	2461	8	0.281299	17	0.00039	2	0.281281	-52.54	2.69	0.03	2.65	2.79	20
F-17.1	2704	7	0.280969	16	0.00092	7	0.280922	-64.21	-4.40	0.04	3.13	3.42	15
F-4.1	3078	4	0.281438	18	0.00332	20	0.281242	-47.62	15.82	0.12	2.67	2.43	20
F-1.1	2229	11	0.281272	17	0.00128	8	0.281217	-53.51	-4.97	0.06	2.75	3.09	18
PE-SM-07 São João da Chapada Fm.													
A-37.1	2492	71	0.281314	15	0.00020	1	0.281304	-52.02	4.25	0.15	2.62	2.71	16
A-27.1	1684	11	0.281483	15	0.00130	8	0.281442	-46.03	-9.58	0.12	2.47	2.95	15
A-24.1	2460	7	0.281128	13	0.00150	9	0.281057	-58.61	-5.28	0.05	2.96	3.28	19
A-21.1	2151	23	0.281528	15	0.00065	4	0.281502	-44.43	3.33	0.06	2.36	2.51	14
A-9.1	2824	9	0.281014	16	0.00108	10	0.280955	-62.63	-0.38	0.00	3.08	3.26	20
A-7.1	2148	18	0.281561	17	0.00103	10	0.281519	-43.28	3.86	0.07	2.34	2.47	17
A-6.1	2935	11	0.280891	14	0.00052	3	0.280862	-66.97	-1.08	0.01	3.20	3.39	17
A-5.1	2716	9	0.281088	14	0.00114	7	0.281029	-60.01	-0.30	0.00	2.99	3.17	16
A-4.1	2880	11	0.280972	15	0.00107	7	0.280913	-64.12	-0.58	0.01	3.14	3.32	17
A-3.1	2702	9	0.281531	17	0.00159	11	0.281448	-44.35	14.30	0.14	2.42	2.24	15
B-18.1	2760	15	0.281088	16	0.00166	13	0.281001	-60.00	-0.27	0.00	3.03	3.20	14
B-17.1	1698	17	0.281502	19	0.00109	8	0.281467	-45.36	-8.36	0.15	2.43	2.88	12

PE-SM-06													
Hematite Phyllite													
A-1.1	2155	7	0.281527	15	0.00053	3	0.281505	-44.50	3.52	0.03	2.36	2.50	18
A-2.1	2682	48	0.280871	16	0.00062	4	0.280839	-67.68	-7.84	0.19	3.24	3.62	16
A-3.1	2154	44	0.281534	15	0.00122	8	0.281484	-44.23	2.77	0.07	2.39	2.54	20
A-4.1	2105	22	0.281554	14	0.00089	7	0.281518	-43.53	2.84	0.05	2.34	2.50	17
A-5.1	2685	58	0.280853	14	0.00061	4	0.280821	-68.33	-8.42	0.24	3.26	3.65	18
A-6.1	2186	40	0.281553	14	0.00105	6	0.281509	-43.58	4.39	0.11	2.36	2.47	17
A-7.1	2126	28	0.281506	18	0.00127	15	0.281455	-45.22	1.07	0.03	2.43	2.63	12
A-8.1	2081	29	0.281579	13	0.00143	9	0.281522	-42.65	2.42	0.05	2.34	2.51	20
A-11.1	2172	42	0.280968	20	0.00251	16	0.280864	-64.25	-18.84	0.49	3.27	3.90	11
A-13.1	2689	38	0.281643	21	0.00360	23	0.281458	-40.37	14.34	0.30	2.39	2.22	16
A-10.1	1718	47	0.281571	14	0.00110	7	0.281536	-42.92	-5.48	0.19	2.33	2.72	14
A-17.1	2125	46	0.281482	32	0.00082	14	0.281449	-46.09	0.83	0.03	2.44	2.64	6
A-18.1	1718	47	0.281554	62	0.00124	8	0.281514	-43.53	-6.25	0.21	2.37	2.77	6
A-19.1	1778	37	0.281565	82	0.00129	11	0.281521	-43.15	-4.60	0.13	2.35	2.71	5
A-20.1	2195	115	0.281470	22	0.00080	9	0.281437	-46.49	2.04	0.13	2.45	2.62	10
PE-GO-59-SB													
Sopa-Brumadinho Fm.													
E-1.1	2710	65	0.281060	16	0.00164	10	0.280975	-61.00	-2.37	0.07	3.07	3.30	17
E-3.1	2897	50	0.280869	12	0.00062	4	0.280835	-67.74	-2.93	0.07	3.24	3.48	24
E-6.1	2677	61	0.280910	13	0.00076	5	0.280872	-66.29	-6.81	0.20	3.20	3.55	21
E-7.1	1371	89	0.281340	13	0.00088	9	0.281317	-51.09	-21.15	1.59	2.63	3.42	21
E-8.1	2091	104	0.281549	17	0.00041	3	0.281533	-43.71	3.03	0.17	2.32	2.48	21
E-23.1	2105	66	0.281561	12	0.00082	6	0.281528	-43.28	3.20	0.12	2.33	2.48	18
E-24.1	2090	96	0.281550	15	0.00078	5	0.281519	-43.66	2.54	0.13	2.34	2.51	20
E-29.1	1878	51	0.281112	14	0.00042	3	0.281097	-59.15	-17.35	0.59	2.90	3.58	14
E-34.1	2101	53	0.281582	16	0.00120	7	0.281534	-42.54	3.31	0.10	2.32	2.47	15
E-39.1	1678	68	0.281615	18	0.00561	37	0.281436	-41.39	-9.93	0.47	2.58	2.97	18
D-38.1	2944	47	0.280872	14	0.00058	4	0.280839	-67.67	-1.70	0.04	3.23	3.43	21
D-33.1	2566	67	0.280886	14	0.00118	12	0.280828	-67.17	-10.96	0.40	3.26	3.72	21

D-32.1	2641	36	0.280913	14	0.00103	10	0.280861	-66.21	-8.04	0.19	3.22	3.60	21
D-31.1	2017	61	0.281679	15	0.00299	19	0.281564	-39.12	2.43	0.09	2.30	2.46	17
D-30.1	1440	121	0.281014	17	0.00108	9	0.280984	-62.64	-31.41	2.89	3.08	4.09	18
D-24.1	3382	73	0.280418	15	0.00194	20	0.280291	-83.72	-10.83	0.35	3.97	4.34	24
D-25.1	2823	80	0.280974	15	0.00113	7	0.280913	-64.04	-1.92	0.07	3.14	3.35	19
D-19.1	2581	68	0.281235	21	0.00221	15	0.281126	-54.81	0.00	0.00	2.87	3.05	16
D-10.1	2016	61	0.281427	15	0.00128	8	0.281377	-48.04	-4.22	0.16	2.54	2.87	20
D-11.1	1256	59	0.281506	15	0.00065	4	0.281491	-45.22	-17.62	0.94	2.39	3.11	20
PE-EX-34 C Matrix													
Sopa-Brumadinho Fm.													
A-1.1	2155	37	0.281009	15	0.00049	3	0.280989	-62.82	-14.82	0.35	3.05	3.64	17
A-4.1	2133	33	0.281575	16	0.00116	7	0.281528	-42.78	3.85	0.08	2.33	2.46	14
A-11.1	2690	47	0.280991	13	0.00052	3	0.280964	-63.45	-3.21	0.08	3.07	3.33	17
A-18.1	2110	29	0.281474	15	0.00053	5	0.281453	-46.37	0.63	0.01	2.43	2.64	15
C-1.1	2773	18	0.281000	15	0.00054	4	0.280971	-63.13	-1.02	0.01	3.06	3.26	17
C-3.1	2127	37	0.281415	14	0.00068	4	0.281387	-48.44	-1.29	0.03	2.52	2.78	19
C-14.1	2169	31	0.281563	14	0.00131	11	0.281509	-43.20	4.00	0.09	2.36	2.48	20
C-22.1	1224	29	0.281913	16	0.00080	5	0.281894	-30.85	-4.05	0.12	1.85	2.25	16
C-25.1	2062	89	0.281521	18	0.00117	10	0.281475	-44.69	0.32	0.02	2.41	2.63	15
PE-EX-34 D Matrix													
Sopa-Brumadinho Fm.*													
A1	1176	19	0.28193	0	0.00079	0	0.281917	-30.09	-4.34	0.42	1.82	2.23	
A2	1303	16	0.28201	0	0.00050	0	0.281995	-27.51	1.32	0.33	1.71	1.97	
A3	2175	20	0.28151	0	0.00078	0	0.281473	-45.24	2.87	0.05	2.40	2.55	
A5	2161	17	0.28141	0	0.00062	0	0.281384	-48.66	-0.64	0.03	2.52	2.76	
A6	1842	27	0.28136	0	0.00057	0	0.281343	-50.28	-9.45	0.23	2.58	3.06	
A7	1765	57	0.28110	0	0.00046	0	0.281089	-59.42	-20.24	0.82	2.92	3.67	
A8	1761	29	0.28142	0	0.00071	0	0.281392	-48.41	-9.57	0.49	2.52	3.01	
A9	2649	18	0.28075	0	0.00037	0	0.280729	-72.02	-12.52	0.22	3.38	3.88	
A10	1198	19	0.28167	0	0.00052	0	0.281655	-39.56	-13.13	0.34	2.17	2.79	

A12	1188	17	0.28128	0	0.00076	0	0.281264	-53.19	-27.22	1.10	2.70	3.64	
A13	1227	27	0.28188	0	0.00039	0	0.281866	-32.17	-4.97	0.21	1.88	2.31	
A14	1187	19	0.28182	0	0.00058	0	0.281807	-34.14	-7.99	0.16	1.97	2.46	
A15	2056	15	0.28099	0	0.00024	0	0.280977	-63.61	-17.53	0.51	3.06	3.73	
A16	2121	13	0.28141	0	0.00044	0	0.281395	-48.51	-1.15	0.02	2.51	2.76	
A19	1176	22	0.28149	0	0.00053	0	0.281474	-45.93	-20.03	1.42	2.41	3.20	
A20	2121	13	0.28086	0	0.00047	0	0.280844	-67.98	-20.75	0.37	3.24	3.98	
A22	1176	15	0.28184	0	0.00037	0	0.281831	-33.44	-7.37	0.43	1.93	2.42	
A23	1174	24	0.28206	0	0.00057	0	0.282043	-25.80	0.08	0.00	1.65	1.95	
A24	1164	39	0.28214	0	0.00103	0	0.282115	-22.91	2.40	0.42	1.56	1.80	
A26	2077	20	0.28149	0	0.00052	0	0.281471	-45.74	0.52	0.01	2.41	2.63	
A27	1178	14	0.28191	0	0.00096	0	0.281888	-30.98	-5.33	0.93	1.87	2.29	
A28	2116	14	0.28138	0	0.00041	0	0.281366	-49.60	-2.32	0.03	2.54	2.83	
A30	2121	29	0.28146	0	0.00044	0	0.281441	-46.92	0.46	0.01	2.44	2.66	
A32	2654	16	0.28108	0	0.00064	0	0.281046	-60.35	-1.14	0.07	2.96	3.18	
A33	2617	16	0.28101	0	0.00096	0	0.280957	-62.92	-5.17	0.17	3.09	3.40	
A34	1227	39	0.28218	0	0.00159	0	0.282139	-21.54	4.70	0.52	1.52	1.70	
A35	2100	20	0.28119	0	0.00069	0	0.281167	-56.24	-9.74	0.73	2.81	3.28	
A36	1948	15	0.28157	0	0.00086	0	0.281538	-42.97	-0.09	0.00	2.32	2.56	
A37	2100	20	0.28116	0	0.00064	0	0.281134	-57.46	-10.91	0.60	2.86	3.35	
A38	1195	19	0.28195	0	0.00077	0	0.281930	-29.62	-3.44	0.37	1.80	2.19	
A39	1877	5	0.28157	0	0.00103	0	0.281530	-43.08	-2.01	0.26	2.34	2.63	
A40	2652	24	0.28114	0	0.00067	0	0.281105	-58.22	0.89	0.07	2.89	3.05	
A41	1171	15	0.28194	0	0.00062	0	0.281923	-30.01	-4.24	0.64	1.81	2.22	
A42	1149	14	0.28187	0	0.00101	0	0.281846	-32.42	-7.45	0.31	1.92	2.40	
A43	1790	15	0.28170	0	0.00119	0	0.281661	-38.32	0.63	0.05	2.16	2.40	
PE-EX-34 B Pebble Sopa-Brumadinho Fm.													
D-20.1	2131	11	0.281556	18	0.00116	7	0.281509	-43.46	3.12	0.04	2.36	2.50	16
D-11.1	2136	13	0.281531	17	0.00196	13	0.281451	-44.35	1.18	0.01	2.44	2.63	15
D-1.1	2132	22	0.281629	16	0.00096	6	0.281590	-40.87	6.02	0.10	2.25	2.32	16
E-4.1	2695	8	0.280887	15	0.00047	3	0.280862	-67.13	-6.72	0.07	3.20	3.56	18

E-6.1	2780	10	0.280991	14	0.00057	4	0.280960	-63.45	-1.24	0.01	3.08	3.28	16
E-14.1	2698	12	0.281547	19	0.00073	5	0.281509	-43.78	16.37	0.17	2.34	2.10	17
E-21.1	2141	12	0.281584	17	0.00172	17	0.281514	-42.46	3.54	0.06	2.35	2.48	16
E-28.1	2116	19	0.281562	15	0.00119	9	0.281514	-43.26	2.95	0.05	2.35	2.50	14
E-29.1	2967	61	0.280963	13	0.00144	9	0.280881	-64.42	0.35	0.01	3.18	3.32	20
E-38.1	2132	12	0.281557	16	0.00193	21	0.281479	-43.42	2.06	0.03	2.40	2.57	19
F-37.1	2152	13	0.280952	15	0.00093	7	0.280914	-64.83	-17.55	0.24	3.16	3.80	16
F-34.1	2100	27	0.281380	14	0.00134	9	0.281326	-49.70	-4.10	0.08	2.61	2.93	17
F-22.1	2127	28	0.281603	16	0.00137	9	0.281547	-41.81	4.38	0.09	2.31	2.42	13
F-20.1	2104	41	0.281481	15	0.00076	5	0.281451	-46.11	0.42	0.01	2.43	2.65	17
F-18.1	2576	57	0.281205	23	0.00126	11	0.281143	-55.86	0.49	0.02	2.84	3.01	19
F-6.1	2141	18	0.281540	14	0.00055	3	0.281518	-44.02	3.67	0.05	2.34	2.48	18
F.2.1	2780	23	0.280906	18	0.00093	7	0.280856	-66.45	-4.94	0.08	3.22	3.51	16
PE-CM-14 Galho do Miguel Fm. Mar													
A-38.1	1583	16	0.281632	11	0.00057	4	0.281615	-40.76	-5.75	0.10	2.22	2.63	20
A-37.1	2199	10	0.281679	15	0.00242	16	0.281578	-39.11	7.14	0.08	2.26	2.30	21
A-35.1	2099	14	0.281362	14	0.00108	8	0.281319	-50.31	-4.37	0.06	2.62	2.95	20
A-30.1	2205	14	0.281341	17	0.00052	3	0.281319	-51.06	-1.91	0.02	2.61	2.88	16
A-27.1	2190	11	0.281342	13	0.00038	2	0.281326	-51.03	-2.00	0.02	2.60	2.87	19
A-22.1	2539	11	0.281052	14	0.00140	11	0.280984	-61.30	-6.06	0.08	3.06	3.39	20
A-18.1	2459	9	0.281318	13	0.00075	5	0.281282	-51.89	2.70	0.03	2.65	2.78	19
A-11.1	2908	12	0.280876	16	0.00099	9	0.280820	-67.52	-3.21	0.04	3.26	3.50	18
A-6.1	2140	15	0.281509	15	0.00032	6	0.281496	-45.13	2.85	0.08	2.37	2.53	19
B-10	2100	31	0.281501	15	0.00061	4	0.281476	-45.42	1.24	0.03	2.40	2.60	19
B-14	2257	83	0.281519	18	0.00025	2	0.281508	-44.77	6.02	0.26	2.35	2.42	15
B-17	2141	34	0.281573	13	0.00061	4	0.281548	-42.86	4.74	0.10	2.30	2.41	17
B-20.1	2118	11	0.281445	15	0.00084	7	0.281411	-47.39	-0.66	0.01	2.49	2.73	20
B-21.1	2132	13	0.281525	17	0.00069	5	0.281496	-44.57	2.69	0.03	2.37	2.53	17
B-34	2083	14	0.281662	12	0.00078	5	0.281631	-39.72	6.33	0.08	2.19	2.26	16
C-3.1	2079	10	0.281442	14	0.00052	4	0.281422	-47.48	-1.18	0.01	2.47	2.73	18

C-7.1	2098	10	0.281423	12	0.00055	6	0.281402	-48.15	-1.46	0.02	2.50	2.77	12
C-9.1	2003	14	0.281521	13	0.00117	10	0.281477	-44.69	-1.00	0.02	2.41	2.66	15
PE-CM-15a													
Galho do Miguel Fm. Eol													
D-3.1	2805	13	0.281220	20	0.00147	11	0.281141	-55.33	5.79	0.07	2.84	2.86	15
D-9.1	2097	15	0.281520	28	0.00102	9	0.281479	-44.73	1.28	0.02	2.40	2.59	13
E-2.1	2153	11	0.281393	13	0.00050	3	0.281373	-49.21	-1.21	0.01	2.54	2.79	17
E-5.1	2115	8	0.281424	15	0.00104	7	0.281382	-48.12	-1.75	0.02	2.53	2.80	18
E-6.1	2763	25	0.280884	18	0.00091	6	0.280836	-67.24	-6.08	0.09	3.24	3.57	15
E-7.1	2137	14	0.281553	22	0.00052	5	0.281532	-43.57	4.06	0.06	2.32	2.45	15
E-10.1	2087	13	0.281485	14	0.00059	9	0.281461	-45.98	0.40	0.01	2.42	2.64	17
E-11.1	2179	13	0.281279	18	0.00075	5	0.281248	-53.27	-5.06	0.07	2.71	3.05	13
E-12.1	2071	20	0.281430	15	0.00081	10	0.281398	-47.91	-2.21	0.05	2.51	2.79	16
E-14.1	2065	21	0.281459	18	0.00035	2	0.281445	-46.90	-0.69	0.01	2.44	2.69	14
E-19.1	1843	12	0.281667	19	0.00093	6	0.281635	-39.53	0.92	0.01	2.19	2.42	14
E-21.1	2151	20	0.281572	19	0.00019	1	0.281564	-42.91	5.53	0.09	2.28	2.37	20
E-22.1	2142	11	0.281382	153	0.00054	5	0.281360	-49.60	-1.91	0.03	2.55	2.83	1
E-23.1	2161	11	0.281472	21	0.00035	2	0.281457	-46.43	1.98	0.02	2.42	2.60	19
E-25.1	2095	23	0.281565	37	0.00047	6	0.281546	-43.15	3.60	0.09	2.30	2.45	15
E-27.1	2114	8	0.281564	27	0.00052	4	0.281543	-43.17	3.94	0.05	2.31	2.44	11
PE-CM-15b													
Galho do Miguel Fm. Eol													
A-1.1	2070	33	0.281442	13	0.00025	2	0.281432	-47.50	-1.04	0.02	2.46	2.72	24
A-7.1	2085	41	0.281399	14	0.00035	2	0.281385	-49.00	-2.35	0.06	2.52	2.81	22
A-14.1	2157	43	0.281483	15	0.00101	10	0.281441	-46.04	1.32	0.04	2.45	2.64	16
A-19.1	2119	38	0.281594	14	0.00113	7	0.281549	-42.11	4.25	0.10	2.30	2.42	14
B-6.1	2156	34	0.281546	14	0.00050	3	0.281526	-43.80	4.30	0.09	2.33	2.45	20
B-13.1	2257	34	0.281501	21	0.00144	13	0.281439	-45.40	3.57	0.09	2.45	2.57	10
C-10.1	3272	72	0.280793	18	0.00172	11	0.280685	-70.45	0.58	0.02	3.44	3.54	14
C-26.1	2234	23	0.281408	55	0.00069	8	0.281379	-48.69	0.89	0.02	2.53	2.72	8

C-30.1	2865	25	0.281054	22	0.00162	11	0.280966	-61.20	0.95	0.01	3.07	3.21	10
PE-SC-43 Galho do Miguel Fm. Mar													
A-15.1	1598	10	0.281635	14	0.00114	7	0.281600	-40.67	-5.93	0.07	2.25	2.66	18
A-16.1	1545	22	0.281612	17	0.00125	8	0.281576	-41.48	-8.02	0.17	2.29	2.74	19
A-19.1	1607	13	0.281623	12	0.00125	10	0.281585	-41.09	-6.28	0.10	2.27	2.68	19
A-20.1	1919	13	0.281263	14	0.00055	4	0.281243	-53.82	-11.24	0.16	2.71	3.23	16
A-31.1	2124	15	0.281574	16	0.00064	4	0.281548	-42.83	4.33	0.06	2.30	2.42	12
B-41.1	2046	14	0.281529	30	0.00100	7	0.281490	-44.42	0.47	0.01	2.38	2.60	8
B-21.1	2089	9	0.281141	17	0.00059	4	0.281118	-58.13	-11.76	0.13	2.88	3.40	12
B-24.1	1560	11	0.281658	14	0.00110	7	0.281625	-39.86	-5.92	0.08	2.22	2.63	17
B-12.1	2173	13	0.281636	16	0.00299	21	0.281512	-40.64	4.20	0.06	2.36	2.47	18
B-11.1	1607	14	0.281140	13	0.00055	3	0.281123	-58.18	-22.66	0.34	2.88	3.69	18
B-10.1	2013	10	0.281644	14	0.00109	7	0.281602	-40.36	3.70	0.04	2.23	2.38	17
B-4.1	2192	10	0.281489	15	0.00086	6	0.281453	-45.82	2.56	0.03	2.43	2.59	14
B-1.1	1611	13	0.281627	16	0.00065	4	0.281607	-40.95	-5.39	0.08	2.23	2.63	18
C-2.1	2737	32	0.280988	17	0.00064	4	0.280954	-63.55	-2.47	0.04	3.08	3.32	15
C-19.1	2692	17	0.281041	23	0.00177	17	0.280950	-61.66	-3.67	0.06	3.10	3.36	11
C-29.1	2197	12	0.281421	20	0.00070	6	0.281392	-48.22	0.50	0.01	2.51	2.72	12
C-33.1	2034	14	0.281512	15	0.00089	6	0.281477	-45.03	-0.26	0.00	2.40	2.64	18
PE-SM-16 Santa Rita Fm.													
D-1.1	2076	39	0.281131	15	0.00067	6	0.281105	-58.48	-12.52	0.35	2.90	3.44	17
D-8.1	3328	27	0.280644	20	0.00108	6	0.280575	-75.72	-2.01	0.03	3.58	3.75	12
D-12.1	3545	20	0.280733	20	0.00257	16	0.280557	-72.58	2.53	0.03	3.60	3.63	16
D-16.1	2095	21	0.281445	14	0.00066	6	0.281419	-47.37	-0.92	0.02	2.48	2.73	18
D-29.1	2152	20	0.281469	19	0.00169	28	0.281399	-46.54	-0.29	0.01	2.51	2.73	11
E-1.1	2678	24	0.280962	18	0.00120	8	0.280900	-64.48	-5.78	0.09	3.16	3.48	18
E-2.1	2043	23	0.281069	17	0.00102	6	0.281029	-60.69	-15.97	0.28	3.01	3.62	18

E-12.1	2044	24	0.281230	15	0.00042	3	0.281214	-54.99	-9.39	0.18	2.75	3.22	19
E-21.1	2919	25	0.280798	16	0.00095	7	0.280745	-70.27	-5.62	0.09	3.36	3.66	15
E-31.1	2672	32	0.280939	20	0.00069	4	0.280904	-65.29	-5.79	0.11	3.15	3.48	12
E-33.1	2084	21	0.281433	15	0.00067	6	0.281406	-47.82	-1.62	0.03	2.49	2.76	17
F-2.1	2157	28	0.281514	13	0.00073	5	0.281484	-44.94	2.84	0.06	2.39	2.54	18
F-2.2	2032	23	0.281210	14	0.00113	7	0.281166	-55.71	-11.36	0.20	2.83	3.33	19
F-6.1	2032	32	0.281069	15	0.00031	2	0.281057	-60.68	-15.23	0.34	2.95	3.57	17
F-14,1	2611	36	0.281027	13	0.00049	3	0.281003	-62.17	-3.69	0.07	3.02	3.30	20
F-17.1	3192	32	0.280702	15	0.00066	4	0.280661	-73.67	-2.16	0.04	3.46	3.65	17
F-18.1	2612	36	0.280957	15	0.00119	8	0.280897	-64.65	-7.42	0.15	3.17	3.54	17
PE-CM-17													
Santa Rita Fm.													
D-1.1	1576	24	0.281766	15	0.00065	4	0.281746	-36.03	-1.25	0.03	2.04	2.35	22
D-2.1	1524	32	0.281824	20	0.00180	11	0.281772	-33.98	-1.53	0.04	2.03	2.32	11
D-3.1	1551	30	0.281838	14	0.00076	5	0.281815	-33.50	0.62	0.02	1.95	2.21	13
D-14.1	1538	29	0.281831	14	0.00054	3	0.281816	-33.72	0.34	0.01	1.95	2.22	18
D-23.1	2598	27	0.281016	17	0.00067	5	0.280983	-62.54	-4.70	0.08	3.05	3.35	17
D-24.1	1971	26	0.281452	16	0.00166	18	0.281390	-47.13	-4.82	0.12	2.53	2.88	17
D-25.1	1489	29	0.281657	18	0.00060	4	0.281640	-39.90	-7.03	0.19	2.19	2.64	15
D-32.1	1988	34	0.281663	53	0.00277	39	0.281558	-39.69	1.55	0.05	2.31	2.49	9
E-17.1	2123	30	0.281491	21	0.00083	5	0.281458	-45.75	1.12	0.02	2.42	2.62	9
E-18.1	2122	28	0.281513	15	0.00033	2	0.281500	-44.98	2.58	0.05	2.37	2.53	19
E-19.1	2115	37	0.281500	14	0.00086	5	0.281465	-45.45	1.20	0.03	2.42	2.61	15
F-11.1	2177	77	0.281473	15	0.00038	4	0.281457	-46.41	2.33	0.11	2.42	2.59	21
F-20.1	2793	65	0.280837	15	0.00046	3	0.280812	-68.88	-6.19	0.18	3.27	3.60	20
PE-CM-19													
Córrego dos Borges Fm.													
A-1.1	2177	19	0.281399	12	0.00037	3	0.281383	-49.02	-0.29	0.00	2.52	2.75	17
A-3.1	2117	13	0.281512	16	0.00071	4	0.281484	-45.00	1.90	0.02	2.39	2.57	18
A-5.1	2845	5	0.281105	19	0.00240	15	0.280974	-59.42	0.77	0.01	3.07	3.20	16

A-7.1	2127	7	0.281464	12	0.00076	5	0.281434	-46.70	0.34	0.00	2.46	2.67	22
A-8.1	1966	12	0.281423	14	0.00046	3	0.281406	-48.16	-4.37	0.06	2.49	2.84	22
A-11.1	1972	15	0.281526	16	0.00045	3	0.281509	-44.52	-0.56	0.01	2.36	2.61	19
A-12.1	1499	27	0.281667	12	0.00053	3	0.281652	-39.53	-6.36	0.15	2.17	2.61	20
A-15.1	1737	19	0.281728	11	0.00095	6	0.281697	-37.37	0.69	0.01	2.11	2.35	18
A-19.1	1951	18	0.281454	14	0.00127	9	0.281407	-47.07	-4.69	0.07	2.50	2.85	18
A-20.1	2121	9	0.281321	14	0.00058	4	0.281297	-51.78	-4.63	0.05	2.64	2.98	20
A-27.1	2884	6	0.280961	12	0.00072	4	0.280921	-64.51	-0.20	0.00	3.13	3.29	24
A-36.1	1548	17	0.281818	15	0.00055	3	0.281802	-34.21	0.07	0.00	1.97	2.24	19
B-1.1	3227	14	0.280702	15	0.00089	6	0.280647	-73.65	-1.82	0.02	3.48	3.66	20
B-2.1	2708	7	0.280900	14	0.00061	4	0.280868	-66.66	-6.21	0.05	3.20	3.53	20
B-6.1	1750	15	0.281720	17	0.00092	6	0.281690	-37.66	0.73	0.01	2.12	2.36	16
B-14.1	1441	13	0.281795	15	0.00062	5	0.281778	-35.01	-3.22	0.05	2.00	2.36	18
B-18.1	1407	22	0.281827	14	0.00048	3	0.281814	-33.89	-2.73	0.06	1.95	2.31	16
B-28.1	1544	27	0.281828	15	0.00063	5	0.281809	-33.85	0.25	0.01	1.96	2.23	18
B-30.1	1753	30	0.281780	16	0.00151	9	0.281729	-35.55	2.21	0.05	2.07	2.27	16
C-18.1	3022	8	0.280790	15	0.00093	13	0.280737	-70.53	-3.49	0.06	3.37	3.61	16
C-33.1	1500	24	0.281844	19	0.00142	15	0.281804	-33.28	-0.96	0.03	1.98	2.27	17
PE-SC-42 **Córrego dos Borges Fm.**													
D-2.1	1780	20	0.281734	17	0.00100	7	0.281701	-37.15	1.81	0.03	2.11	2.31	20
D-5.1	1764	10	0.281677	14	0.00136	9	0.281632	-39.18	-1.01	0.01	2.20	2.48	10
D-8.1	1555	65	0.281808	16	0.00097	6	0.281779	-34.55	-0.57	0.03	2.00	2.29	65
D-15.1	2072	15	0.281667	15	0.00129	9	0.281616	-39.53	5.55	0.08	2.21	2.30	15
D-23.1	1775	14	0.281510	20	0.00080	5	0.281484	-45.07	-6.01	0.08	2.40	2.80	14
D-27.1	2861	26	0.280840	22	0.00074	8	0.280799	-68.79	-5.06	0.10	3.29	3.58	26
D-33.1	2532	22	0.281002	14	0.00131	10	0.280939	-63.04	-7.81	0.13	3.12	3.50	22
E-1.1	2067	12	0.281363	14	0.00070	4	0.281336	-50.27	-4.52	0.05	2.59	2.93	12
E-2.1	1761	14	0.281700	19	0.00121	8	0.281660	-38.37	-0.08	0.00	2.16	2.42	14
E-10.1	1650	23	0.281720	15	0.00057	4	0.281702	-37.66	-1.12	0.02	2.10	2.40	23
E-21.1	2662	13	0.281000	14	0.00060	4	0.280969	-63.13	-3.69	0.04	3.07	3.34	13
E-22.1	2212	15	0.281541	19	0.00227	14	0.281445	-44.00	2.72	0.04	2.45	2.59	15

F-1.1	1491	26	0.281698	16	0.00129	11	0.281661	-38.45	-6.22	0.16	2.17	2.59	26
F-4.1	1516	13	0.281328	16	0.00035	2	0.281318	-51.51	-17.82	0.26	2.61	3.33	13
F-8.1	2387	24	0.281519	18	0.00110	7	0.281469	-44.78	7.65	0.12	2.40	2.42	24
F-10.1	2187	15	0.281490	19	0.00105	7	0.281446	-45.78	2.20	0.03	2.44	2.61	15
F-12.1	2671	13	0.281074	15	0.00250	25	0.280946	-60.52	-4.31	0.06	3.12	3.39	13
F-18.1	2524	16	0.281146	18	0.00065	4	0.281115	-57.95	-1.74	0.02	2.88	3.11	16
F-20.1	2090	24	0.281292	11	0.00060	11	0.281268	-52.79	-6.38	0.19	2.68	3.07	24
PE-CM-18													
Córrego Pereira Fm.													
E-15.1	2657	23	0.281031	16	0.00026	2	0.281018	-62.02	-2.08	0.03	3.00	3.24	17
F-3.1	2671	25	0.281001	14	0.00030	2	0.280985	-63.10	-2.91	0.05	3.04	3.30	23
F-4.1	1763	34	0.281723	18	0.00075	6	0.281698	-37.54	1.33	0.04	2.11	2.33	18
F-17.1	1629	21	0.281718	14	0.00051	3	0.281702	-37.73	-1.61	0.03	2.10	2.41	18
F-18.1	2716	27	0.281093	15	0.00130	11	0.281025	-59.84	-0.43	0.01	3.00	3.18	26
F-24.1	2100	34	0.281619	13	0.00078	5	0.281588	-41.25	5.19	0.12	2.25	2.35	17
F-37.1	1802	26	0.281689	21	0.00135	9	0.281643	-38.74	0.28	0.01	2.19	2.43	12
F-35.1	1797	29	0.281629	12	0.00042	3	0.281614	-40.89	-0.86	0.02	2.22	2.49	18
E-3.1	1445	16	0.282010	18	0.00030	2	0.282002	-27.39	4.82	0.08	1.70	1.86	15
D-21.1	1404	32	0.281985	16	0.00030	2	0.281977	-28.28	3.01	0.09	1.73	1.95	14
E-8.1	1978	28	0.281655	16	0.00099	7	0.281618	-39.96	3.45	0.07	2.21	2.36	16
D-23.1	1796	38	0.281807	16	0.00051	3	0.281790	-34.57	5.35	0.15	1.98	2.10	17
D-20.1	1966	33	0.281564	14	0.00114	7	0.281521	-43.18	-0.28	0.01	2.35	2.59	17
D-15.1	1978	29	0.281496	13	0.00103	7	0.281458	-45.57	-2.25	0.05	2.43	2.72	18
D-14.1	2460	32	0.281236	14	0.00061	4	0.281207	-54.77	0.06	0.00	2.75	2.95	13
D-2.1	1978	23	0.281409	17	0.00047	12	0.281391	-48.65	-4.60	0.17	2.51	2.87	19
D-5.1	1981	29	0.281568	17	0.00070	4	0.281542	-43.03	0.80	0.02	2.31	2.53	18
E-1.1	2457	34	0.281219	16	0.00075	4	0.281184	-55.39	-0.86	0.02	2.79	3.01	13
E-3.1	1445	40	0.281847	16	0.00077	5	0.281826	-33.16	-1.42	0.05	1.94	2.26	16
E-13.1	1748	43	0.281763	17	0.00049	3	0.281747	-36.14	2.72	0.09	2.04	2.23	15
PE-CM-35													

Rio Pardo Grande Fm.													
A-1.1	2001	29	0.281567	16	0.00037	2	0.281553	-43.07	1.67	0.03	2.30	2.49	18
A-2.1	1939	16	0.281574	15	0.00041	3	0.281559	-42.82	0.45	0.01	2.29	2.52	20
A-4.1	2900	19	0.280853	13	0.00072	5	0.280813	-68.33	-3.67	0.05	3.27	3.52	23
A-5.1	2070	16	0.281299	14	0.00039	3	0.281284	-52.54	-6.30	0.09	2.65	3.05	20
A-10.1	1991	22	0.281588	16	0.00063	4	0.281564	-42.34	1.83	0.03	2.28	2.48	16
A-12.1	2001	22	0.281625	15	0.00077	9	0.281596	-41.01	3.20	0.07	2.24	2.40	18
A-13.1	1886	28	0.281567	12	0.00156	10	0.281511	-43.06	-2.47	0.05	2.37	2.66	22
A-15.1	1956	16	0.281550	17	0.00036	2	0.281536	-43.67	0.04	0.00	2.32	2.56	18
A-22.1	2003	25	0.281564	14	0.00054	3	0.281544	-43.17	1.38	0.03	2.31	2.51	18
A-25.1	2008	25	0.281530	15	0.00035	2	0.281516	-44.39	0.52	0.01	2.34	2.57	17
A-31.1	2459	34	0.281246	20	0.00091	8	0.281203	-54.42	-0.12	0.00	2.76	2.96	12
A-37.1	2004	31	0.281520	22	0.00110	7	0.281478	-44.75	-0.93	0.02	2.40	2.66	13
B-23.1	1517	12	0.281618	15	0.00074	4	0.281597	-41.27	-7.92	0.11	2.25	2.72	18
B-31.1	2681	19	0.280986	12	0.00078	5	0.280945	-63.63	-4.10	0.06	3.10	3.38	17
B-35.1	1874	16	0.281608	23	0.00121	8	0.281565	-41.61	-0.83	0.01	2.29	2.55	12
C-37.1	1752	21	0.281689	13	0.00066	5	0.281667	-38.76	-0.03	0.00	2.15	2.41	18
C-30.1	1536	29	0.281761	14	0.00067	4	0.281742	-36.21	-2.34	0.06	2.05	2.38	19
C-26.1	1983	23	0.281748	15	0.00058	4	0.281726	-36.68	7.39	0.13	2.07	2.12	18
C-20.1	2667	18	0.280935	15	0.00051	3	0.280909	-65.43	-5.73	0.08	3.14	3.47	17
C-15.1	1810	20	0.281658	17	0.00089	6	0.281627	-39.86	-0.10	0.00	2.20	2.46	16

Assumed Values

t (Ma)	4560
l (Ga-1) [a]	0.01867
(^{176}Hf/^{177}Hf)^{0}chur [b]	0.282785
(^{176}Hf/^{177}Hf)^{i} chur	0.279718
(^{176}Lu/^{177}Hf)^{0} chur [b]	0.0336
(^{176}Hf/^{177}Hf)DM [c]	0.28325
(^{176}Lu/^{177}Hf)DM [c]	0.0388
(^{176}Lu/^{177}Hf)UCC [d]	0.015

a ^{176}Lu decay constant (Söderlund et al., 2004)

b Chondritic values (Bovier et. Al, 2008)

c Present day Depleted Manlte (Giffin et al., 2000; updated by Andersen et al., 2009)

d Goodge and Vervoort, EPSL 243, 711-731 (2006)

*** Lu-Hf isotope data from Guadagnin et al. (2015)**